

## SIXTH INTERNATIONAL WORKSHOP

### ON LASER RANGING INSTRUMENTATION

ANTIBES JUAN-LES-PINS



6<sup>e</sup> COLLOQUE INTERNATIONAL  
SUR L'INSTRUMENTATION  
DE LA TELEMETRIE LASER

EDITED BY / EDITE PAR :

- JEAN GAIGNEBET
- FRANCOISE BAUMONT

WE WISH HEREBY TO EXPRESS OUR THANKS TO /  
NOUS TENONS A REMERCIER ICI :

- MINISTERE DES AFFAIRES ETRANGERES
- ASSOCIATION INTERNATIONALE DE GEODESIE
- UNION GEODESIQUE ET GEOPHYSIQUE INTERNATIONALE
- INSTITUT NATIONAL DES SCIENCES DE L'UNIVERS
- CENTRE NATIONAL D'ETUDES SPATIALES
- AEROSPATIALE
- BRASSARD MICHELET INDUSTRIES
- QUANTEL
- SOCIETE D'ETUDES ET DE CONSTRUCTION D'INSTRUMENTS ASTRONOMIQUES

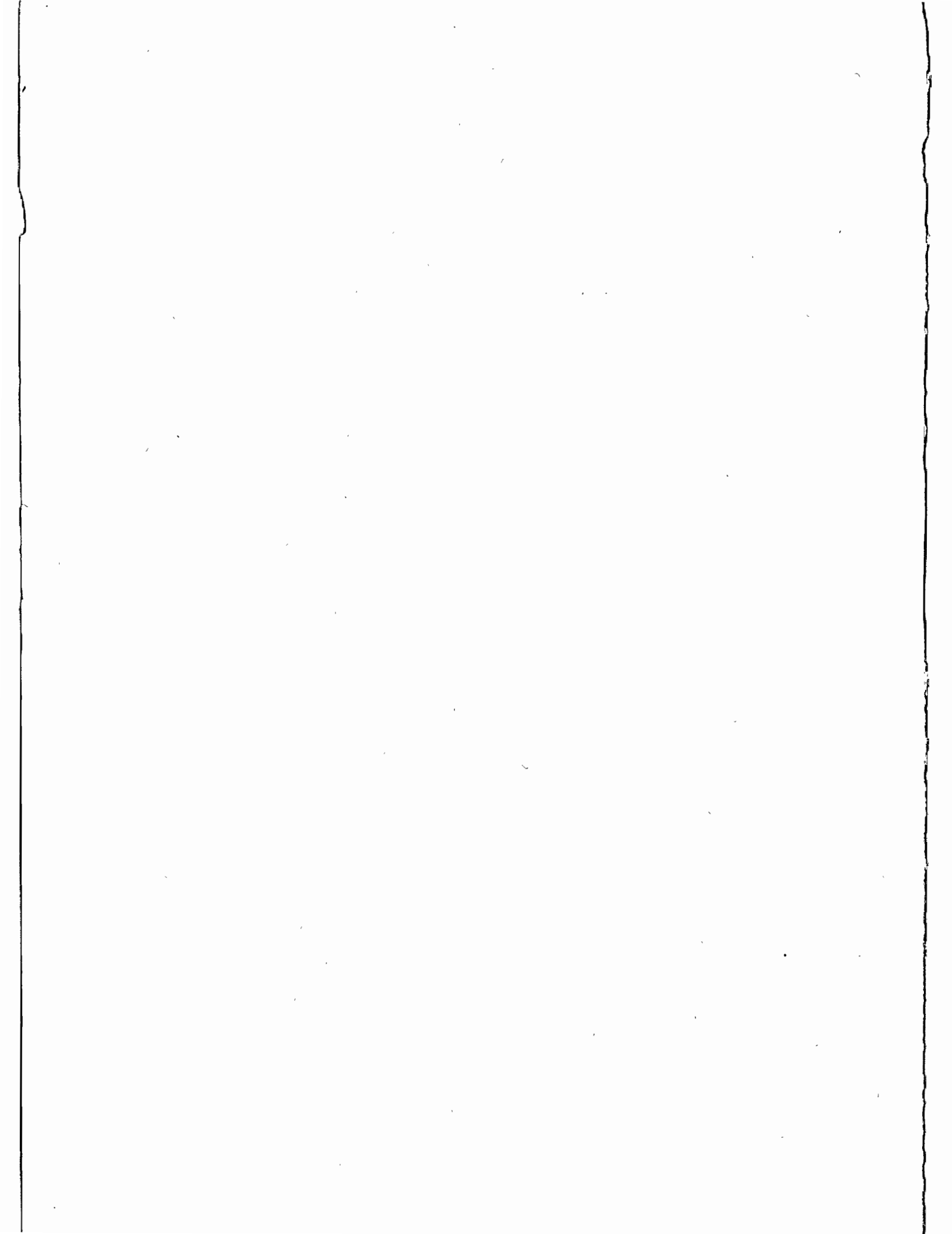


TABLE OF CONTENTS  
=====

	PAGE
WELCOMING ADDRESS            J.P. Rozelot	V
PREFACE                        J. Gaignebet	VII
RESOLUTIONS	XI
LIST OF PARTICIPANTS	XVI
 <u>SCIENTIFIC RESULTS AND FUTURE GOALS OF LASER RANGING</u>	
Chairman : F. Barlier (Invited Papers)	
 I. Ciufolini	
New Relativistic Measurements With Laser Ranged Satellites	1
 <u>NORMAL POINTS</u> Chairman : D. Leigeman	
 R. Kolenkiewicz et al.	
Comparison Of Lageos Satellite Ranging Normal Points	11
 <u>SATELLITE MOBILE STATIONS</u> Chairman : P. Wilson	
 T. Varghese, M. Hernick	
Sub Cm Multiphotoelectron Satellite Laser Ranging	21
 T. Varghese et al.	
TLRS-1 ; System Upgrade And Performance Results	33
 N. Sasaki, Y. Suzuki	
Satellite Laser Ranging System At The Simosato Hydrographie Observatory And The Transportable system, HTLRS	45
 Z. Wen-Yao, T. De Tong	
Progress In SLR At Shanghai Observatory	59
 K. Hamal et al.	
Interkosmos Laser Radar, Version Mode Locked Train	69
 F. Pierron et al.	
Upgrades And New Developments On Satellite Laser Ranging Station From Grasse	73
 L. Grunwaldt et al.	
The SBG Laser Radar Stations Potsdam And Santiago De Cuba Status And Performance Report	93
 K. Hamal et al.	
3. Generation Laser Radar, Version Mode Locked Train Proposal	109
 A. Banni, V. Capoccia	
The New Satellite Laser Ranging System At Cagliari Observatory	113
 P. Kloeckler, Th. Schildknecht	
Zimmerwald Satellite Observation Station	123

LUNAR AND COMBINED Chairman : K. Hamal

Ch. Veillet et al. The New CERGA LLR Station	129
M.L. White Recent Improvements And Future Plans At The University Of Hawaïi Lunar And Satellite Ranging Station	135
J.R. Wiant, P.J. Shelus The McDonald Observatory Laser Ranging Station : MLRS	139

DETECTORS : SOLID STATE AND PMT Chairman : S.R. Bowman

I. Prochaska Start Detector For The Mode Locked Train Laser Radar	145
R. Neubert et al. Ambiguity And Resolution of A Mode Locked Pulse Train Laser Radar	149
I. Prochaska, J. Gaignebet Microchannel/Dynode Photomultipliers Comparison Experiment	161
Z. Neumann Detectors For III Generation Laser Ranging Systems	165
S.R. Bowman et al The Use Of Geiger Mode Avalanche Photodiodes For Precise Laser Ranging At Very Low Light Levels : An Experimental Evaluation	173
K. Hamal et al. Single Photon Solid State Detector For Ranging At Room Temperature	185
W.A. Kielek "Constant Fraction" Discriminators In Few And Multiphotoelectron Laser Ranging	189

TIMING AND EPOCH Chairman : C.A. Steggerda

B.A. Greene Calibration Of Sub-Picosecond Timing Systems	197
P. Dachel et al. Recent Advances In The GLTN Timing And Frequency Instrumentation	205
C.A. Steggerda The Development Of A Dual Frequency Event Timer	225

LASERS Chairmen : F. Moya, H. Jelinkova

K. Hamal, H. Jelinkova Saturable Dye For 1.06 $\mu$ m	243
H. Jelinkova et al. Spatial Structure Of The Doubled Nd:YAG Laser Transmitter Beam	251
L. Jiyu Some Special Requirements To Lasers For Satellite Laser Ranging	261

OPTICS, TRACKING AND MOUNTS Chairman : M.L. White

S.R. Bowman et al. Analysis And Performance Of A Passive Polarization Telescope Coupling Switch For Lunar Laser Ranging	273
H. Feng et al. An Accurate Test Of The Azimuth Axis Of A 1.2M Alt-AZ Telescope Mount For The Lunar Laser Ranging And The Analysis Of The Results	281
M.L. White Double Peak Polarized Interference Filters	289
R. Korakitis Effects Of Telescope Design On Laser Beam Pointing Accuracy	297

CALIBRATION Chairman : M. Pearlman

T. Varghese System Characterization Of Moblas-7 For Colocation With TLRS-1 & 2	311
R. Appller Calibration Error Sources	323
B.A. Greene Calibration Of Sub-Millimeter Precision Satellite Laser Ranging Systems	331
P. Kloeckler, T. Schildknecht Measuring And Modelling Pulse Discriminator Amplitude Dependence	343
H. Junginger MTLRS Ground Tests	357
J.D. Rayner et al. Zero Range Realtime Calibration	373
K. Hamal, I. Prochaska System Stability Using Mode Locked Train	377
L. Jiyu Satellite Laser Ranging Errors	379

SOFTWARE BENCHMARKING AND COLOCATION Chairman : E. Vermaat

M.R. Pearlman Some Current Issues On Laser Collocations	399
A. Cenci Management Of The Laser Ranging Systems Colocation	409
D.L.F. Van Loon Eccentricity Vectors For Colocation Purposes	441
V. Husson, D. Edge Polyquick Collocation Analysis	453
A. Caporali Colocation Data Analysis : Dynamical Approach	467
R. Kolenkiewicz Geodyn Collocation Analysis And Its Comparison With Polyquick	481

RAPID ON SITE DETERMINATION OF THE EARTH ROTATION

Chairmen : D. Smith, Ch. Veillet

- P.J. Shelus, R. Ricklefs  
Real Time, On Site Earth Orientation Parameter Generation At  
The MLRS Using Laser Ranging Data 493
- G.M. Appleby, A.T. Sinclair  
A Note On The Use Of The CRS Lageos Ephemerides 499
- Ch. Veillet et al.  
Real Time UTO Determination At CERGA LLR Station 507
- P.J. Shelus  
A Simple Software Scheduling Tool For Efficient Observing  
Operations At A Lunar/Lageos Laser Ranging Station 511

HIGHT AVERAGE POWER AND NEW LASERS, NEW SATELLITES

Chairman : C.O. Alley

- S.R. Bowman et al.  
A Neodimium YAG Active Mirror For The Amplification Of Mode  
Locked Laser Pulses 523
- M. Sasaki  
Japanese Geodetic Satellite "AJISAI" Launched In August 1986 527
- F.M. Yang  
The Proposal Of Strictly Simultaneous Satellite Laser Ranging 549

TWO WAVELENGTH SYSTEMS AND STREAK CAMERA Chairman : B. Greene

- I. Prochaska, K. Hamal  
Streak Camera Based Laser Radar Receiver. Its Performance and  
Limitations 559
- J. Gaignebet et al., K. Hamal et al.  
Two Wavelength Ranging On Ground Target Using Nd:YAG 2HG and  
Raman 0.68  $\mu\text{m}$  Pulses 565
- I. Prochaska, K. Hamal  
Picosecond Laser Ranging Using Photodiode 577
- B.A. Greene  
Multiple Wavelength Laser ranging 581
- F. Guerin, G. Cerutti-Maori  
Problems Induced By Multicolor Telemetry On Laser Retroreflector  
Development 593

SPECIAL STUDY GROUP ON LUNAR LASER RANGING

Report prepared by Ch. Veillet 623

LUNAR AND COMBINED (Additive)

- C.O. Alley et al.  
First Lunar Ranging Results From The University Of Maryland  
Research Station At The 1.2M Telescope Of The GSFC 625

WELCOMING ADDRESS AT THE JUAN-LES-PINS  
WORKSHOP ON LASER INSTRUMENTATION

J.P. ROZELOT  
Directeur du CERGA  
Avenue Copernic  
06130 - Grasse - France -

First at all, on behalf of the local organizing committee, I would like to welcome you here in Juan-Les-Pins for this Sixth International Workshop on Laser Instrumentation.

The intent of the scientific committee is to summarize the advances in this technique in the broader context of current research in the physics of lasers, and I am not afraid to say that this symposium is almost unique in bringing together a large scientific community that includes not only physicists but also astrophysicists, atmospheric specialists, fluid mechanics specialists, and so on.

LASER : what a magic name nowadays ! Lasers in theaters, laser in night-club and cabarets, compact discs with lasers, medical therapy with laser, what else more ? Every one knows now this word, laser, but what a long way ! Remember. In July 1960, MAIMAN, working at the Hughes Aircraft Company was the first man to notice that a rubis, in special conditions of lightning, was able to flash in a monochromatic way. A few months later, JAVAN at the Bell Telephone laboratories was able to do the same thing with an Helium-neon blending. The Light Activation by Simulated Emission of Radiations, which was abbreviated in laser, was born. And noticing that the light in one picosecond cover 0.3 millimeter, the high accuracy telemetry was also born...

As Director of the CERGA, this well-known Agency for research in the field of Geodynamics and Astronomy, it is my pleasure to thank all the participants of this meeting for their enthusiasm and I am sure, for their generous cooperation. The brunt of responsibility during this meeting fall to the working group leaders, and especially to Mrs. Françoise BAUMONT, Dr. Jean GAIGNEBET, and Prof. C.O. Alley, Dr. B.A. Greene, Dr. K. Hamal. I would like to extend my warm congratulations to all experts who worked in the shadow to make this meeting a success.

An international technical meeting is one of the effective ways to propel the World's science forward. I believe that this exchange and discussion not only be beneficial to the academic researches carried out by every country's laser engineers, but also can promote the existing friendship between people, and further the mutual understanding and cooperation among the scientists of all countries.

Friends and colleagues from distant part of the World ! It is Apollo's rover that has brought you here from all different directions, from the States, from China, from Eastern Countries, from all Europe. The Rendez-Vous is not Olympia, but a city where we can have dialogue with Apollo for about 300 days in the year. A marvellous city, where flowers blossom in all four seasons. Every cloud has a silvery nimbused : take this one and don't forget to go back home with the last jasmine or a lot of carnations.

At last, I am impressed by the High quality of the program booklet : this guarantee that we may look forward to a highly inspiring and successful meeting.

Thank you for all that you have done so far !

I wish you all success in this workshop, and a pleasant stay on the French Riviera.



## PREFACE

Le Sixième Colloque International sur l'Instrumentation en Télémétrie s'est déroulé du 22 au 26 Septembre 1986 à Antibes Juan-Les-Pins (France).

Comme lors des précédents colloques, un nombre important de présentations ont eu lieu. Les progrès accomplis depuis la dernière réunion (Herstmonceux) sont spectaculaires et extrêmement prometteurs. L'exactitude des stations a continué à s'améliorer grâce aux avancées technologiques et à une meilleure maîtrise des problèmes liés à la calibration. La mobilité et la fiabilité opérationnelle de quelques stations ouvrent la voie à des systèmes complètement automatisés. De nouveaux concepts (2 couleurs, haute cadence de répétition, logiciels de traitement, photodiodes en régime Geiger,...) ouvrent le champ à un nouveau progrès des performances (stations millimétriques) et à la possibilité de concevoir des équipements embarqués.

Ce tableau impressionnant des progrès réalisés et à venir, ne doit pas masquer quelques problèmes qui me semblent apparaître :

Le développement de systèmes de positionnement "Tout Temps" comme le système GPS Navstar (D.O.D), du V.L.B.I. va concurrencer sérieusement la télémétrie laser dans ses applications traditionnelles (Géodésie, Geodynamique) et l'application de notre technique à des domaines et objectifs moins additionnels (relativité, altimétrie spatiale laser sur les continents et les glaces, synchronisation horaire de très haute exactitude...) me semble nécessaire pour continuer à exister à moyen ou long terme. La part de plus en plus grande prise par les sessions non techniques (organisation de campagnes) au cours des derniers colloques me semble également dangereuse. Les discussions et les contacts personnels entre techniciens deviennent difficiles, donc rares, tant le programme est chargé. Par ailleurs les organisateurs de campagnes ont déjà à leur disposition un nombre annuel important de réunions spécialisées. Je pense que le temps dédié à l'instrumentation laser tous les deux ou trois ans doit être sauvegardé. Enfin la représentation de plus en plus fréquente de groupes par un seul exposé de "manager" exclu les rapports techniques détaillés qui me semblent le sang de ce type de colloque.

Ces remarques pour personnelles quelles soient et n'entraînant que ma responsabilité me semblent néanmoins refléter la sensibilité d'un nombre non négligeable de participants. Elles peuvent servir à ouvrir une réflexion générale, je serais heureux de connaître la réaction de notre Communauté.

Avant de terminer en souhaitant bonne chance au Nouveau Comité Scientifique d'Organisation, je tiens à remercier tous ceux qui ont aidé à faire de ce colloque une réussite. C'est à dire :

- Les participants sans lesquels nous n'existerions pas,
- les responsables de session dont la tâche ne s'arrête pas à la fin du colloque, puisqu'ils ont collecté les exposés pour les minutes,
- le Comité Local d'Organisation et en particulier Madame F. Baumont sans qui le colloque eut été assez "pagaille",
- le Comité Scientifique d'organisation :  
C.O. Alley, son dynamisme inlassable a apporté beaucoup aux derniers colloques et à la télémétrie laser en général,  
B.A. Greene dont les idées nouvelles et non conformistes ont dynamisées la discipline,  
K. Hamal, pilier infatigable de la physique du laser et hôte à plusieurs reprises de comités d'organisation
- enfin, Madame M. Perrin pour la préparation du tirage des minutes.

Merci à tous et que vive la télémétrie laser.

J. GAIGNEBET

Membre du Comité Scientifique et Responsable du  
Comité Local d'Organisation du VI I.W.L.R.I.

## PREFACE

The Sixth International Workshop On Laser Ranging Instrumentation was held in Antibes Juan-Les-Pins (France) 22-26 September, 1986. A large number of presentations was given as in the previous workshops. The improvements accomplished since the last meeting (Herstmonceux) are spectacular and very promising. The accuracy of the station is still increasing thanks to the technological progress and to a better knowledge of the problems related to calibration. Completely automated systems are foreseen driven by the need for the mobility and operational efficiency of some stations.

We have to be aware of some approaching problems despite the impressive progress of our technique. Development of all weather and accurate positioning networks such as GPS/NAVSTAR (D.O.D.) or the VLBI will present competition to some traditional of laser ranging (Goedesy and Geodynamics). I feel that our technique has to aim towards less conservative goals (relativity, spaceborne altimetry to the ground and ice caps, time synchronization,..) to be able to grow in the medium and long term. I feel a dangerous trend in the increase of the time devoted to the technical sessions. The difficulties in holding adequate discussions and in managing personal contact among those participants interested in improving the experimental techniques of laser ranging have increased as the schedule has become really crowded. Campaign organizers have at their disposal a number of specialized meetings every years for that purpose. I do not think they need to take a substantial part of the time intended for laser ranging instrumentation during the only meeting every two or three years devoted to this topic. Last of all we see more and more managers representing their group with a single presentation. This tendency eliminates detailed technical reports wich are the life blood of such workshop. These personal remarks are on my own responsibility but I feel that they reflect the sensitivity of a non negligible part of the attendees. They may be a starting point for a general discussion and I would be happy to know the reaction of the community.

Prior to ending with my best wishes to the New Scientific Organizing Committee, I want to thank everyone who helped to make a success of this Workshop, that is to say :

- Participants,
- session chairmen and cochairmen for their task during and after the workshop,
- local organizing committee and particularly Mrs. F. Baumont whose work prevented the transformation of the workshop into a happy jumble,
- scientific organizing committee.:
- C.O. Alley whose permanent dynamism was a great support for the organization of the session and laser ranging in general,
- B.A. Greene whose bright new ideas and 'non conformism' have boosted the discipline,
- K. Hamal tireless pillar of the laser physics and host of many organizing committees
- at last but not the least, Mrs. M. Perrin for the preparation of the proceedings.

Thanks to everyone and hurrah for laser ranging.

J. GAIGNEBET  
Member of the Scientific Organizing Committee  
and Chairman of the Local Organizing Committee  
of the 6th I.W.L.R.I.

The 6th International Workshop Laser Ranging Instrumentation  
meeting at Antibes Juan-Les-Pins, France,

RECONGNISING the unique value and complementary nature of joint  
lunar/artificial satellite tracking stations for the determination  
of earth orientation parameters and recognising that new facilities  
of this kind are under development, strongly recommends that due  
attention be given to ensuring the continuation of these measurements  
and their exploitation to the fullest extent.

The 6th International Workshop on Laser Ranging Instrumentation meeting at Antibes Juan-Les-Pins, France,

NOTING that since October 1983 the Royal Greenwich Observatory's laser ranging group has been one of the major contributors to international collaborative programmes related to the dynamics of earth satellites and the surface and body of the earth and

RECOGNISING that the quality and quantity of these observations are comparable with the best achieved elsewhere,

VIEWS with concern the uncertain future of the group and

REQUESTS that all feasible steps be taken to ensure its continued activity in a suitable environment.

The 6th International Workshop on Laser Ranging Instrumentation meeting at Antibes Juan-Les-Pins, France,

RECOGNISING that most institutions creating normal points are conforming now to the Herstmonceux recommendations and recognising the normal point comparison experiment initiated by NASA,

STRONGLY recommends that all institutes performing normal point calculations should create normal points for the October 1983 Lageos test data set and send the results to NASA for detailed intercomparisons which may lead to further refinements and definitions.

The 6th International Workshop on Laser Ranging Instrumentation,  
meeting at Antibes Juan-Les-Pins, France,

· RECOGNIZING the important scientific results being obtained with  
the LAGEOS spacecraft, and recognizing the remarkable improvements in  
ground-based laser ranging technology that have occurred in the last  
decade since the launch of LAGEOS,

strongly endorses

- (1) the plans to develop and launch a second LAGEOS (LAGEOS II)  
in support in geodetic, geodynamics, and technology objectives  
and urges its launch at the earliest possible opportunity.

In addition,

recognizing the unique value of precise laser ranging to satellites  
in increasing our knowledge and understanding of fundamental forces  
of nature , including the "gravito-magnetic force" predicted by  
Einstein's theory of gravity,

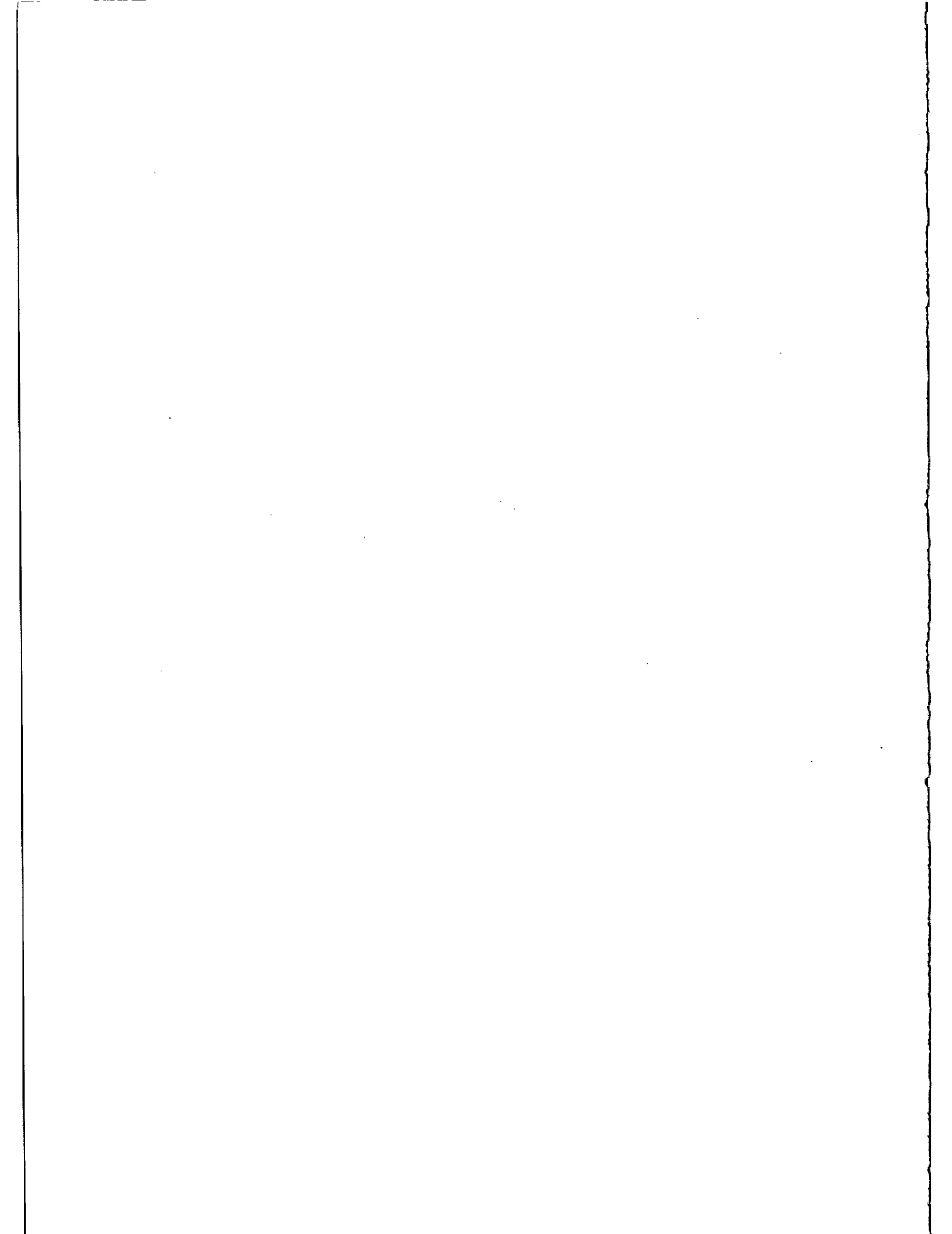
urges strongly

- (2) that a third LAGEOS satellite (LAGEOS III) be constructed and  
launched into an appropriate orbit allowing the detection and  
measurement of the gravito-magnetic orbit precession produced  
by the rotating Earth, as well as increasing our ability to  
monitor Universal Time.



The 6th International Workshop on Laser Ranging Instrumentation  
meeting at Antibes Juan-Les-Pins, France,

· RECOGNISING the significant contributions that Laser Ranging  
systems are making to geodesy, geophysics, geodynamics and other  
disciplines hereby GRATEFULLY ACKNOWLEDGES the dedicated efforts of  
the crews operating these systems for the benefit of the scientific  
community.



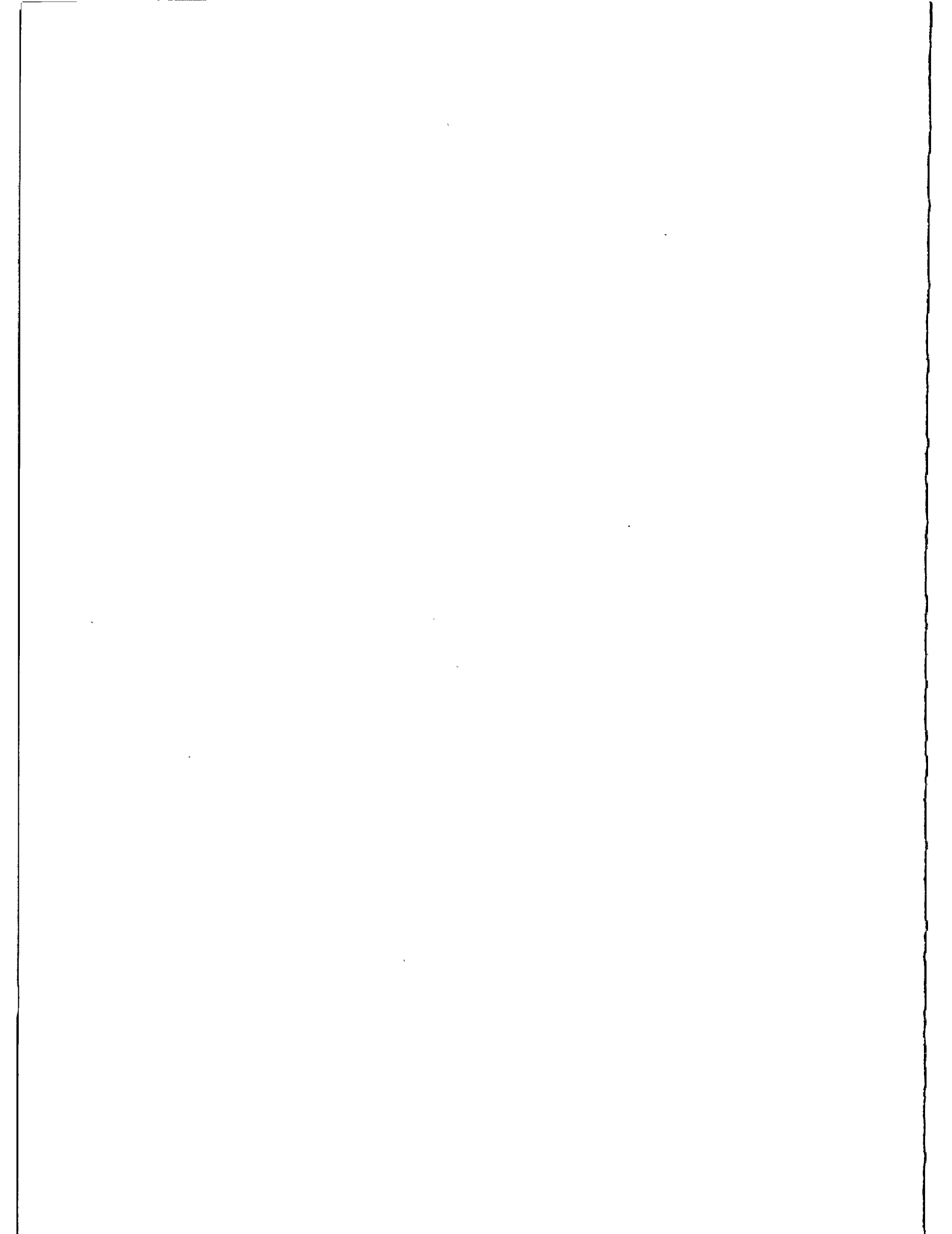
The 6th International Workshop on Laser Ranging Instrumentation meeting at Antibes, France,

NOTING that since October 1983 the Royal Greenwich Observatory's laser ranging group has been one of the major contributors to international collaborative programmes related to the dynamics of earth satellites and the surface and body of the earth and

RECOGNISING that the quality and quantity of these observations are comparable with the best achieved elsewhere,

VIEWS with concern the uncertain future of the group and

REQUESTS that all feasible steps be taken to ensure its continued activity in a suitable environment.



AT ANTIBES JUAN LES PINS ON 22 - 26 SEPTEMBER 1986  
=====

LIST OF PARTICIPANTS  
-----

Prof. C.O. ALLEY  
Dept of Physics & Astronomy  
University of Maryland  
Code def 3  
College Park, MD 20742  
U.S.A.

Tel : (301) 4543405  
Telex : 908787 PHY UN MD CORK

Dr. R. APPLER  
Code 601  
G.S.F.C.  
Greenbelt, MD 20771  
U.S.A.

Tel : (301) 286 8119  
Telex : 257559

Dr. S.G. ALBANESI  
Piano Spatiale Nazionale  
CNR  
Via Regina Margherita, 202  
00198 ROMA  
ITALIE

Tel : 64 76 72 35  
Telex : 616162 CNRTSN

F. BARLIER  
CERGA / GRGS  
Avenue Nicolas Copernic  
06130 GRASSE  
FRANCE

Tel : 93 36 58 49  
Telex : 470865 F.

F. BAUMONT  
CERGA/GRGS  
Avenue Nicolas Copernic  
06130 GRASSE  
FRANCE

Tel : 93 36 58 49  
Telex : 470865 F.

Dr. W. BEEK  
Dept. of Geodesy  
Delft University of Technology  
Observatorium Kootwijk  
Postbus 581  
7300 AN APELDOORN  
PAYS BAS

Tel : 057 69 341  
Telex : 36 442 (SATKO UL)

Prof. B. BERTOTTI  
University of Cambridge  
Institute of Astronomy  
CAMBRIDGE  
ROYAUME UNI

Tel : 382 31 341  
Telex : 817 297 (ASTRON G)

Dr. J. BIANCO  
Piano Spatiale Nazionale  
CNR  
Via Regina Margherita, 202  
00198 ROMA  
ITALIE

Tel : 64 76 72 35  
Telex : 616162 CNRTSN

Mr. BOKOBZA  
QUANTEL  
B.P. 23  
91941 LES ULIS CEDEX  
FRANCE

Tel : (1) 690 76 615  
Telex : 691329

Dr. S.A. BOWMAN  
Physics and Astronomy  
University of Maryland  
College Park, MD 20742  
U.S.A.

Tel : 301 454 3405  
Telex : 908797 PHY UN MD CORK

Dr. J. A. BUISSON  
Naval Research Laboratory (NRL)  
Code 7773  
4555 Overlook Ave S.W  
WASHINGTON, DC 20375  
U.S.A.

Tel : (202) 767 2595  
Telex :

Dr. A. CAPORALI  
Dipartimento di Fisica G. Galilei  
Universita di Padova  
Via Marzolo N 8  
I-35131 PADOVA  
ITALIE

Tel : 49 844 278  
Telex : 43330308 (DFGGPD-I)

Dr. G. CECCHET  
I.N.F.N.  
University of Pavia  
V. Bassi 6  
I-27100 PAVIA  
ITALIE

Tel :  
Telex :

Dr. A. CENCI  
Telespazio, Via Bergamini 50  
ROMA  
ITALIE

Tel : 64 987 254  
Telex : 620424 (TSPZRO I)

Dr. I. CIUFOLINI  
University of Texas  
AUSTIN, TX 78712  
U.S.A.

Tel : (512) 471 5573  
TWX : 910 874 1351

Dr. R. J. COATES  
Code 904  
NASA/G. S. F. C.  
GREENBELT, MD 20771  
U.S.A.

Tel : 301 286 8809  
Telex : 257559

E. CUOT  
CERGA  
Avenue Nicolas Copernic  
06130 GRASSE  
FRANCE

Tel : 93 36 58 49  
Telex : 470 865 F

Dr. P. R. DACHEL  
Bendix Field Engineering Corp.  
1 Bendix Road  
COLUMBIA, MD 21045  
U.S.A.

Tel : 301 964 7189  
Telex : 198120

Dr. P. J. DUNN  
Analytical Services Center,  
Inc. Lanham,  
MARYLAND 20752  
U.S.A.

Tel : 301 731 2044  
Telex : 590613

Dr. R. J. EANES  
Dept. of Aerospace Eng.  
University of Texas  
AUSTIN, TX 78712  
U.S.A.

Tel : (512) 471 4273  
Telex : 7044265 (CSRUTX UD)

Dr. D. R. EDGE  
Bendix Aerospace  
One Bendix Road  
COLUMBIA, MD 21045  
U.S.A.

Tel : (301) 344 5013  
Telex : 197700 (GLTN)

P. EXERTIER  
CERGA/GRGS  
Avenue Nicolas Copernic  
06130 GRASSE  
FRANCE

Tel : 93 36 58 49  
Telex : 470865 F

Dr. A.N. M.FADHL  
Director  
King Abdul Aziz City of Science  
P.O. Box 6086  
RIYADH  
11442 ARABIE SAOUDITE

Tel : 478-8000:580  
Telex : 401590 (KACST SJ)

Dr. FALCONER  
Divison of National Mapping  
P.O. Box 31  
BELCONNEN A.C.T. 2616  
AUSTRALIE

Tel : 61 52 50 95  
Telex : 62 230 (NATMAP)

D. FERAUDY  
CERGA/GRGS  
Avenue Nicolas Copernic  
06130 GRASSE  
France

Tel : 93 36 58 49  
Telex : 470 865 F.

Dr.M. FERMI  
Telespazio SPA  
via Bergamini, 50  
00159 ROMA  
ITALIE

Tel : 64 987 489  
Telex : 620424(TSPZRO I)

Dr. T. FISCHETTI  
2609 Village Lane  
Silver Spring, Md 20906  
U.S.A.

Tel : (301) 871 6272  
Telex : 650 272 86 72 (MCI)

Dr. E. A. FLINN  
Mail Code EEG  
NASA Headquarters  
WASHINGTON DC 20546  
U.S.A.

Tel : (202) 453 1675  
Telex : 89530 (NASA WSH)

Dr. H. FUNG  
Yunnan Observatory  
P.O. Box 110  
KUNMING  
Yunnan Province  
R.P. CHINE

Tel : 72 946  
Telex : 64040 (YUOBS.FN)

J. GAIGNEBET  
CERGA/GRGS  
Avenue Nicolas Copernic  
06130 GRASSE  
FRANCE

Tel : 93 36 58 49  
Telex : 470 865 F.

Dr. B.A. GREENE  
Division of National Mapping  
P.O. Box 31  
BELCONNEN A.C.T. 2616  
AUSTRALIE

Tel : 61 52 5095  
Telex : 62 230 (NATMAP)

P. GRUDLER  
CERGA/GRGS  
Avenue Nicolas Copernic  
06130 GRASSE  
FRANCE

Tel : 93 36 58 49  
Telex : 470 865 F.

Dr. L. GRUNWALTD  
Central Institute for  
Physics of the Earth  
Telegrafenberg A17  
DDR 1500 POTSDAM  
R.D.A

Tel :  
Telex : 15305 (VDEPDM DD)

Mr. F. GUERIN  
Aerospatiale  
100. Boulevard du Midi  
06322 CANNES LA BOCCA Cedex  
FRANCE

Tel : 93 90 00  
Telex : 470 902F (AECAN)

Dr. K. HAMAL  
Faculty of Nuclear Science  
Physical Engineering  
BREHOVA 7  
115 19 PRAGUE 1  
TCHECOSLOVAQUIE

Tel : 284 8840  
Telex : 121254 (FJFI)

J.L. HATAT  
CERGA/GRGS  
Avenue Nicolas Copernic  
06130 GRASSE  
FRANCE

Tel : 93 36 58 49  
Telex : 470 865 F.

Prof. H. FENG  
Deputy Director of Yunnan  
Observatory  
P.O. Box 110  
KUNMING, YUNNAN Province  
R.P. CHINE

Tel : 72 946  
Telex : 64040 (YUOBS CN)

Dr. R. HOPFL  
Satellitenbeobachtungsstation  
Wettzell  
8493 KOETZTING  
R.F.A.

Tel : 09941 / 8643  
Telex : 69 937 (WESAT D)

Dr. B. HYDE  
Alpoptics  
267, Rue du Chateau du Roi  
38220 VIZILLE  
FRANCE

Tel : 76 68 24 05  
Telex :

Mr. P. JAQUET  
Hamamatsu Photonics France  
49-51 Rue de la Vanne  
92120 MONTROUGE  
FRANCE

Tel : 46 55 47 58  
Telex : 631 895

Dr. H. JELINKOVA  
Faculty of Nuclear Science  
Physical Engineering  
BREHOVA 7  
115 19 PRAGUE 1  
TCHECOSLOVAQUIE

Tel : 284 8840  
Telex : 121254 (FJFI)

Dr. H. JUNGINGER  
Satellitenbeobachtungsstation  
Wettzell  
8493 KOETZTING  
R.F.A.

Tel : 09941/8643  
Telex : 69937 (WESAT D)

Mr. M. KASSER  
I.G.N.  
2. Avenue Pasteur  
94160 SAINT MANDE  
FRANCE

Tel : 43 74 12 15  
Telex : 210 551 F.

Dr. W. KIELEK  
Warsaw Radiotechnical Institute  
Faculty of Electronics  
Institute of Radioelectronics  
00-665 NOVOWIEJSKA STR. 15/19  
VARSOVIE POLOGNE

Tel :  
Telex : 813307 (PW PL)

Dr. D. KIRCHNER  
Technische Universitat  
Inffeldgasse 12  
A-8010 GRAZ  
AUTRICHE

Tel : 316 70 61  
Telex : 311221 (TUGRZ A)

DR.G. KIRCHNER  
Observatory of Graz Lustbuehel  
Lustbuehelstrasse 46  
A-8042 GRAZ  
AUTRICHE

Tel : (316) 42 231  
Telex : 311 078 (OBSLG A)



Dr. W. J. KLEPCZYNSKI  
U.S. Naval Observatory  
Washington, D.C.20390  
U.S.A.

Tel : 19 1 (202) 653 15 21  
Telex : 710 822 1970

Dr. P. KLOECKLER  
Astronomisches Institut  
Bern Universitat  
Sidlerstrasse 5  
CH-3012 BERNE  
SUISSE

Tel : 31 65 85 91  
Telex : 32 320 (PHYBE)

Dr. R. KOLENKIEWICZ  
NASA/G. S. F. C.  
Code 621  
GREENBELT, MD 20771  
U.S.A.

Tel : 301 286 5373  
Telex : 710 828 9716

Dr. KORAKITIS  
National Technical University  
9 K. Zographou  
ATHENES 624  
GRECE

Tel : 18131961  
Telex : 215032 (GEO GR)

Dr. S. LABINI  
Piano Spatiale Nazionale  
Via Regina Margherita, 202  
OO198 ROMA  
ITALIE

Tel : 64 76 72 75  
Telex : 616162 (CNRTSN)

J.G. LANGLOIS  
CERGA/GRGS  
Avenue Nicolas Copernic  
06130 GRASSE  
FRANCE

Tel : 93 36 58 49  
Telex : 470 865 F.

M. LAPLANCHE  
CERGA/GRGS  
Avenue Nicolas Copernic  
06130 GRASSE  
FRANCE

Tel : 93 36 58 49  
Telex : 470 865 F.

Dr. J. LATKA  
Space Research Center  
UL Bartycka 18  
00-716 WARSZAWA  
POLOGNE

Tel : 41 00 41  
Telex : 081 56 70 (CBK PL)

Dr. D. LELGEMAN  
Technische Universitat  
Schr. H. 12  
Strasse Des 17 Juni, 135  
1000 BERLIN 12  
R.F.A.

Tel : 30 314 3205  
Telex : 184 262 (TUBLN D)

Prof. S. LESCHIUTA  
Dipartimento Electronica  
Politecnico  
Coso Duca Degli Abruzzi, 24  
10123 TORINO  
ITALIE

Tel : 11 55 67 235  
Telex : 220 646

Dr. H.L. LINDER  
Code 634  
NASA/G.S.F.C.  
GREENBELT MD 20771  
U.S.A.

Tel : (301) 2865373  
Telex : 710 828 9716

J.F. MANGIN  
CERGA/GRGS  
Avenue Nicolas Copernic  
06130 GRASSE  
FRANCE

Tel : 93 36 58 49  
Telex : 470865 F

Mr. J.M. MARTEAU  
QUANTEL  
Avenue de l'Atlantique  
Z.I. Courtaboeuf  
91940 LES ULIS  
FRANCE

Tel : 69 07 66 15  
Telex :

Mr. F. H. MASSMANN  
Deut. Geod. Forschlings Inst.  
Marstallplatz 8  
D8000 MUNCHEN 22  
R.F.A.

Tel : (089) 230 31 217  
Telex : 5213 550 (DGFI D)

Dr. W.E. MATTHEWS  
Royal Greenwich Observatory  
Herstmonceux Castle  
HAILSHAM, EAST SUSSEX  
ROYAUME UNI

Tel : 323 83 31 71  
Telex : 87451

Dr. J.J. MILLER  
Bendix Field Engin. Corp.  
1 Bendix Road  
COLUMBIA, MD 21045 1897  
U.S.A.

Tel : (301) 344 75 30  
Telex : 197700 (GLTN)

Mr. F. MOYA  
B.M.I.  
26 Rue du Petit Fief  
Z.I. La croix blanche  
91700 STE GENEVIEVE DES BOIS  
FRANCE

Tel : 60 16 12 45  
Telex :

O. MULHOLLAND-CALAME  
CERGA/GRGS  
Avenue Nicolas Copernic  
06130 GRASSE  
FRANCE

Tel : 93 36 58 49  
Telex : 470865F

Dr. H. MULLER  
Deut. Geod. Forschlings Inst.  
Marstallplatz 8  
D8000 MUNCHEN 22  
R.F.A.

Tel : (089) 230 31 217  
Telex : 5213 550 (DGFI D)

Dr. Z. NEUMANN  
Observatory Ondrejov  
25165 ONDREJOV  
TCHECOSLOVAQUIE

Tel : 27 245 25  
Telex : 121579 (ASTR C)

Dr. S. NEWHALL  
JPL, 138.208  
4800 Oak Grove DR.  
PASADENA, CA 91109  
U.S.A.

Tel : 818 354 4371  
Telex : 675 429 (JPL COMM PSD)

Dr. A. NOVOTNY  
Faculty of Nuclear Science  
and Physical Engineering  
Brehova 7  
115 19 PRAGUE 1  
TCHECOSLOVAQUIE

Tel : 2 84 88 40  
Telex : 121254 (FJFI)

Dr. K.H. OTTEN  
Delft University of Technology  
P.O. BOX 581  
7300 AN APELDOORN  
PAYS-BAS

Tel :  
Telex :

J. PARIS  
CERGA/GRGS  
Avenue Nicolas Copernic  
06130 GRASSE  
FRANCE

Tel : 93 36 58 49  
Telex : 470865F

Dr. M. PAUNONEN  
Finnish Geodetic Institute  
Ilmalankatu 1A  
00240 HELSINKI  
FINLANDE

Tel : 358 0 26 4994  
Telex : 12 2771 (ROKTA SF)

Dr. M.R. PEARLMAN  
Smithsonian Astrophysical Obs.  
60. Garden St.  
CAMBRIDGE, MASS 02138  
U.S.A.

Tel :  
Telex : 921428 (SATELLITE CAM)

Dr. P. PETRONI  
Lab. CISI  
Via Reggio Emilia, 39  
20090 SEGRATE  
ITALIE

Tel :  
Telex :

F. PIERRON  
CERGA/GRGS  
Avenue Nicolas Copernic  
06130 GRASSE  
FRANCE

Tel : 93 36 58 49  
Telex : 470 865F.

Dr. J.D.H. PILKINGTON  
Royal Greenwich Observatory  
Herstmonceux Castle  
HAILSHAM, EAST SUSSEX BN27 1RP  
ROYAUME UNI

Tel : 323 83 3171  
Telex : 87451

Dr. P. PIZZOLATI  
Lab. CISI  
Via Reggio Emilia, 39  
20090 SEGRATE  
ITALIE

Tel :  
telex :

J. PHAM-VAN  
CERGA/GRGS  
Avenue Nicolas Copernic  
06130 GRASSE  
FRANCE

Tel : 93 36 58 49  
Telex : 470 865 F.

Dr. I. PROCHAZKA  
Faculty of Nuclear Science  
Physical Engineering  
BREHOVA 7  
115 19 PRAGUE 1  
TCHECOSLOVAQUIE

Tel : 284 88 40  
Telex : 121254 (FJFI C)

Prof. S.A. RAMSDEN  
Dept. of Applied Physics  
University of Hull  
HULL HU6 7RX  
ROYAUME UNI

Tel : 482 46 51 24  
Telex : 592530 (UNIHUL G)

Dr. J.D. RAYNER  
Physics Dept.  
University of Maryland  
College Park, MD 20742  
U.S.A.

Tel : 301 454 34 05  
Telex : 908 787 (PHY UN MD CORK)

Dr. G. REICHERT  
Geodetic Institute  
University of Bonn  
Nussallee 17  
D 5300 BONN  
R.F.A.

Tel : 223 33 77 33  
Telex : 88 69693 (PHYBE D)

Dr. T. SCHILTKNECHT  
Astronomisches Institut  
Universitat Bern  
Sidlerstrasse 5  
CH-3012 BERNE  
SUISSE

Tel : 41 65 85 91  
Telex : 32320 (PHYBE)

Dr. W. SCHLUTER  
Institut fur Angewandte Geod.  
(ABT,II DGF I)  
Richard Stauss Allee 11  
D-6000 FRANKFURT AM MAIN 70  
R.F.A.

Tel : 069 63 331  
Telex : 413592

Dr. B.E. SCHUTZ  
Center for Space Research  
University of Texas  
AUSTIN, TX 78712  
U.S.A.

Tel : (512) 471 42 67  
Telex : 704265 (CSRUTX UD)

Mr. B. SERENE  
Centre Spatial de Toulouse  
18. Avenue E. Belin  
31055 TOULOUSE Cedex  
France

Tel : 61 27 35 63  
Telex : 520 862 (ESA TLS F)

Dr. P. SHELUS  
Dept. of Astronomy  
University of Texas  
AUSTIN, TEXAS 787 12  
U.S.A.

Tel : (512) 471 339  
TWX : 910 874 1351

Dr. D. E. SMITH  
Code 621  
NASA/G.S.F.C.  
GREENBELT, MD 20771  
U.S.A.

Tel : (301) 286 85 55  
TWX : 710 828 97 16

Dr. C. A. STEGGERDA  
Physics & Astronomy  
University of Mariland  
College Park, MD 20742  
U.S.A.

Tel : (301) 454 34 05  
Telex : 90 87 87 (PHY UN MD CORK)

Dr. Y. SUZAKI  
Defense Electronic Systeme Dpt.  
Totsuka Works, Hitachi, LTD  
216 Totsuka-Machi, Totsuka-Ku  
YOKOYAMA 244  
JAPAN

Tel :  
Telex : 3823 503 (HITUKA J)

J.M. TORRE  
CERGA/GRGS  
Avenue Nicolas Copernic  
06130 GRASSE  
FRANCE

Tel : 93 36 58 49  
Telex : 470 865 F.

Dr. M. TORRENCE  
EG&G  
5000 Philadelphia Way  
Sweet J  
LANHAM, MD 20706  
U.S.A.

Tel : 301 731 20 44  
Telex :

Dr. M.R. VAN DER KRAAN  
C/O Technisch Physische  
Dients Tno-Th  
Postbus 155  
Stieltjesweg 1  
200 AD DELFT-NL  
PAYS BAS

Tel : 15 78 71 49  
Telex : 38091 (TPDDT NL)

Dr. D.L.F. VAN LOON  
Observatory for Satellite  
Geodesy Kootwijk  
P.O. Box 581  
7300 AN APELDOORN  
PAYS-BAS

Tel : 57 69 341  
Telex : 36442 (SATKO UL)

Dr. T. K. VARGHESE  
Bendix Aerospace  
1 Bendix Road  
COLUMBIA, MD 21045  
U.S.A.

Tel : (301) 345 56 40  
Telex : 197 700 (GLTN GRNBLT UT)

C. VEILLET  
CERGA/GRGS  
Avenue Nicolas Copernic  
06130 GRASSE  
FRANCE

Tel : 93 36 58 49  
Telex : 470 865 F.

Dr. E. VERMAAT  
Delft University of Technology  
P.O. Box 581  
7300 AN APELDOORN  
PAYS BAS

Tel : 57 69 341  
Telex : 36 442 (SATKO NL)

Dr. H. VISSER  
Technisch Physische Dienst Tno-th  
Stielljesweg 1  
Postbus 155  
2600 AD DELFT  
PAYS BAS

Tel : 15 78 72 10  
Telex : 38091 (TPDDT NL)

Mr. P. VOLUER  
Quantel  
B.P. 23  
91941 LES ULIS Cedex  
FRANCE

Tel : (1) 690 76 615  
Telex : 691329

Dr. B. C. WANG  
P.O. Box 110  
KUNMING Yunnan Province  
R.P. CHINE

Tel : 72 946  
Telex : 64 040 (YUOBS.FN)

Dr. M.L. WHITE  
Institute for Astronomy  
University of Hawaii  
P.O. Box 209  
KULA, HI 96790  
U.S.A.

Tel :  
Telex : 723 8459 (UH AST HR)

Dr. J. WIANZ  
MacDonald Observatory  
FT. Davis, TX 79734  
U.S.A.

Tel : (915) 426 36 68  
TWX : 910 874 1351

Dr. P. WILSON  
Institute fur Angewandte  
Geodasie  
Richard Strausse Allee 11  
D-6000 FRANKFURT M70  
R.F.A.

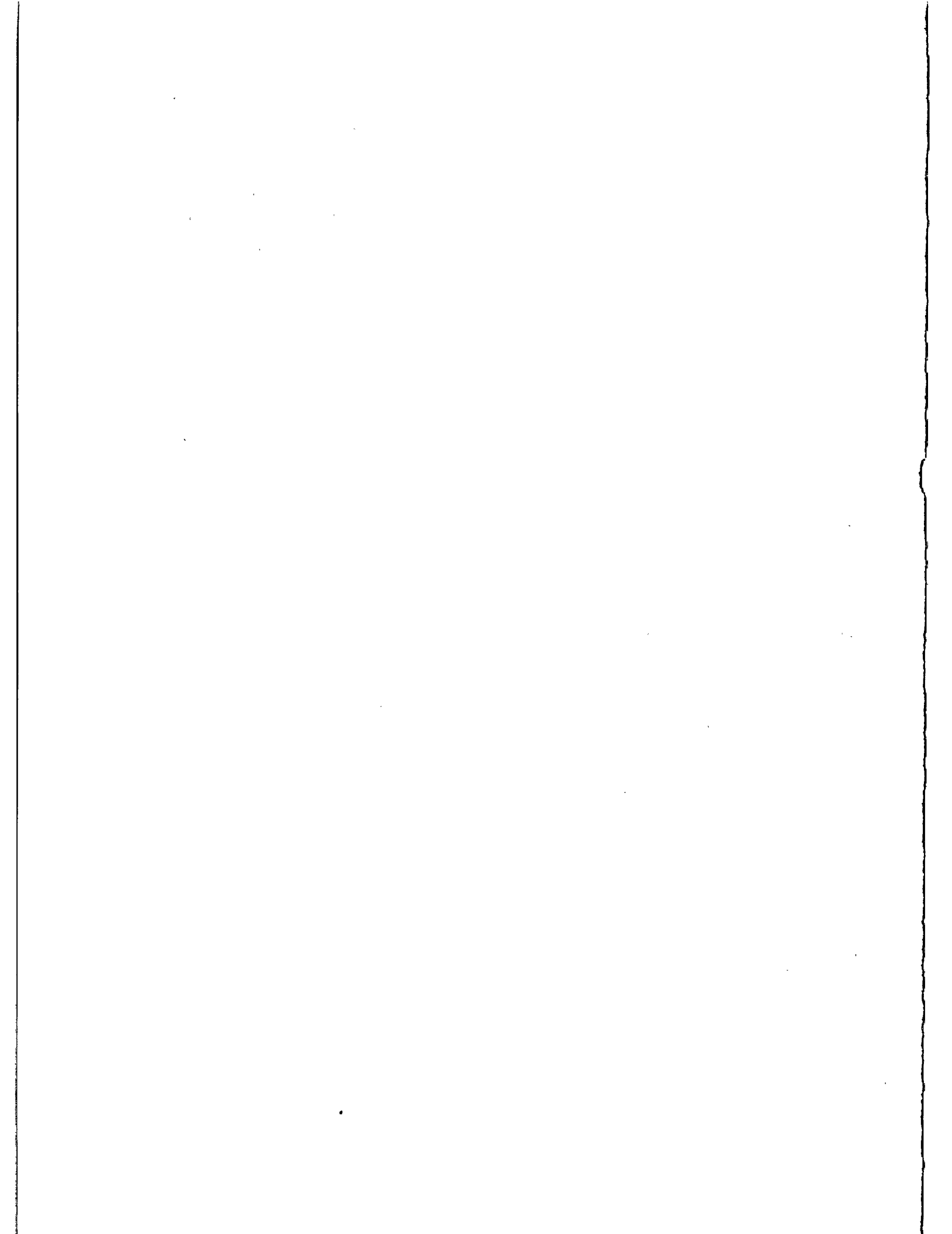
Tel :  
Telex : 413592 (JPA D)

Dr. Z. W. YAO  
Shanghai Observatory  
Academia Sinica  
SHANGHAI  
R.P. CHINE

Tel : 386 191  
Telex : 33164 (SHAO CN)

Dr. YANG  
Shanghai Observatory  
Academia Sinica  
SHANGHAI  
R.P. CHINE

Tel : 386 191  
Telex : 33164 (SHAO CN)



NEW RELATIVISTIC MEASUREMENTS WITH LASER RANGED SATELLITES

I. Ciufolini  
Center for Space Research  
The University of Texas at Austin  
Austin, Texas 78712 - USA -

Telephone (512) 471 5573  
TWX 910874-1351

ABSTRACT

The accuracy of laser ranging associated with the use of a LAGEOS like satellite (inclination supplementary to the existing LAGEOS) allows the measurement of the gravitomagnetic field of the earth.

The proposal of a satellite for this determination is developed here.

# NEW RELATIVISTIC MEASUREMENTS WITH LASER RANGED SATELLITES

Ignazio Ciufolini  
Center for Space Research  
The University of Texas at Austin  
Austin, Texas 78712\*

Telephone (512) 471-5573

The importance of measuring the gravitomagnetic field is comparable to the importance of measuring gravitational waves.

In electrodynamics the wave equation describing electromagnetic waves in vacuum is, in the Lorentz gauge:

$$\square A^\alpha = 0 \quad (1)$$

where  $\square = \eta^{\alpha\beta} \frac{\partial^2}{\partial x^\alpha \partial x^\beta}$  and  $A^\alpha$  is the 4-vector potential.

Similarly in General Relativity <sup>(1), (2), (3)</sup> in the weak field limit, the wave equation describing gravitational waves in vacuum is:

$$\square h_{\alpha\beta} = 0 \quad (2)$$

where  $\square = g^{\alpha\beta} \frac{\partial^2}{\partial x^\alpha \partial x^\beta}$  is the D'Alambertian operator in curved spacetime and in the weak field limit:  $h_{\alpha\beta} \approx g_{\alpha\beta} - \eta_{\alpha\beta}$  ( $g_{\alpha\beta}$  is the spacetime metric tensor and  $\eta_{\alpha\beta}$  is the Minkowski metric tensor).

A similar analogy is valid for the gravitomagnetic field.

In electrodynamics the equation of motion of a particle with mass  $m$  and charge  $q$  subjected to an electric field  $\vec{E}$  and a magnetic field  $\vec{B}$  is the Lorentz equation:

$$m \frac{d^2 \vec{x}}{dt^2} = q (\vec{E} + \vec{v} \times \vec{B}) \quad (3)$$

The torque acting on a test magnet with magnetic dipole moment  $\vec{\mu}$  is  $\vec{\tau} = \vec{\mu} \times \vec{B}$  and the force on the magnetic dipole is  $\vec{F} = (\vec{\mu} \cdot \nabla) \vec{B}$  where  $\vec{B} = \nabla \times \vec{A}$  and for a source with magnetic moment  $\vec{m}$ :  $\vec{B} = \frac{3\vec{n}(\vec{n} \cdot \vec{m}) - \vec{m}}{|\vec{x}|^3}$  and  $\vec{A} = \frac{\vec{m} \times \vec{x}}{|\vec{x}|^3}$ .

Similarly in General Relativity <sup>(4), (5)</sup> the equation of motion of a test particle in the field of a central body with mass  $M$  and angular momentum  $\vec{J}$ , can be written in the weak field and slow motion

\* Supported by Grant NAS 5-28192



limit:

$$m \frac{d^2 \vec{x}}{dt^2} = m(\vec{g} + \frac{d\vec{x}}{dt} \times \vec{H}) \quad (4)$$

where  $\vec{g} \equiv -\frac{M}{r^2} \hat{r}$  is the standard, radial Newtonian acceleration,  $\vec{H}$  is the gravitomagnetic field given in this limit by  $\vec{H} \equiv \nabla \times \vec{\beta} \equiv 2 \left[ \frac{\vec{J} - 3(\vec{J} \cdot \hat{r})\hat{r}}{r^3} \right]$  and  $\vec{\beta}$  is the gravitomagnetic or Lense-Thirring potential  $\vec{\beta} = (\beta^r, \beta^\theta, \beta^\phi) = \left[ 0, 0, -\frac{2J}{r^3} \right]$ , in geometrized units:  $G \equiv c \equiv 1$ . Furthermore in General Relativity <sup>(4), (5)</sup> the torque acting on a gyroscope with spin angular momentum  $\vec{s}$  is in the weak field and slow motion approximation:

$$\vec{\tau} = \frac{d\vec{s}}{dt} = \frac{1}{2} \vec{s} \times \vec{H} \quad (5)$$

and therefore the gyroscope precesses with respect to an asymptotic inertial frame, defined by the distant stars, with angular velocity:

$$\vec{\Omega} = -\frac{1}{2} \vec{H} = \frac{-\vec{J} - 3(\vec{J} \cdot \hat{r})\hat{r}}{r^3} \quad (6)$$

This phenomenon is the "dragging of gyroscopes" or "dragging of inertial frames" of which the gyroscopes define the axes. The force exerted on the gyroscope by the gravitomagnetic field  $\vec{H}$  is

$$\vec{F} = \left( \frac{1}{2} \vec{s} \cdot \nabla \right) \vec{H} \quad (7)$$

Finally, due to the second term in the force (4), the orbital plane (and the orbital angular momentum) of a test particle - which can be thought as an enormous gyroscope - is dragged in the sense of rotation of the central body. This dragging of the whole orbital plane is described by the formula for the rate of change of the longitude of the node discovered by Lense and Thirring in 1918 <sup>(6), (7)</sup>:

$$\Omega^{\text{Lense-Thirring}} = \frac{2J}{a^3(1-e^2)^{3/2}} \quad (8)$$

where  $a$  is the satellite semimajor axis,  $e$  the eccentricity and  $J$  the angular momentum of the central body.

Many experiments have been proposed to measure the gravitomagnetic field: Everitt - 1974 and Lipa, Fairbank and Everitt - 1974; Van Patten and Everitt - 1976; Braginski, Caves and Thorne - 1977; Scully - 1979; Braginski and Polnarev - 1980; Braginski, Polnarev and Thorne - 1984. In particular the experiment of Lipa, Fairbank and Everitt <sup>(8)</sup> will try to measure the gravitomagnetic precession (6) of a gyroscope orbiting the Earth.

We propose here a different experiment based on the Lense-Thirring effect (8). The idea <sup>(9), (10), (11), (12)</sup> is to measure the gravitomagnetic nodal precession (8) due to the angular momentum of the Earth on laser ranged satellites like LAGEOS <sup>(13), (14)</sup>. The Lense-Thirring precession (8) is for LAGEOS  $\Omega^{\text{Lense-Thirring}} \approx 31$  milliarcsec/year. The total nodal precession is <sup>(14)</sup> for LAGEOS  $\Omega^{\text{total}} \approx 126^\circ$  and can be measured <sup>(15)</sup> with laser ranging with an accuracy of 1 or 2 milliarcsec/year. Therefore, if all the classical perturbations on LAGEOS were known, it would be possible to measure  $\Omega^{\text{LT}}$  with a few percent accuracy. The deviations of the Earth gravity field from

spherical symmetry - quadrupole and higher mass moments of the Earth - are responsible for the most part of the total nodal precession<sup>(16)</sup>. Even though the Earth's multiple mass moments are very well known<sup>(17), (18)</sup>, they are unfortunately not known at the level of accuracy to measure the Lense-Thirring precession. The uncertainty in the even zonal harmonic coefficients  $J_{2n}$  relative to  $J_2$  is<sup>(17)</sup>,

<sup>(18)</sup> of the order of  $\frac{\delta J_{2n}}{J_2} \approx 10^{-6}$ , which uncertainty corresponds for  $J_2$  to an uncertainty in the nodal precession of  $\pm 450$  milliarcsec/year, much larger than the Lense-Thirring precession (8).

The idea<sup>(9), (10), (11), (12)</sup> is to launch a tandem laser ranged satellite "LAGEOS-X" with the same orbital parameters of LAGEOS apart from a supplementary inclination i.e.  $I_{\text{LAGEOS-X}} \approx 70^\circ$  ( $I_{\text{LAGEOS}} \approx 110^\circ$ ). In such a way the classical precession will be equal and opposite for the two satellites; in fact this classical precession is proportional to the cosine of the inclination  $I$  and is a function of even trigonometric functions of  $I$ <sup>(16)</sup>. On the contrary, the Lense-Thirring precession will be the same in both magnitude and sign, thus allowing<sup>(9), (10), (11), (12)</sup> the extraction of the general relativistic drag.

In other words, the two tandem satellites define a "gyroscope".

The bisector of the angle between the nodal lines of the two satellites is not affected by the Earth's multipole mass moments but only by the Lense-Thirring drag and by other small calculable classical precessions<sup>(12)</sup>. Since the precession of the nodal lines of the two satellites, due to the Earth's multiple moments, is equal and opposite, the precession of the bisector between the two nodal lines is zero, apart for other small classical precessions<sup>(12)</sup>.

We studied<sup>(12)</sup> several non-gravitational nodal perturbations.

The result<sup>(12)</sup> is that the error in the calculated value of the secular nodal precession or the value of the secular nodal precession itself is for each perturbation less than 1% of the Lense-Thirring drag, we list some of the dominant perturbations.

**Direct solar radiation pressure:**

The rate of change of the nodal longitude  $\Omega$ , due to an external force  $\vec{f}$ , can be written<sup>(16)</sup>:

$$\frac{d\Omega}{dt} = \frac{1}{na \sin I} (1-e^2)^{-1/2} f W \frac{r}{a} \sin(\nu + \omega) \quad (9)$$

where  $n$  is the mean motion,  $a$  the semimajor axis,  $I$  the inclination,  $e$  the eccentricity,  $r$  the radial coordinate,  $\omega$  the argument of the pericenter,  $\nu$  the mean anomaly,  $f$  is the magnitude of the external force per unit satellite mass and  $W$  is the direction cosine of the force  $\vec{f}$  along the normal to the orbital plane, which can be written<sup>(19), (20), (21)</sup>:

$$W = \sin I \cos^2 \frac{\epsilon}{2} \sin(\lambda_0 - \Omega) - \sin I \sin^2 \frac{\epsilon}{2} \sin(\lambda_0 + \Omega) - \cos I \sin \epsilon \sin \lambda_0 \quad (10)$$

where  $\epsilon$  is the obliquity of the ecliptic and  $\lambda_0$  is the ecliptic longitude of the Sun.

The acceleration  $f_\odot$  due to direct solar radiation pressure on a spherical satellite like LAGEOS, can be written<sup>(20), (21)</sup>:

$$f_\odot = s \frac{A}{m} P \left[ \frac{a_0}{r_0} \right]^2 \quad (11)$$

where  $s$  is a number between 0 and 2, depending on the reflection properties of the satellite surface,  $\frac{A}{m}$  is the satellite cross-sectional area to mass ratio and  $P \equiv \frac{\phi}{c} = \frac{\text{solar constant}}{\text{speed of light}} \approx 4.65 \times 10^{-5} \text{ dyn} \times \text{cm}^{-2}$

is the solar radiation pressure at the Earth when the geocentric distance  $r_0$  is equal to its mean distance  $a_0$ .

Integrating equations (9) and (10) with the proper initial conditions <sup>(15)</sup>, we found <sup>(12)</sup> that over one orbital period  $P = 3.758h$ :

$$\dot{\Omega}^{\text{Direct radiation pressure}}|_P \approx 10^{-1} \dot{\Omega}^{\text{Lense-Thirring}}|_P \quad (12)$$

Since <sup>(15)</sup> the uncertainty in the value of  $f_0$  is for LAGEOS less than 1%, the error in the calculated nodal precession due to direct solar radiation pressure is over one orbital period  $P$ :

$$\text{Error} \left[ \dot{\Omega}^{\text{Direct radiation pressure}}|_P \right] \lesssim 10^{-3} \dot{\Omega}^{\text{Lense-Thirring}}|_P \quad (13)$$

#### Earth's albedo:

On the basis of works of Lautmann <sup>(22), (23)</sup> and Bender <sup>(24), (25)</sup> and due to the periodicity in the sign of  $W$ , we found that the secular nodal precession due to the Earth's albedo is over one year:

$$\dot{\Omega}^{\text{Albedo}}|_{1y} \lesssim 10^{-1} \dot{\Omega}^{\text{Lense-Thirring}}|_{1y} \quad (14)$$

Assuming a 10% error in the model <sup>(22), (23)</sup> we have:

$$\text{Error} \left[ \dot{\Omega}^{\text{Albedo}}|_{1y} \right] \lesssim 10^{-2} \dot{\Omega}^{\text{Lense-Thirring}}|_{1y} \quad (15)$$

#### Satellite eclipses by the Earth:

Because of the change of sign of  $W$ , when the Sun is in opposite regions with respect to the satellite orbital plane, we have that the secular nodal precession due to satellite's eclipses is small over one year <sup>(12)</sup>:

$$\dot{\Omega}^{\text{Eclipses}}|_{1y} \lesssim 10^{-1} \dot{\Omega}^{\text{Lense-Thirring}}|_{1y} \quad (16)$$

Assuming <sup>(15), (26)</sup> an uncertainty of  $10^{-2}$  radians in the determination of the boundary of the shadow's region and an uncertainty <sup>(15)</sup> in  $f_0$  of less than 1%, we have that the error in the calculated secular nodal precession due to satellite's eclipses by the Earth, is over one year:

$$\text{Error} \left[ \dot{\Omega}^{\text{Eclipses}}|_{1y} \right] \lesssim 10^{-3} \dot{\Omega}^{\text{Lense-Thirring}}|_{1y} \quad (17)$$

#### Neutral and charged particles drag:

The neutral particle drag force on a satellite can be written <sup>(16), (27)</sup>:

$$F = \frac{C_D}{2} A \rho v^2 \quad (18)$$

where  $C_D$  = drag coefficient,  $\rho$  is the density of the atmosphere and  $v$  is the velocity of the satellite relative to the atmosphere.

Even with the extreme hypothesis that the atmosphere is corotating with the Earth at the LAGEOS altitude - 12,270 km - and with the hypothesis that the total drag on LAGEOS - neutral plus charged particles - is <sup>(26), (27)</sup> of the order of  $2.3 \times 10^{-10} \text{ cm/sec}^2$  ( $\approx 6$  times the neutral drag (18)), we find <sup>(12), (25)</sup> that the secular nodal precession due to atmospheric drag is:

$$\dot{\Omega}^{\text{Total drag}} \lesssim 10^{-2} \dot{\Omega}^{\text{Lense-Thirring}} \quad (19)$$

### Anisotropic thermal radiation:

Due to the finite heat conductivity of the body, there is an anisotropic distribution of temperature on the satellite <sup>(26)</sup> and therefore an anisotropic flux of radiation causing its acceleration. Over one period  $P$ , the corresponding secular nodal precession is <sup>(7)</sup>:

$$\dot{\Omega}^{\Delta T} | P \lesssim 1.3 \times 10^{-3} \dot{\Omega}^{\text{Lense-Thirring}} | P \quad (20)$$

### Satellite albedo:

Due to the anisotropic temperature distribution on LAGEOS, there is an anisotropic flux of reflected radiant energy from the satellite. The corresponding secular nodal precession is <sup>(12)</sup>:

$$\dot{\Omega}^{\text{Albedo}} | P \lesssim 6.6 \times 10^{-4} \dot{\Omega}^{\text{Lense-Thirring}} | P \quad (21)$$

### Poynting-Robertson effect:

Because of the relative velocity between LAGEOS and the Sun there are <sup>(28), (29)</sup> small corrections, of the order of  $v$ , to the formula (11); over one period  $P$ , we have <sup>(12)</sup>:

$$\dot{\Omega}^{\text{Poynting-Robertson}} | P \lesssim 7.2 \times 10^{-7} \dot{\Omega}^{\text{Lense-Thirring}} | P \quad (22)$$

### Infrared radiation:

The Earth's infrared radiation contribution to the nodal precession was studied by Sehnal-81 <sup>(30)</sup>. From his work we find that:

$$\dot{\Omega}^{\text{Infrared-radiation}} |_{1 \text{ day}} \approx \dot{\Omega}^{\text{Lense-Thirring}} |_{1 \text{ day}} \quad (23)$$

and assuming an error of less than 10% in the model we have:

$$\text{Error} \left[ \dot{\Omega}^{\text{Infrared radiation}} |_{1 \text{ day}} \right] \lesssim 10^{-1} \dot{\Omega}^{\text{Lense-Thirring}} |_{1 \text{ day}} \quad (24)$$

However, the infrared radiation is mainly described by zonal terms of zero and second degree, that is the flux of infrared radiation has <sup>(30)</sup> a latitudinal dependence:

$$\sigma = A_0 + A_2 P_2(\sin\phi) \quad (25)$$

therefore, for the particular configuration LAGEOS plus LAGEOS X, we have:

$$\dot{\Omega}_{\text{LAGEOS}}^{\text{Infrared radiation}} \approx -\dot{\Omega}_{\text{LAGEOS X}}^{\text{Infrared radiation}} \quad (26)$$

and consequently a null contribution from the Earth's infrared radiation to the uncertainty in the measurement of the Lense-Thirring drag.

### Solar wind:

With a calculation similar to the atmospheric drag, for the neutral and charged solar wind <sup>(31)</sup> drag, we have <sup>(12)</sup>:

$$\dot{\Omega}^{\text{Solar wind}} | P \lesssim 2.1 \times 10^{-3} \dot{\Omega}^{\text{Lense-Thirring}} | P \quad (27)$$

### Drag from interplanetary dust:

With a similar calculation, we have <sup>(12)</sup>:

$$\dot{\Omega}^{\text{Cosmic dust}}|_P \lesssim 1.8 \times 10^{-3} \dot{\Omega}^{\text{Lense-Thirring}}|_P \quad (28)$$

#### Earth's magnetic field:

Assuming <sup>(27)</sup> a LAGEOS total surface charge  $q_L \approx 3.3 \times 10^{-11}$  C, we have:

$$\dot{\Omega}^{\text{B e}}|_P \lesssim 1.6 \times 10^{-4} \dot{\Omega}^{\text{Lense-Thirring}}|_P \quad (29)$$

In conclusion, formulae (13), (15), (17), (19), (20), (21), (22), (26), (27), (28), (29) show that each non-gravitational perturbation contributes to the secular rate of nodal precession of LAGEOS less than 1% of the Lense-Thirring drag, or can be calculated to an accuracy better than 1% of the Lense-Thirring precession.

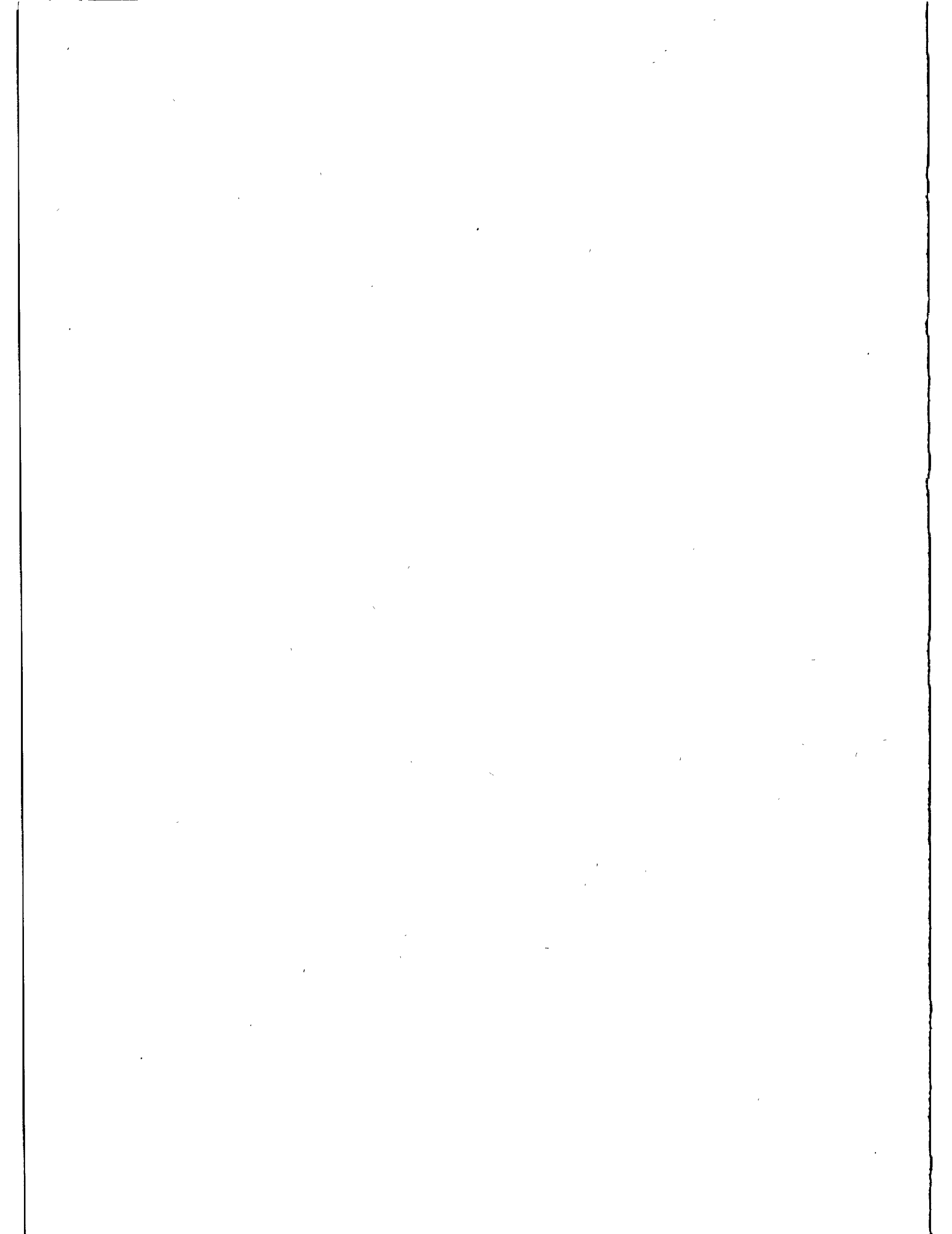
Concerning the earth's tides, due to the periodicity of the Earth's tides, the measurement of the total nodal precession should be taken over a period of a few years, over such a period of time the corresponding uncertainty should be of a few milliarcsec <sup>(15), (32)</sup>. We must also consider the accuracy of our knowledge of the orbital parameters. For the special configuration LAGEOS plus LAGEOS X with supplementary inclinations, the error in the measurement of  $\Omega^{LT}$  due to errors in the determination of the inclination, including polar motion determination errors, should be <sup>(15), (32)</sup> of a few milliarcsec when averaged over a period of a few years. Finally we observe that to have less than 3% individual contribution to the experimental uncertainty - with the hypothesis of improvements in the uncertainties  $\frac{\delta J_{2n}}{J_2}$  to  $3 \times 10^{-7}$  - the differences between the orbital parameters of two satellites should be:  $a_e = (a_x - a_l) \lesssim \pm 16$  km,  $I_e = (I_x - I_l) \lesssim \pm 0.13^\circ$ , and  $e_e = (e_x - e_l) \lesssim \pm 0.04$ .

I thank C. Alley, P. Bender, B. Bertotti, R. Eanes, P. Farinella, R. Matzner, W. Miller, J. Ries, D. Rubincam, B. Schutz, D. Smith, B. Tapley, K. Thorne, H. Yilmaz and J. A. Wheeler for helpful discussions.

## REFERENCES

1. C. W. Misner, K. S. Thorne and J. A. Wheeler, Gravitation (Freeman, San Francisco, 1973).
2. S. Weinberg, Gravitation and Cosmology: Principles and Applications of the General Theory of Relativity (Wiley, New York, 1972).
3. J. Weber, General Relativity and Gravitational Waves (Wiley-Interscience, New York, 1961).
4. K. S. Thorne, Rev. Mod. Phys. 52, 299 (1980).
5. K. S. Thorne, R. H. Price, and D. A. Macdonald, eds., Black Holes, the Membrane Paradigm (Yale University Press, New Haven and London, 1986), p. 72.
6. J. Lense and H. Thirring, Phys. Z. 19, 156 (1918), english translation by:
7. B. Mashhoon et al., Gen. Relativ. Gravit. 16, 711 (1984).
8. J. A. Lipa, W. M. Fairbank, and C. W. F. Everitt, in: Experimental Gravitation, B. Bertotti, ed. (Academic Press, New York, 1974), p. 361.
9. I. Ciufolini, Bull. Am. Phys. Soc., Cleveland, Ohio, October 1984, 6, 1169 (1985).
10. I. Ciufolini, Phys. Rev. Lett. 56, 278 (1986).
11. I. Ciufolini, Found. of Phys. 16, 259 (1986).
12. I. Ciufolini, to be published in Celestial Mechanics.
13. D. E. Smith and P. J. Dunn, J. Geophys. Res. Lett. 7, 437 (1980).
14. C. F. Yoder, J. G. Williams, J. O. Dickey, B. E. Schutz, R. J. Eanes, and B. D. Tapley, Nature 303, 757 (1983).
15. B. D. Tapley, B. E. Schutz and R. J. Eanes, private communication (1984).
16. W. M. Kaula, Theory of Satellite Geodesy (Blaisdell, Waltham, 1966).
17. F. J. Lerch et al., J. Geophys. Res., A84, 3879 (1979).
18. F. J. Lerch et al., J. Geophys. Res., 90, 9312 (1985).
19. Y. Kozai, Smithsonian Astrophys. Obs. Spec. Rep. No. 56.
20. K. Aksnes, Cel. Mech., 13, 89 (1976).
21. L. Anselmo, B. Bertotti et al., Cel. Mech., 29, 27 (1983).
22. D. A. Lautmann, Cel. Mech., 15, 387 (1977).
23. D. A. Lautmann, Cel. Mech., 16, 3 (1977).
24. P. Bender in The Use of Satellites for Geodesy and Geodynamics Volume II; Proceedings of the Second International Symposium on the use of Artificial Satellites for Geodesy and Geodynamics, G. Veisard and E. Livieratos editors, National Technical University of Athens (1979), p. 145.
25. P. Bender, private communication.
26. F. Barlier et al., to be published in Cel. Mech.
27. D. P. Rubincam, Cel. Mech., 26, 361 (1982).

28. H. P. Robertson, Mon. Not. Roy. Astron. Soc. 97, 423 (1937).
29. R. R. Allan, Planet. Space Sci. 15, 53 (1967).
30. L. Sehnal, Cel. Mech. 25, 169 (1981).
31. V. M. Blanco and S. W. McCuskey, Basic Physics of the Solar System, Addison-Wesley, Reading, Mass., USA (1961).
32. I. Ciufolini, paper in preparation.





## COMPARISON OF LAGEOS SATELLITE LASER RANGING NORMAL POINTS

R. Kolenkiewicz  
NASA Goddard Space Flight Center  
Greenbelt, Maryland

P.J. Dunn  
EG & G Washington Analytical Services Center, Inc.  
Lanham, Maryland

R.J. Eanes  
Center for Space Research  
University of Texas at Austin

R. Johnson  
Bendix Field Engineering Corp.  
Columbia, Maryland

### ABSTRACT

The high repetition rates of currently deployed satellite laser ranging instruments allow the data to be compressed into normal points which will contain the essential characteristics of the original data. The generation of normal points is desirable in that it reduces both the computer storage space and time necessary for the analyses of these data to obtain the final end product of geophysical parameters. Several groups have been generating the LAsER GEODynamics Satellite (LAGEOS) normal points, and the resulting points can be evaluated by subjecting them, and the full rate data from which they come, to a common geodetic test. For this evaluation the raw full rate laser measurements were comprised of an edited set of LAGEOS observations taken by 20 laser stations, located worldwide, and collected in October 1983. The noise level of the 206,000 range measurement residuals varied between 1 and 20 cm, and when compressed yielded approximately 5800 two-minute normal points. The geodetic test consisted of a data reduction, using the GEODYN computer program, to obtain a simultaneous estimate of the orbit parameters and station positions. In particular, the laser site heights were compared among the four data sets used in each reduction. The overall fit of the normal point residuals to the finally adjusted satellite and station parameters was 8 cm, with individual stations fitting between 5 and 20 cm. The expected standard error in the estimated station heights varied between 1 and 3 cm, and in every case the difference in the estimated heights from each normal point data set fell within this expected range. The conclusion is that starting with the same set of LAGEOS edited data, the algorithms used by the various groups are adequate in producing normal points which are in agreement with each other.

### Normal Point Generation

At the Fifth International Workshop on Laser Ranging Instrumentation at Herstmonceux, England in September 1984 a procedure for generating normal points from full-rate laser ranges was adopted. The steps in the procedure are listed in Table 1, which also indicates at which stage a choice of technique is necessary for its implementation. Even when a particular step is so rigorously defined that no choice is required, alternative algorithms are possible which can improve data concentration or computational efficiency.

The choices of technique at each stage are listed in Table 2, which shows, for example, in step 6 the possibility of starting a bin interval at the first point in the pass instead of at an even UTC time. This alternative allows more information to be concentrated in the first normal point in the pass, but could reduce the total number of points in each pass by one. The median epoch time within the bin interval is simpler to compute than the arithmetic mean suggested in the Herstmonceux standard and is therefore presented as an alternative in step 7.

### Normal Point Test Date

Each of the groups represented by the co-authors of this paper applied their normal point generation technique to a test data set comprising of edited LAGEOS observations collected by the global laser ranging network during the month of October 1983. The quantity of data from each station in the reference set is shown in the second column of Table 3. When the first point acquired within each second was chosen to reduce the normal point computation time, the number of ranges in the third column were obtained. The fourth column of Table 3 gives the number of normal points obtained with the regular UTC bin intervals recommended at Herstmonceux, and the reduced number of observations given by starting the bin interval at the first point in the pass is shown in the last column.

The data set generated by the Bendix group (BEN HER) adheres most closely to the Herstmonceux standard, although the University of Texas normal points were adopted as the base in the tests described here. They differ from the strict convention by the occasional estimate of a linear trend within each two-minute bin interval (choice 7(c) in Table 2). The normal point generation at GSFC (GOD MED) was based on one second samples (choice 1(c) in Table 2) and the choice 7(b) of the median epoch time tag. Another reasonable option (GOD FIRST) employed choice 6(b) for the bin interval. A final coarse data set was generated by simply taking the actual range at the times of the GOD FIRST normal points with no bin correction at all (2 MIN.DATA).

### Normal Point Testing Procedure

Each normal point data set was subjected to a common geodetic test, which corresponds to the standard dynamic technique used by the Goddard Space Flight Center's Geodynamics Branch for laser data analysis. To assess the quality of the observations from each station, the 30-day data arc was reduced adjusting six orbital elements, an along-track orbit

acceleration parameter, a solar radiation coefficient and all components of station position except for three. The latitude and longitude of the Greenbelt station and the latitude of the Hawaii laser were fixed at arbitrary values to stabilize the reference system for the adjustment of earth orientation parameters every 5 days. The characteristics of each of the test data sets were essentially the same and are given in Table 4.

To monitor the differences between the test data sets, all parameters of the orbit, force model and earth orientation were fixed at the same reasonable values and all components of each station were estimated. The differences in millimeters for the height components of each station are tabulated in Table 5. The formal standard deviation for data at the 10cm. noise level (20cm. for station 7181) is also given in Table 5. A key to the station numbers used throughout this analysis is presented in Table 6.

### Test Results

Examination of Table 5 shows that necessary choices in normal point generation make insignificant differences to the results of a properly designed geodetic experiment. Some differences are detectible in the results from sparse, noisy data such as provided by stations 7181 and 7833. Possible choices of procedure such as sampling the original observations each second, taking the median epoch time and starting the bin interval at the first point in the pass, give acceptable differences in results, which are always within the expected uncertainties. Simply sampling the data every two minutes gave a data set which occasionally yielded results outside the allowable formal error. It should finally be pointed out that editing procedures, which are likely to cause the greatest differences in alternative normal point generation procedures, were not examined in the tests described here.

TABLE 1. NORMAL POINT GENERAL PROCEDURE

- \*\* 1. GENERATE RESIDUALS
- \*\* 2. COARSE EDIT
- \*\* 3. COMPUTE TREND FUNCTION
- \*\* 4. FINE EDIT
- 5. GO TO 3
- \* 6. CHOOSE BIN INTERVAL
- \* 7. COMPUTE MEAN RESIDUAL AND MEAN EPOCH WITHIN BIN
- \*\* 8. LOCATE CLOSEST RANGE TO MEAN EPOCH
- 9. APPLY RESIDUAL BIN CORRECTION
- 10. COMPUTE STATISTICS
- 11. REPORT STATISTICS
- 12. FOLLOW STANDARD FORMAT
- 13. QUICK LOOK CARRY OVER CHECK
- 14. REPORT SCREENED FULL-RATE DATA

\*\*A CHOICE OF TECHNIQUE IS NECESSARY

\* A CHOICE OF TECHNIQUE IS POSSIBLE

## TABLE 2. CHOICES OF TECHNIQUE

### \*\*1. GENERATE RESIDUALS

- a. FIT or FIX 'PREDICTION'
- b. If FIX go to 2
- c. Sample data
- d. Fit ORBIT over arc
- e. Fit FORCE MODEL over some interval
- f. Fit EARTH ORIENTATION over some interval
- g. Fit STATIONS over arc
- h. Fit RB/TB over pass

### \*\*2. COARSE EDIT

- a. Sample data
- b. Choose RMS multiplier per arc
- c. Choose RMS Multiplier per pass

### \*\*3. COMPUTE RESIDUAL TREND FUNCTION

- a. Fit ORBIT over pass
- b. Fit POLYNOMIAL over pass
- c. Fit RB/TB over pass

### \*\*4. FINE EDIT

- a. Choose RMS multiplier per pass

### \*6. CHOOSE BIN INTERVAL

- a. Count from zero hours UTC
- b. Count from first point in pass

### \*7. COMPUTE MEAN RESIDUAL AND MEAN EPOCH

- a. Pick arithmetic MEAN TIME
- b. Pick MID.TIME (MEDIAN)
- c. Fit residual TB/RB as well as MEAN

### \*\*8. LOCATE CLOSEST RANGE

- a. Equidistant TIMES from MEAN (eg: 2 points)
- b. Even number of points for MEDIAN

TABLE 3. 8310 TEST DATA QUANTITY

STATION	TOTAL OBS	SAMPLED ONE SEC.	NORMAL ZERO UTC	NORMAL FIRST POINT
7062	3,800	2,600	108	101
7086	1,800	1,400	66	61
7090	7,200	3,000	40	39
7105	91,500	36,800	507	492
7109	52,900	24,800	343	335
7110	71,600	32,000	521	508
7112	5,500	5,500	220	211
7121	4,500	4,500	175	176
7122	21,400	21,400	313	299
7181	100	100	43	40
7210	13,800	13,800	390	371
7220	51,900	19,800	504	489
7831	16	16	7	6
7833	229	229	79	77
7834	15,000	9,900	252	240
7838	5,100	4,100	204	186
7839	6,400	5,800	271	256
7840	1,600	1,500	241	231
7907	12,300	12,300	1122	1085
7939	<u>6,400</u>	<u>6,400</u>	<u>437</u>	<u>430</u>
TOTAL	373,300	206,100	5843	5633

TABLE 4. 8310 TEST DATA QUALITY

STATION	NORMAL POINTS	BEST NOISE NORMAL PT.	FINAL 30 DAY FIT	BEST NOISE SINGLE SHOT
7062	108	1 cm.	6 cm.	8 cm.
7086	66	2	7	7
7090	40	1	2	2
7105	507	1	7	2
7109	343	1	6	2
7110	521	1	7	4
7112	220	3	9	12
7121	175	2	9	10
7122	313	1	7	7
7181	43	16	22	16
7210	390	1	5	4
7220	504	1	8	7
7831	7	21	21	23
7833	79	10	14	15
7834	252	1	7	7
7838	204	2	11	8
7839	271	1	8	4
7840	241	1	7	4
7907	1122	3	10	13
7939	437	3	<u>13</u>	12
TOTAL			9 cm.	

TABLE 5. DIFFERENCES OF HEIGHT ESTIMATES  
FROM THOSE USING TEST DATA SET

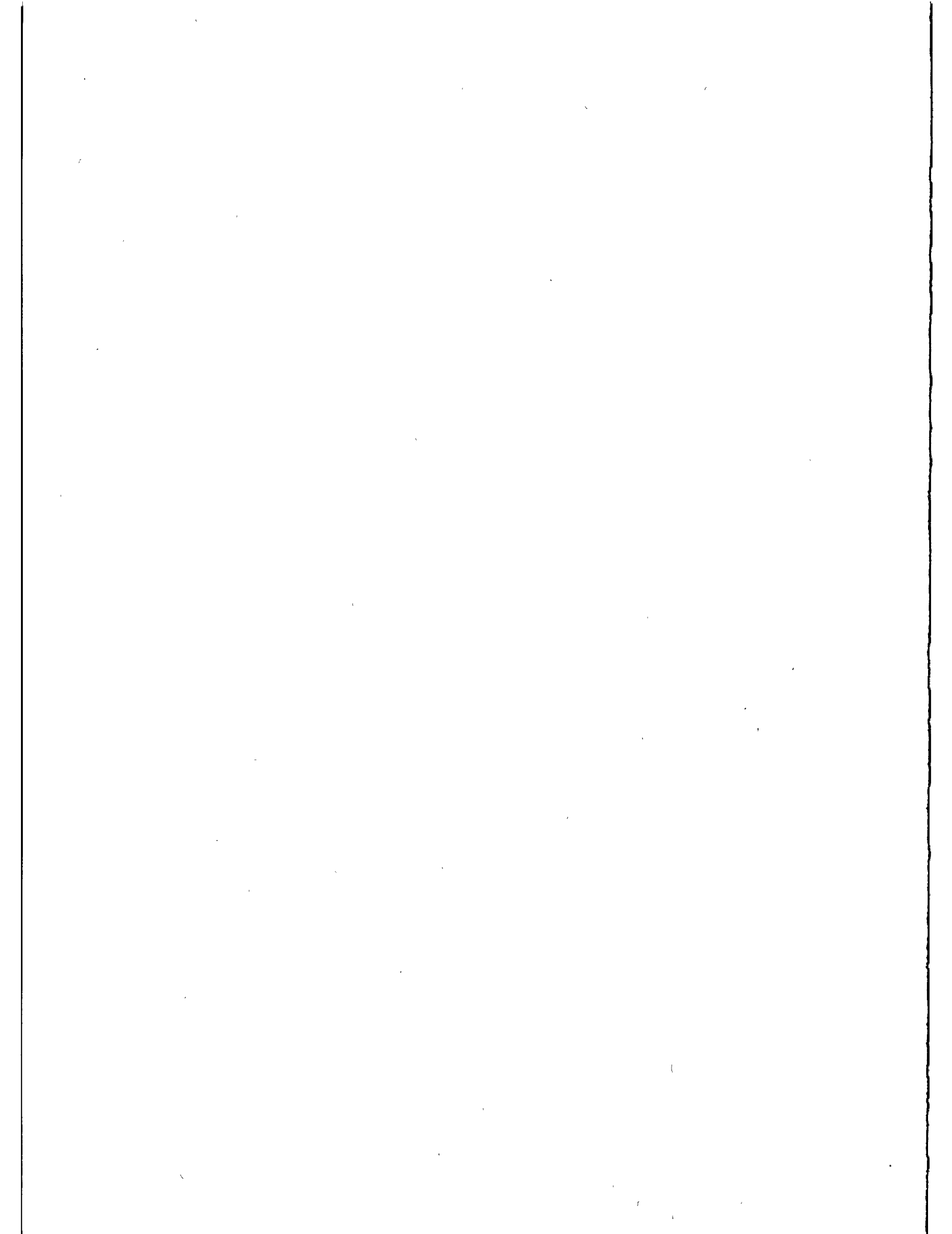
STATION	FORMAL SIGMA	BEN HER	GOD MED	GOD FIRST	2 MIN. DATA	FORMAL SIGMA
7062	14 mm.	0 mm.	0 mm.	-3 mm.	- 6 mm.	14 mm.
7086	21	- 1	-1	-1	.23	21
7090	26	- 1	1	4	6	26
7105	7	- 1	0	-3	1	7
7109	10	0	2	1	- 1	10
7110	7	0	-1	0	1	7
7112	10	1	-1	8	- 8	10
7121	11	0	-1	-9	-11	11
7122	9	- 1	-1	-2	- 7	9
7181	42	-37	-2	21	54	42
7210	8	1	0	4	6	8
7220	7	0	2	7	10	7
7831	∞	-	-	-	-	∞
7833	30	5	7	4	27	30
7834	8	0	-1	1	-10	8
7838	11	- 2	-1	9	13	11
7839	9	0	0	3	1	9
7840	8	0	0	1	3	8
7907	5	1	0	-2	- 5	5

HER: STRICT HERSTMONCEUX  
MED: MEDIAN EPOCH IN BIN  
FIRST: BIN STARTS AT FIRST POINT



TABLE 6. KEY TO STATION NUMBERS

STATION	NO.	OCC.	NAME	LOCATION
7062	12	05	TLRS-2	OTAY MOUNTAIN
7086	24	03	MLRS	MACDONALD OBS.
7090	05	01	MOBLAS-5	YARRAGADEE
7105	07	02	MOBLAS-7	GREENBELT
7109	08	02	MOBLAS-8	QUINCY
7110	04	02	MOBLAS-4	MONUMENT PEAK
7112	02	01	MOBLAS-2	PLATTEVILLE
7121	01	01	MOBLAS-1	HUAHINE
7122	06	01	MOBLAS-6	MAZATLAN
7181	39	01	GRDLAS	POTSDAM
7210	23	01	HOLLAS	HALEAKALA
7220	11	01	TLRS-1	MONUMENT PEAK
7831	46	01	HELLAS	EGYPT
7833	32	01	KOOLAS	KOOTWIJK
7834	30	01	WETLAS	WETZELL
7838	36	01	SHOLAS	SIMOSATO
7839	34	01	AUSLAS	GRAZ
7840	35	01	RGOLAS	RGO
7907	40	01	SAO201	AREQUIPA
7939	41	01	SAO102	MATERA



SUB-CM MULTIPHOTOELECTRON SATELLITE LASER RANGING

T. Varghese, M. Heinick  
Allied Bendix Aerospace  
BFEC, GLTN  
10210 Greenbelt Road Seabrook  
Maryland 20706 - USA -

Telephone (301) 7318916  
Telex 197700 GLTN

ABSTRACT

A satellite laser ranging receiver configuration has been developed and tested to generate sub-cm precision in laser ranging to earth-bound satellites. Multiphotoelectron data taken within the dynamic range of the receiver has shown a standard deviation of 5 mm on ground targets and 7-9 mm on Lageos satellite data residuals. The systematic error from this receive package is measured to be less than 3 mm and is a significant improvement over the previous configuration.

## 1. INTRODUCTION

The projected requirements of the NASA Crustal dynamics program for the 1990s include sub-cm observational accuracy in laser ranging to Lageos. This would be particularly relevant since Lageos-II is projected for deployment in the not so distant future and accuracy enhancement would significantly impact the high volume data period. The precision of Mobile Laser ranging systems (MOBLAS) of the NASA Goddard Laser Tracking Network (GLTN) has been receiver limited above 1cm. To meet the program requirements of increased accuracy and precision, Bendix designed a receiver system based on a Microchannel plate photomultiplier tube (MCP-PMT) and a Tennelec constant fraction discriminator. Prototype testing of this advanced receiver package in the laboratory yielded RMS around 3.5mm over a dynamic range  $\sim 15$ , and during the field tests in November of 1984 the system produced calibration rms of 4.5mm and satellite data RMS of 9-10mm. Further improvements were made to the system which was installed for field operation in April of 1986. This paper describes briefly the device characteristics and performance features of the receiver package in the laboratory, and also sub-cm satellite data results from approximately 1 year operation from Moblas-7.

## 2.0 DEVICE CHARACTERISTICS

The desirable device features for precision opto-electronic detection of low photoelectron are high gain, low electron transit time (and jitter), and low pulse spread. Conventional photomultipliers have a fairly large electron transit time and have an impulse response time of several nanoseconds, and, hence, are not suitable for low photoelectron optical detection with sub-cm precision. The use of a proximity focussed microchannel plate in the pmt instead of conventional electron photomultipliers generates all of the above desirable features. Besides, it has low transit time, large dynamic range, and is well suited for precision laser ranging.

GLTN requirements for satellite ranging include daytime tracking. Although a 10 angstrom spectral filter is used for daytime tracking, the 30 inch telescope still produces a large mean background. The lifetime of the DC biased (normally-ON) device would be considerably reduced if used for daylight tracking due to increased charge accumulation at the anode from high continuous background noise. However, electronic gating of the device would alleviate this problem. We have performed qualitative and quantitative evaluation to examine spatial and temporal ON-voltage uniformity of the tube under gated conditions to determine problems in the mm domain.

Our receiver package consisted of ITT F4129f 3-stage MCP-PMT,

Tennelec TC 454 constant fraction discriminator, a gating module with output of -600 volts, and a delay unit for delayed proportional gating of the discriminator. In laboratory measurements, the system produces 3-4mm rms data over a dynamic range  $\sim 15$  and hence covers 5-60 photoelectrons. This design also accomplishes electron isolation of  $\sim 500$ . The gate is adjustable from 100ns-10us and the time walk is  $\sim 1$ mm within this interval. The discriminator response also is adjusted to have variation of no more than 2mm.

### 3.0 MOBLAS 7 DATA AND DATA PROCESSING

Targets currently used by MOBLAS 7 are the satellites LAGEOS, Starlett, and Ajisai, corner cubes mounted as ground targets at ranges from 75 to 3500 meters, and an internal calibration target.

Raw ranging data from the station contain the round trip time of flight of the laser pulse, the epoch time at which the pulse is transmitted, meteorological data consisting of pressure, temperature, and humidity, and system measurements of transmit and receive energy.

Data processing takes place on two levels, operational data processing and engineering analysis processing. For operational data processing, the rigidly controlled and heavily benchmarked DSG Laser Processor is used to prepare satellite data for release to the scientific community and to provide basic information on data quality. During operational data processing, time of flight measurements are converted to ranges and corrected for system delays, atmospheric refraction, and satellite center of mass. The epoch times of the range measurements are corrected to the times the laser pulses are at the satellite. For MOBLAS 7, a single system delay is applied throughout each pass. A 15 degree polynomial is fit to the ranges in each pass for an analysis of data quality.

Engineering analysis processing utilizes several specialized routines to provide information beyond the scope of the DSG Laser Processor on tracking system characteristics. For the data presented here, a 20 degree polynomial was fit to the time of flight measurements of each pass without corrections. The least squares fitting procedure includes editing of data beyond 3 sigma (standard deviation) from the polynomial and refitting of the remaining data. Editing and refitting cycles are repeated until no improvement in the standard deviation is obtained, or a maximum of 10 iterations is reached. The residuals are then used in several types of analysis plots including those displayed in the text.

#### 4.0 RESULTS

The plots which follow demonstrate the sub-centimeter precision of the MOBLAS-7 ranging system. Fig.1 displays the RMS value of every LAGEOS pass(day and night) and associated combined pre-post pass calibration tracked by MOBLAS-7 during the month of November, 1986. All rms values were taken from the DSG Laser Processor. Of the 30 LAGEOS passes tracked, only two passes have RMS values greater than or equal to 1.00 centimeter(cm). The mean RMS of all 30 passes is 0.866cm, and the mean RMS of the combined calibrations is 0.595cm. A corner cube mounted on a water tower at a range of 3482.547 meters from MOBLAS-7 was the operational calibration target during this time frame. Targets located at distances of 200 meters show data RMS of ~5mm. The larger RMS in calibration on the operational target is a consequence of the target distance, the meteorological variations and the dynamics of the target. Results from four individual passes are illustrated in Fig.2-4 where satellite residuals are displayed using 20 degree polynomial least squares fitting and editing (as described above). These passes include:

DATE	TIME (GMT)	OBSERVATIONS	RMS (CM)
June 18, 1986	01:18	7537	0.79
Nov. 17, 1986	07:19	8546	0.80
Nov. 22, 1986	07:30	8995	0.88
Nov. 25, 1986	06:57	10233	0.89

Satellite range residuals vs. time(minutes) into the pass are shown in Fig.2(a),3 and 4. Two of these plots have polynomial fit errors as can be seen in Fig.2(a) and 3(b) while fig.3(a) and Fig.4 show no such problems.

Two types of Receive Energy Dependence plots illustrate the response of the system over a wide range of receive energies. In Fig.2(a), a scatter plot of satellite residuals vs. relative receive energy is provided. The anomalous accumulation of long residuals just above the value of 1200 is due to a hardware/software limitation(bit error) which reduces the values above 1999 by 1000 units. These very high energy returns represent data around 80-100 photoelectrons and are present only in high elevation passes under very good tracking conditions. Typically, this constitutes less than 5% of the data within a pass and have little impact on overall data.

quality. Fig.2(c),3(c-d)& 4 display the mean and rms of all residuals within 20 standard deviations of the polynomial with a bin resolution of 20 units of relative receive energy. The slight increase in the variation of the mean and larger RMS values at the higher receive energies are due, in part, to the small number of data occurring within each receive energy interval.

#### 5.0 SUMMARY

We have shown for the first time the possibility of obtaining consistent ranging precision of sub-cm on Lageos. The proven dynamic range in this design is particularly relevant considering the transmitted power level and the telescope aperture. The Goddard Laser Tracking Network is presently undergoing the necessary hardware upgrade to meet sub-cm satellite laser ranging goal of NASA Crustal Dynamics program.

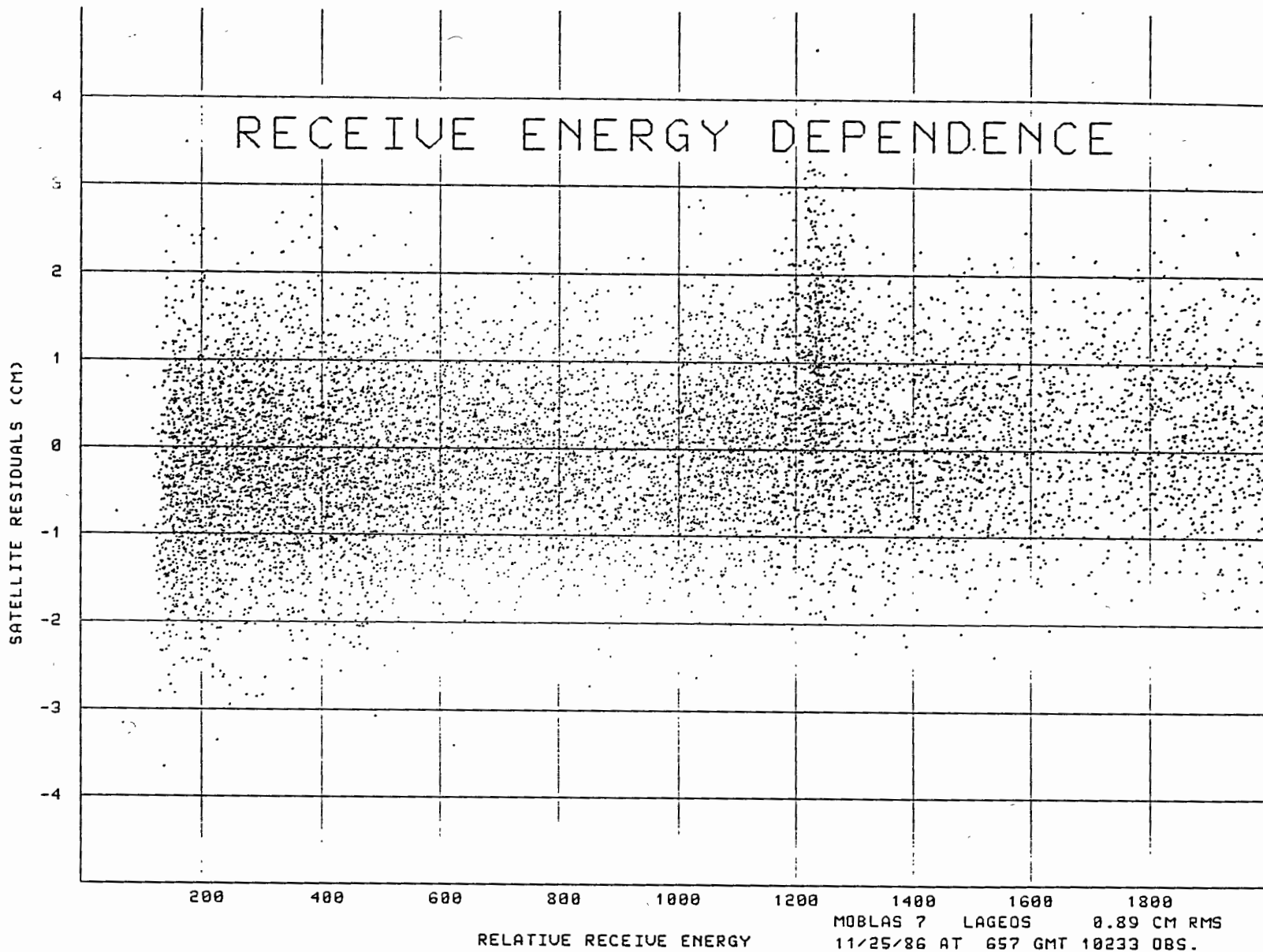


FIG. 2(B)



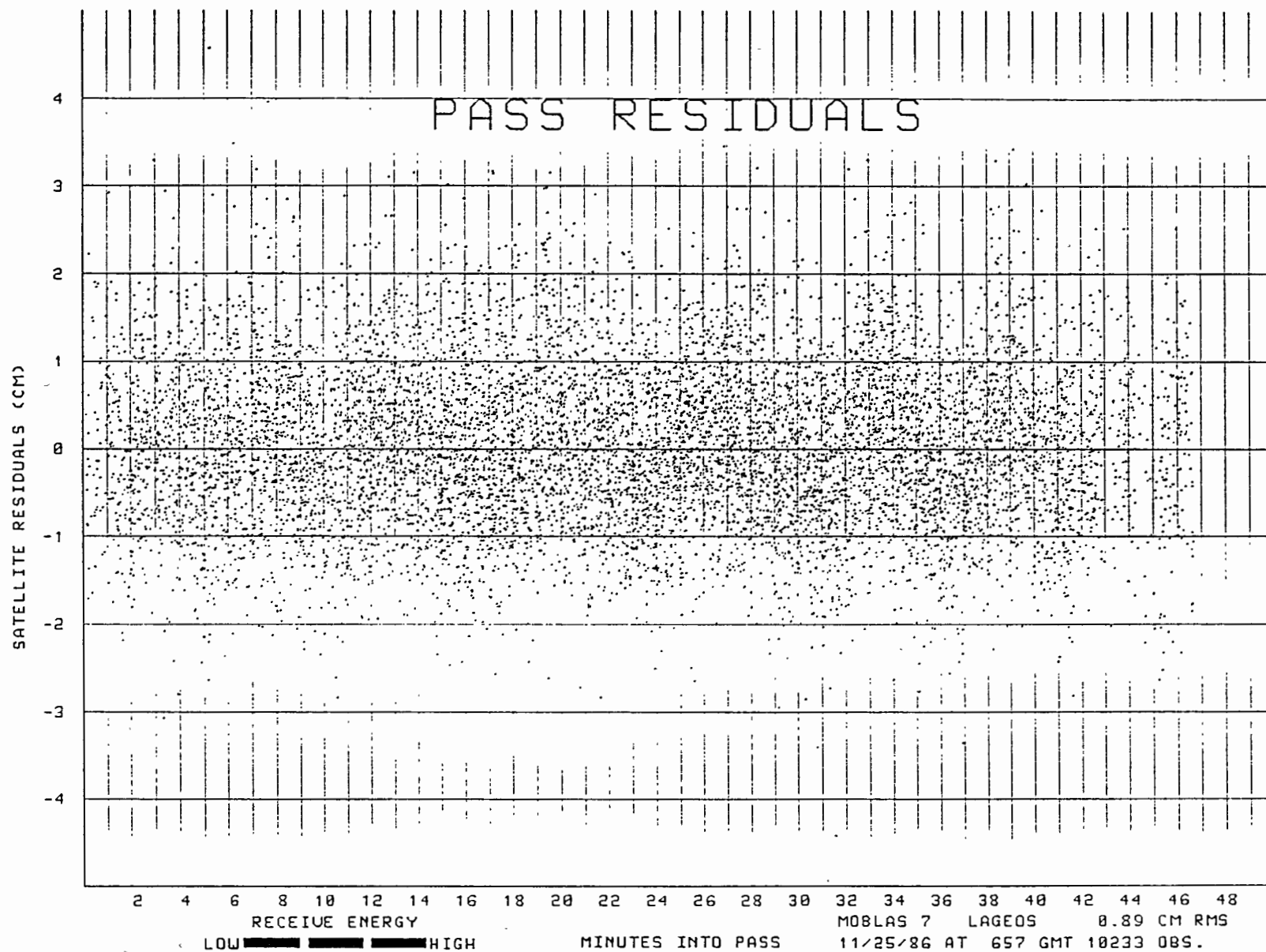


FIG. 2(A)

# LAGEOS & CALIBRATION RMS

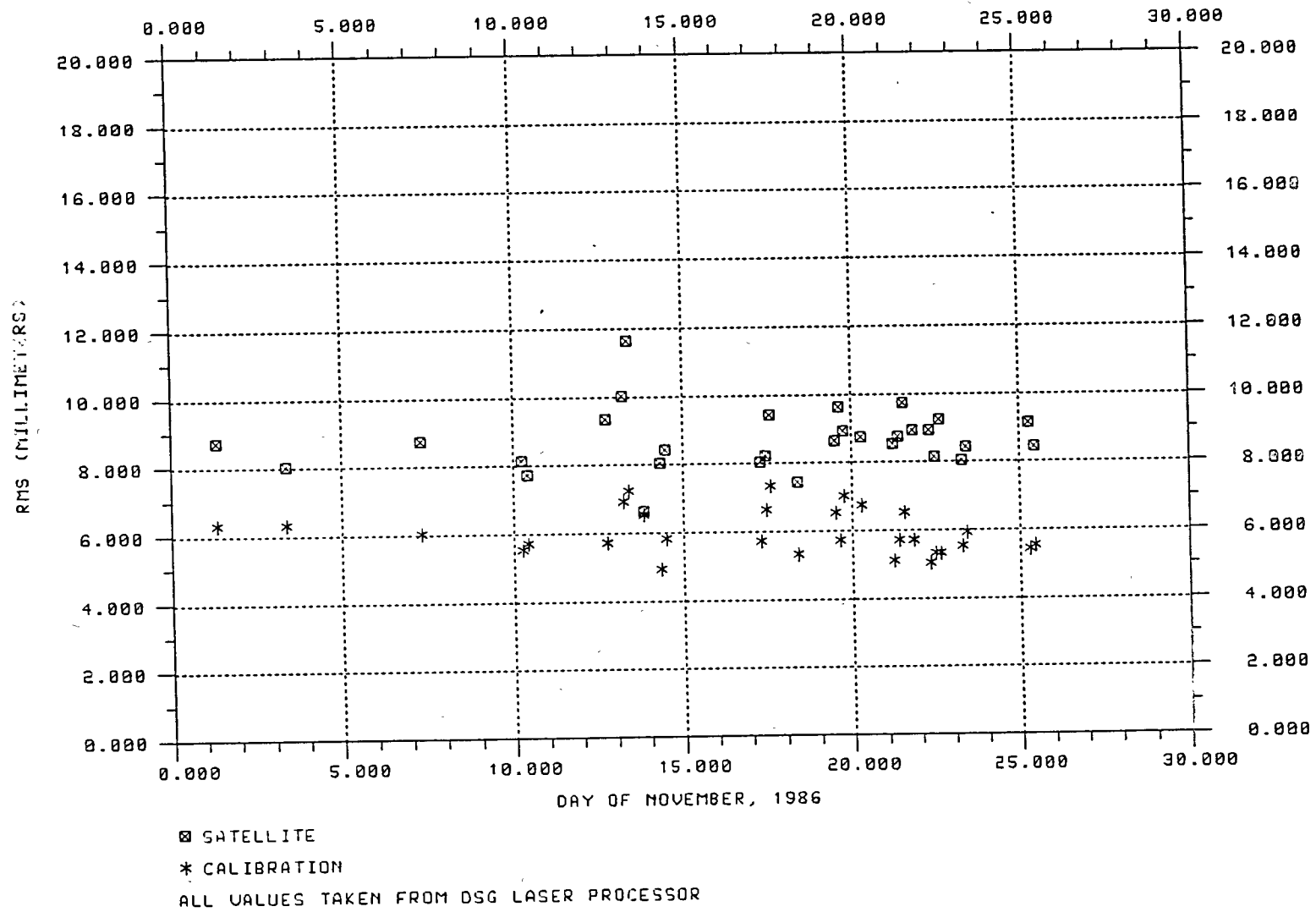


FIG. 1

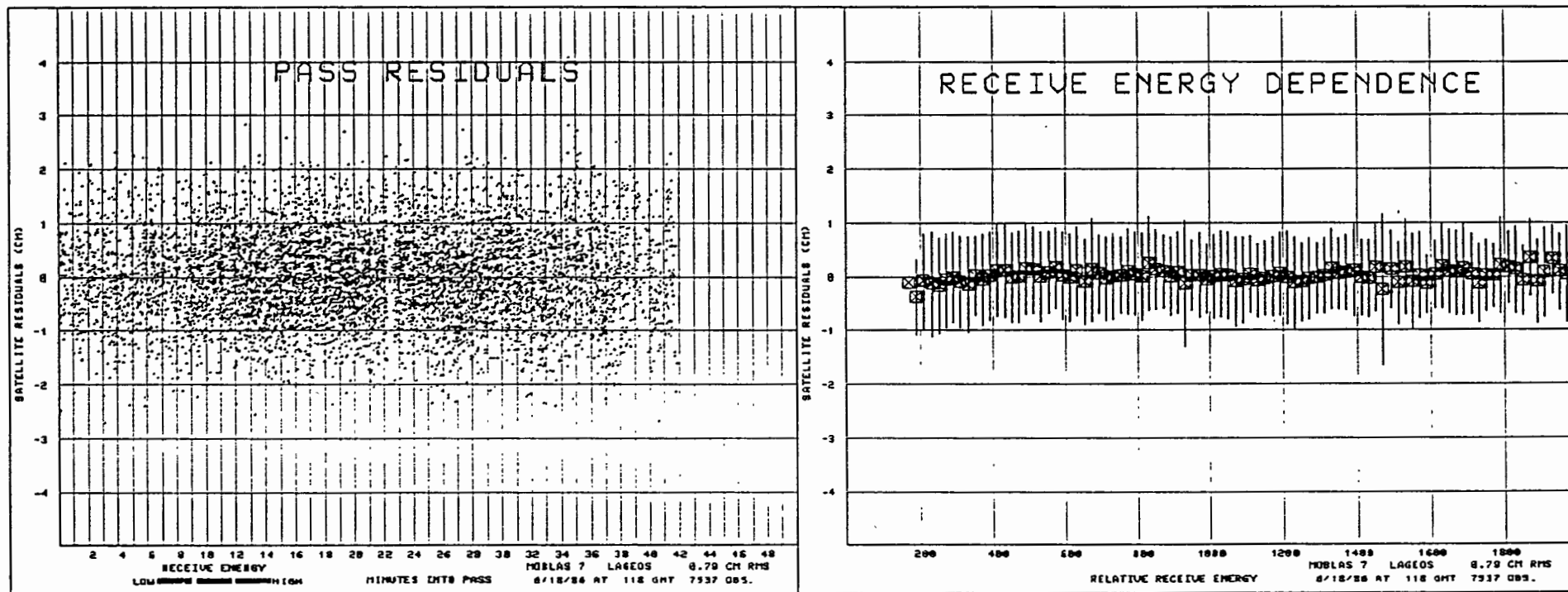


FIG. 4

FIG. 3(A)

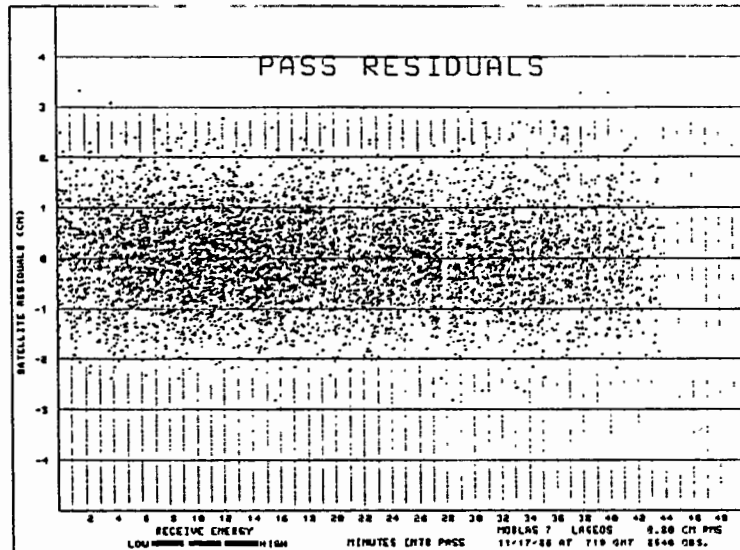


FIG. 3(C)

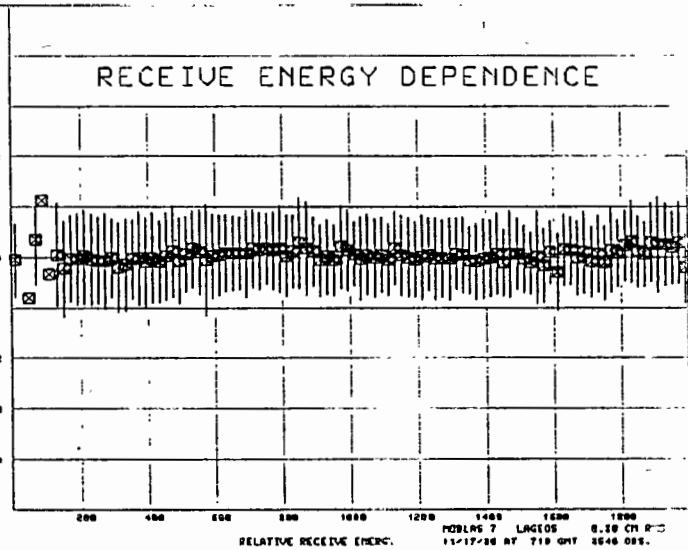


FIG. 3(B)

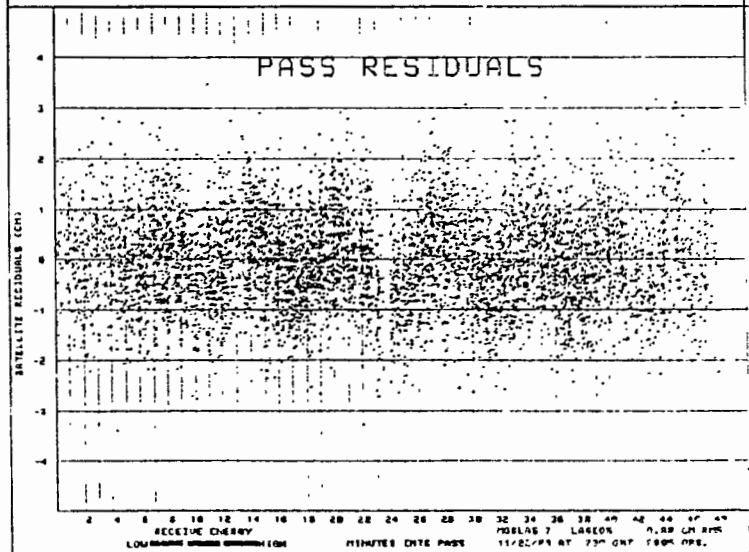
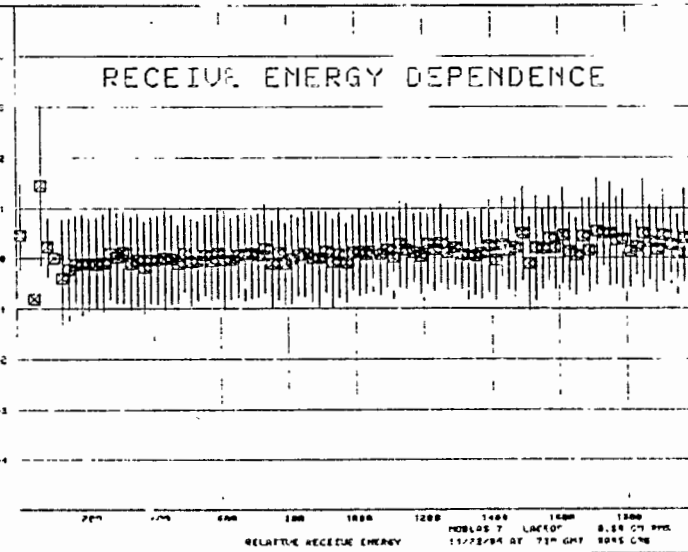


FIG. 3(D)



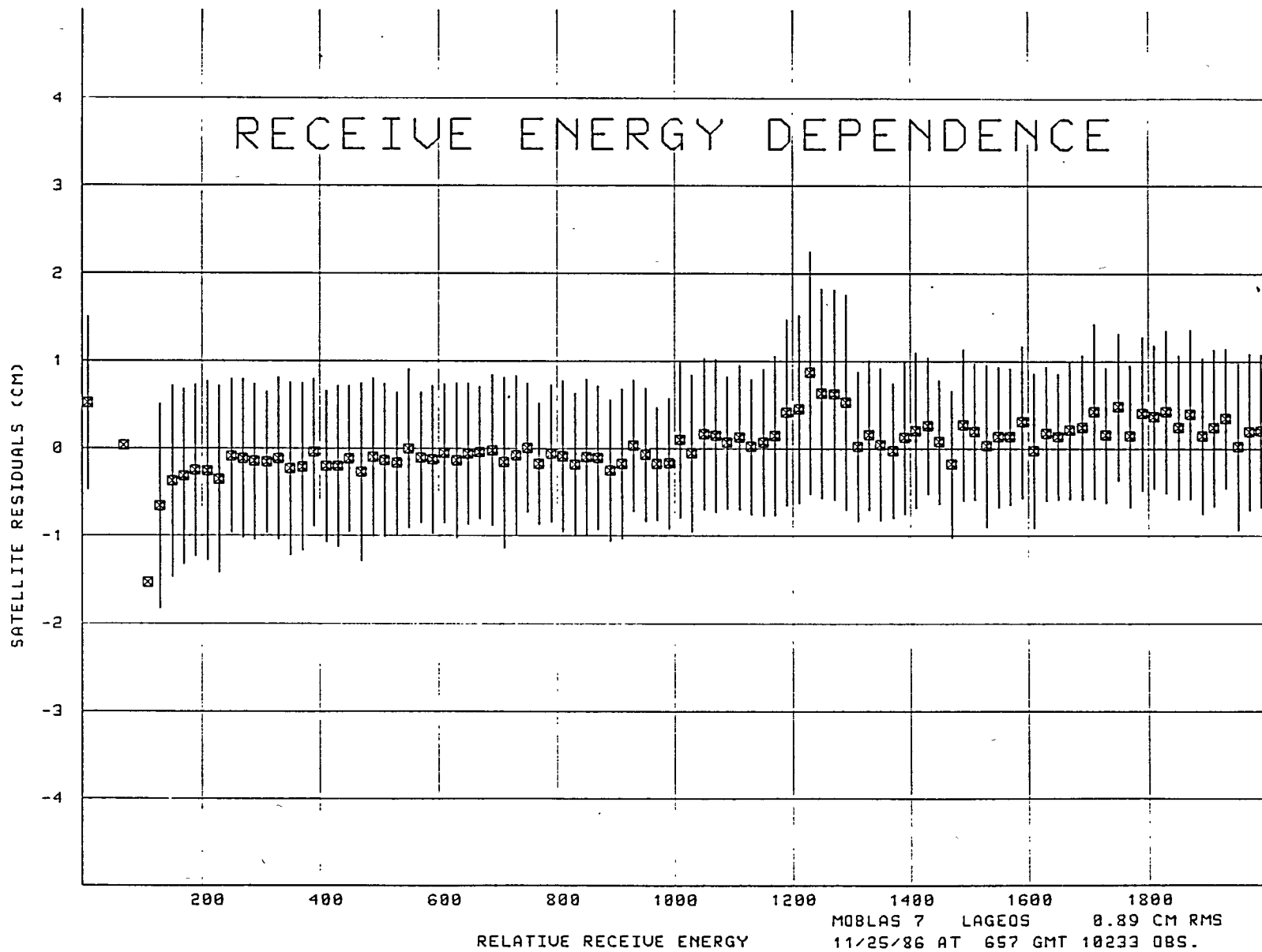
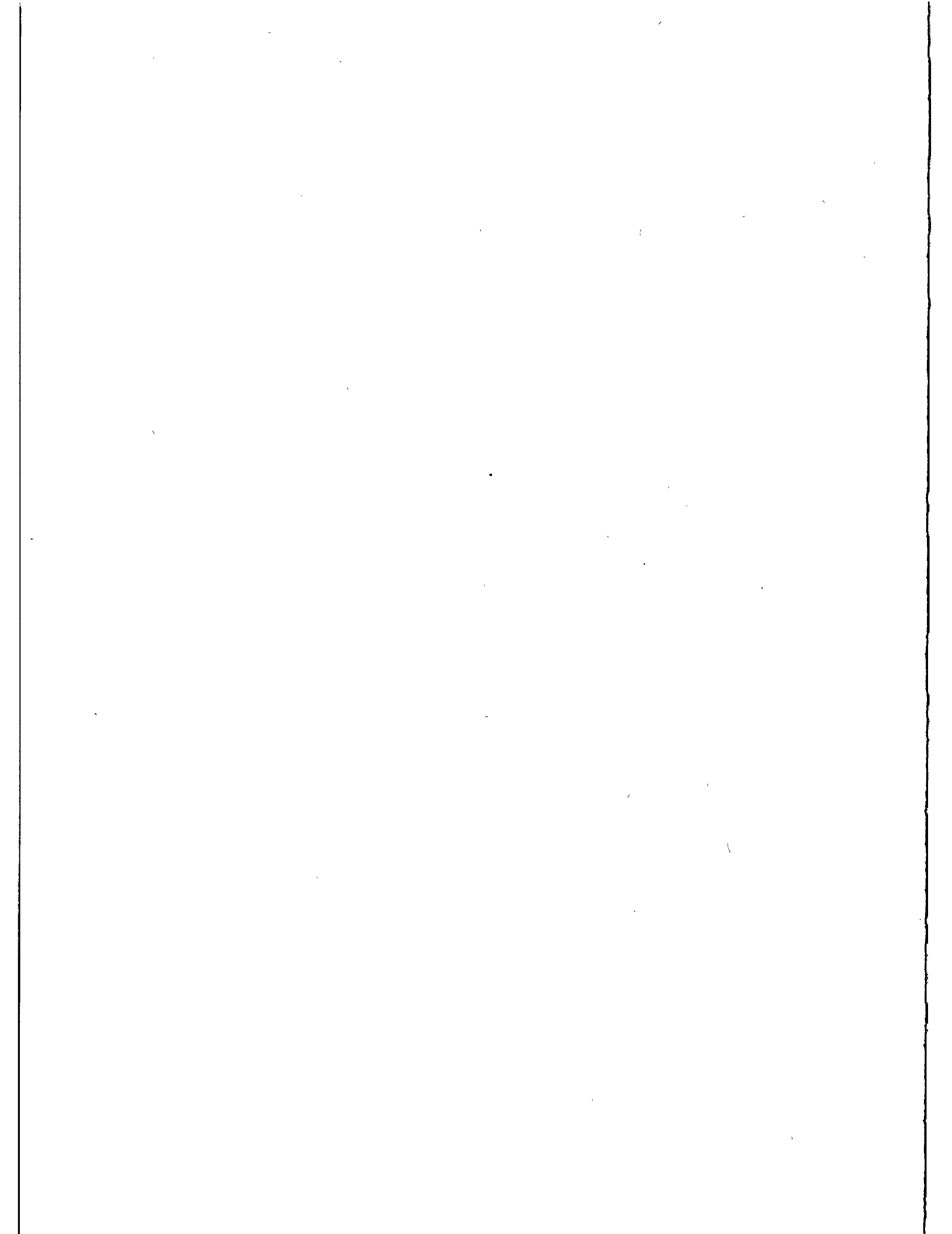


FIG. 2(c)



## TLRS-1 ; SYSTEM UPGRADE AND PERFORMANCE RESULTS

T. Varghese, P. Seery, H. Donovan, Patterson,  
K. Emenheiser, D. Gurovich, D. Yannuzzi  
Allied Bendix Aerospace  
BFEC, GLTN  
Seabrook, MD 20706 - USA -

Telephone (301) 2867743  
Telex 19770 GLTN

R. Appler  
Code 601 NASA  
Goddard Space Flight Center  
Greenbelt MD 20770 - USA -

Telephone (301) 2868119  
Telex 257559 CDPO UR

### ABSTRACT

A major system upgrade was undertaken in TLRS-1 to improve the ranging accuracy as well as to eliminate the biases observed during collocation with Moblas-4 & -8. The goal is to obtain collocated Lageos passes with Moblas-7 at the sub-cm level with calibration and satellite data residual RMS values of  $\sim 1$  cm and comparable ground calibration data. Recent operational results show satellite and ground data close to the projected performance. In this paper we overview past system bias characteristics, causes for the bias and engineering upgrades accomplished to meet the goals.

## 1.0 INTRODUCTION

The collocation of TLRS-1 (Transportable Laser Ranging System) with MOBLAS-4 in Monument Peak and MOBLAS-8 in Quincy, California, during Sept. 1984-July 1985, revealed an azimuth dependent bias of approximately 10cm. Extensive investigations were carried out by the crew in the field with external help to identify and correct the problem to no avail. Hence the NASA Crustal dynamics program decided to bring the system to Goddard Optical Research Facility for detailed engineering evaluation and analysis by Bendix Engineering group and to make appropriate modifications to the system so as to reduce the bias to the 1-cm level.

## 2.0 COLLOCATION RESULTS FROM QUINCY AND MONUMENT PEAK

Fig.1 illustrates the bias as a function of azimuth angle. It is evident that the data shows a transition to 1.0 cm bias in the azimuth angle range of 30 - 210 degrees ("frontside"), and is close to zero in the range of 211 - 29 degrees ("backside"). An important feature to recognize here is the difference in the nature of the bias when the mount is switching from "backside" to "frontside" mode.

## 3.0 ENGINEERING EVALUATION

The AZ-EL mount of TLRS-1 has a 2 feet lever-arm and this produces two equivalent orientations for the mount which are mutually realizable by azimuth rotation of 180 degrees and elevation rotation of twice the angle with respect to zenith. These two equivalent orientations are known as backside and frontside modes. The mount can exhibit few mm of optical path length difference depending on the orientation. The magnitude of the observed bias was too large to be a consequence of the mount orientation. However, if the optical alignment of the system is such that the beam shifts at the field of view of the telescope depending on the orientation, this can produce significant bias if the detector is sensitive to the spatial positioning of the beam.

For optoelectronic detection of the received signal from the satellite the system had a high quantum efficiency Varian photomultiplier tube as the detector. Laboratory experiments have shown that the tube can exhibit 6-8cm time-walk even for few mm of spatial displacement of the beam on the photocathode. The electron beam inside this tube has a cycloidal trajectory between dynodes due to the longitudinal electric field and hence the transit time is not space-invariant. The single largest contribution towards the bias could thus be attributed to the detector. The errors in calibration



path distances, discriminator calibration, nonlinearity in the TD811 time interval counter etc., may be considered as additional sources for the observed bias.

#### 4.0 HARDWARE/SOFTWARE UPGRADES AND PERFORMANCE RESULTS

The need for hardware/software upgrade was imperative following the determination of the above problems. To verify that the data-loop hardware changes (Table-1) would accomplish the set objectives, horizontal ranging was performed on 8 targets. These targets were located to provide fairly uniform azimuth angle coverage and had ranges of 50-400 meters. Fig.2 illustrates the measured system delay as a function of azimuth angle for various targets. Each division on the horizontal axis is 15 degrees while that on the vertical axis is 50ps (~7.5mm). Measurements were performed on the front and backside modes. As can be seen from the plot the azimuth dependence was not more than 6mm and is within the uncertainty of the hardware and survey measurement. The mean difference between the front and backside mode was less than 2mm and the upgraded hardware thus should meet the projected goals.

Table-1 illustrates the hardware configuration before and after the upgrade. Major software upgrade was also necessary for hardware interface, system diagnostics, shot-shot measurements of system parameters, and real-time computation/display of the statistics of ranging. A new analytical mount model was also developed to provide smoother alignment and tracking capability and is expected to become operational in the near future.

The system has been subjected to extensive ground testing prior to the commencement of collocation to meet collocation prerequisites. These tests included cube map, system stability as a function of time, range, signal amplitude, temperature and azimuth. These results are displayed in Fig.3-6 and it is clear that the system is capable of providing sub-cm collocation data.

Collocation is presently underway at Goddard Optical Research facility between TLRS 1 and MOBLAS 7 and the initial results are meeting the sub-cm criteria and look very encouraging. More collocated passes are to be taken and analyzed and the results will be published at a future time.

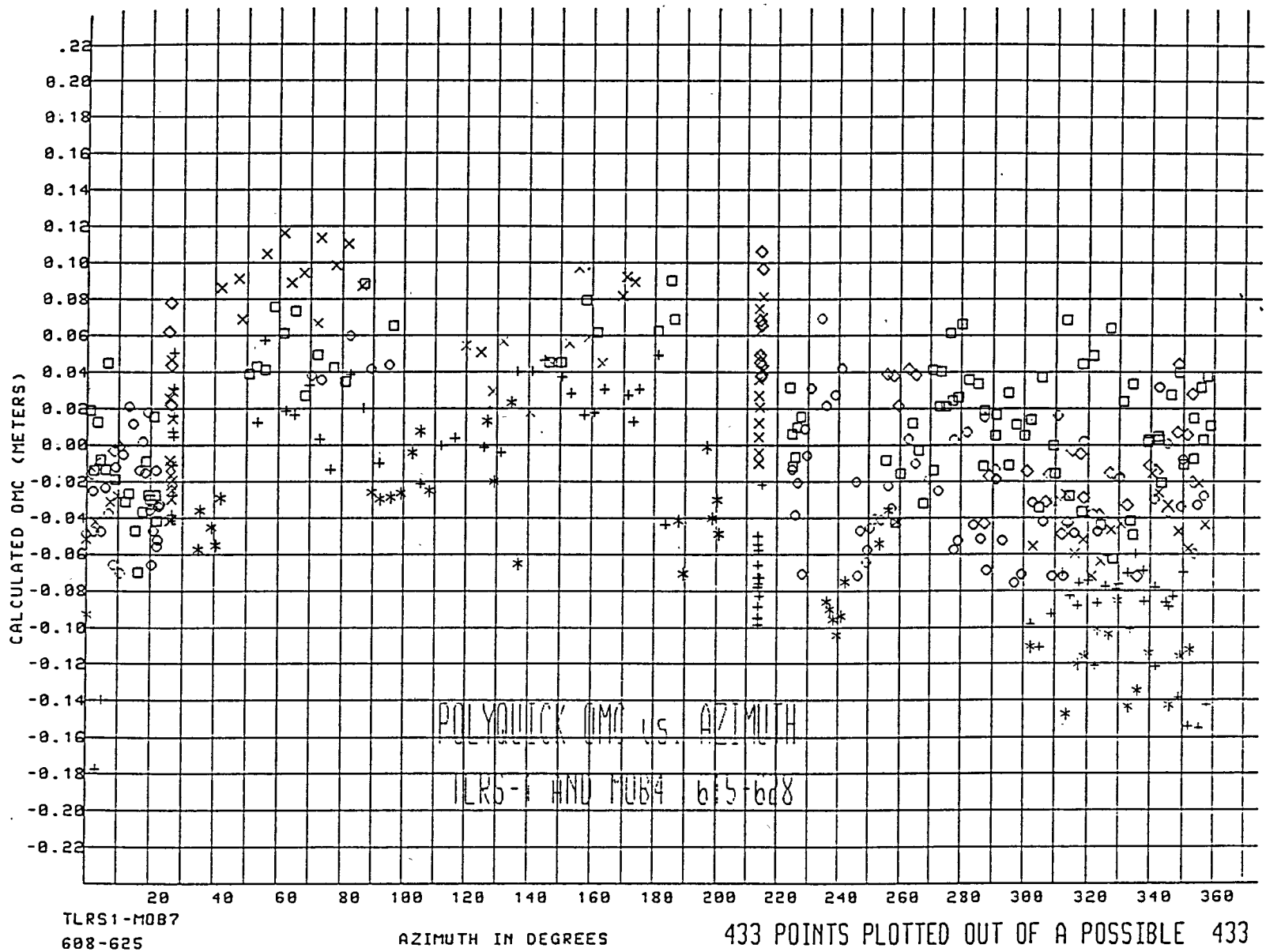


FIG. 1

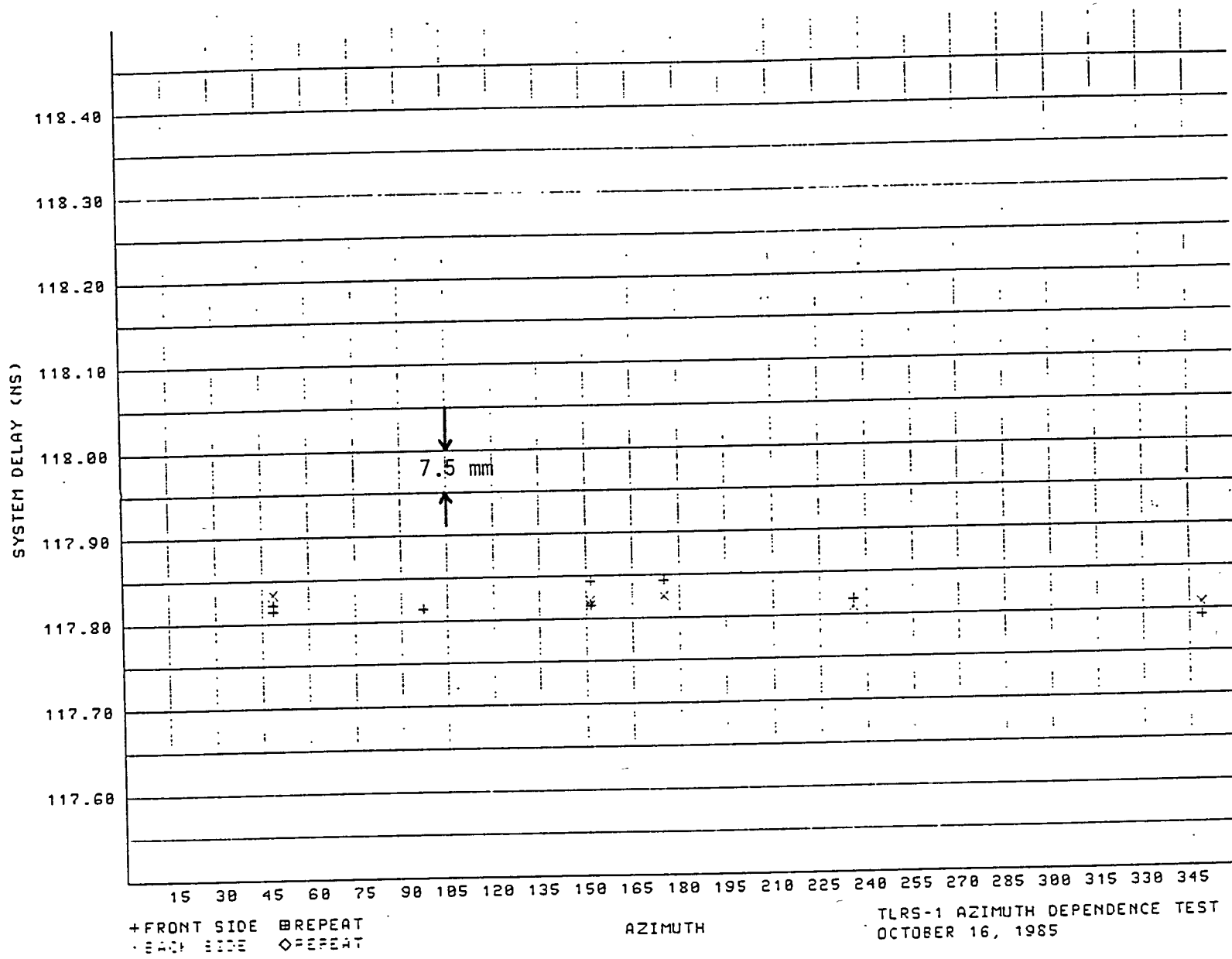


FIG. 2

TLRS-1 SYSTEM CONFIGURATION

	<u>BEFORE UPGRADE</u>	<u>AFTER UPGRADE</u>
o LASER	QUANTEL YG441ML	QUANTEL YG402DP
- OUTPUT ENERGY	4 MJ	100 MJ
- PULSE WIDTH	200 PICOSECONDS (PS)	200 PICOSECONDS (PS)
- PULSE RATE	5 PULSES PER SECOND (PPS)	5 PULSES PER SECOND (PPS)
o RECEIVE ELECTRONICS		
- PHOTOMULTIPLIER TUBE	VARIAN	ITT MICROCHANNEL PLATE
- DISCRIMINATOR	ORTEC 934	TENNELEC TC 454
- TIME TO DIGITAL CONVERTOR	TD 811	HP 5370B
- DETECTION	SINGLE PE	SINGLE PE
o OPTICAL SYSTEM		
- TELESCOPE	25 CM REFRACTIVE	SAME

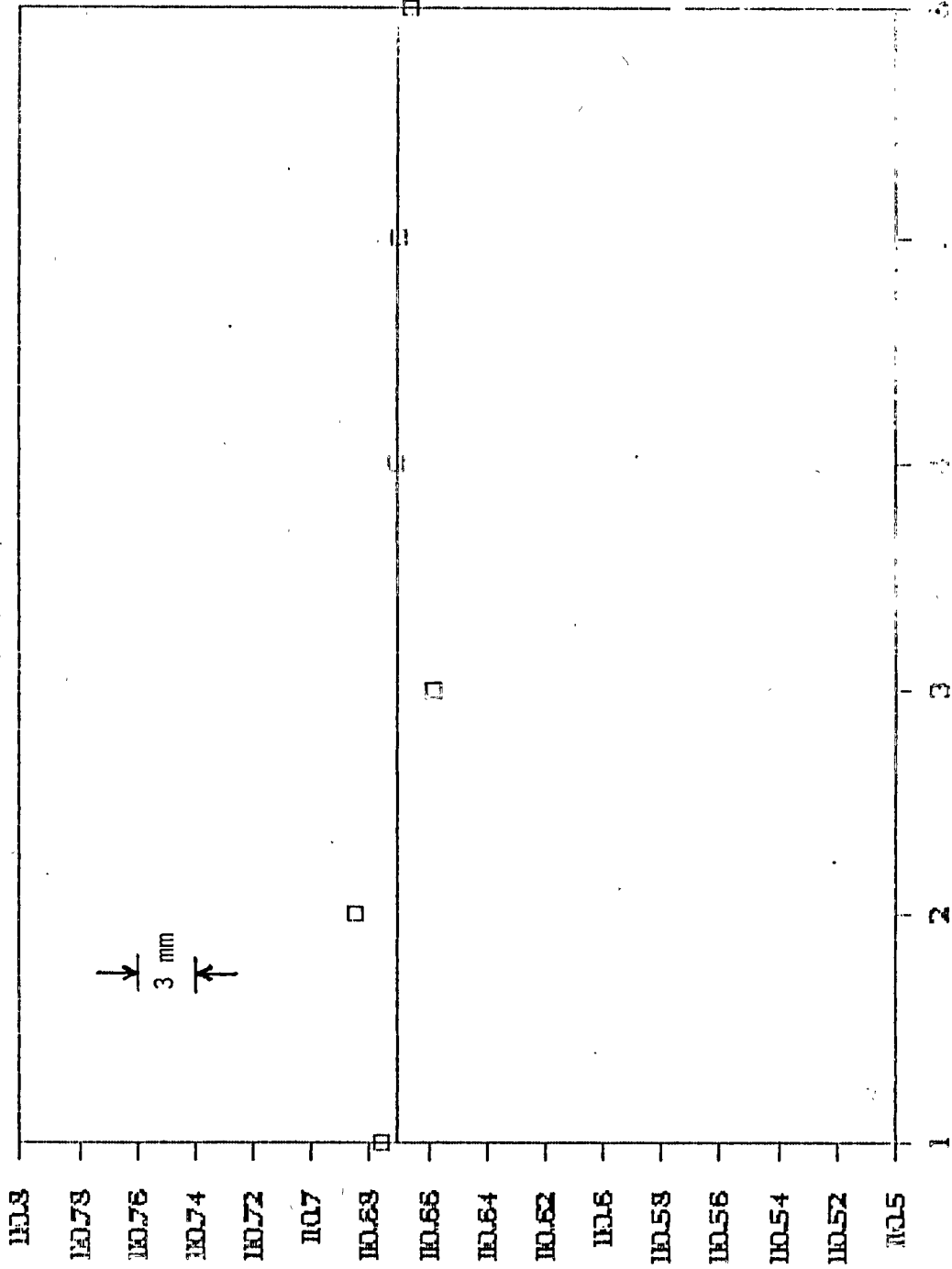
TABLE 1

● TRACKING MOUNT		
- TYPE	AZ-EL (U. OF TX DESIGN)	SAME
- ENCODER RESOLUTION	$2^{22}$ (.31 ARC SEC)	SAME
● TIMING ELECTRONICS		
- SHORT TERM STANDARD	CESIUM	SAME
- EPOCH STANDARD	LORAN RECEIVER	GPS RECEIVER (TRIMBLE)
● COMPUTER		
- HARDWARE	NOVA	SAME
- SOFTWARE	U. OF TEXAS	U. OF TEXAS + BFEC
● CALIBRATION	INTERNAL CALIBRATION (INSENSITIVE TO POSSIBLE MOUNT BIASES)	EXTERNAL + INTERNAL
● ENVIRONMENTAL CONTROL		
- TEMPERATURE	CONTROLLED BUT	$70 \pm 5^{\circ}\text{F}$
- HUMIDITY	RANGE UNKNOWN	$50\% \pm 10\%$

TABLE 1 (CONT'D.)

# CUBE MAP ON TARGET #1 FROM TLRS 1

JULY 28, 1955



□ SYSTEM DELAYS

FIG. 3

# STABILITY TEST OF TLRS 1 ON TARGET #1

JULY 28, 1955

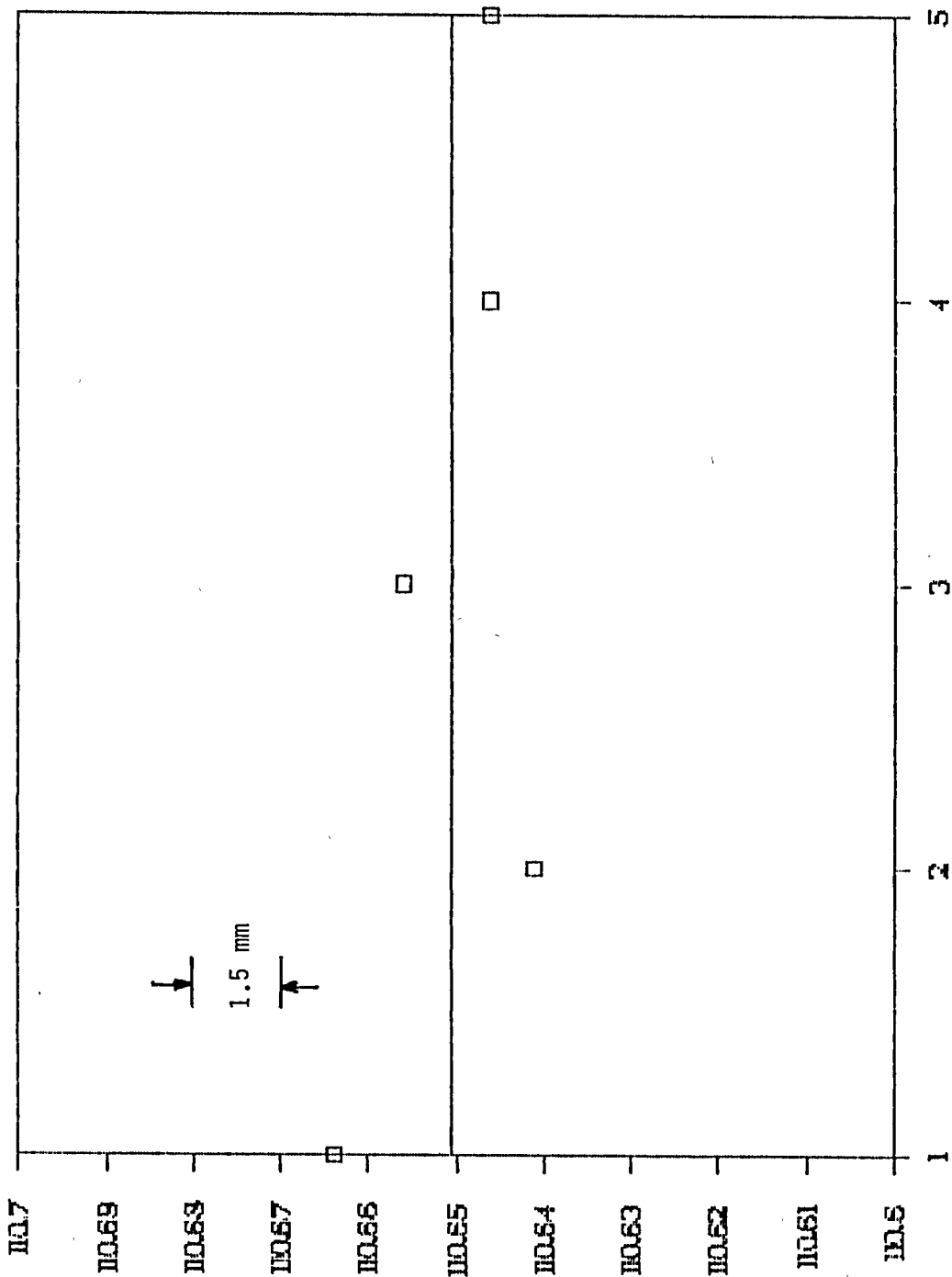


FIG. 4

# MULTITARGET RANGE STABILITY

JULY 26 - 27, 1995

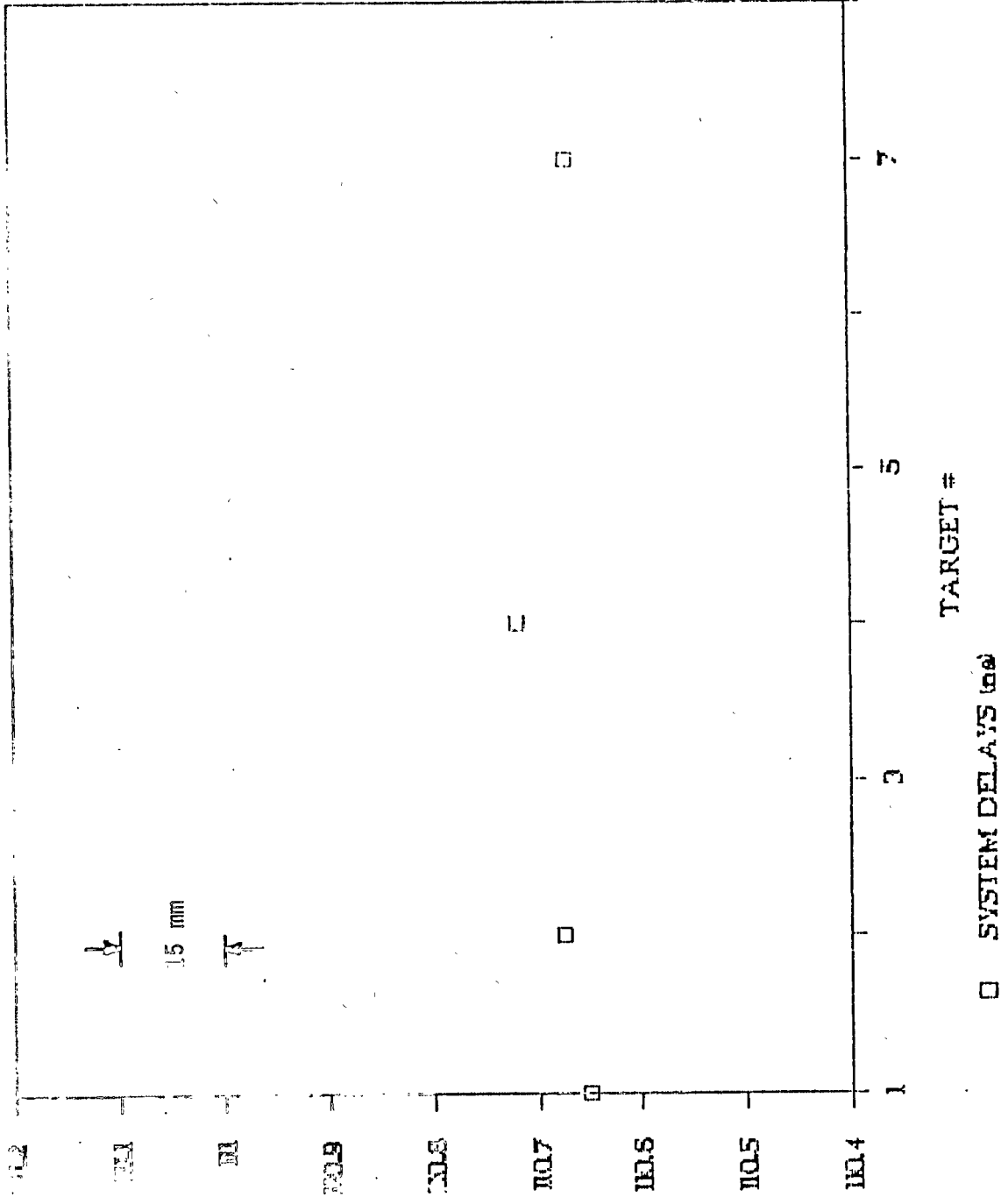


FIG. 5



# AZIMUTH DEPENDENCE (FOUR TARGETS)

JULY 26 - 27, 1985

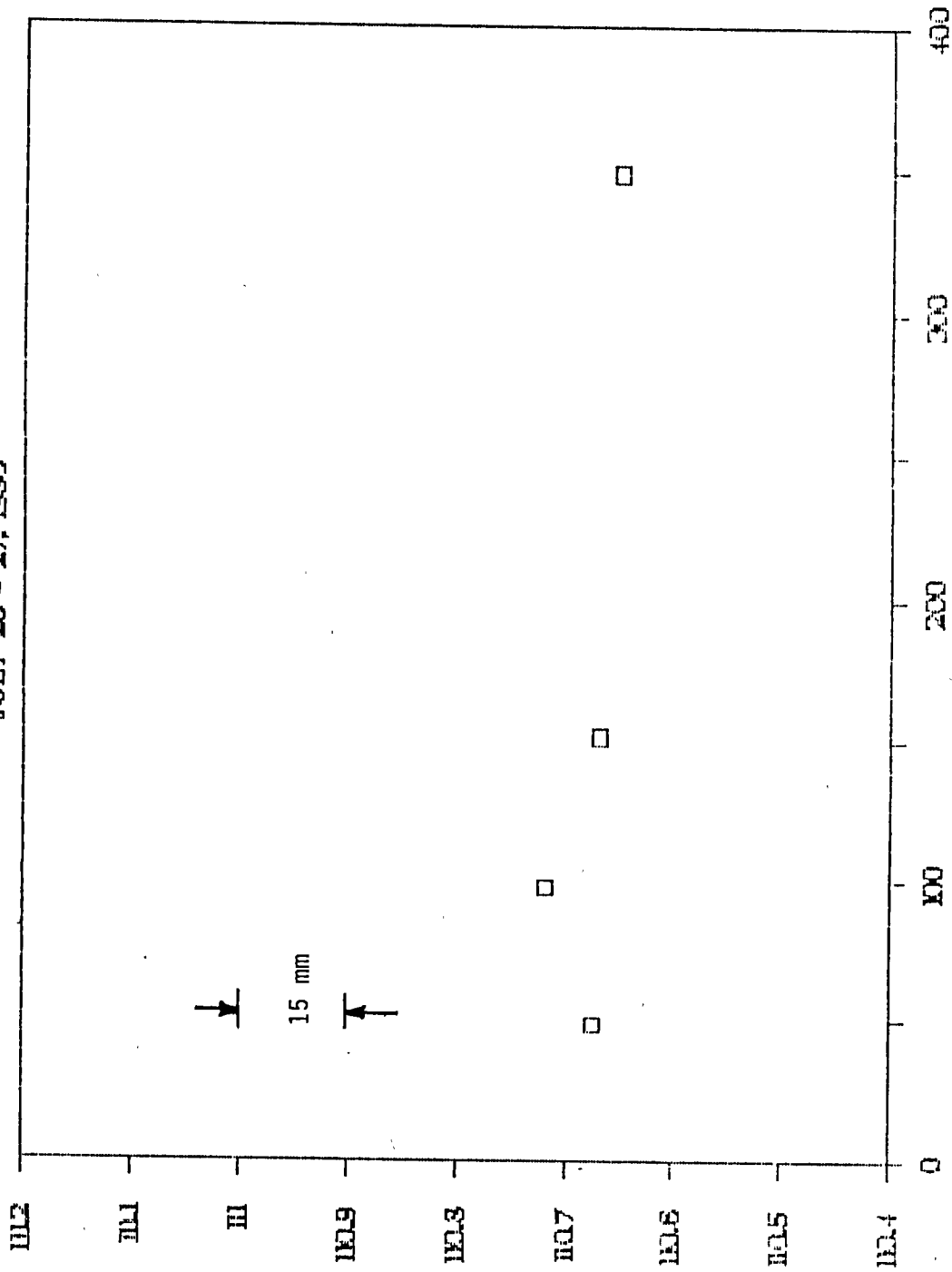
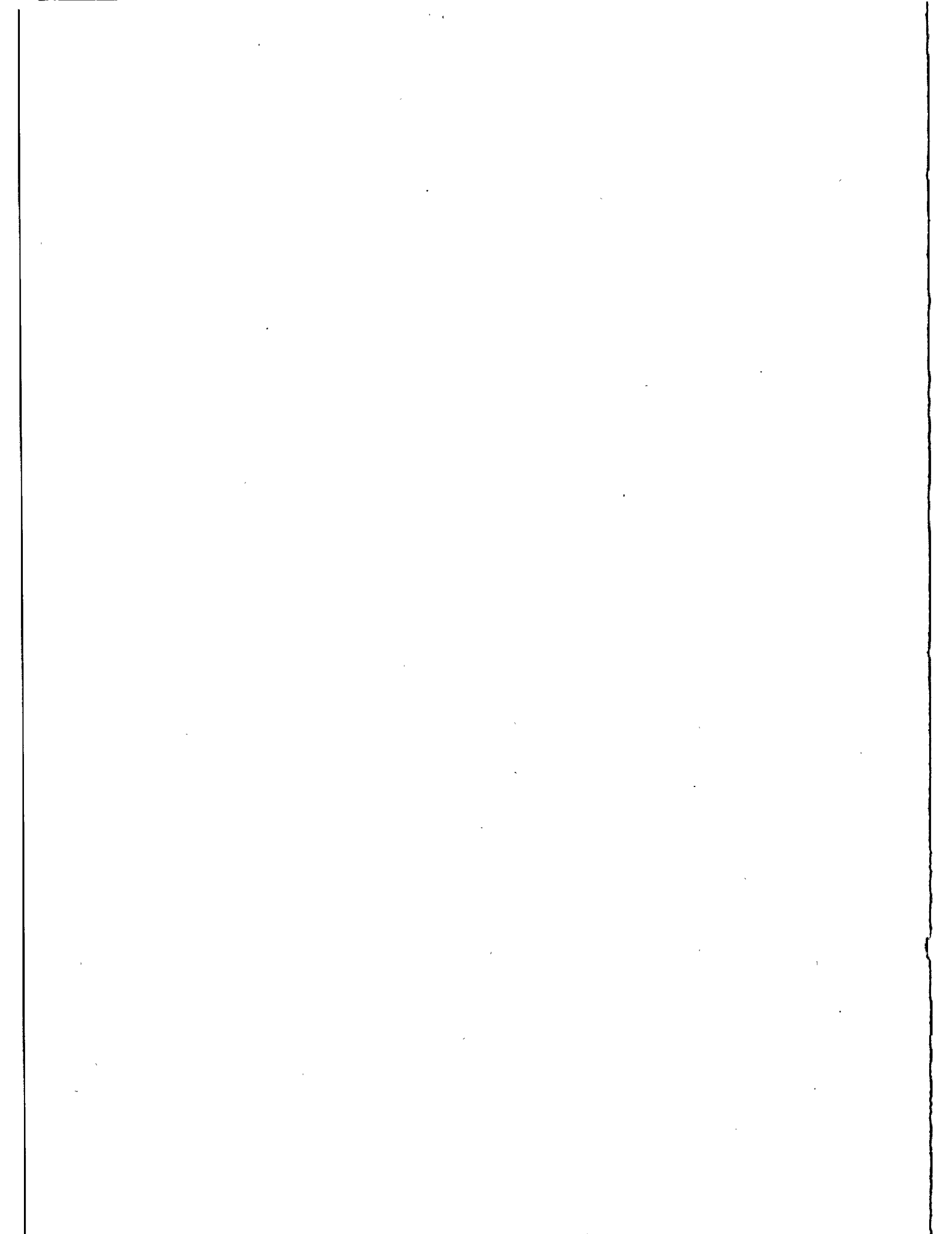


FIG. 6



SATELLITE LASER RANGING SYSTEM AT THE SIMOSATO HYDROGRAPHIC  
OBSERVATORY AND THE TRANSPORTABLE SYSTEM ; HTLRS

M. Sasaki  
Hydrographic Department,  
Maritime Safety Agency  
Tsukiji-5, Chuo-ku, Tokyo 104 - Japan -

Telephone (03) 541 3811  
TWX 2522 452 HDJODC J

Y. Suzuki  
Totsuka Works, Hitachi Ltd.  
216 Totsuka-machi, Totsuka-ku  
Yokohama 244 - Japan -

Telephone (045) 881 1221  
TWX 3823 503

ABSTRACT

The paper outlines the history of laser ranging in Japan, and introduces the SLRS installed in the Simosato Hydrographic Observatory of Hydrographic Department, Maritime Safety Agency. It also describes the transportable system ; TLRS now under development for determining the locations of isolated islands around Japan.

## INTRODUCTION

The work on laser ranging in Japan began with an experiment of ranging the GEOS and DIADEME satellites at the Dodaira Station of Tokyo Astronomical Observatory (TAO) in December 1968. A satellite laser ranging system (SLRS) using a receiving telescope with diameter of 60 cm, and a ruby laser with pulse width of 50 ns, output of 1 J, 1 pps, was manufactured for the experiment<sup>(1)(2)</sup>.

A lunar ranging experiment was made at the Okayama Astrophysical Observatory in 1971 with the target of the retro-reflector installed by Apollo 11 on the surface of the moon. The experiment employed an astronomical telescope with diameter of 188 cm as the transmitting and receiving optics, and a ruby laser with output of 5 J, 12 ppm<sup>(3)(4)</sup>. Above two systems were developed by TAO and Hitachi.

The work of TAO has since been continued at the Dodaira Station, and the system was improved several times.

A test model of an SLRS for geodetic observation was built up jointly by the Hydrographic Department (JHD) of Maritime Safety Agency (MSA) and Geographical Survey Institute (GSI) and installed at the Kanozan Geodetic Observatory in 1976. The system employed a receiving optics with diameter of 40 cm, a ruby laser, and a three-axis mount<sup>(5)</sup>.

Upon reviewing the experiment results and the world's technological trends, the JHD decided to use an SLRS for marine geodetic control, and to determine the locations of isolated islands around Japan. The JHD introduced a fixed type SLRS for the base station into the Simosato Hydrographic Observatory (SHO)<sup>(6)</sup>.

The SLRS is of the same size with the system of the IFAG station in West Germany. It is provided with a receiving telescope, 60 cm in diameter, and an Nd-YAG laser having a pulse width of 200 ps, 4 pps.

Japan's first geodetic satellite "AJISAI" which means "HYDRANGER" of flower in Japanese was launched on an orbit on August 12, 1986(UT), by the first H-1 rocket which was developed by the National Space Development Agency (NASDA).

Following the introduction of the fixed type SLRS, the MSA has started developing a transportable SLRS:TLRS which is intended for determining the locations of isolated islands in combination with the satellite "AJISAI". The TLRS, now being manufactured by Hitachi Limited, is expected to be completed in October 1987.

#### THE SLRS AT SIMOSATO

The laser site of the Simosato Hydrographic Observatory is situated close to the point of Kii Peninsula of Honshu Island (135° 56 min. E, 33° 34 min.). The site, at an altitude of 60 meters above the sea level, faces the Sea of Kumano. With annual precipitation of more than 2,700 mm, the climate is not so suitable for satellite ranging.

The SLRS at Simosato was manufactured jointly by GTE of the U.S.A. and Hitachi of Japan under the supervision of JHD. GTE manufactured the laser, optics and mount, control and data-processing equipment subsystem, and main software. Hitachi took the roles of manufacturing the timing system, the system calibration equipment including the ground target, various types of support software for operation and data processing,

and of integrating, installing and adjusting the entire system.

The SLRS was brought into the Simosato site in February 1982. Regular observation was started in April after some adjustment and testing. Since then, the SLRS has been continuously operating for four years to date.

Figure 1 shows an external view of the entire Simosato station. The SLRS installation is housed in the building on the right side. Figure 2 shows the electronics including the control and data-processing equipment subsystem. Figure 3 shows the optics and mount.

Table 1 lists the main items of the system specification.

During the discussions on the proposed SLRS installation at Simosato, those who concerned with the project were afraid that satisfactory observation might not be performed at the low-altitude, seashore site, where the climatic conditions are not favorable for the purpose. Table 2 lists the results of the observation during the past four years, which indicate that the number of annual data acquisitions has been increasing. Ranging data of 297 passes and 243,800 ranges was acquired for the LAGEOS in 1985.

System operation and ranging of LAGEOS, STARLETTE and BEACON-C is conducted around-the-clock by five staff members headed by Mr. E. Nishimura. One of the ranging objects was changed from BEACON-C to AJISAI last August. Figure 4 shows the ranging data of AJISAI obtained immediately after its launching.

Hitachi has been contracting with JHD for the SLRS maintenance.

The coordinates of the base point at the SHO were estimated from the satellite ranging data obtained at the Simosato site, and were reported<sup>(7),(8)</sup>.

In addition to the main work for marine geodetic control, the JHD participates in the efforts to detect plate motions and crustal movements in the SLRS observation project which will contribute to estimating the earth rotation and geophysical parameters.

The following additions and changes were made to the SLRS:

(1) Laser attenuator

The ground target is used to calibrate the system delay time. An attenuator of the construction shown in Fig. 5 is added to the system in order to assure safety against the laser beam and to match the signal intensity with the level of the signal reflected by the satellite. A high attenuation ratio is obtained from the diffractive effect of a pin hole aperture and a beam splitter with high reflection ratio.

(2) Photomultiplier tube (PMT)

The static crossed field type photomultiplier tube initially employed for the system caused deterioration of the dynode gain in about two years after the start of its use, and needed to be replaced. However, the PMT was then out of production. Its substitute selected was the Micro channel plate PMT with gate. At the same time, a wideband amplifier (DC to 3.15 GHz) was added to the back of the PMT in order to

prevent the output from being saturated by the strong background light in the daytime, and to improve the signal level detectable by the system.

Its employment resulted in the increase in the data acquisition rate and similar ranging accuracy to the initial PMT, helped by the additional amplifier.

### (3) Software

Support software was developed and added to the main software. The major items of the support software include the satellite path charting feature for observation scheduling, the star position computing and tracking feature for correcting mount pointing errors, the ranging accuracy calculating feature, satellite position calculating feature using numerical integration method, and the joystick hold feature for facilitating satellite tracking with offset error.

Prior to the construction of the Simosato site, the one of authors visited the laser sites of CERGA in France, IFAG in West Germany, NASA Goddard, SAO Boston and Hawaii Haleakala in the U.S.A. The authors wish to thank the personnel of these organizations for their kind advice and useful suggestions.



## TRANSPORTABLE SYSTEM; HTLRS

The transportable system: HTLRS the JHD plans to introduce is to be used for AJISAI satellite ranging to determine the locations of ten major isolated islands around Japan. Figure 6 shows these ten islands (marked with a double circle) where mobile observation is expected.

The observation is scheduled to be done on two islands a year. The SLRS will be transported by truck, by ship (cargo boat or ferry boat), or by aircraft.

To permit transportation by the above means, the entire system will be housed in two shelters as shown in Fig. 7 and designed to weigh less than five tons.

The optics/mount and the laser are assembled on the same bench. Upon arrival at the site, the bench is installed on a concrete pier constructed on the ground independently of the shelters. The electronics including the control and data processing equipment subsystem are housed in the other shelter.

Table 3 lists the major specifications of the system. Figure 8 is a block diagram showing the system configuration. The major target satellite of the HTLRS is the AJISAI. It is, however, designed to be capable of ranging the LAGEOS.

The ability of a ranging system is represented by the concept of system size<sup>(9)</sup>. The authors defined the system size parameter S for the SLRS as follows:

$$S = n \cdot E_0 \cdot A_r \cdot \alpha \beta \gamma \cdot \eta \dots\dots\dots (1)$$

where,

Table 2 Data Acquisition at Simosato Hydrographic  
Observatory and Its Mean Range Accuracy

year	LAGEOS		STARLETTE		BEACON C		AJISAI	
	passes	ranges	passes	ranges	passes	ranges	passes	ranges
1982	47	11,000	36	4,700	59	11,900	-	-
1983	137	30,000	116	29,400	199	92,200	-	-
1984	223	93,300	118	37,800	150	56,100	-	-
1985	297	243,800	108	38,800	154	67,500	-	-
~Aug 1986	156	103,900	53	11,700	56	15,400	27	25,300
accuracy	9.0 cm		9.8 cm		9.2 cm			

n : Laser output repetitions  
E<sub>0</sub> : Laser output energy  
A<sub>r</sub> : Area of receiving optics  
αβγ: Efficiency of transmitting and receiving optics  
η : Quantum efficiency of detector.

Figure 9 shows the system size of the transportable SLRS defined by the equation (1) above. The horizontal axis in Fig. 9 represents "S" in equation (1), while the vertical axis shows the beam divergence of the transmitting laser. The oblique lines in the diagram indicate the relationship between system size S to detect reflected signals from the LAGOS and the GS-1 at an output of rate of one photoelectron per second, and beam divergence θt.

System size S of the transportable SLRS is designed to be 3.5 to 17 w.sq.cm, which means that the detection of one photoelectron output per second can be obtained (detectable) by shooting at the LAGEOS with beam divergence of approximately 100 arc seconds.

The HTLRS is expected to be operated with beam divergence of 40 arc seconds. Then, the theoretical value of the signal level received from the LAGEOS will be 10 to 1 p.e. per shot. The system is designed to operate during the period of night to twilight time.

Figure 10 shows the calculated results of the detection probability of a few receiving systems based on the authors' studies on weak pulse light detection<sup>(10),(11),(12)</sup>. The horizontal axis in the diagram shows the noise level per gate 10

microsec., while the vertical axis shows the detection probability. Parameter  $N_s$  indicates the average number of received photons. The curves of detection probability are, from left to right, the results of threshold detection at single p.e. level, multichannel (8 channel) detection, and coincidence detection using double pulses by two output branching, respectively.

One-channel threshold detection (single p.e. detection) will be conducted in the early days of the transportable system introduction, although the multichannel or coincidence system is more desirable for twilight operation. Possibility of day time ranging may be discussed by narrowing range gate from 10  $\mu$ s to 100 ns and the bandwidth of interference filter from 8 Å to 1 Å.

The HTLRS will employ the Nd-YAG laser. Its output is 50 mJ per pulse, pulse width is up to 200 ps, and repetition is 10 pps.

Hitachi's personal computer, Model B16/FX will be used to control the system and process data.

The Rb frequency standard with a time calibration by Loran will be employed for the timing subsystem.

The detector will be used for the micro channel PMT with gate, similarly to the Simosato system.

The optics/mount subsystem will be of a new configuration. Figure 11 illustrates a rough sketch of the optics/mount subsystem, while Fig. 12 shows its configuration. The receiving telescope is arranged so that the light axis will coincide with the elevation axis, and will be stationary for the elevation axis. The transmitting laser beam passes along the azimuth

axis, and is shot via the reflector mirror on the rear of the secondary mirror of the receiving telescope and the tracking mirror. Only the tracking mirror, installed at an angle of  $45^\circ$  to the elevation axis, revolves around the elevation axis. This arrangement has such advantages as that the receiving telescope can be stabilized because it is used in a nearly stationary state, that the load can be reduced because the elevation axis needs to drive only the tracking mirror, and that the transmitting optics can be simplified.

The two axes, elevation and azimuth, are driven by a direct drive torque motor.

The HTLRS is provided with an additional for detecting the flash light of the sun reflected by the AJISAI (star of magnitude 2 to 4, 2 pps, 5 ms width) and determining the flash times (rise and fall) besides the main feature for tracking and ranging the satellite. This additional feature is used to fix the time of photographic observation of the AJISAI with fixed stars in the background.

#### REFERENCES

- (1) T. Takenouchi, K. Tomita, S. Yamamoto and Y. Suzaki: Experimental Laser Ranging of Artificial Satellites, Nat'l. Conv. Record of I.E.C.E., Japan, 659 (1969)
- (2) T. Takenouchi, K. Tomita, S. Yamamoto, Y. Hasegawa, A. Tachibana, S. Yamamoto and M. Takatsuji: Satellite Ranging with a Laser, Hitachi Review (1972) Vol. 19, No. 4 pp 153-164

- (3) A. Tachibana, Y. Yamamoto, M. Takatsuji, K. Murasawa and Y. Kozai: A Preliminary System of Lunar Laser Ranging, Space Research XII-Akademie-Verlag, Berlin (1972) pp 179-195
- (4) Y. Kozai: Lunar Ranging Experiments in Japan, Space Research XII-Akademie-Verlag, Berlin (1972) pp 212-217
- (5) Research Coordination Bureau, Science and Technology Agency: Comprehensive Study on the Development of the Laser Ranging System; Performance Report, (1977)
- (6) M. Sasaki, Y. Ganeko, and Y. Harada: Satellite Ranging system at Simosato Hydrographic Observatory. Data Rep, Hydrogr. Obs. Series of Astronomy and Geodesy, JHD, No. 17 (1983), pp 49-60
- (7) M. Sasaki: Satellite Laser Ranging at the Simosato Hydrographic Observatory and its Preliminary Results., Journal of Geodetic Society of Japan, Vol. 30, No. 1 (1984) pp 29-40
- (8) M. Sasaki: Algorithm for Determination of a Satellite Orbit and Geodetic Parameters by Using Laser Ranging Data and Preliminary Results of its Application, Report of Hydrographic Researches, No. 19, March (1984) pp 107-132
- (9) E.C. Silverberg: Operation and Performance of a Lunar Laser Ranging Station Applied Optics, Vol. 13, No. 3, March (1974) pp 565-574
- (10) Y. Suzaki and A. Tachibana: Detection Probability of Laser Radars for Satellite Ranging, Trans. IECE Vol 55-B No. 10 '72/10 pp 569-576

- (11) Y. Suzaki and A. Tachibana: Influence of the Photo-electron Fluctuations on Accuracy of Ranging by Pulsed Laser Radar, Trans. IECE Vol. 56-c, No. 11 '73/11 pp 609-614
- (12) Y. Suzaki and A. Tachibana: Detection Times and Errors of Returned Optical Pulses for Satellite Ranging, Trans. IECE Vol. 63-c, No. 8, '80/8 pp 500-506

Table 1 Major Specifications of the SLRS at Simosato

Subsystem	Specification
<b>Mount</b>	
Configuration	elevation over azimuth
Transmitter system	laser stationary – two axes Coudé path
Tracking rate	from sidereal to 1° per second
Orthogonality	±5 arcsec
Wobble	±2 arcsec in elevation, ±5 arcsec in azimuth
Angular resolution	20 bits (1.2 arcsec)
Drive	DC direct drive torque motors
<b>Transmitting optics</b>	
Type	Galilean
Diameter	17 cm
Beam divergence	25 μrad – 2 mrad (computer controlled)
Start pulse detector	common with receiver electronics connected by fiber optics
<b>Receiving optics</b>	
Type	Cassegrain
Diameter	60 cm
Field of view	100 μrad – 2 mrad (computer controlled)
Sun shutter	automatic
Spectral filter	0.8 nm bandpass (temperature controlled)
Optical attenuator	0 – 40 dB (computer controlled)
<b>Laser</b>	
Type	Nd:YAG
Wave length	532 nm
Output energy	150 mJ (normal)
Pulse width	200 ps
Repetition rate	1 – 4 pps (4 pps normal)
<b>Receiving electronics</b>	
Detector type	PMT (static crossed-field)
Quantum efficiency	29 %
Rise time	120 ps
Gate position	2 μs – 130 ms (computer controlled)
Gate width	0.2 μs – 33 ms (computer controlled)
Flight time counter	20 ps resolution
<b>Control</b>	
Mount control	DC servo amplifiers (45 A peak current) with torque motors, tachometers and encoders (manual, computer and computer aided)
Data flow rate	30 Hz
<b>Clock</b>	
Frequency standard	a Rubidium ( $2 \times 10^{-11}$ ) oscillator
Comparison	multi-Loran C waves (NW Pacific Chain)
<b>Computer</b>	
CPU	PDP 11/60 (64 kw Mos- and 1 kw cache memory)
Peripherals	two 5.2 Mbyte disk drives, a magnetic tape unit, a paper tape reader/punch, a hardcopy terminal and a CRT display



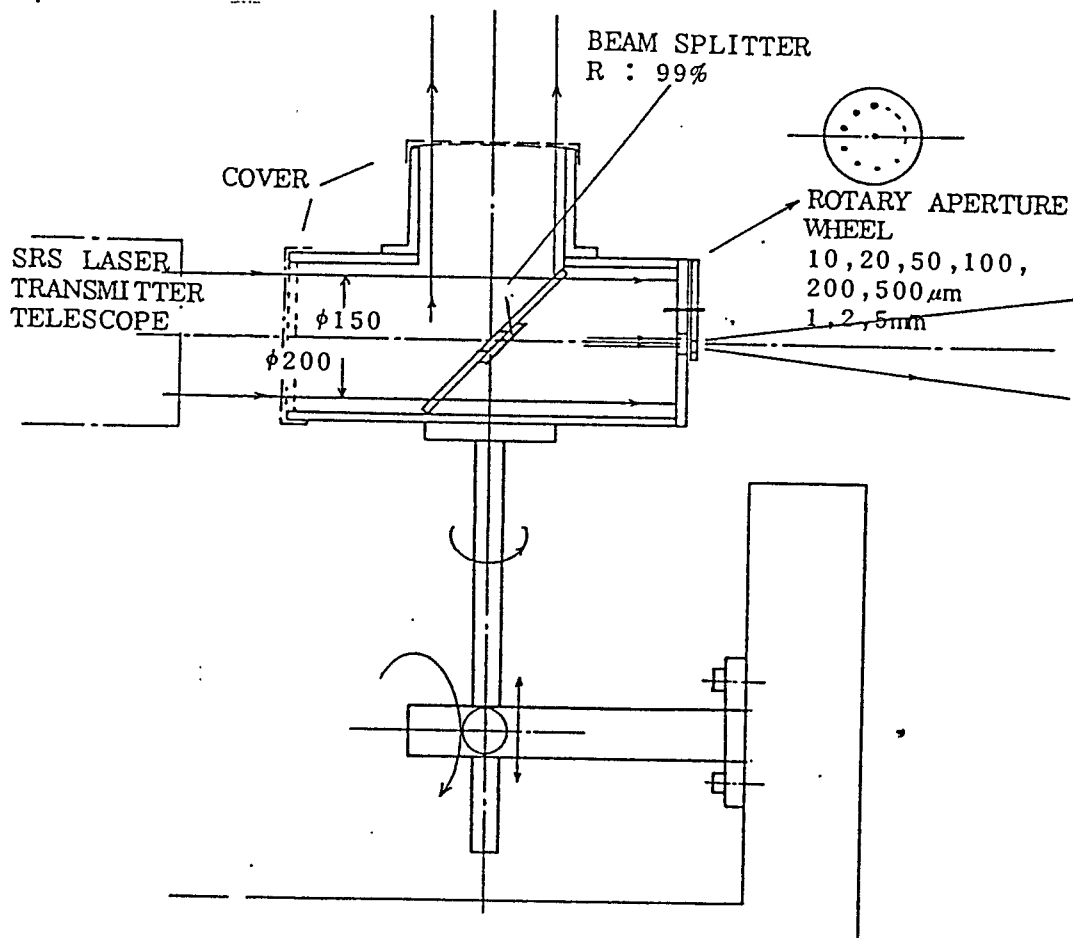
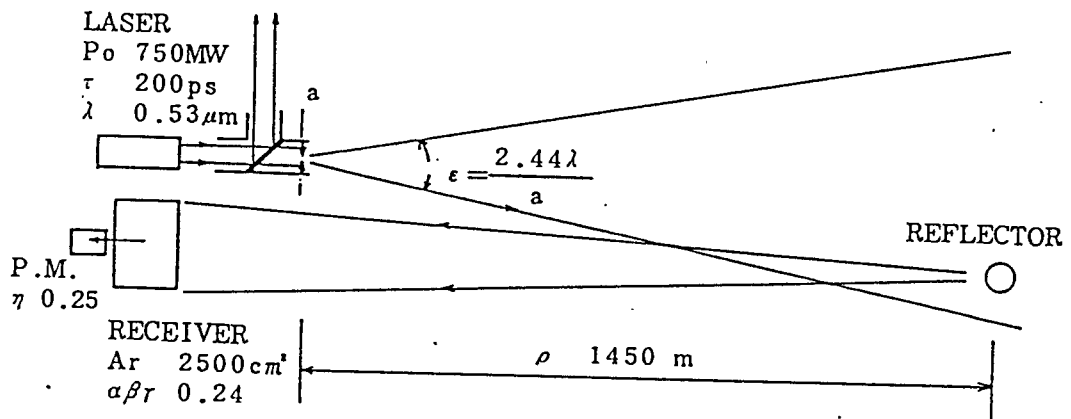


Fig. 5 Laser Attenuator for Ground Target Ranging

# Marine Geodetic Controls around Japan

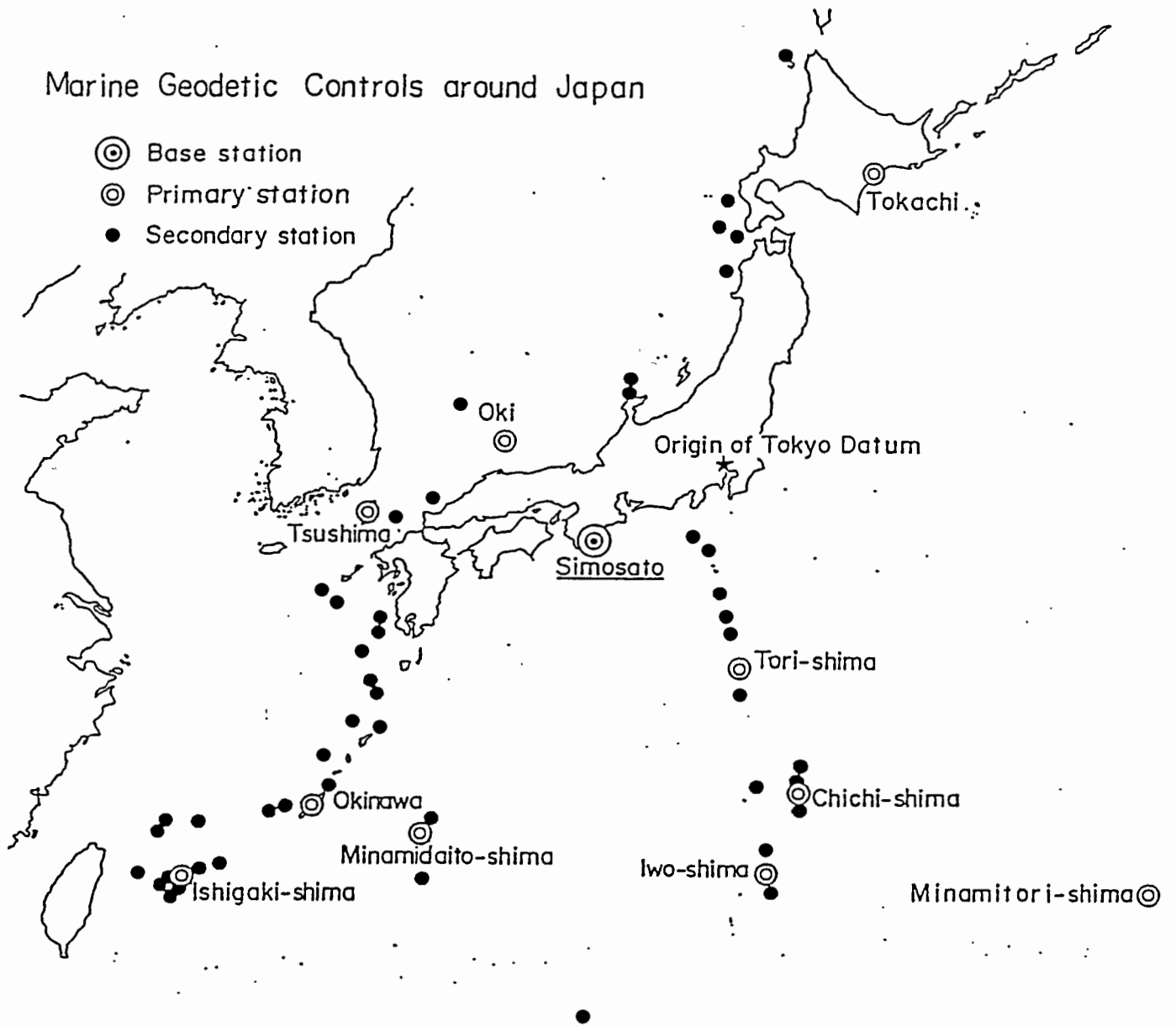


Fig. 6 Isolated Island where Observation by HTLRS is expected ( with double circle )

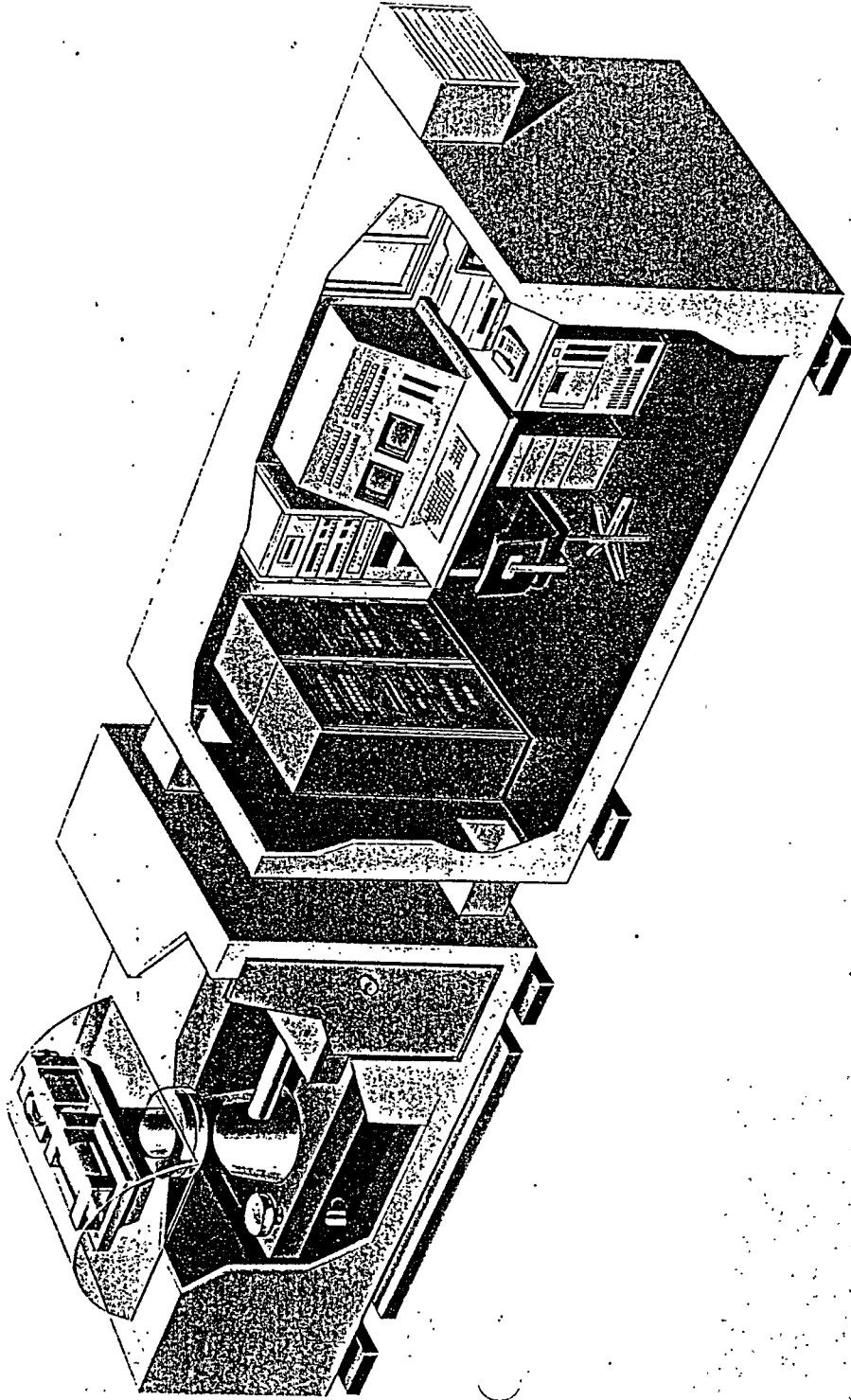


Fig. 7 HTLRS Housed in Shelters

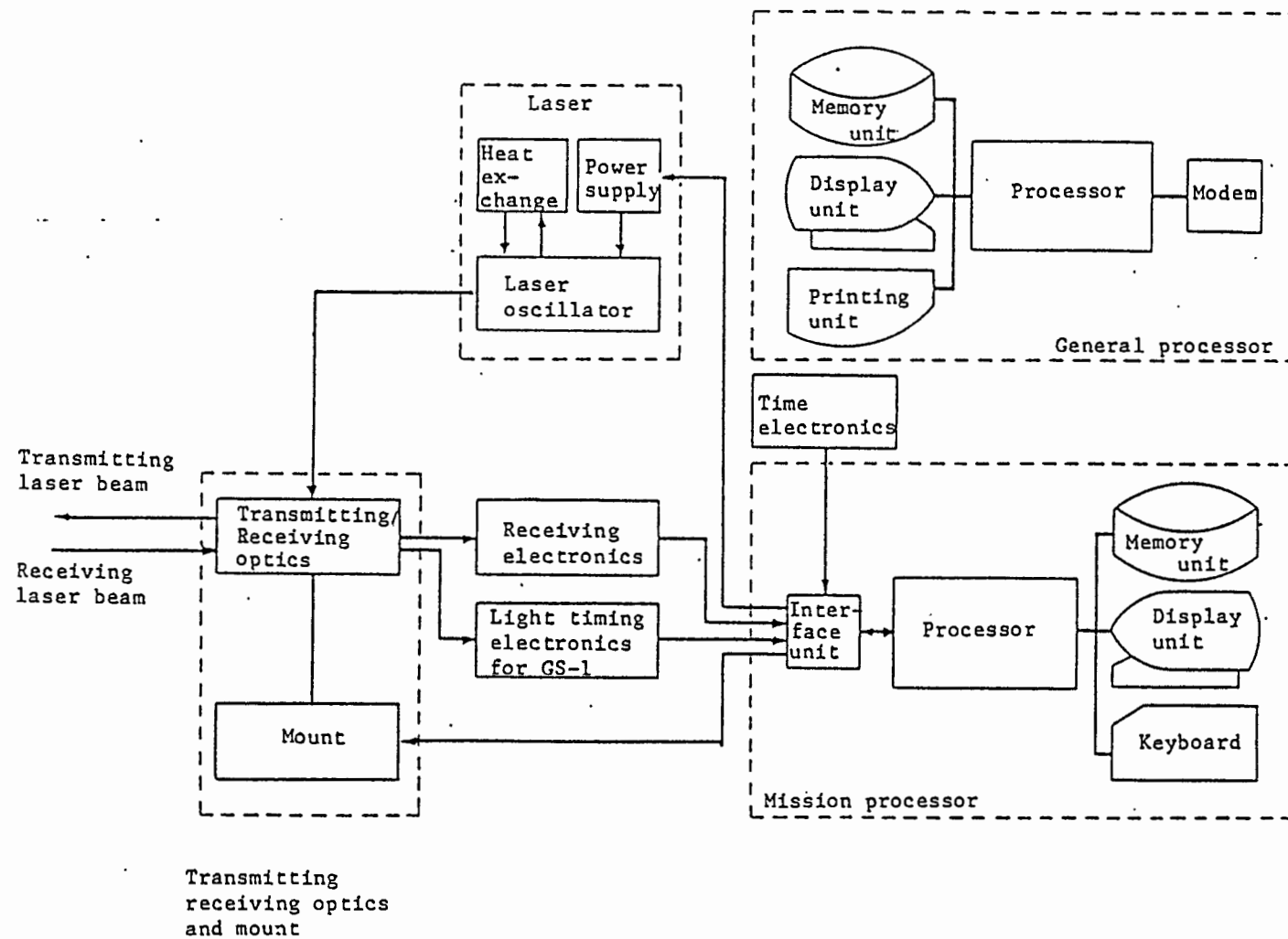


Fig. 8 System Cofiguration of the HTLRS

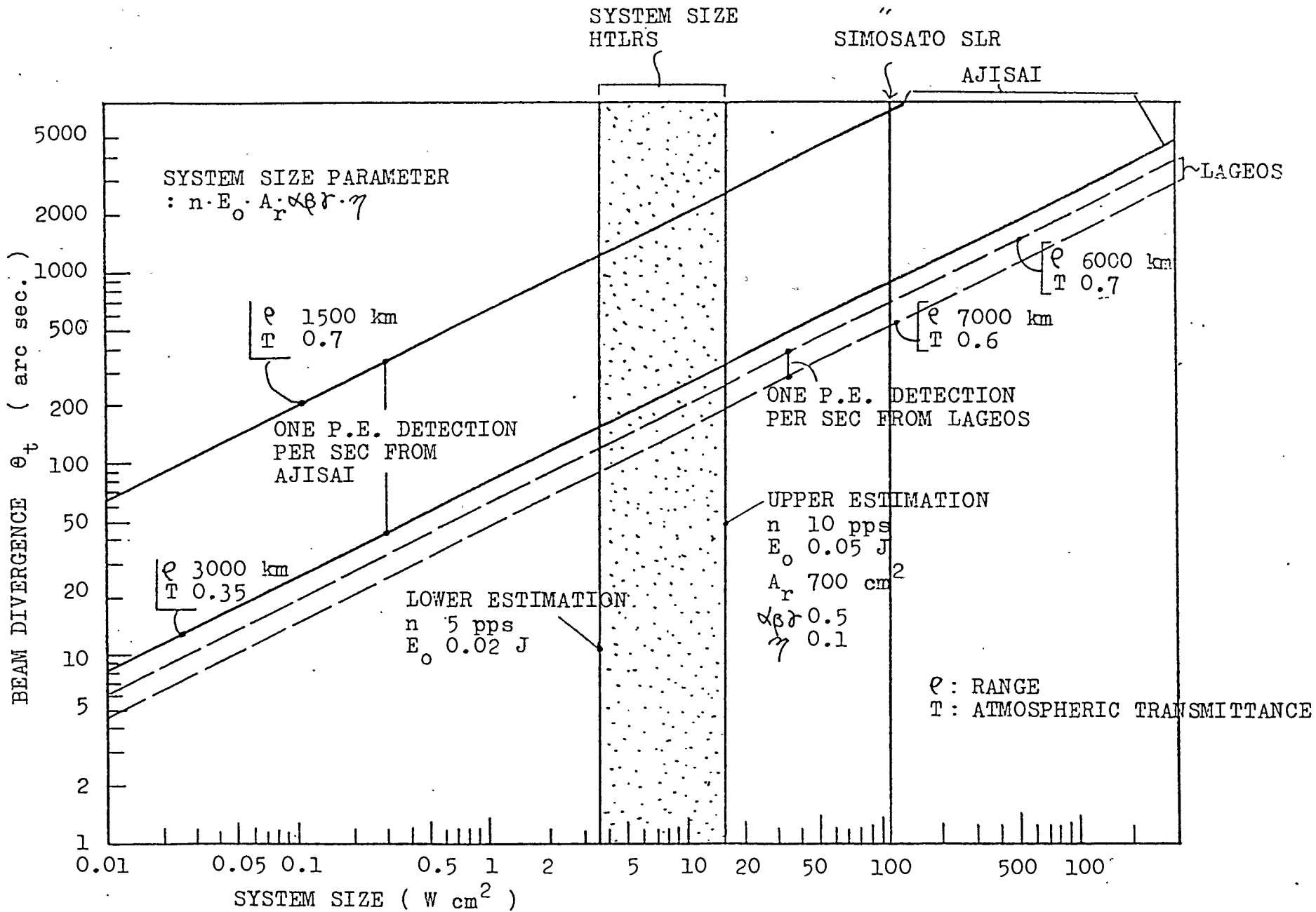


Fig. 9 System Size of the HTLRS

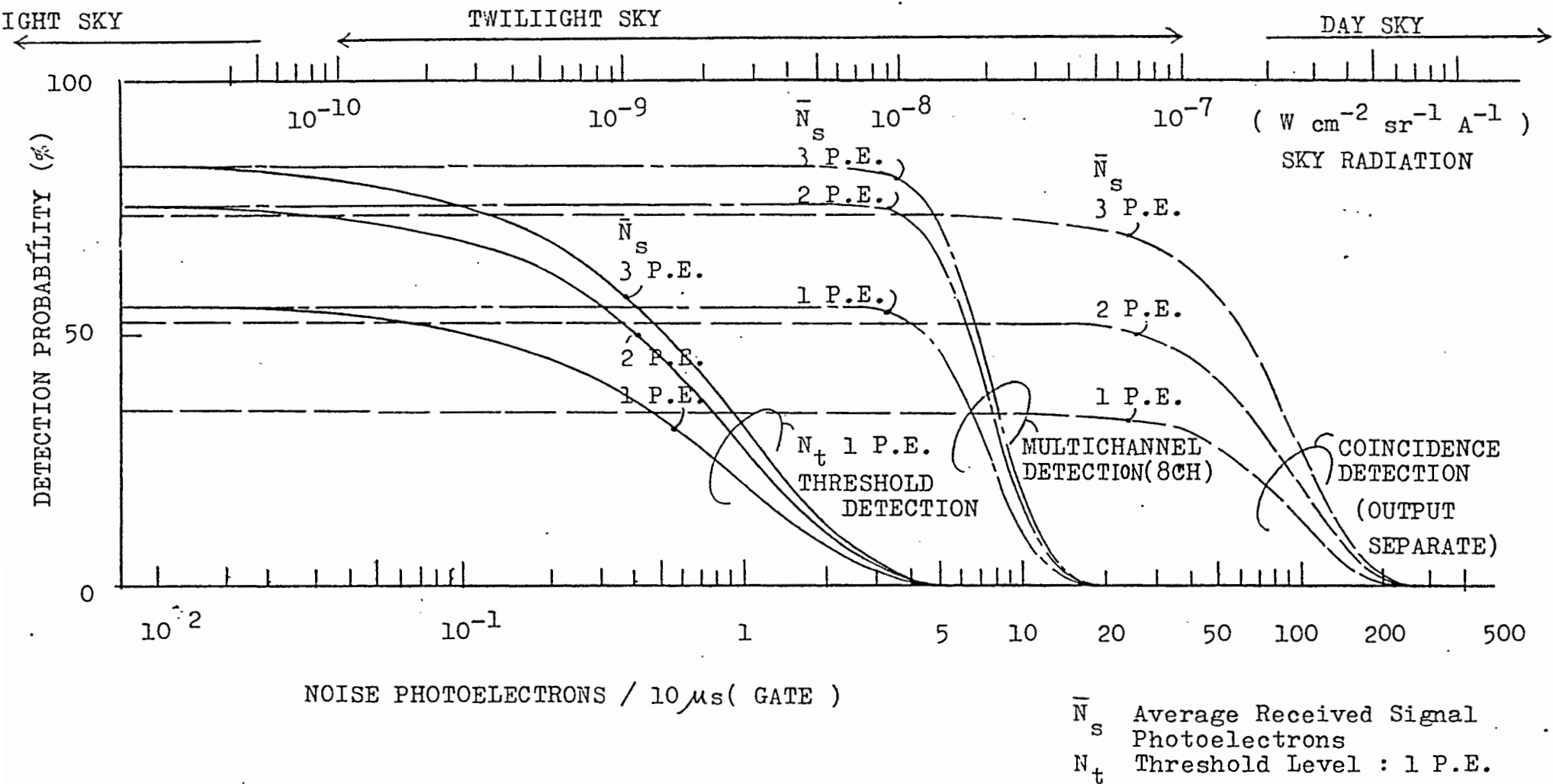


Fig. 10 Calculated Detection Probability of the HTLRS

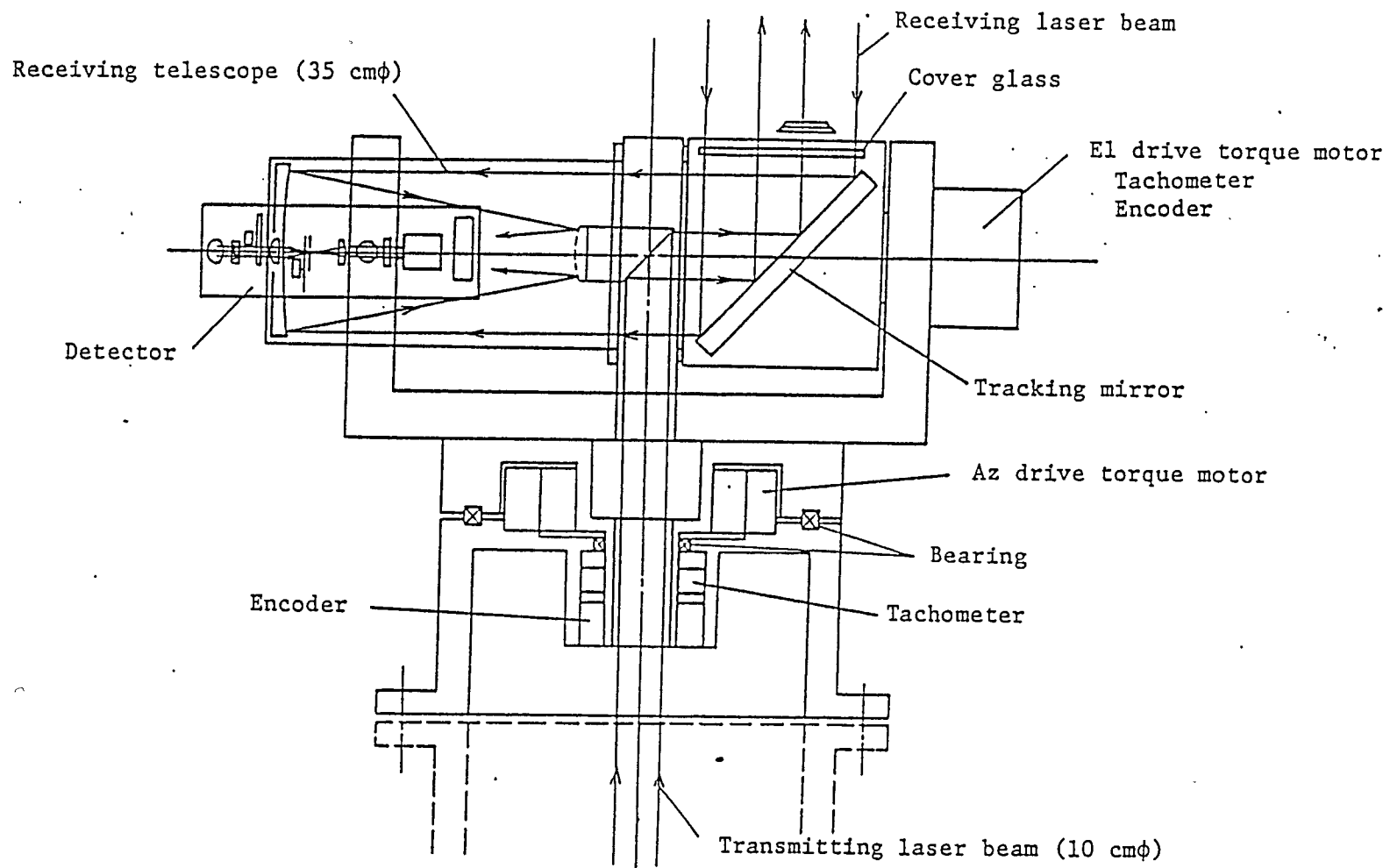


Fig. 11 Optics / Mount of the HTLRS

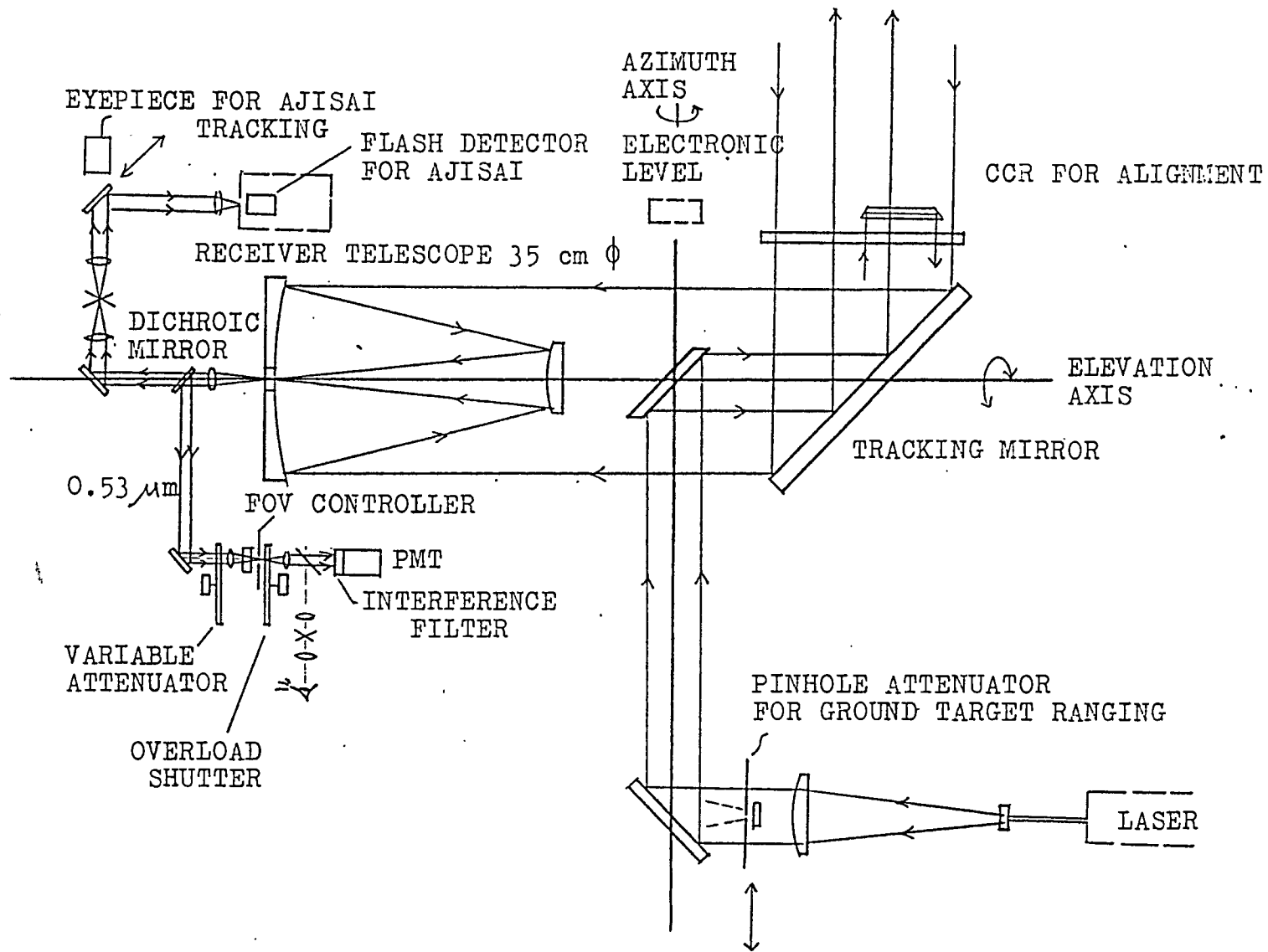


Fig. 12 Optical Configuration of the HTLRS



## PROGRESS IN SLR AT SHANGHAI OBSERVATORY

Z. Wen-Yao, T. De-Tong  
Shanghai Observatory  
Academia Sinica  
Shanghai - China -

Telephone 386191  
Telex 33164 SHAO CN

### ABSTRACT

SLR work at Shanghai Observatory was started in 1975, while development of the second-generation SLR system, with the aperture of the telescope 60 cm and the width of the Nd:YAG laser pulse 4-5 nsec, was begun in 1978. During the MERIT Main Campaign the Laser Geodynamic Satellite LAGEOS has been successfully observed with this laser system. According to the CSR analyses, the accuracy of our data for single shot is about 15 cm. In that period, the system has the capability of a maximum range of about 8542 km, the lowest elevation angle of 20 degrees for LAGEOS and the longest track arc of 45 minutes in a pass.

After MERIT Campaign we began to set up a new Nd/YAG frequency-doubled mode-locked laser ranging system in order to improve the accuracy of LAGEOS ranging.

## PROGRESS IN SLR AT SHANGHAI OBSERVATORY

Contact: Zhu Wen-yao, Tan De-tong  
Shanghai Observatory  
Academia Sinica  
Shanghai, China

Tel: 386191  
Telex: 33164 SHAO CN

### 1. THE SLR EXPERIMENTAL SYSTEM WITH 5 CM ACCURACY AT SHANGHAI OBSERVATORY

SLR work at Shanghai Observatory was started in 1975, while development of the second-generation SLR system, with the aperture of the telescope 60 cm and the width of the Nd:YAG laser pulse 4-5 nsec, was begun in 1978. During the MERIT Main Campaign the Laser Geodynamic Satellite LAGEOS has been successfully observed with this laser system. According to the CSR analyses, the accuracy of our data for single shot is about 15 cm. In that period, the system has the capability of a maximum range of about 8542 km, the lowest elevation angle of 20 degrees for LAGEOS, and the longest track arc of 45 minutes in a pass.

After MERIT Campaign we began to set up a new Nd:YAG frequency-doubled mode-locked laser ranging system in order to improve the accuracy of LAGEOS ranging. This system consists of an oscillator, a pulse selector, two amplifiers and a frequency-doubler. The oscillator mode-locked by using both acousto-optic modulator and saturable dye produces a sequential laser pulse trains.

The width of each pulse with TEMOO mode is 32 picoseconds. The pulse selector extracts one single pulse out of the pulse train, then is amplified through the two amplifiers. The output energy from the amplifiers is about 100 mj per pulse at 1.06  $\mu\text{m}$ . In order to match the pulse width with the rise time of receiving system, the pulse width are expanded to 120 ps by using two F-P mirrors. After frequency doubled with a KDP crystal, the output energy is now 30-50 mj at 0.53  $\mu\text{m}$ . The block diagram of Nd:YAG mode-locked laser system is shown in Fig. 1. The width of output pulse has been measured with a streak camera, it is shown in Fig. 2.

A 8-bit microcomputer with 64k byte memory is used for real-time tracking control which is made in China. The accuracies of both predicting and tracking are about 10 arcseconds.

In Nov. 1985, the mode-locked laser system was set up at Zo-Se Station of the Shanghai Observatory. On Dec. 12, 1985, we received the first echo from LAGEOS by the new laser system. Five passes with 606 data were obtained

during the experimental stage. These data had been preprocessed with a residual analytic program of our Observatory. The result is shown in Table 1 and Fig. 3-6. Meanwhile we transmitted these quick-lock data to NASA/GITN. The GITN and CSR have analyzed these data, Table 2 lists their results.

From Table 1, 2, we can see that the accuracy of this new SLR system is about 5 cm for single shot.

In order to explore the stability of the experimental system, a ground target set on the top of a water tower separated by 675.6 meters away from the laser, is used for calibration of the laser system. apertures of different size representing different return signal strength have been used on both receiving and transmitting telescopes to simulate the return signal strength from the satellite. The results of the calibration for ground target indicate that the stability of mode-locked ranging system is about 0.11 ns (2 cm). See Table. 3.

It is expected that the third-generation SLR system at Shanghai Observatory will be in routine operation from Sept. 1986 onwards.

## 2. SLR DATA ANALYSIS

During the MERIT Main Campaign, as one of the Associated Analysis Center, the Shanghai Observatory had processed the global data of LAGEOS satellite, using the software named SHORDE, which stands for Shanghai Observatory Orbit Determination Processor. The results obtained are A series of ERP-ERP (SHA) 85L01. It lists the solutions for two components of polar motion for each 5-day arc since the beginning of Sept. 1983. The interval precision is approximately 2.1 mas for  $x_p$ , 2.2 mas for  $y_p$  and 0.13 ms for  $D_R$ . In addition, the ability to detect the rate of change of polar motion  $\dot{x}_p$  and  $\dot{y}_p$ , with 5-day arc solution has been estimated to be approximately 1 mas/day.

The accuracy of the determination of the orbit of LAGEOS satellite is about 14 cm for each 5-day arc from the overall weighted RMS fit of the laser observations to the orbits.

Using SHORDE software, we determined the length of the baseline between two Chinese SLR stations of Shanghai Observatory and Xian Institute of Geodesy and Cartography. All observational data are divided into two arcs: 5-day arc from 18 through 22, Oct. 1984 and 4-day arc during 23-26, Oct. 1984. They are processed respectively. The weighted mean value of two solutions is equal to  $1192562.89 \pm 0.11$  m. The obtained result can be for checking the length survey of geodetic triangulated network. The researching work of the determination of global plate motion and deformation using LAGEOS tracking data is also underway.

Recently we have also completed a program for the transfer of the full-rate data to normal point data. This program includes: (1) pre-processing of full-rate data, (2) generating short-arc/long-arc trajectories for LAGEOS and removing some of the effects of the unmodeled perturbations, and (3) obtaining normal point data and identifying bad observations.

## 3. THE CHINESE SLR NETWORK

The Chinese SLR network is also being developed. At present, this network consist of seven stations located at Shanghai, Wuhan, Changchun, Kunming,

Xian, Guangzhou, and Zhengzhou. The ranging accuracy of these stations, except the Shanghai and Wuhan Stations, is about 2. cm for single shot. By 1988, two SLR systems of the third generation will be joined into this network. The Chinese SLR network is aimed at geodesy, astronomy and geodynamcis applications such as building of the zero order geodetic controlling network, monitoring of the regional crustal deformation and so on.

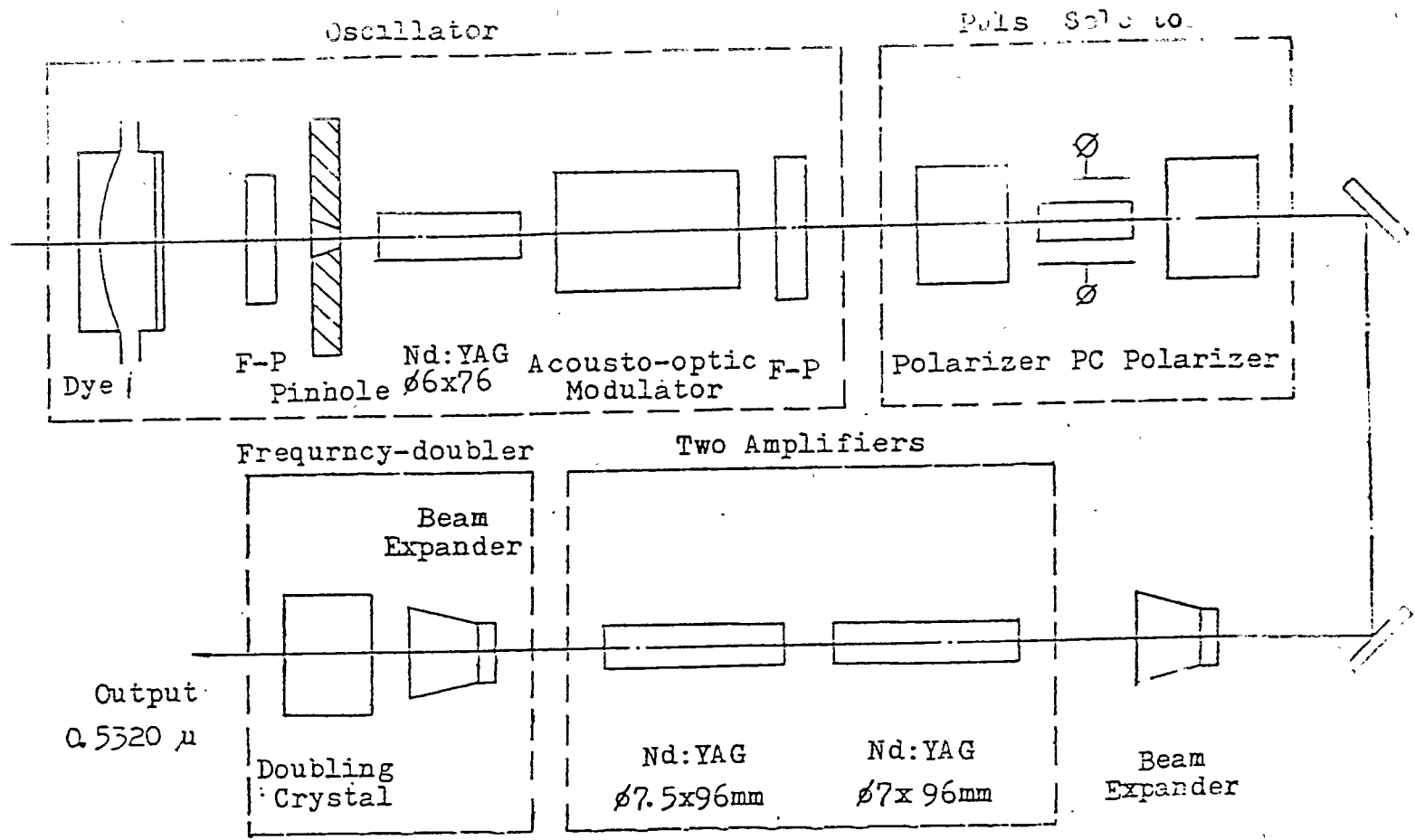


Fig.1 The Block Diagram of Nd:YAG Frequency-Doubled Mode-Locked Laser System

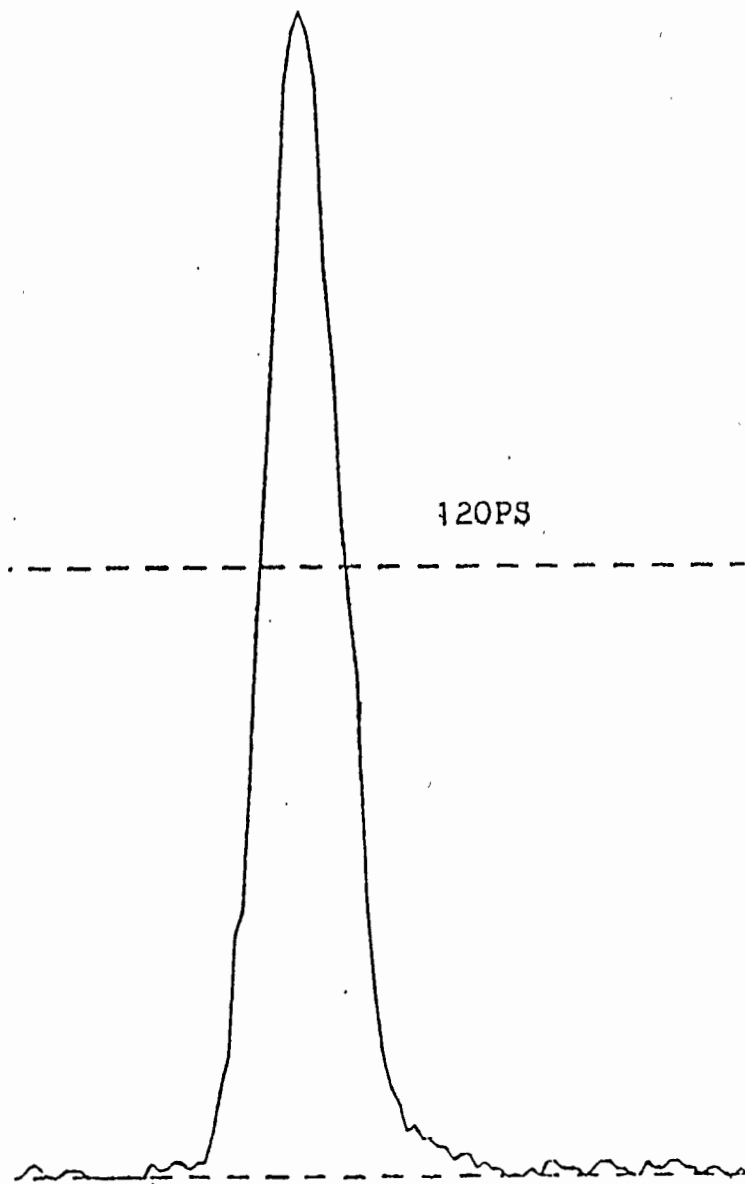


Fig.2 Pulse Width Measured with Streak Camera .

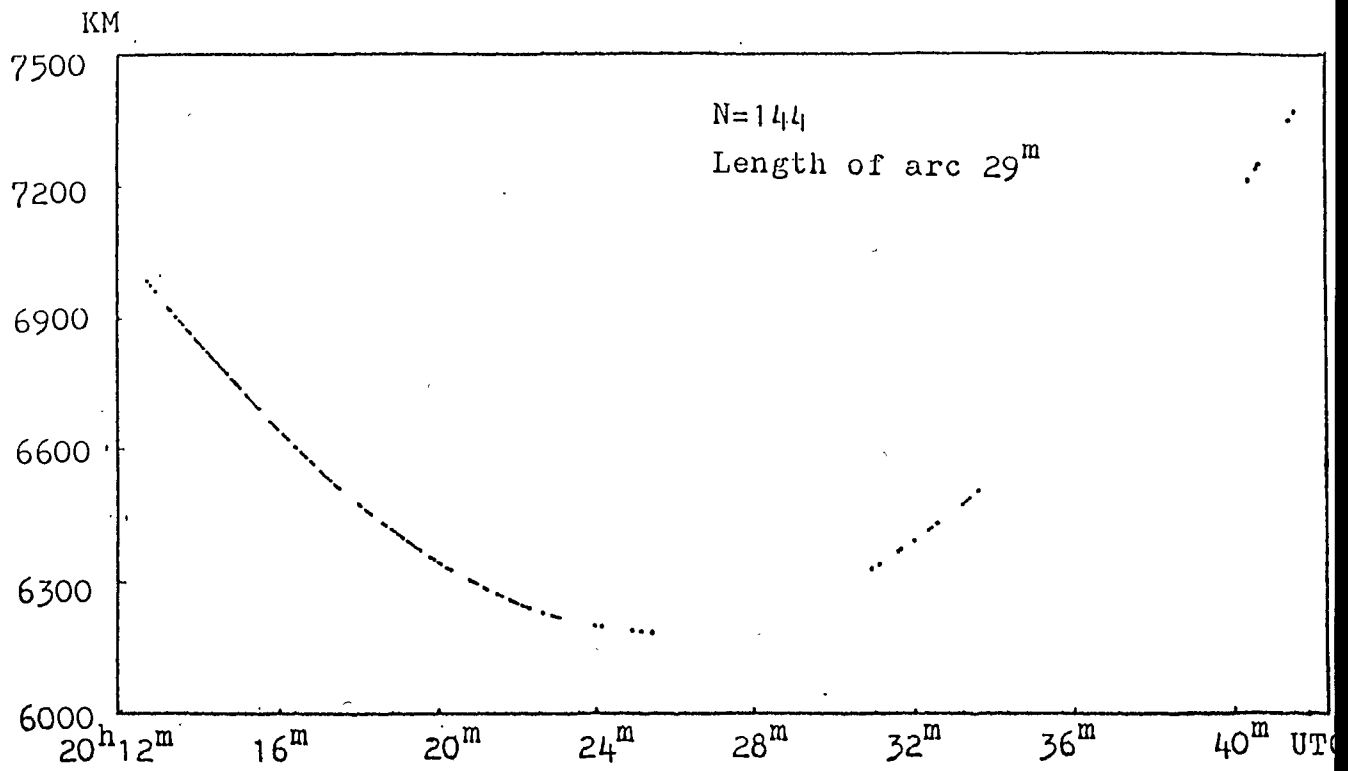


Fig.3 The Observing values for LAGEOS (Dec.16,1985)

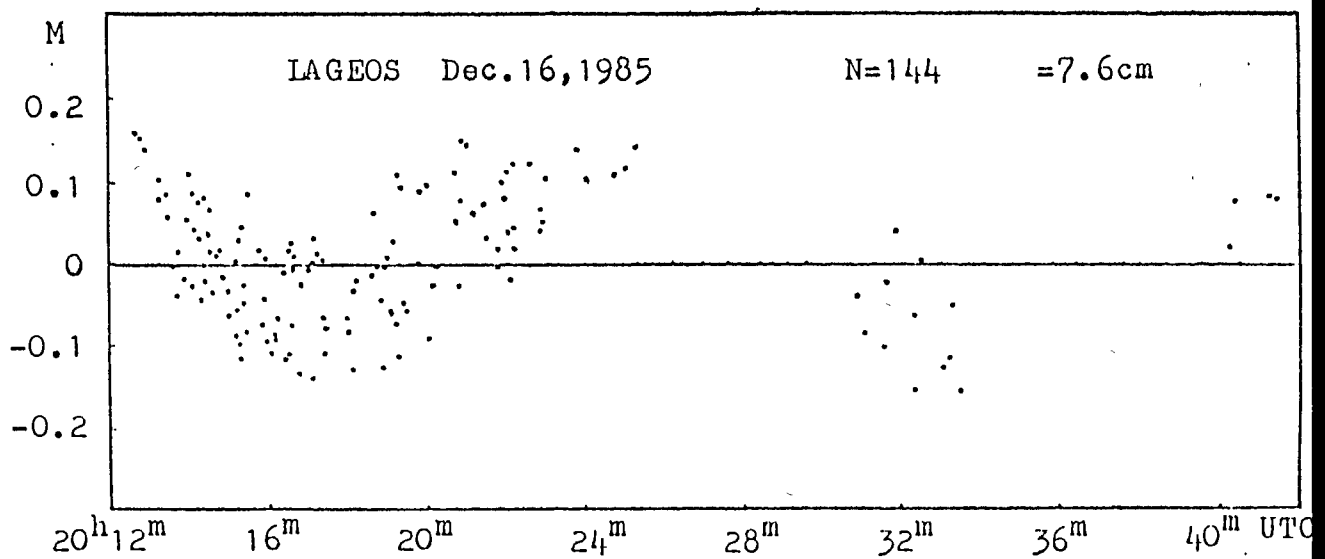


Fig.4 The residuals after polynomial fitting

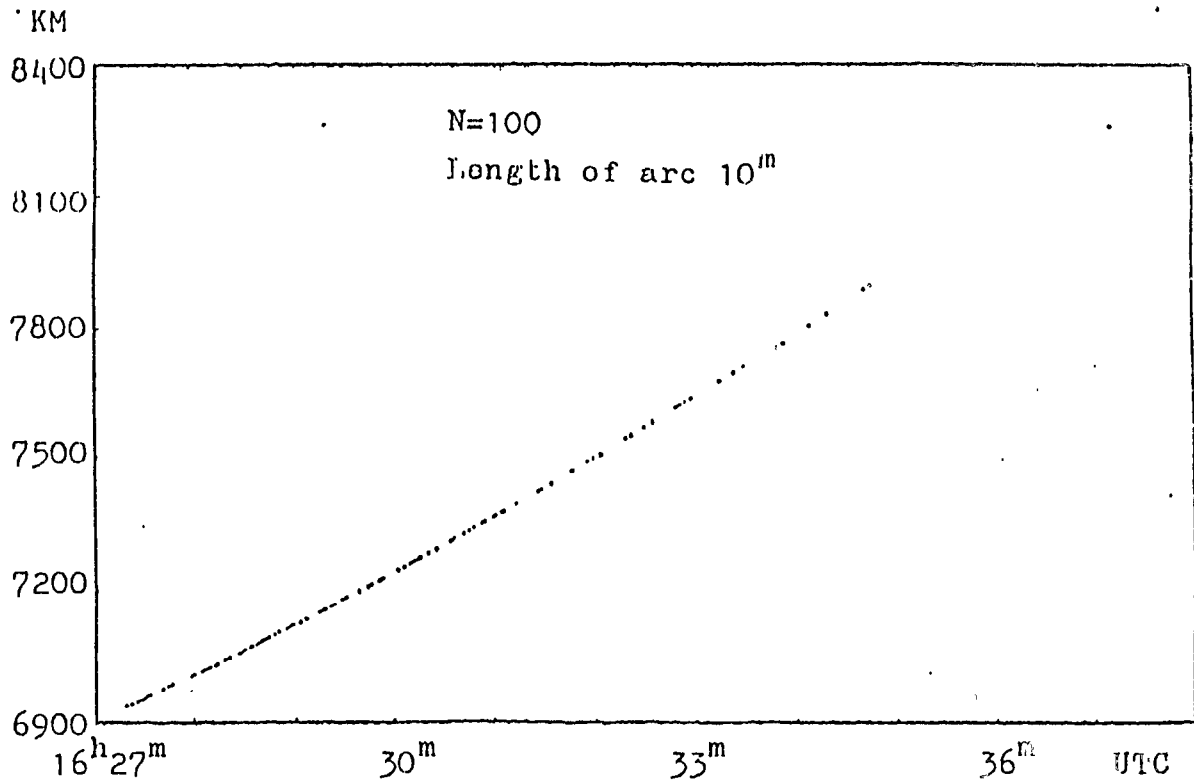


Fig.5 The Observing values for LAGEOS (Jan. 8, 1986)

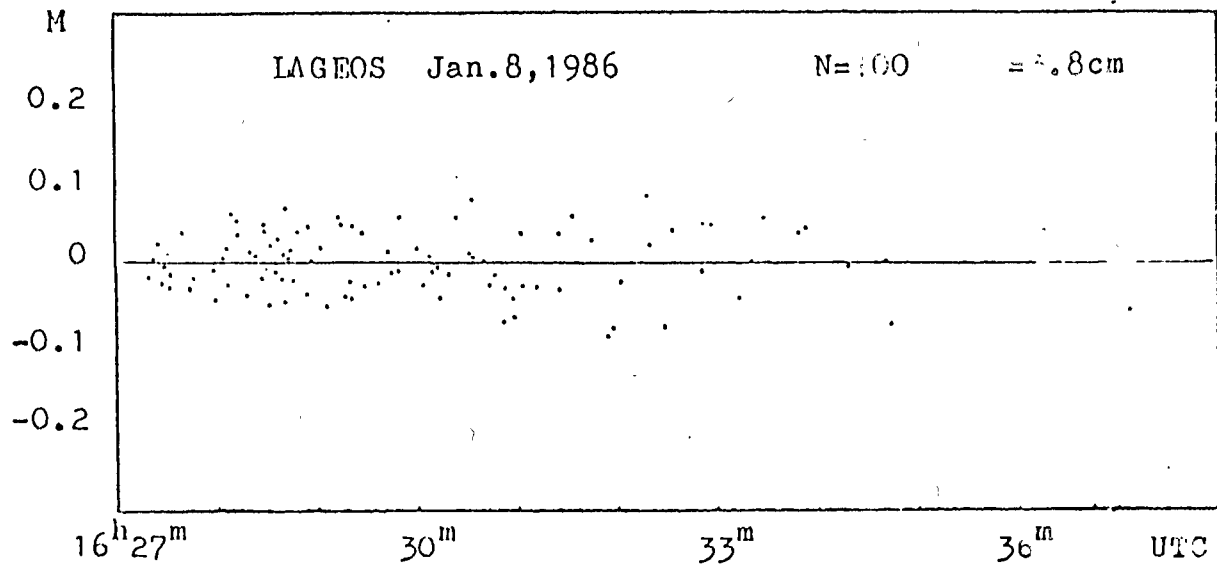


Fig.6 The residuals after polynomial fitting



Table 1 The Summary of Observation for IAGEOS with Mode-Locked Laser

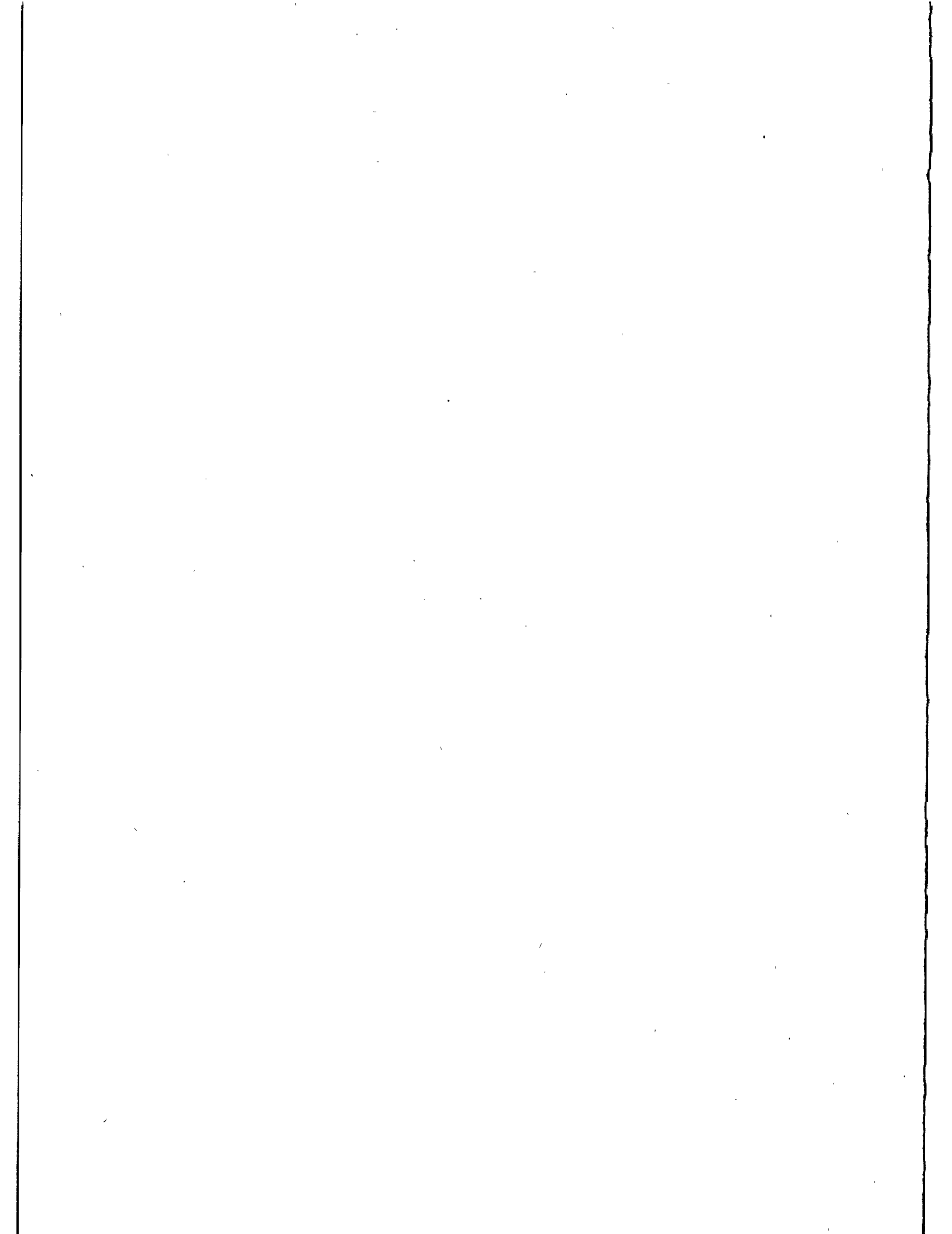
Date	Time	Length of arc	Total Obs.	Accuracy (cm)
Dec. 12, 1985	18 <sup>h</sup> 48 <sup>m</sup> --18 <sup>h</sup> 59 <sup>m</sup>	11 <sup>m</sup>	182	6.3
Dec. 16, 1985	20 <sup>h</sup> 12 <sup>m</sup> --20 <sup>h</sup> 41 <sup>m</sup>	29 <sup>m</sup>	144	7.6
Jan. 5, 1986	17 <sup>h</sup> 43 <sup>m</sup> --17 <sup>h</sup> 56 <sup>m</sup>	13 <sup>m</sup>	133	6.1
Jan. 8, 1986	17 <sup>h</sup> 21 <sup>m</sup> --17 <sup>h</sup> 37 <sup>m</sup>	10 <sup>m</sup>	131	6.9
Jan. 9, 1986	19 <sup>h</sup> 16 <sup>m</sup> --19 <sup>h</sup> 23 <sup>m</sup>	7 <sup>m</sup>	16	5.0

Table 2 The Results of Analysis at GLTN and CSR

Date	No. of the Obs. Sent	GLTN		CSR	
		Good Obs.	Accuracy (cm)	Good Obs.	Accuracy (cm)
Dec. 12, 1985	80	61	7.2	75	6.4
Dec. 16, 1985	50	49	4.9	49	5.9
Jan. 5, 1986	100	97	4.5	97	4.4
Jan. 8, 1986	100	100	3.5	100	3.8
Jan. 9, 1986	15	14	6.0	14	5.2

Table 3 Calibrated Stability for Ground Target (Dec. 16, 1985)

Transmitter Aperture(cm )	Receiver Aperture(mm )	No. of Measure	Value of Obs.(ns)
1 x 4	2	51	4650.19
1 x 4	8	54	4650.15
1 x 4	2	97	4650.09
0.5 x 4	2	53	4649.97
1 x 4	2	69	4649.91
0.3 x 4	1	11	4650.16
Average			4650.08 ± 0.11



## INTERKOSMOS LASER RADAR, VERSION MODE LOCKED TRAIN

K. Hamal, M. Cech, H. Jelinkova  
A. Novotny, I. Prochazka  
Czech Technical University  
Faculty of Nuclear Science and Physical Eng.  
Brehova 7, 115 19 Prague - Czechoslovakia -

Telephone 848840  
TWX 121254 FJFI C

B.B. Baghos, M. Tawadros, Y. Helali  
Helwan Institute of Astronomy and Geophysics  
Academy of Scientific Research and Technology  
Helwan, Cairo - Egypt -

TWX 93070 HIAG UN

### ABSTRACT

The INTERKOSMOS 2.generation satellite laser station, built in 1980, located in Helwan, has been operating since 1982 in the mode locked train version. To improve the performance several upgradings have been made since 1984. To improve RMS, the new Start detector and HP5370B counter have been implemented. To improve the reliability the transmitter has been placed into the Coude. To study new detectors, the independent receiver chain No.2, consisting of Newtonian 32 cm telescope, detector and HP5360 counter has been implemented. This arrangement allows to apply different detectors including solid state silicon diode operating at room temperature on single/multi photon signal level.

## INTERKOSMOS LASER RADAR, VERSION MODE-LOCKED TRAIN

K.Hamal, M.Čech, H.Jelínková, A.Novotný, I.Procházka  
B.B.Baghos, M.Tawadros, Y.Helali

The INTERKOSMOS 2.generation laser radar, built in 1980 [1] located in Helwan, has been operating since 1982 in mode-locked train version [2]. To improve the performance several upgradings have been made since 1984.

To improve RMS, the new Start detector and HP5370B counter have been implemented. The Start Detector [3], using a transistor, contributed 50 psec to the RMS budget. The detector chain Nr.1 consists of PMT RCA31034A, two HP8447 amplifiers, ORTEC 473A discriminator and HP5370B counter.

To improve the reliability, the transmitter has been placed into Coude focus. A tremendous increase of the laser output stability was resulted. The laser transmitter itself was examined to identify the optical elements influencing the beam quality [4]. The saturable dye was tested under different conditions [5].

To study new detectors [6], the independent receiver chain Nr.2, consisting of the Newtonian 32cm telescope, detector and HP5360 counter has been implemented. This arrangement allows to apply different detectors (solid state diode [6]), while routine ranging has been provided using the original receiver chain Nr.1. To have a comparison, the MCP PMT Varian has been tested at the indoor calibration facilities [7].

To collect data from both chains, the computer software package has been modified. To simplify the calibration, ranging and data processing procedures, some other modifications have been implemented into the software package.

The calibration and system stability tests have been acomodated to the upgraded version [10].

The strong signal response from the photodiode was measured at the indoor calibration facilities [9].

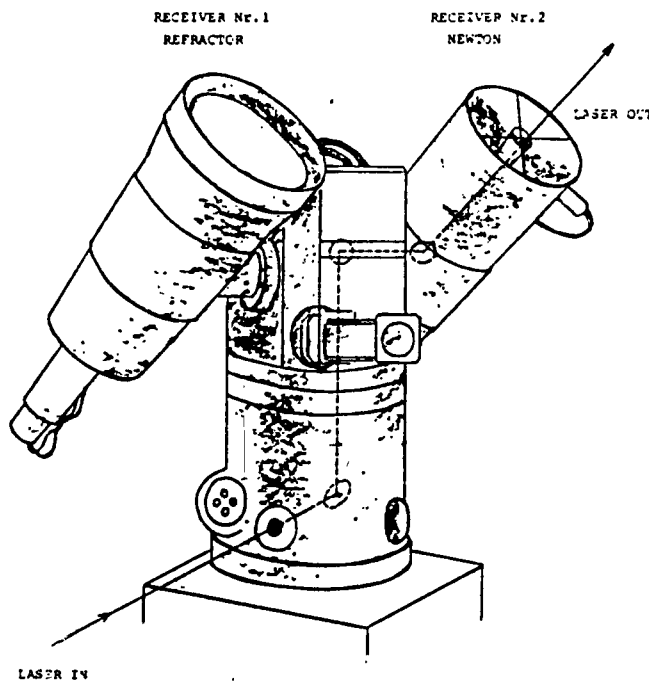
### Summary.

	before upgrading 1984	after upgraging 1986		
		PMT	MCP-PMT	diode
System stability (ps)	150	110		25
System jitter (ps)	520	300	100	100

Upgrading of the existing 2.generation laser station into 3.generation has been proposed [10].

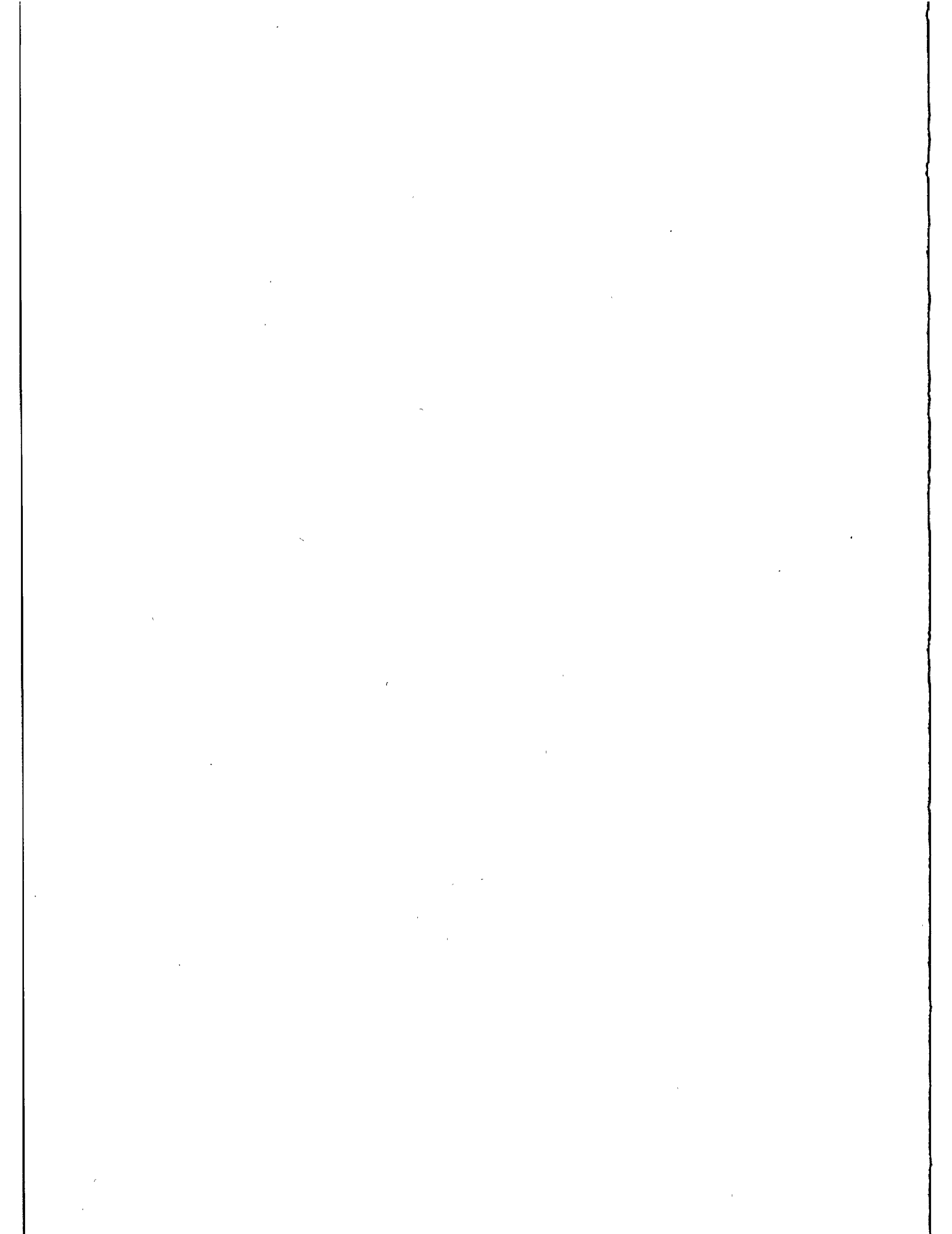
Abstracts:

- [1] K.Hamal, H.Jelinkova, A.Novotny, I.Prochazka, M.Cech  
INTERKOSMOS SECOND GENERATION SATELLITE LASER RADAR  
Proceedings of The Fourth International Workshop, Austin, 1983
- [2] K.Hamal, H.Jelinkova, A.Novotny, I.Prochazka  
INTERKOSMOS LASER RADAR, VERSION MODE LOCKED TRAIN  
Proceedings of The Fifth International Workshop, Greenwich, 1984  
In this Proceedings:
- [3] I.Prochazka  
START DETECTOR FOR MODE LOCKED TRAIN LASER RADAR
- [4] H.Jelinkova, J.del Pino, P.Valach  
SPATIAL STRUCTURE OF THE DOUBLED ND:YAG LASER TRANSMITTER BEAM
- [5] K.Hamal, H.Jelinkova, STABLE SATURABLE DYE FOR 1.06UM
- [6] K.Hamal, H.Jelinkova, I.Prochazka, B.Sopko, SINGLE PHOTON  
SOLID STATE DETECTOR FOR RANGING AT ROOM TEMPERATURE
- [7] I.Prochazka, K.Hamal, J.Caignebet, MICROCHANNEL/DYNODE PMT  
COMPARISON EXPERIMENT
- [8] K.Hamal, I.Prochazka, SYSTEM STABILITY USING MODE LOCKED TRAIN
- [9] I.Prochazka, K.Hamal, H.Jelinkova, PICOSECOND LASER RANGING  
USING PHOTODIODE
- [10] K.Hamal, I.Prochazka, 3.GENERATION/VERSION MODE LOCKED TRAIN



View of the mount. Refractor receiver Newton receiver.

2.Generation Mode Locked Train, Helwan 1986				
UPGRADINGS 1985 - 1986				
RMS	START DETECTOR <50ps COUNTER HP5370B			
LASER RELIABILITY	COUDE LASER SYSTEM BEAM STRUCTURE SATURABLE DYE			
EXPERIMENTAL RECEIVER No.2	NEWTONIAN 32CM			
SOLID STATE DETECTOR	SINGLE MULTI PHOTON DETECTION			
SOFTWARE PACKAGE	MODIFICATION TO SIMPLIFY CALIBRATION RANGING, DATA PROCESSING PROCEDURE			
	1984	1986		
	PMT	PMT	MCP PMT	DIODE
SYSTEM STABILITY ps	150	110		25
SYSTEM JITTER ps	528	308	100	100
K. Hamal, M. Cech, H. Jelinkova, A. Novotny, I. Prochazka Interkosmos Laser Radar, Version Mode Locked Train				1



UPGRADES AND NEW DEVELOPMENTS  
ON SATELLITE LASER RANGING  
STATION FROM GRASSE

F. Pierron and the laser staff  
Observatoire de Calern  
Causols  
06460 Saint Vallier de Thiey - France -  
  
Telephone 93 42 62 70 - 93 36 58 49  
Telex 470865 F

ABSTRACT

The Grasse Satellite Laser Station, operating since 1978, in a first step with a decimeter accuracy has successively been upgraded.

At first the ruby laser was replaced by an active mode locked Nd:YAG laser in 1984 and it puts the system at a centimeter level.

After that, in view to give to this station a total efficiency and autonomy the replacement of the computer was undertaken and this improvement should be ready before the end of 1986.

This paper describes the station today (hardware and software), its performances and its possibilities.

## 1.OVERVIEW OF THE SATELLITE LASER RANGING FROM GRASSE

=====

The Satellite Laser Ranging of GRASSE is, in fact, installed in the mountains just above Grasse where the astronomical Observatory of the CERGA has been built. (Annexe 1.)

The site is a plateau at a 1250 meter altitude at 20 Kilometers from Grasse and the weather is particularly favorable to Laser Ranging.

This S.L.R. Station developed in the Years 75-78 and entirely financed by the French Spatial Organisation (C.N.E.S.) obtained the first returns in 1978 and, since this time, in spite of some interruptions, it has provided to the Scientific community a lot of data of an increasing quality.

In order to minimize the interruptions of data, the modifications and upgrade have been carried out in stages.

In a first time the Ruby Laser System (3 Nanosecondes of PWHM) was replaced by an active Mode-locked ND:YAG in 1984 and in a second time (1985) the change of the computer and software was undertaken.

For this occasion, the software was totally refurbished in taking into account the new technology and the requirements for the data (great number of data, need of quick dispatching the results with the new link possibilities, ...)

This very important work is being terminated in a few weeks and so, the station will acquire all the possibilities of a modern station.



## 2.HARDWARE EQUIPMENTS

=====

Except the Mount,the Telescope and the computer,all the hardware equipments are installed in a shelter,where the operators stand during the ranging,close to the building.

The mount rests on a concrete pier at 3 meters from the ground and a floor independant from the mount allows to reach the equipment attached to the telescope.

### 2.1 MOUNT,TELESCOPE(Annexe 2)

-----

The optical system consists of:

- The Telescope(Cassegrain)proper of a diameter of 1 meter and a focal length of 8 meters;it is especially dedicated receiving light from returns.

- The transmitting afocal optics made of lenses with a diameter of 20 Centimeters.

-A sighting Refracting Telescope to achieve some adjustments(particularly the alignment of the transmitting and receiving axes,the firing direction,and to observe the satellites when they are illuminated.

As the Telescope,the Mount was designed,drawn and built in FRANCE,it is an altazimuth system with an absolute accuracy of about 10 arcseconds.

The encoders(absolute)have a resolution of 1.2 arcseconds (20 bits).

The laser beam is going to the transmitting optic through a coude path with five coated mirrors.

## 2.2 ND:YAG LASER(Annexe 3)

---

This transmitter built by QUANTEL FRANCE currently provides a single 200 Picoseconde pulse at a repetition rate of 5 Hertz or 10 Hertz.

One of the distinctive features of this system is that it is possible to operate the oscillator either in passive (with dye) or in active(with pockel cells) mode;this active mode is generally used for an easier operating.

An active mode-locker(at 70 Megahertz)in the cavity increase the stability of the pulse train.

At the outgoing of the oscillator,the slicer(with avalanches transistors)selects one pulse and,after a double pass and the final amplifier,the single pulse energy is currently 100 Millijoules per shot in the green.

## 2.3 TIMING EQUIPMENTS.(Annexe 4)

---

The chronometry is achieved by a Thomson event-timer of for channels(1 start and 3 stop).The resolution of this equipment is of 100 Picosecondes.

The start time is triggerred by a photodiode on the Laser bench and through a TENNELEC discriminator.

The Photomultiplier tube(RTC 2233b)is going replaced in a few time by a Micro channel plate HAMAMATSU PMT in view to increase the RMS of the data and reduce systematic biases. A constant fraction discriminator TENNELEC is used for the stop channels.

With such a configuration,the RMS currently achieved is from 3 to 5 Centimeters on a satellite pass.

## 2.4 COMPUTER:

-----

The Computer is a DIGITAL EQUIPMENT(DEC) PDP 11-73 with a memory size of one Mega-byte and an optional hardware to increase the speed of floating operations.

- Numerous specialized interfaces to control the Servo of mount, the encoders, the event-timer, electronic systems to elaborate the range gate,...

- \* 3 parallel I/O 64 bits

- \* 1 Real-time clock

- \* 1 Digital/Analog converter

-A Track-ball (connected by an asynchronous link) in view:

- \* To introduce corrections during the tracking

- \* To process the data

Different mass storages are connected to this computer:

- Two removable disk systems of 10 Mega-bytes

- \* One for the system.

- \* One for the software developments.

- One Winchester disk of 160 Mega-bytes

- \* Storage and editing the data.

One Magnetic Tape drive(one-half inch,1600 BPI)

\* Disk backups

\* Editing full rate data

\* Different exchanges

This computer is connected(by the VAX in grasse) to the computing center of CNES in TOULOUSE.

### 3.SOFTWARE

=====

The computer is running under the Real-time Multitask, Multiusers RSX 11 M PLUS Operating System.

According to their functions,all the modules were written either in Assembly language(Driver modules,Process control, Interrupt services routine modules,...) or in Fortran 77 Language for all the scientific calculations and every time it was possible.

The programs are accessible to the operators through a system of Menu .

The different possibilities are:

-Computing the shedules of a given satellite.

-Tracking:

\* Stars.

\* Satellite(Ranging)

\*Target(Calibration)

- Preprocessing Data
  - \* Manual
  - \* Automatic

- Editing
  - \*Quick-Look
  - \*Full rate Data

### 3.1 SCHEDULE COMPUTING(Annexe 5)

-----

Once a Month the Operator computes the Schedule of LAGEOS, STARLETTE and AJISAI(Rise time, Set time ,Max Elevation) in view to establish work schedule for the crew.

These computations are achieved with the IRV for LAGEOS and Keplerian Elements for other satellites.

### 3.2 TRACKING(Annexe 6 et 7)

-----

The capability to track the stars(direct and reverse) is needed to adjust the encoders and the parameters of the mount.

The tasks which control the tracking of a satellite are numerous.

-Preliminary computation of Site, Azimuth and range of the satellite every second of time.

In real time:

- Interpolating position(50 Hertz)
- \* Servo control of the mount(activation every 20 Milliseconds by internal clock)
  - Reading Encoders
  - Reading Track-Ball for correction
  - elaborating speed orders for servo amplifier site and azimuth
- \* Interpolating range and derived of range
- \* Loading Range Gate(Activation by an interrupt on firing,5 Hertz)
- \* Reading Start an Stop time on the event timer(Interrupt on the end of gate)
- \* Computing of residuals for the exact firing time(With predicted range and his derived)for later processing and recording on a file.
- \* Ploting on Graphic display residuals and informations for operator.
- \* Reading operator commands.

### 3.3 TARGET CALIBRATION(Annexe 8)

-----

After each pass,a calibration is achieved on a ground target erected at a distance of about 2.5 Kilometers.

Five hundred returns are recorded and processed.

The calibration is appended to the file of the preceding pass with the meteorological data.

### 3.4 PREPROCESSING DATA

-----

The preprocessing of the data is entirely based on the residuals computed during the pass.

To avoid to spend a lot of time to read files and to give more flexibility to the software,all the data are loaded in the memory of the computer at the beginning with managment memory facilities.

The data residuals are plotted on the graphic screen and the operator can execute with the Track-ball a manual cleaning (Annexe 9)of the data,after what an automatic algorithm(with polynomial fitting,elimination at 2.5 RMS and iteration) terminates the processing.(Annexe 10).

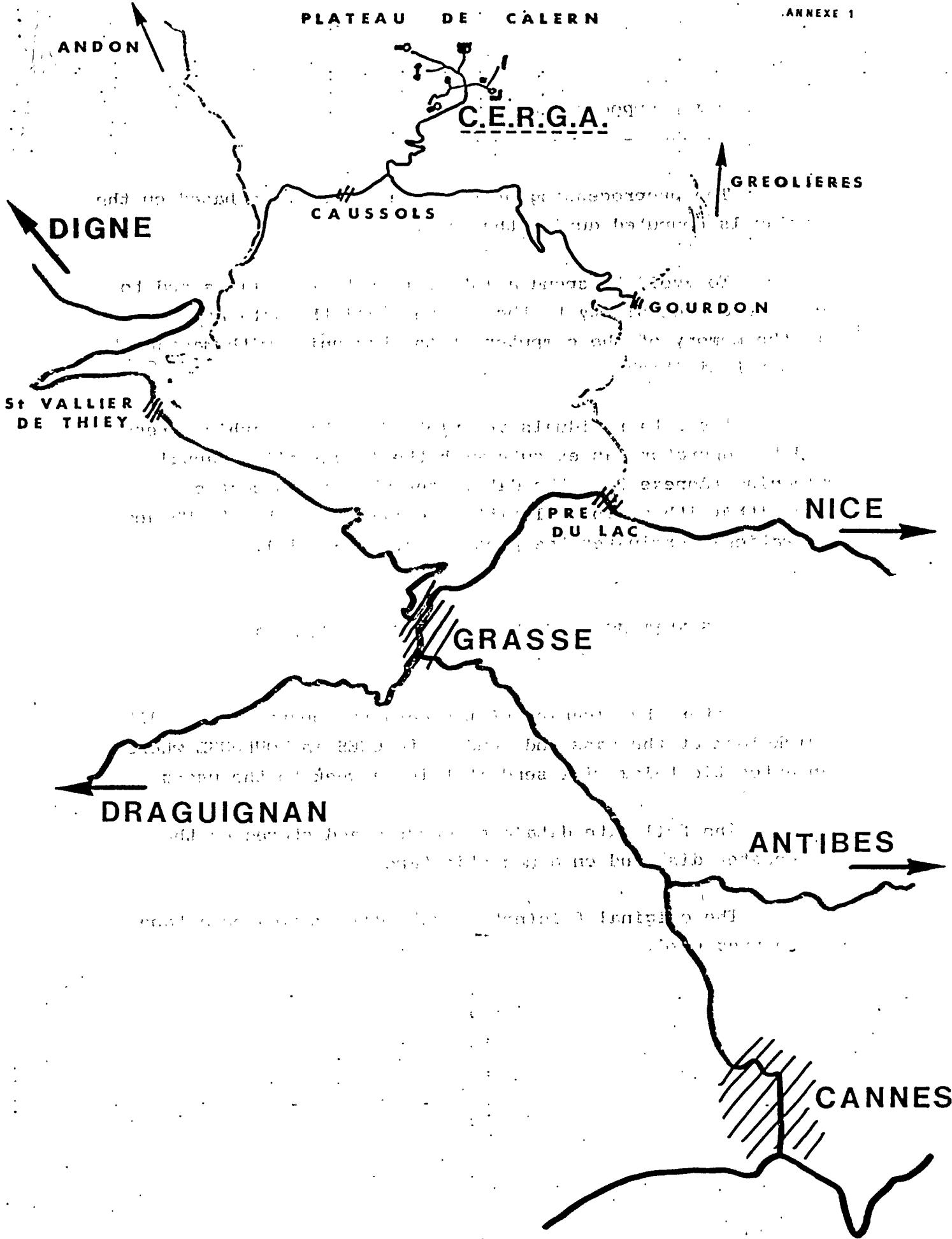
### 3.5 EDITING QUICK LOOK AND FULL RATE DATA:

-----

After the cleaning of the data,the operator can edit quick-look of the pass and send it to CNES in TOULOUSE where an automatic telex will send it twice a week to the users.

The full rate data are computed and stored on the Winchester disk and on a magnetic tape.

The original file(not processed)is copied on a tape to be preserved.



ANDON

C.E.R.G.A.

GREOLIÈRES

DIGNE

CAUSSOLS

GOURDON

St VALLIER  
DE THIEY

PRE  
DU LAC

NICE

GRASSE

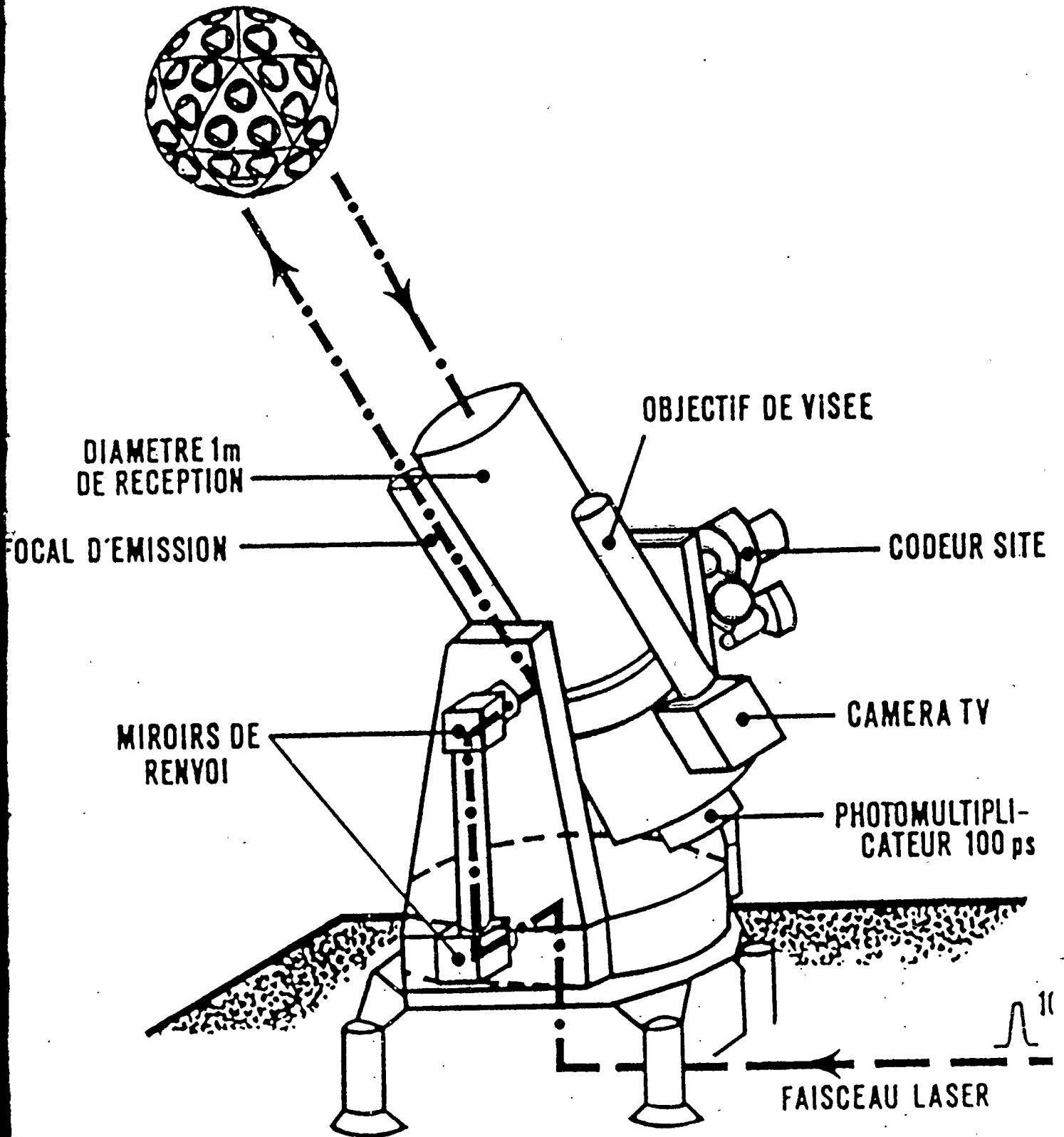
DRAGUIGNAN

ANTIBES

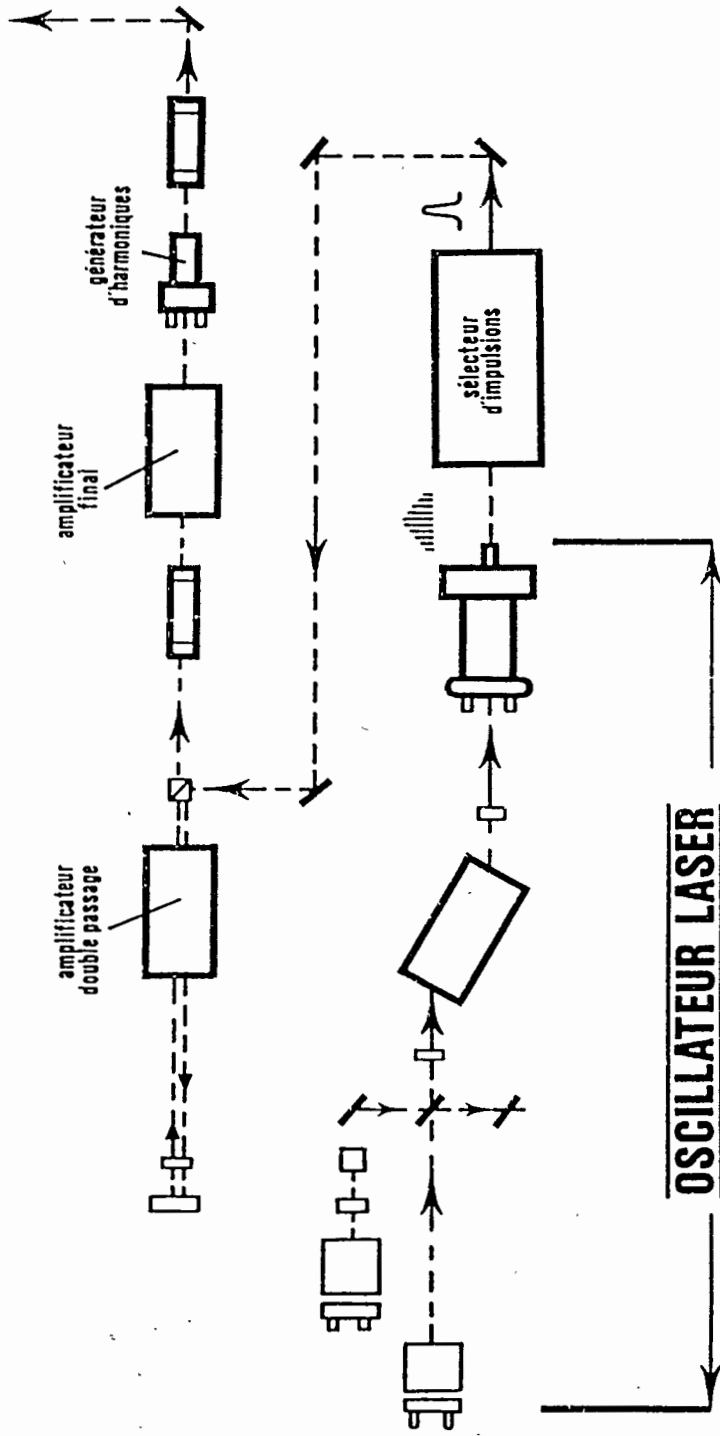
CANNES



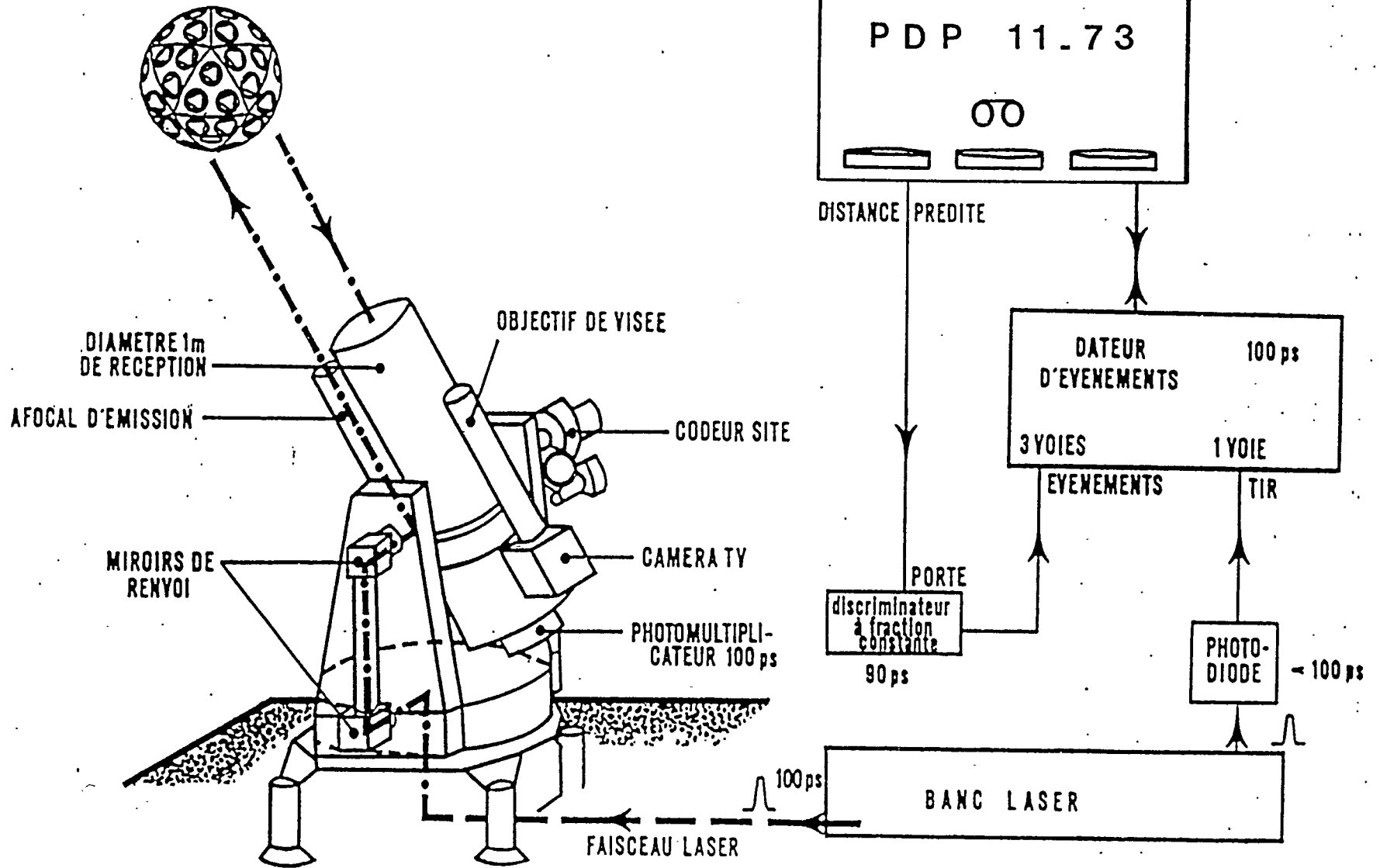
# SATELLITE GEODESIQUE



LASER 406  
100 ps



SATELLITE GEODESIQUE



ANNEXE DE LA BIBLIOTHEQUE

EGS DEBUT: MERCREDI 17 SEPTEMBRE 86

FIN: LUNDI 6 OCTOBRE 86

MERCREDI 17 SEPTEMBRE 86	10H 40H	21	-	164	116	77	+	390451	524031	643049
MERCREDI 17 SEPTEMBRE 86	12H 14H	68	-	223	106	62	+	218467	560735	689738
MERCREDI 17 SEPTEMBRE 86	14H 20H	65	+	264	15	69	-	100085	824278	688200
MERCREDI 17 SEPTEMBRE 86	16H 04H	62	+	290	40	93	-	23830	751231	597680
MERCREDI 17 SEPTEMBRE 86	18H 04H	74	-	296	175	131	+	5333	357961	487389
MERCREDI 17 SEPTEMBRE 86	20H 11H	25	-	284	223	183	+	41960	217866	336681
JEUDI 18 SEPTEMBRE 86	9H 13H	50	-	139	112	92	+	463852	542936	599109
JEUDI 18 SEPTEMBRE 86	11H 08H	12	-	207	119	64	+	264725	522064	681340
JEUDI 18 SEPTEMBRE 86	13H 04H	74	+	253	29	64	-	132543	783577	681815
JEUDI 18 SEPTEMBRE 86	15H 12H	59	+	284	37	83	-	39791	760764	626813
JEUDI 18 SEPTEMBRE 86	17H 14H	86	+	297	105	118	-	4402	563092	524984
JEUDI 18 SEPTEMBRE 86	19H 17H	37	-	288	220	153	+	28191	228312	392761
VENREDI 19 SEPTEMBRE 86	10H 15H	35	-	190	123	67	+	313778	509720	672569
VENREDI 19 SEPTEMBRE 86	12H 15H	83	+	240	59	62	-	169944	697595	687014
VENREDI 19 SEPTEMBRE 86	14H 18H	59	+	277	17	76	-	60790	819111	647626
VENREDI 19 SEPTEMBRE 86	16H 20H	73	+	295	63	106	-	9684	685685	559558
VENREDI 19 SEPTEMBRE 86	18H 22H	52	-	295	196	148	+	10216	298154	438019
VENREDI 19 SEPTEMBRE 86	20H 27H	13	-	266	232	212	+	94406	193534	250312
SAHEDI 20 SEPTEMBRE 86	9H 23H	2								

LACROC DEBUT: JEUDI 18 SEPTEMBRE 86

FIN: LUNDI 3 NOVEMBRE 86

JEUDI 18 SEPTEMBRE 86	4H 11H	68	+	27	119	197	-	790217	521346	294565
JEUDI 18 SEPTEMBRE 86	7H 34H	51	-	35	327	263	+	766184	963706	102786
JEUDI 18 SEPTEMBRE 86	10H 57H	43	-	77	12	315	+	643355	834055	999516
JEUDI 18 SEPTEMBRE 86	14H 20H	83	-	142	329	333	+	454154	957670	948353
JEUDI 18 SEPTEMBRE 86	18H 74H	23	+	222	273	322	-	221659	73941	976419
VENREDI 19 SEPTEMBRE 86	2H 38H	42	+	29	104	170	-	784489	566399	322638
VENREDI 19 SEPTEMBRE 86	6H 12H	68	-	29	309	238	+	783501	1016040	174470
VENREDI 19 SEPTEMBRE 86	9H 40H	40	-	57	354	300	+	703682	886658	1044249
VENREDI 19 SEPTEMBRE 86	13H 04H	66	-	117	32	329	+	526756	775857	958746
VENREDI 19 SEPTEMBRE 86	16H 34H	45	+	186	260	332	-	327508	110665	950227
SAHEDI 20 SEPTEMBRE 86	14 20H	20	+	41	89	134	-	748108	608071	477919
SAHEDI 20 SEPTEMBRE 86	4H 49H	87	+	27	176	214	-	791088	356202	245577
SAHEDI 20 SEPTEMBRE 86	8H 21H	44	-	42	339	278	+	746615	930361	57418
SAHEDI 20 SEPTEMBRE 86	11H 42H	49	-	93	22	322	+	598605	805373	978554
SAHEDI 20 SEPTEMBRE 86	15H 04H	71	+	159	251	333	-	404351	136027	947105
SAHEDI 20 SEPTEMBRE 86	19H 14H	10	+	269	283	296	-	84491	45465	6575
DIMANCHE 21 SEPTEMBRE 86	3H 26H	59	+	27	116	188	-	790916	529219	319703
DIMANCHE 21 SEPTEMBRE 86	7H 04H	55	-	33	321	255	+	772935	982279	125335
DIMANCHE 21 SEPTEMBRE 86	10H 25H	41	-	70	7	310	+	665505	847815	1013104

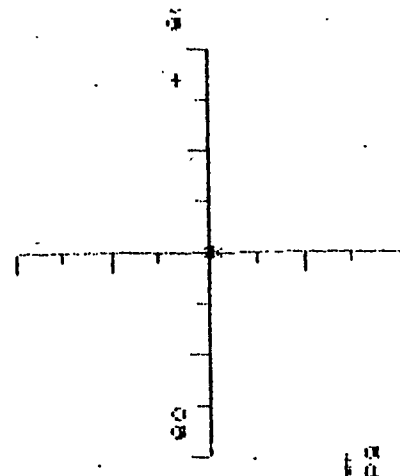
STARLETTE DEBUT: MERCREDI 17 SEPTEMBRE 86

FIN: LUNDI 6 OCTOBRE 86

MERCREDI 17 SEPTEMBRE 86	11H 34H	16	-	160	114	96	+	401014	535892	618366
MERCREDI 17 SEPTEMBRE 86	13H 20H	68	-	226	98	63	+	209713	581577	683986
MERCREDI 17 SEPTEMBRE 86	15H 04H	54	+	270	32	65	-	82235	774941	678679
MERCREDI 17 SEPTEMBRE 86	16H 59H	52	+	294	51	89	-	10776	721191	612214
MERCREDI 17 SEPTEMBRE 86	18H 40H	82	-	296	139	123	+	5598	462472	589379
MERCREDI 17 SEPTEMBRE 86	20H 38H	27	-	278	212	171	+	59090	251288	370234
JEUDI 18 SEPTEMBRE 86	11H 52H	29	-	186	115	71	+	326746	533815	661335
JEUDI 18 SEPTEMBRE 86	13H 39H	77	+	244	54	62	-	158230	709720	687697
JEUDI 18 SEPTEMBRE 86	15H 29H	49	+	282	17	71	-	47553	819227	661568
JEUDI 18 SEPTEMBRE 86	17H 18H	61	+	296	49	99	-	5859	726373	578706
JEUDI 18 SEPTEMBRE 86	19H 04H	57	-	292	173	139	+	19092	365101	464923
JEUDI 18 SEPTEMBRE 86	20H 58H	16	-	268	222	191	+	87692	221607	312149
VENREDI 19 SEPTEMBRE 86	12H 10H	47	-	211	114	65	+	253079	536890	678437
VENREDI 19 SEPTEMBRE 86	13H 54H	64	+	260	20	63	-	111358	810820	684010
VENREDI 19 SEPTEMBRE 86	15H 49H	49	+	291	30	79	-	20417	782230	637767
VENREDI 19 SEPTEMBRE 86	17H 38H	78	+	298	91	112	-	1541	603698	543222
VENREDI 19 SEPTEMBRE 86	19H 27H	38	-	287	201	155	+	31353	282928	417681
SAHEDI 20 SEPTEMBRE 86	10H 43H	18	-	166	118	80	+	384576	524935	634538



CORRECTIONS (G,S)



RESIDUS

TEMPS

( 0 , 0 )

DECALAGE FENETRE = 0  
 DECALAGE TRAJECT = 0  
 NOMBRE ECHOS = 4681

70m

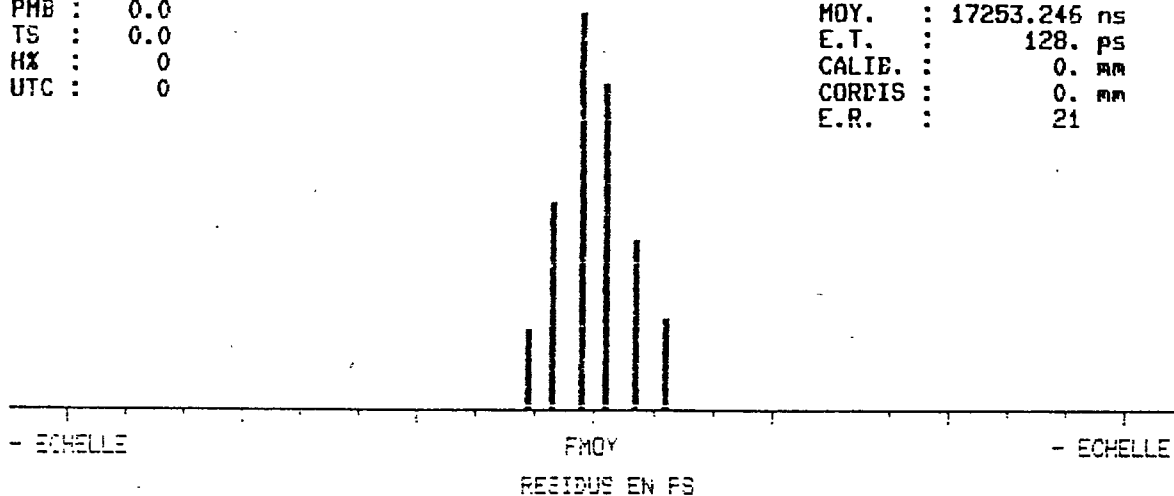
70m

## STATION LASER-SATELLITES DU C.E.R.G.A.

L86082004.46D

PMB : 0.0  
 TS : 0.0  
 HX : 0  
 UTC : 0

MOY. : 17253.246 ns  
 E.T. : 128. ps  
 CALIB. : 0. mm  
 CORDIS : 0. mm  
 E.R. : 21



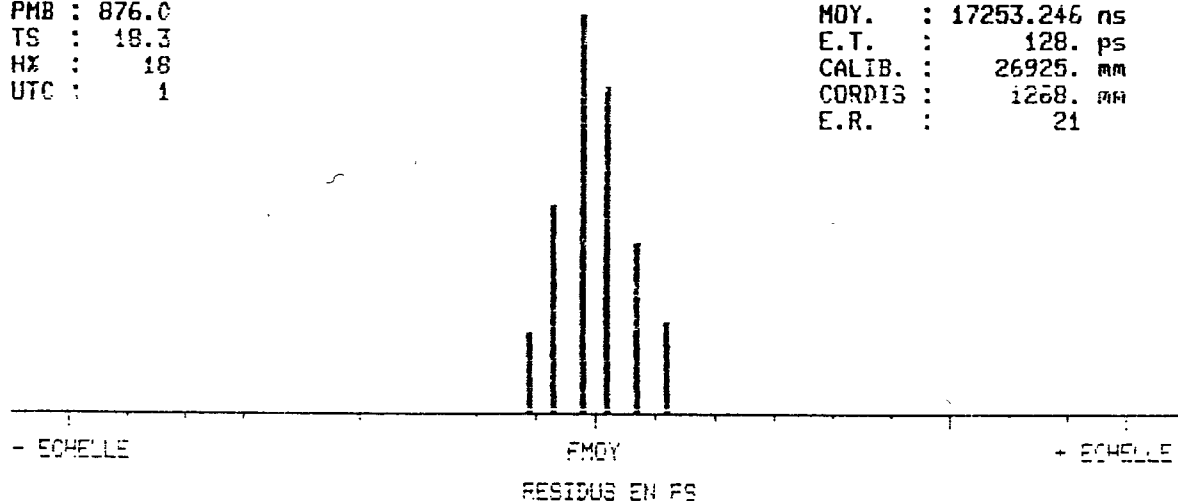
echelle : 2.000 ns largeur des canaux : 22. ps  
 coord. du maximum : X= -44 ps Y= 150 pts

## STATION LASER-SATELLITES DU C.E.R.G.A.

L86082004.46D

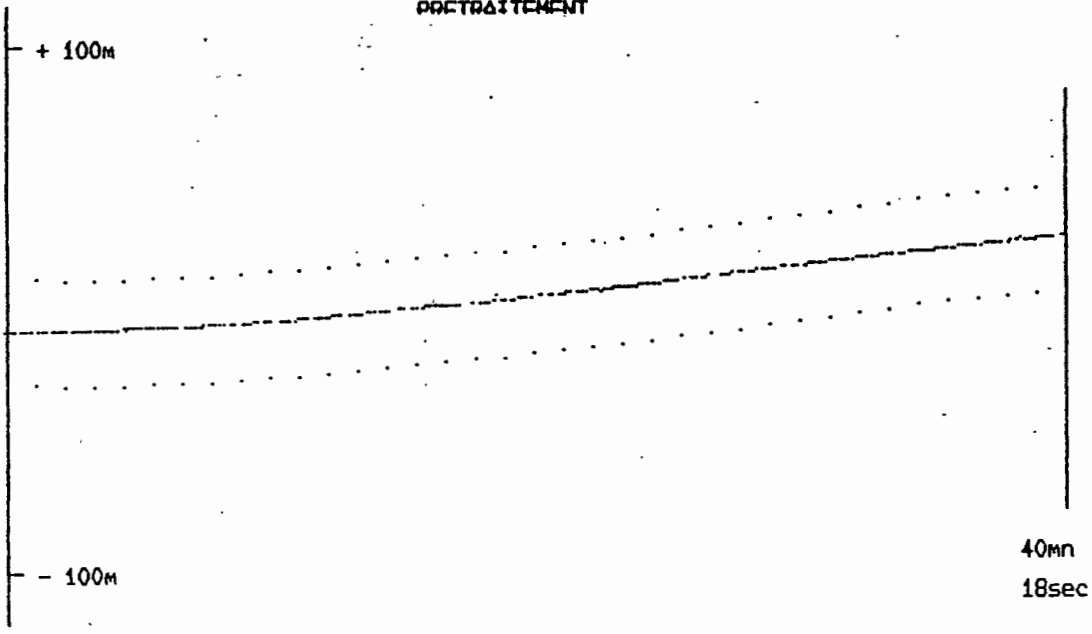
PMB : 876.0  
 TS : 18.3  
 HX : 18  
 UTC : 1

MOY. : 17253.246 ns  
 E.T. : 128. ps  
 CALIB. : 26925. mm  
 CORDIS : 1268. mm  
 E.R. : 21



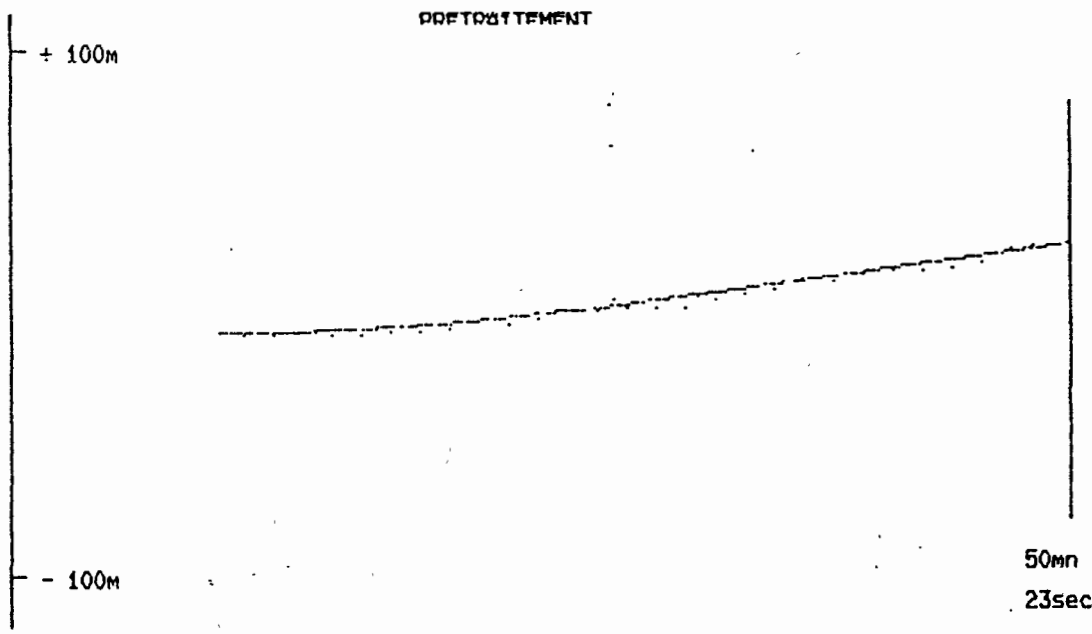
echelle : 2.000 ns largeur des canaux : 22. ps  
 coord. du maximum : X= -44 ps Y= 150 pts

PROFONDITAMENT



40mn  
18sec

PROFONDITAMENT



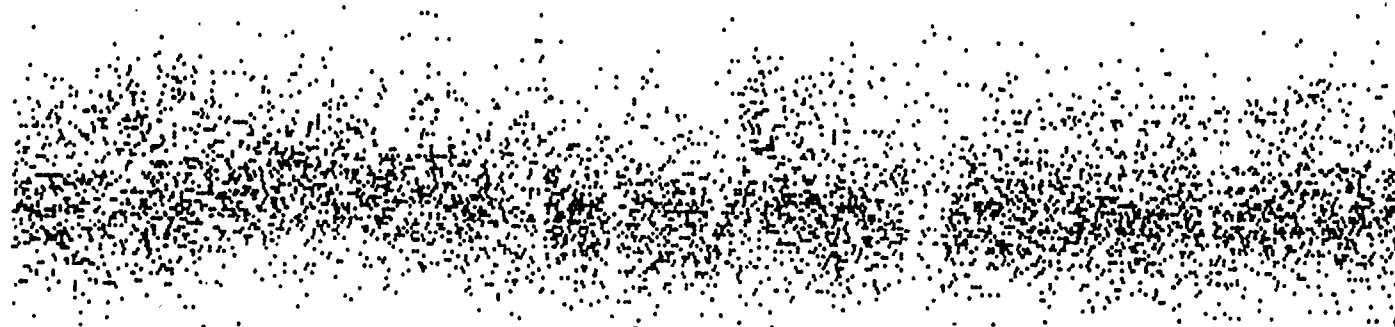
50mn  
23sec



PRETRAITEMENT

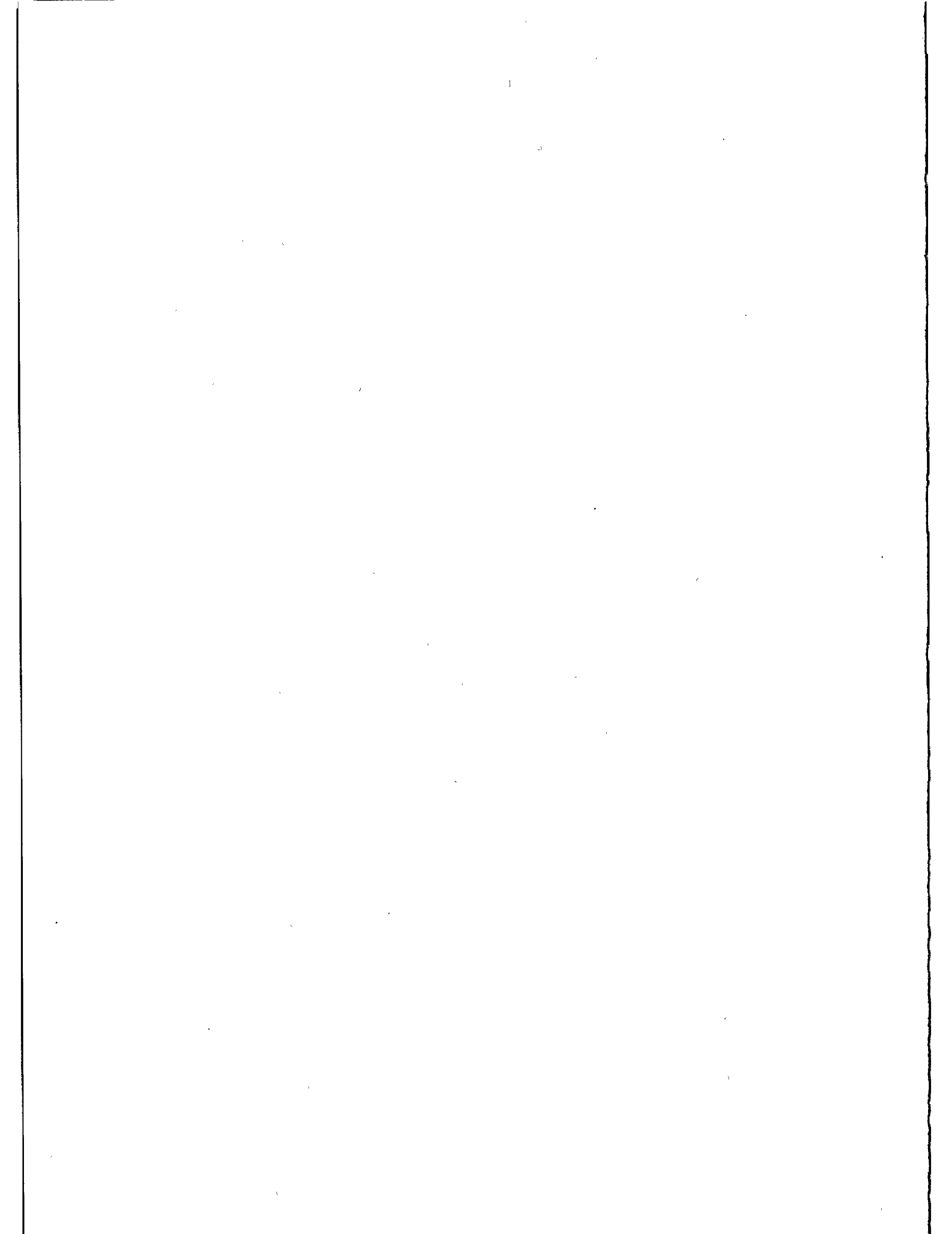
+ 15cm

- 15cm



40mn

18sec



THE SBG LASER RADAR STATIONS POTSDAM AND SANTIAGO DE CUBA  
STATUS AND PERFORMANCE REPORT

L. Grunwaldt, H. Fischer, R. Neubert  
Academy of Sciences of G.D.R.  
Central Institute for Physics of the Earth  
Potsdam 1500, G.D.R.

Telephone  
Telex 15305

J. Del Pino  
Cuban Academy of Sciences  
Institute for Geophysics and Astronomy  
Havana, Cuba

ABSTRACT

The systems are based on a modified 4-axis satellite tracking camera (SBG). Their basic concepts and technical performance are typical for 2nd generation devices. Blind tracking of LAGEOS using narrow beams is possible with the help of a star calibration method. The systems are operated with 2nd generation performance since 1981 and 1985, respectively. The Potsdam station is contributing continuously to the MERIT project since 1980. LAGEOS tracking at Santiago station started in December 1985.

## 1. Station 1181 Potsdam

The SBG telescope was developed in the early sixties as a photographic tracking camera and was operated at Central Institute for Physics of the Earth (ZIPE) since 1966. In its basic construction, it was a Maksutov-Schmidt system (effective diameter of receiver optics 32 cm) on a 4-axis mount with axes no. 1 and 2 fixed and axes 3 (along track) and 4 (cross track) moved during operation. Along track movement was controlled by punch tape with an accuracy sufficient for photographic tracking of GEOS type satellites (SBG mount see Fig.1).

The main modifications to allow laser tracking with the SBG was to mount an additional hinged Cassegrain mirror in front of the photographic unit and to drill a central hole through the main mirror. In this way the receiver optics and related electronics could be placed behind this mirror. A two-stage passively Q-switched ruby laser was mounted on the main tube and moved together with the telescope. By inserting and replacing the Cassegrain mirror, alternating photographic and laser observations became possible. This 1st generation system (laser pulsewidth 20 ns, visual tracking only) was operated successfully since 1974. First LAGEOS returns were obtained in September 1977.

Especially through the years 1979-81, the system was upgraded to a 2nd generation device (possibility of automatic observations, ranging errors of a few decimeters for all existing laser satellites). The main hardware modifications were:

- Equipment of the 3rd and 4th axis with step motor drives and digital encoders for precise positioning, 2nd axis with a theodolite for accurate control of inclination.
- On-line computer control of the mount and related electronics (digital range gate, laser firing etc.). For this purpose, an IEC 625 type interface with a desktop computer (8 - 24 kByte operational memory) as a controller is used.
- Replacement of the former laser transmitter (20 ns) by a 5 ns ruby laser [1].

There are some limitations in further upgrading the system: because of the optical-mechanical layout of the SBG mount there is no possibility to install a Coudé focus. So both laser and receiver have to be moved together with the mount being unfavourable especially for more sophisticated lasers with shorter pulsewidth. Additionally, the mount errors for a 4-axis mount are not so easy to handle and can be controlled exactly only by star calibrations limiting this method to night and twilight observations.

A program system for satellite position prediction, on-line mount control, data reduction and orbital elements improvement from own measurements was developed [2]. Additionally, from star observations an error model for the 4-axis mount can be derived leading to an absolute pointing accuracy of about

+/- 30" which is sufficient for most tracking purposes with wider diffraction angles of the laser. Totally blind tracking of LAGEOS using narrow beams (20 - 30") can be attained by observing the positions of some stars along the track of the satellite and finding the true setting angles of the mount by matching the observed and the catalogue positions of the stars via the computer. In this way the pointing accuracy can be improved to about +/- 10" which is strongly enhancing the reliability of LAGEOS tracking, especially using the long-term predictions of the LAGEOS position edited by the University of Texas [3] to produce osculating elements for the given pass.

The station 1181 Potsdam is contributing continuously to the MERIT project since the short campaign 1980.

## 2. Station 1953 Santiago de Cuba

To improve the INTERKOSMOS station distribution of highly automated stations and according to the good experience with the Potsdam equipment, a second SBG mount was upgraded according to the main construction principles described above. Some slight modifications as enhancement of the laser output energy and simplification of receiver optics were done. The station was equipped in cooperation between G.D.R., U.S.S.R. and Cuba. After the installation in summer/autumn 1985, first performance tests were carried out during Dec.1985/Jan.1986 proving that the main performance data are similar to the Potsdam device. In Fig.2 and 3 typical range-noise histograms on a pass-by-pass basis for both stations are shown. For the Santiago station it was gained from the performance test period, for the Potsdam station it is derived from the whole MERIT main campaign. A comparison of some technical data between both stations can be found in Table 1.

Table 1: Technical data of SBG stations 1181 and 1953

Location	Potsdam, G.D.R.	Santiago de Cuba
Station number	1181	1953
Laser type	Ruby, TEM <sub>00</sub>	Ruby, TEM <sub>00</sub>
Pulsewidth/ns	5	5
Max. output/mJ	200	800
Min. divergency/"	20	20
Q-switch	Dye cell	Dye cell
Receiver type	RCA C 31034A	FEU 79
Quantum eff./% *)	10	3-5
Bus controller	HP 9825 S	EMG 666 B
Oper. memory/kByte	24	8
Time base	ZIPE time service (Cs-clock)	LORAN-C
First operation	March 1974 **)	December 1985

Remarks: \*)  $\lambda = 694 \text{ nm}$   
\*\*) First generation system

#### REFERENCES

- [1] Grunwaldt, L. et al.:  
First Satellite Ranging Results Using a Dual-Pulse Ruby Laser  
Proc. 4th Intern. Workshop on Laser Ranging Instr., vol II  
Edt. by P. Wilson, Bonn (1982), p. 484-87
- [2] Neubert, R.:  
HP 9825-based Software System for Laser Radar  
Proc. 4th Intern. Workshop on Laser Ranging Instr. (Software Session), Edt. by P. Shelus  
The Univ. of Texas Publ. in Astron. 19 (1982), p.77-88
- [3] Schutz, B.E. et al.:  
LAGEOS Ephemeris Predictions  
Proc. 4th Intern. Workshop on Laser Ranging Instr., vol. I  
Edt. by P. Wilson, Bonn (1982), p. 145-71

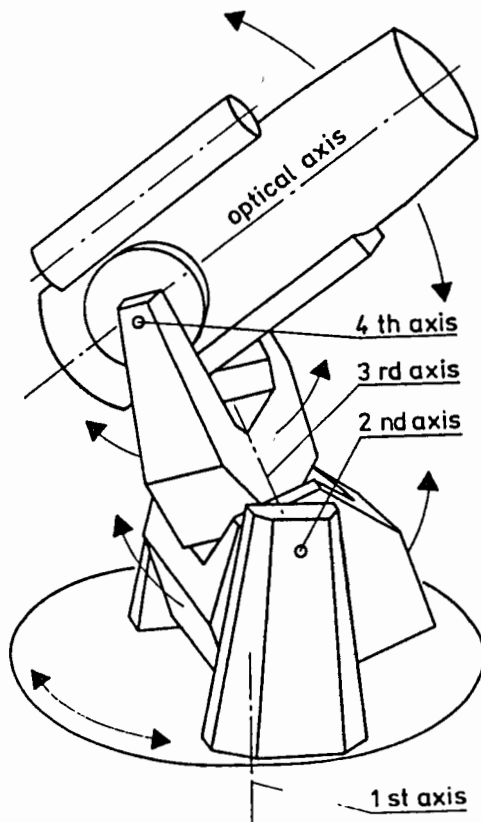


Fig. 1  
Schematic drawing of the SBG - mount

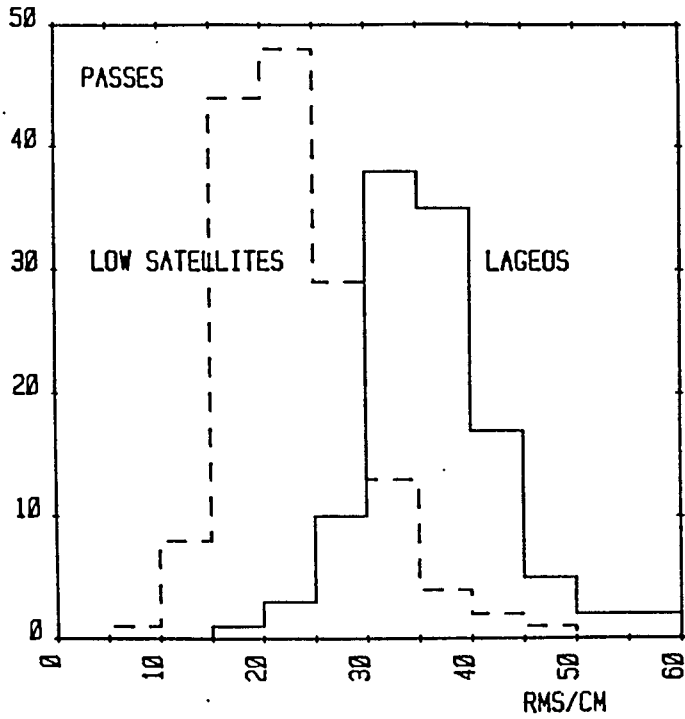


Fig. 2: Pass-by-pass range noise histogram for station 1181 Potsdam, data from the MERIT main campaign

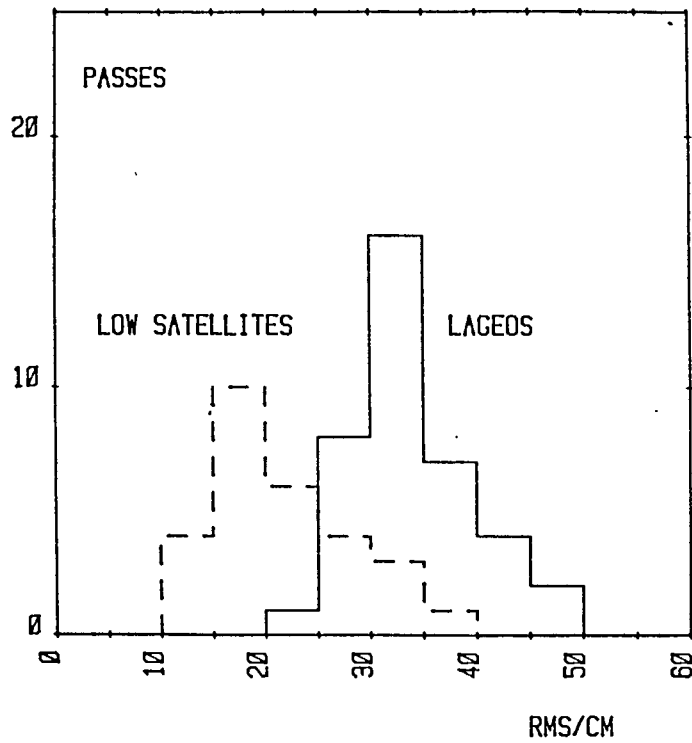
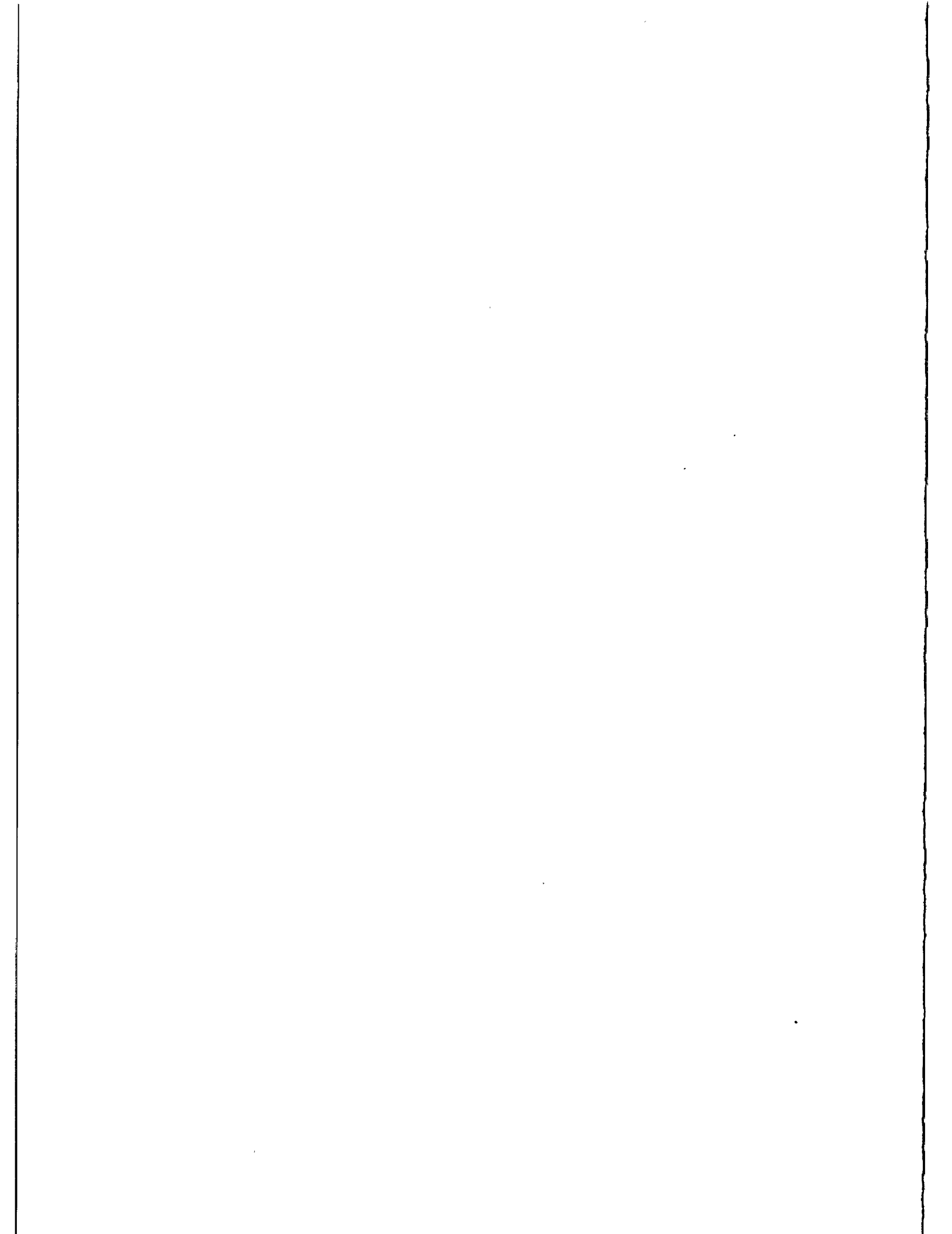


Fig. 3: Pass-by-pass range noise histogram for station 1953 Santiago de Cuba, data from performance test period December 1985 - January 1986





AMBIGUITY AND RESOLUTION OF A MODE-LOCKED  
PULSE TRAIN LASER RADAR

R. Neubert, B. Ritschel, L. Grunwaldt  
Academy of Sciences of G.D.R  
Central Institute for Physics of the Earth  
Telegrafenberg A 17, Potsdam 1500, G.D.R.

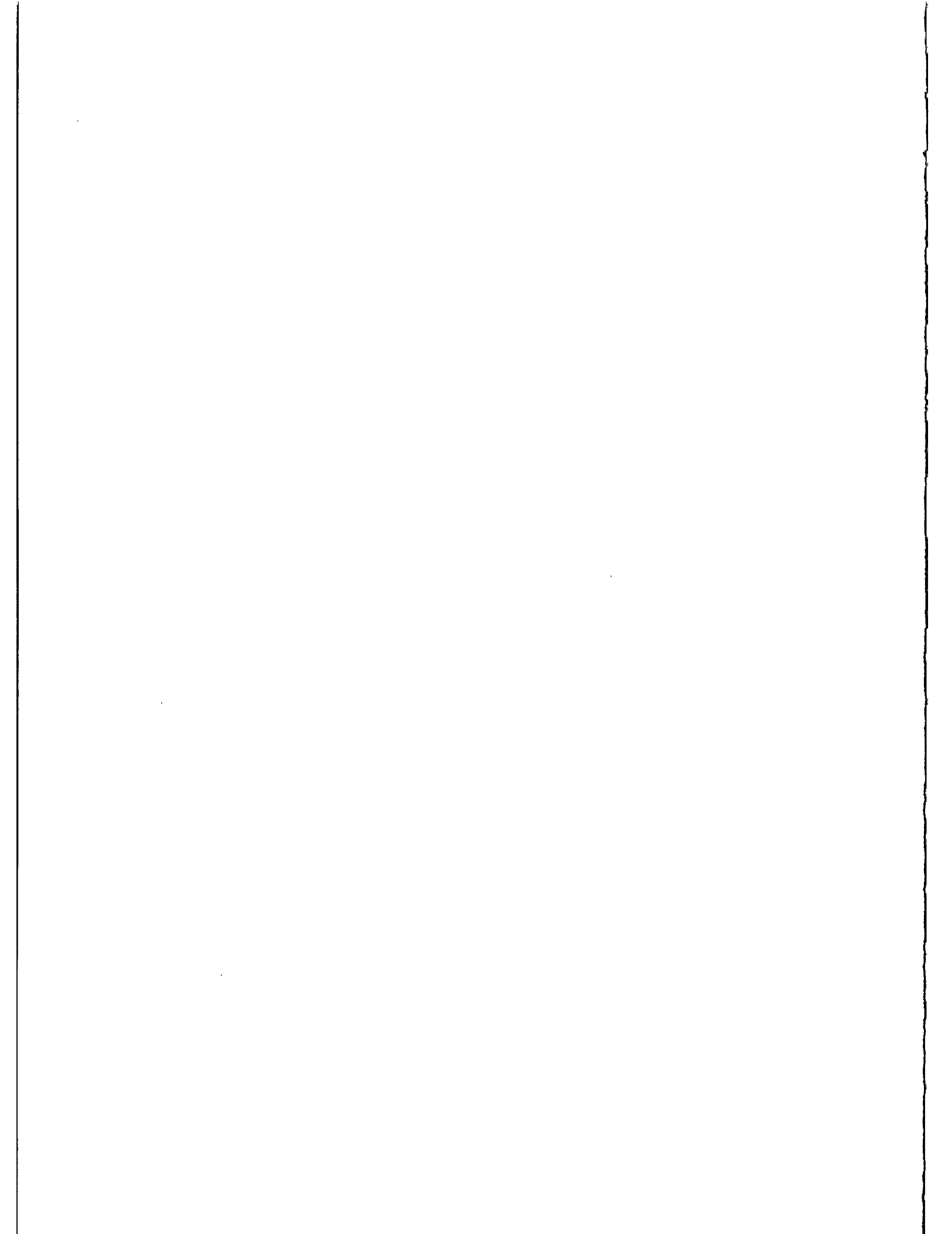
Telex 15305

ABSTRACT

The accuracy of a multipulse laser radar has been studied with indoor experiments and computer simulation. For the experiments a mode-locked Nd-YAG laser producing 7 to 9 pulses of 4.6 ns spacing at 10 Hz repetition rate is used. The frequency-doubled pulses are divided by a beamsplitter and recombined at the photomultiplier which is working at the single photoelectron level. The time-of-flight data are treated by cross-correlating the empirical distributions corresponding to the two light paths. This leads to an estimate of the time-of-flight difference. Using a large amount of data sets, the following parameters are determined:

- a) the percentage of estimates shifted by more than half a pulse spacing
- b) the standard deviation of the unshifted estimates.

For the parameters of our system, the percentage of "good" estimates is higher than 90% if more than 200 measurements are used. A standard deviation of about 100 ps is obtained under the same conditions. These results are obtained using electrostatic PMT's with about 500 ps jitter. Good agreement between the experiments and computer simulations is found. Thus the simulation method is used to determine the system performance in a wider parameter range.



Fernsehelektronik Berlin). Assuming that the start- and stop-time fluctuations are equal and independent in this case, the RMS start-time noise can be calculated to be 100-140 ps. For the experiments with PMT receiver, the SP 109 was always used. Thus, the jitter of the RCA C 31034A can be estimated by quadratic subtraction of the start noise to be around 350 ps. From this example it can be seen, that the start-time noise has only small influence on the overall resolution in our experiments.

#### The precision of the cross-correlation method

The generally adopted method for treating the data of a mode-locked train laser radar is to calculate first the frequency distributions of the calibration- and the ranging-measurements separately, and then to determine the time shift for maximum correlation of the two distributions. An example distribution is shown in Fig.2. The two subdistributions according to path 1 and 2 are well separated from each other by roughly 60 ns. Convoluting both distributions, Fig.4 was obtained. In this figure the convolution sum is plotted like a polygon linking the points separated by the bin width of 250 ps. The maximum can be determined very accurately using some interpolation method. In our case we obtain for the time shift of maximum correlation  $(61.16 \pm 0.1)$ ns.

To investigate the precision of the method, the measurements of this and several other experiments were arranged into groups. Then the cross-correlation method was applied to each group so that an ensemble of time shifts is obtained from which statistical estimates for the precision can be gained. The parameters under consideration are:

1. the percentage of time shift results deviating from the real value not more than half a pulse separation (this quantity called "uniqueness")
2. the RMS error of the results deviating not more than half a pulse separation

These parameters are plotted in Fig. 5 and 6 in dependence of the quantity of measurements. As a normalized measure of the data quantity we are using  $(1/n_1 + 1/n_2)^{1/2}$ , where  $n_1$  and  $n_2$  are the number of measurements for path 1 and path 2, respectively. This is just the probable error of the ranging average for a single pulse system, expressed in terms of the standard deviation of a single time interval measurement. To estimate the uniqueness (resp. ambiguity) and precision from the measurements, 10 runs of 1000 points each are used. The total ensemble of 10000 measurements is arranged into groups of  $n_1 + n_2 = 60, 120, 240, 480$  individual measurements. For each group the cross-correlation method is applied resulting in the generation of an ensemble of ranges from which the interesting average parameters are estimated. The return rates for the two light paths are slightly changing

from run to run. Therefore averages for the parameter  $(1/n_1 + 1/n_2)^{1/2}$  have to be determined also. The resulting experimental values for the uniqueness and precision are plotted with the symbol "+" in Fig. 5 and 6.

For comparison with theoretical values and to obtain more general results (including different shapes of the laser signal like reduced pulse numbers), computer simulations were carried out assuming the photodetection process to be described by Poisson statistics and the timing jitter to have a Gaussian distribution. The simulator is a pseudo random number generator which outputs two possible numbers: 0 (corresponding to no detection) and 1 (detection). The probabilities of the two states are determined by the average number of photoelectrons ( $s$ ) of the pulse according to:

$$P(0) = \exp(-s); \quad P(1) = 1 - \exp(-s)$$

The simulator is called for each consecutive pulse of the group using the pulse intensities as input parameters. When the first positive answer occurs, the corresponding pulse number is stored together with some added Gaussian timing noise. By repeating this process, 5000 simulated time intervals for both the calibration and the ranging channel are generated and stored into the memory. In this process, the average return rate for the calibration is set to be 50% and for the other channel 25%.

To estimate now the performance parameters of the system in dependence on the amount of measurements, example realizations are selected from simulated measurements and then treated by the cross-correlation method in the same way as is done with the real measurements.

The selection of the individual values from the memory is done by calling an equally distributed pseudo random number generator to determine the addresses. 500 example realizations are used to estimate the performance parameters, i.e. the uniqueness and the RMS error of a cross-correlation result.

To compare the experimental values with the simulations, the average shape of the time interval histogram is needed. It has been approximated by 9 Gaussian peaks with Gaussian envelope according to

$$h = a_0 \sum_{k=-4}^4 \exp(k^2/U) \cdot \exp((t - t_k)^2 / 2\sigma^2) \quad (1)$$

The average experimental parameters are  $U = 4.61$ ,  $\sigma = 386$ ps. The separation of consecutive pulses is

$$\Delta t = t_{k+1} - t_k = 4.55 \text{ ns.}$$

So the relative resolution is  $C = \sigma / \Delta t = 0.0848$ . Using these parameters the results marked in Fig. 5 and 6 by "\*" are generated. They agree reasonably well with the experimental points, especially for the uniqueness (Fig.5). This

agreement is somewhat surprising because the laser pulse shape fluctuations are not directly modelled in the simulations. Instead, the pulse shape is chosen in agreement with the observed histograms. Note further that the simulated results showed almost no dependence from  $n_1 / n_2$  if the above introduced parameter  $(1/n_1 + 1/n_2)^{1/2}$  is kept constant. This is proved in the range  $n_1/n_2 = 1 \dots 10$ .

For the conditions used in our experiments, the following conclusions can be drawn:

- the performance of the system can be reasonably well determined by the described simulation method
- 200 measurements for both calibration and ranging are required to have 90 per cent probability of correct assignment of the data (not shifted by a multiple of the pulse separation)
- the standard deviation of a result generated from 200 measurements is in the order of 100 ps.

The good representation of the experiments by the simulation encouraged us to study the dependence of the system performance from the laser pulse shape and the timing resolution more detailed. Some of the results are graphically represented in Fig.7 and 8. In these figures, both the uniqueness parameter (broken lines, 1 at the vertical scale corresponds to 100%) and the ratio of the RMS error of the cross-correlation result to the single-shot timing jitter (full lines) are plotted in dependence on the amount of measurements. The relative RMS error as defined describes the effect of averaging.

In Fig.7 for a fixed laser pulse shape the influence of the timing resolution is represented. As a measure of the resolution, the parameter C (defined as the ratio of the overall RMS jitter of the timing system to the pulse separation of the laser pulses) is used. The time resolution is visualized by the probability distributions of the time intervals, i.e. the shapes of the histograms for very large amounts of measurements.

As can be seen from Fig.7, the timing resolution has a very small influence on the uniqueness (resp. ambiguity) but some effect on the relative RMS error. This behaviour is to be expected. We conclude from Fig.7 that the resolution parameter C should be smaller than 0.2. Note that for a given resolution of the timing system, the parameter C can be adjusted by the separation of the laser pulses which is possible by choosing the laser resonator length.

The number of pulses in a laser pulse group is represented by the parameter U. More precisely, this is the overall width of the probability distribution of the time intervals according to equ.(1). The parameter U is chosen to be  $U = 6$  in Fig.7.

The dependence of the system performance on the parameter U

for a fixed resolution (  $C = 0.1$  ) is shown in Fig.8. As expected, the parameter  $U$  has almost no effect on the error, but strong influence on the ambiguity. Fig.8 may be used to determine the amount of data to reach a given uniqueness level. A uniqueness of 90% in connection with  $U = 2$  is reached for  $n_1 = n_2 \approx 50$ . For  $U = 1$  only 20 measurements are needed in both channels to reach 90% uniqueness. There are some methods to minimize the parameter  $U$  including laser design, the combined use of nonlinear optical effects and well matched start detectors. With generally available technology,  $U = 1...2$  should be a realistic value.

### Conclusion

From the results of this study we conclude that the mode-locked train laser radar remains to be an attractive variant. Its main limitation, the ambiguity, can be reasonably overcome using a sufficient data quantity. The minimum data amount for a given probability of correct assignment can be gained from this paper. As a guide to good performance, one should restrict the number of pulses per group to a minimum and adjust the pulse separation to roughly 10 times the timing jitter. A special advantage of the rigorous use of single photoelectron detection is the low level of systematic errors. This gives the possibility to attain normal point errors near 1 cm even by using conventional electrostatic photomultiplier tubes.

### REFERENCES

- [1] Silverberg, E.C.: The Feedback Calibration of the TLRS Ranging System  
Proc. 4th Intern. Workshop on Laser Ranging Instr.,  
Austin 1981  
Edt. P. Wilson, Bonn 1982, p. 331-37
- [2] Hamal, K. et al.: INTERKOSMOS Laser Radar, Version Mode-Locked Train  
Proc. 5th Intern. Workshop on Laser Ranging Instr., vol.II  
Herstmonceux 1984  
Edt. J. Gaignebet, Bonn 1985, p. 214-18
- [3] Neubert, R.: Simulation Studies on the Statistics of a Multipulse Laser Radar Working at the Single Photoelectron Level  
Nabl. Isk. Sput. Zemli, Prague 23 (1984), p.93-102
- [4] Fischer, H.: Empfangsdiskriminator fuer Satellitenentfernungsmessung mit verbessertem Zeitverhalten  
Radio Fernsehen Elektronik, Berlin 31 (1982) 8, p.491-92

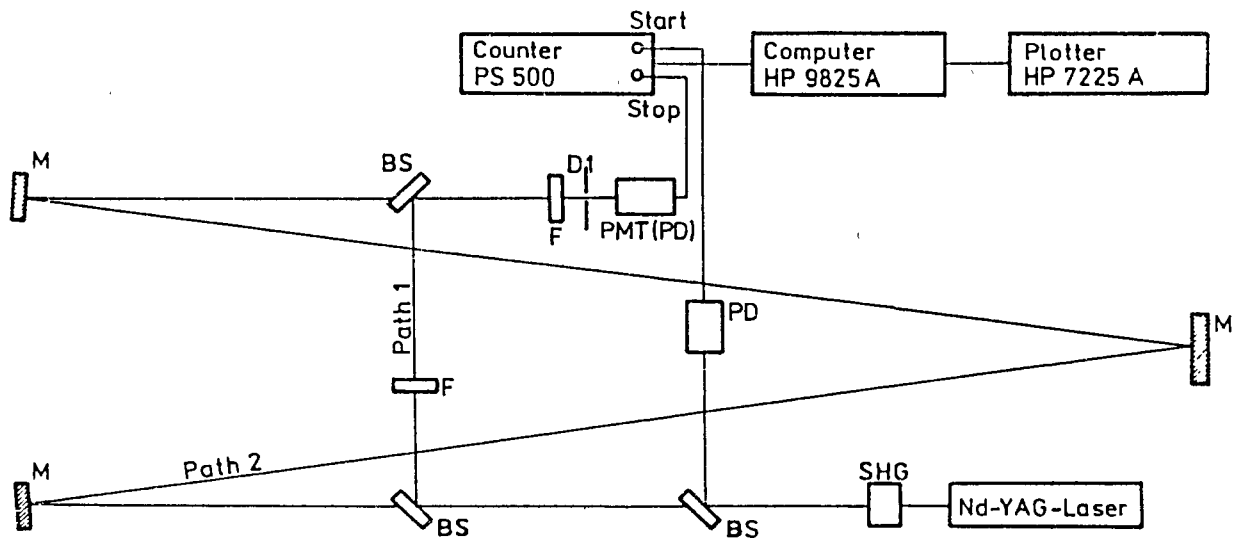


Fig. 1: Scheme of the experimental setup

BS - beam splitter, D - diaphragm  
 F - neutral density filter, M - mirror  
 PD - photo diode

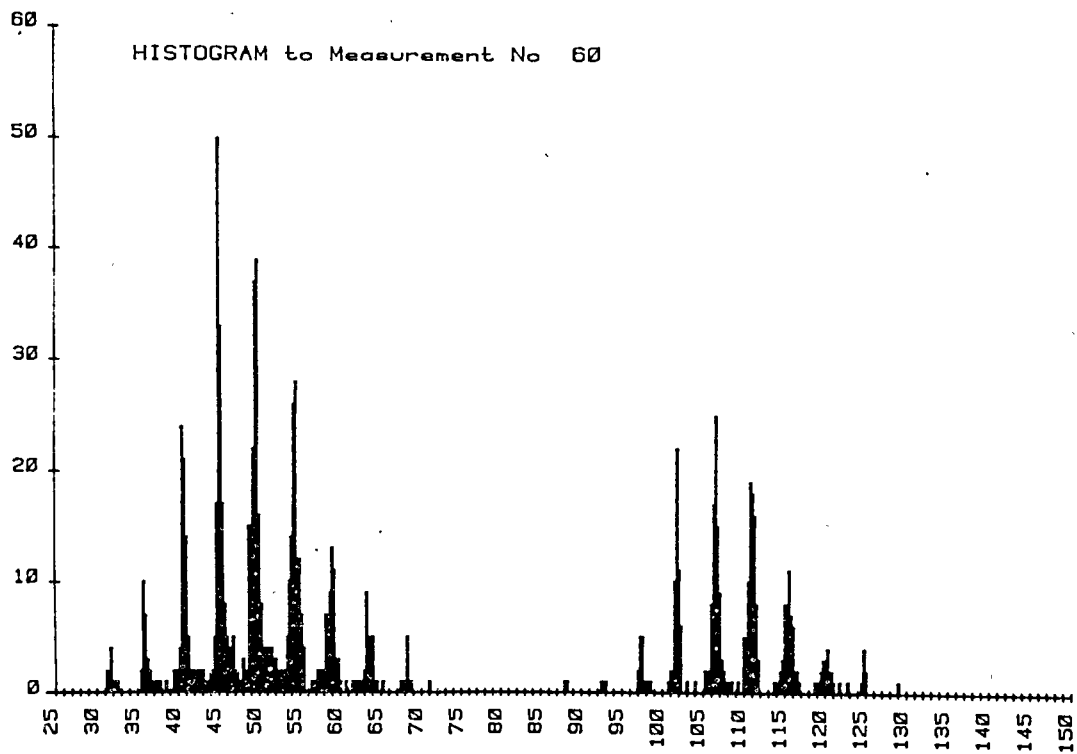


Fig. 2: Histogram of the time of flight values for a typical ranging experiment  
 Abscissa: Time interval in ns  
 ordinate: Number of measurements

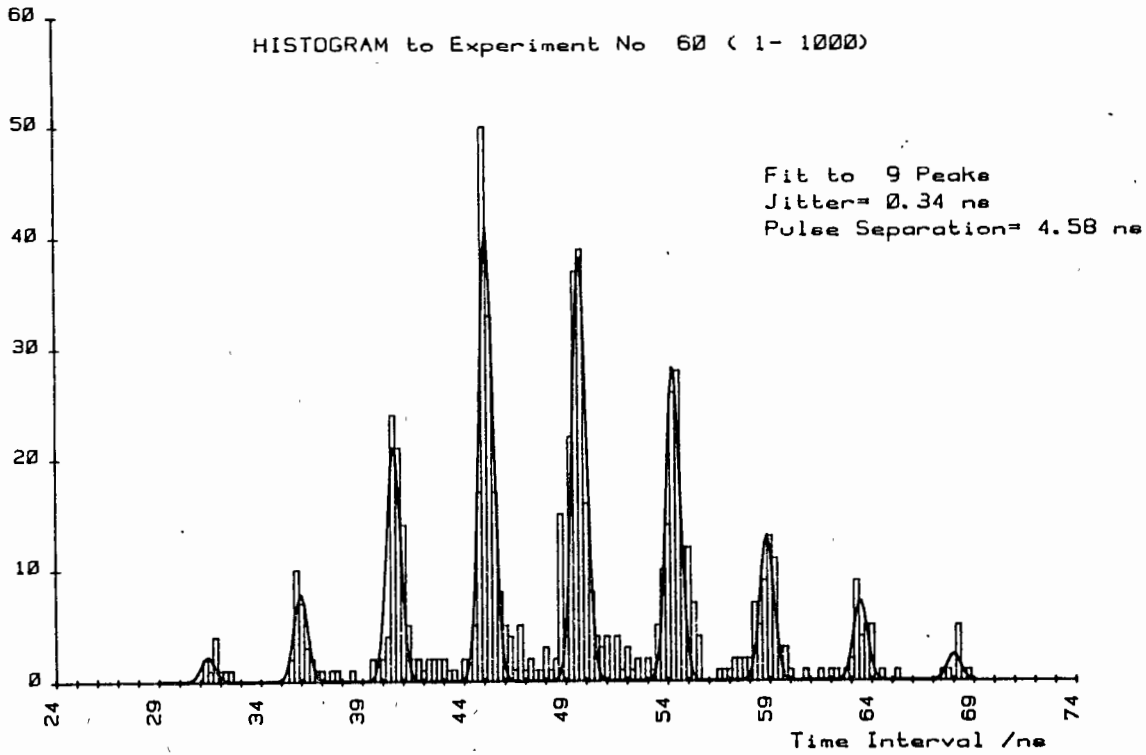


Fig. 3: Least square fit of a sum of Gaussian functions to the calibration part of experiment No. 60 (Fig. 2) bin width: 0.25 ns, RMS resolution: 0.34 ns, peak separation: 4.58 ns

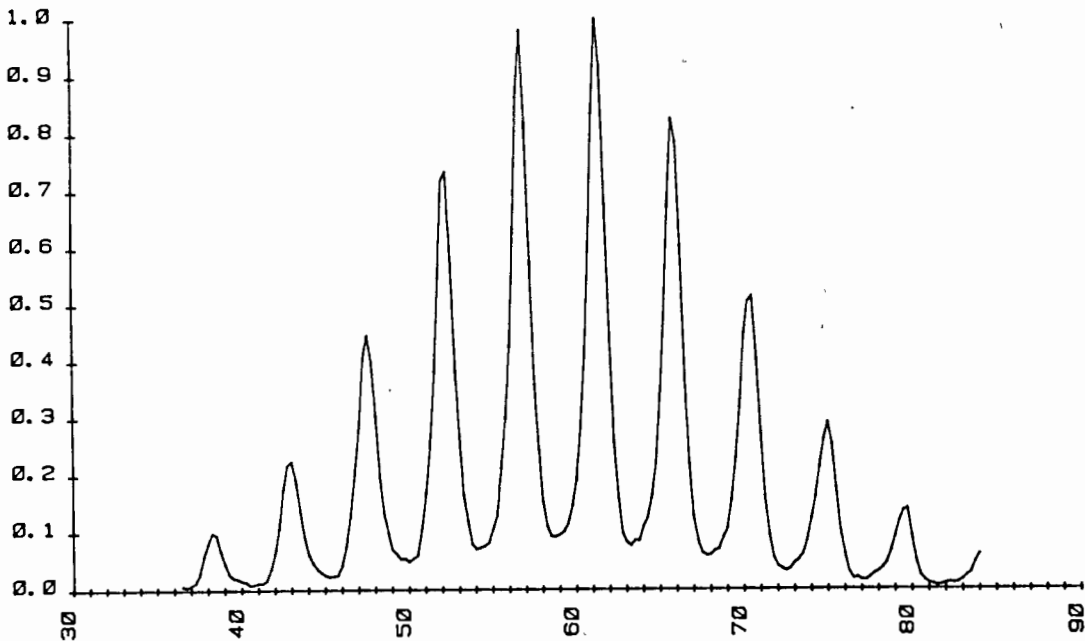


Fig. 4: Empirical cross-correlation to experiment No. 60 (convolution sum of the histograms corresponding to ray path 1 and 2 resp.)



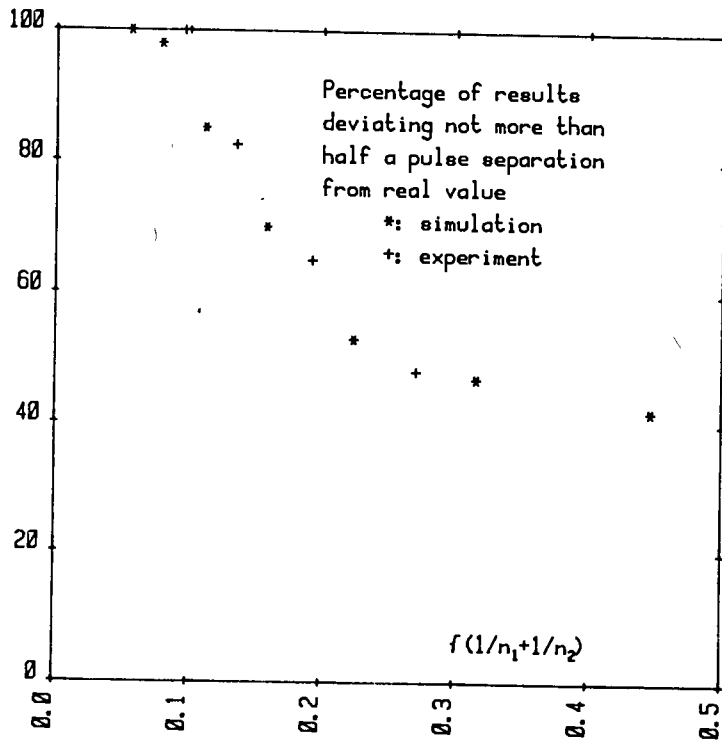


Fig. 5: Uniqueness in dependence of the amount of measurements: comparison of experiment and simulation.  
 $n_1$  - number of measurements for path 1  
 $n_2$  - number of measurements for path 2

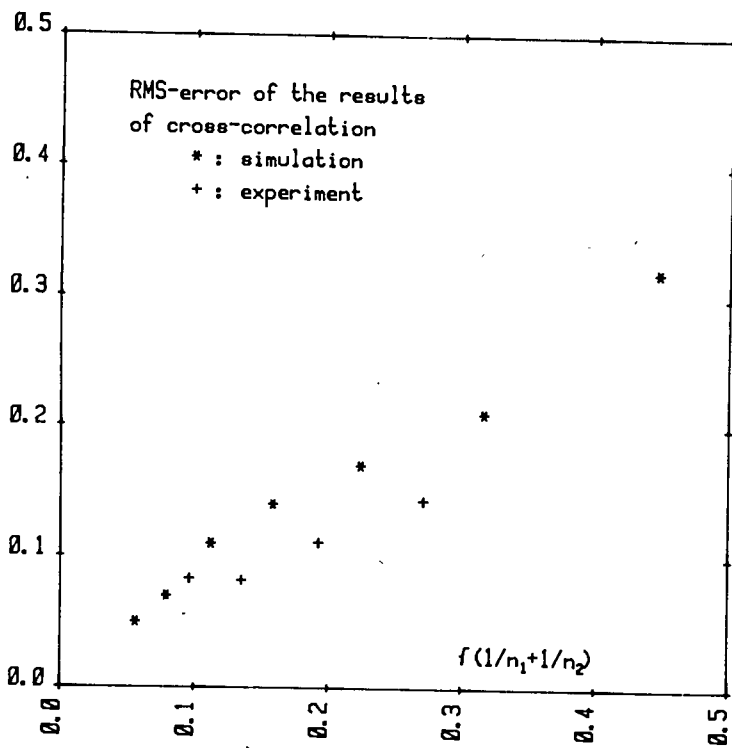


Fig. 6: RMS-error of the time shift corresponding to maximum cross-correlation: comparison of experiment and simulation

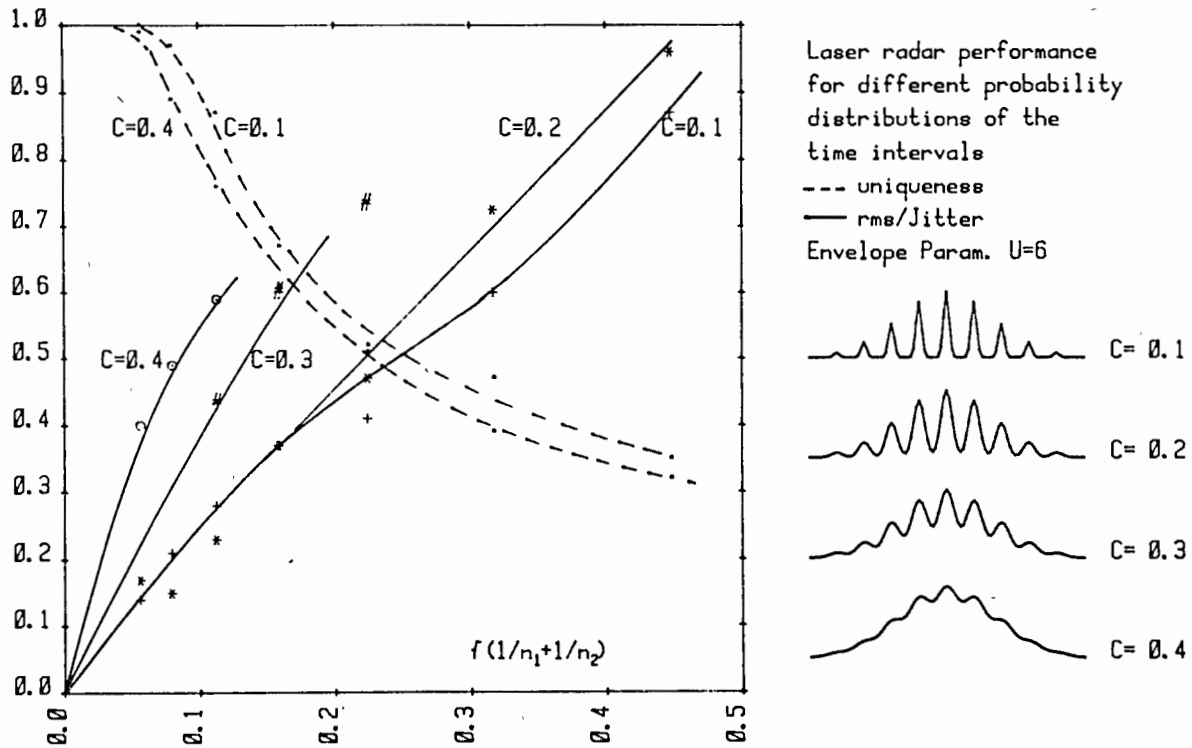


Fig. 7: Uniqueness and error obtained from simulations: dependence from timing resolution

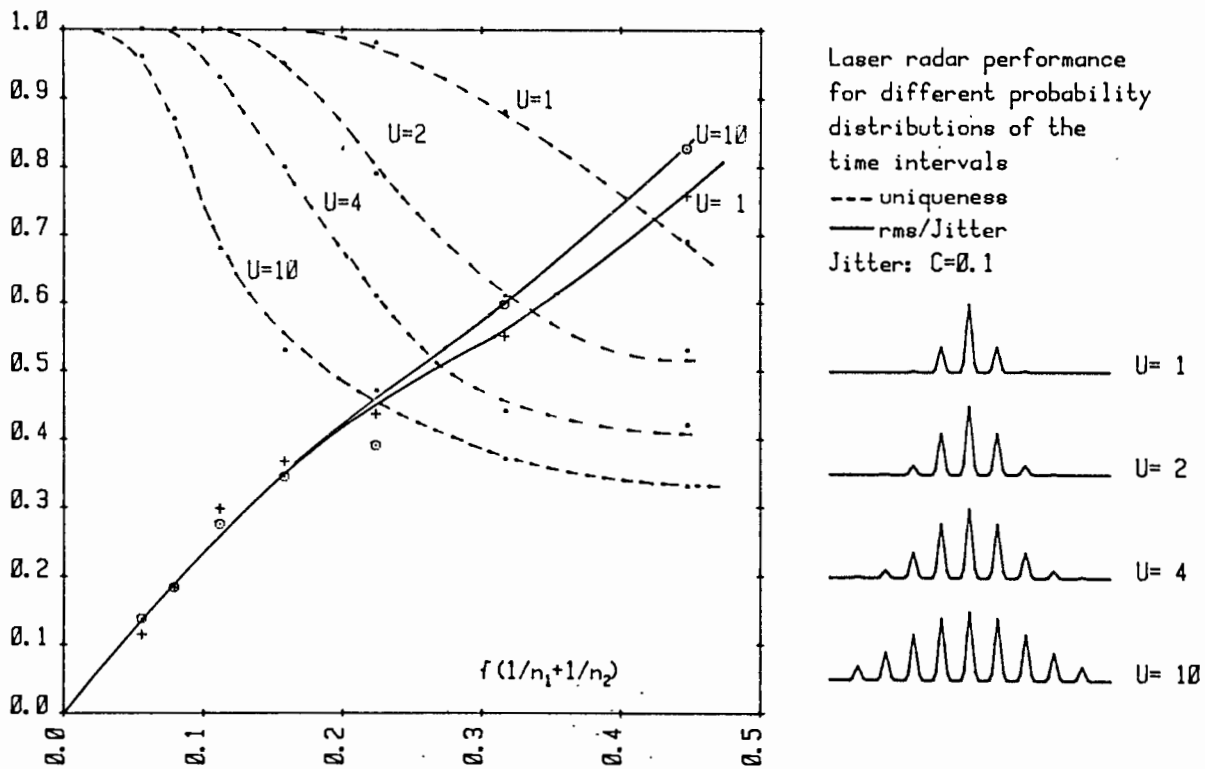


Fig. 8: Uniqueness and error obtained from simulations: dependence from the number of peaks

### 3.GENERATION LASER RADAR, VERSION MODE LOCKED TRAIN PROPOSAL

K. Hamal, I. Prochazka  
Czech Technical University  
Faculty of Nuclear Science and Physical Eng.  
Brehova 7, 115 19 Prague 1 - Czechoslovakia -

Telephone (1) 848840  
TWX 121254 FJFI C

#### ABSTRACT

To range the satellites and the Moon at the 3rd generation level ( $\text{rms} < 9 \text{ cm}$ ), laser transmitters generating mostly single pulse are exploited. Following the idea of E. Silverberg (4WLRI, 1981) and B. Greene (5WLRI, 1984) we propose to exploit the full train of mode locked pulses. The simplification of the laser transmitter is tremendous, the laser output average power may be 3 to 5 times higher for the same material damage threshold. To avoid the ambiguity in range determination we propose to use the transient digitizers as the START/STOP discriminators. The ambiguity is removed by START/STOP signal crosscorrelation on the shot by shot basis for satellite/multi-photon/ranging. Assuming the Moon ephemeris quality, the possible ambiguity in Moon ranging at single photoelectron level may be removed by ranging data processing.

### 3.Generation laser radar /version mode locked train/proposal

REQUIREMENTS : RMS single shot ( 3cm (200 picoseconds)

JITTER budget main contributors - detector  
- laser pulse  
- discriminator

DETECTOR jitter contribution :

$$\begin{array}{ll} \text{RMS /multi PE detection/} & \sqrt{[\text{pulse energy}]^{-1}} \\ \text{Normal point accuracy} & \sqrt{[\text{average power}]^{-1}} \end{array}$$

#### PROJECT PROPOSAL

LASER - mode locked train, 3-5ML pulses, pulse HAFW 30psec

DETECTOR - microchannel PMT

DISCRIMINATORS - Tranzient digitizer /Tektronix 7912AD/

bandwidth 400MHz, 10nV/div sensitivity

discriminators software modelled

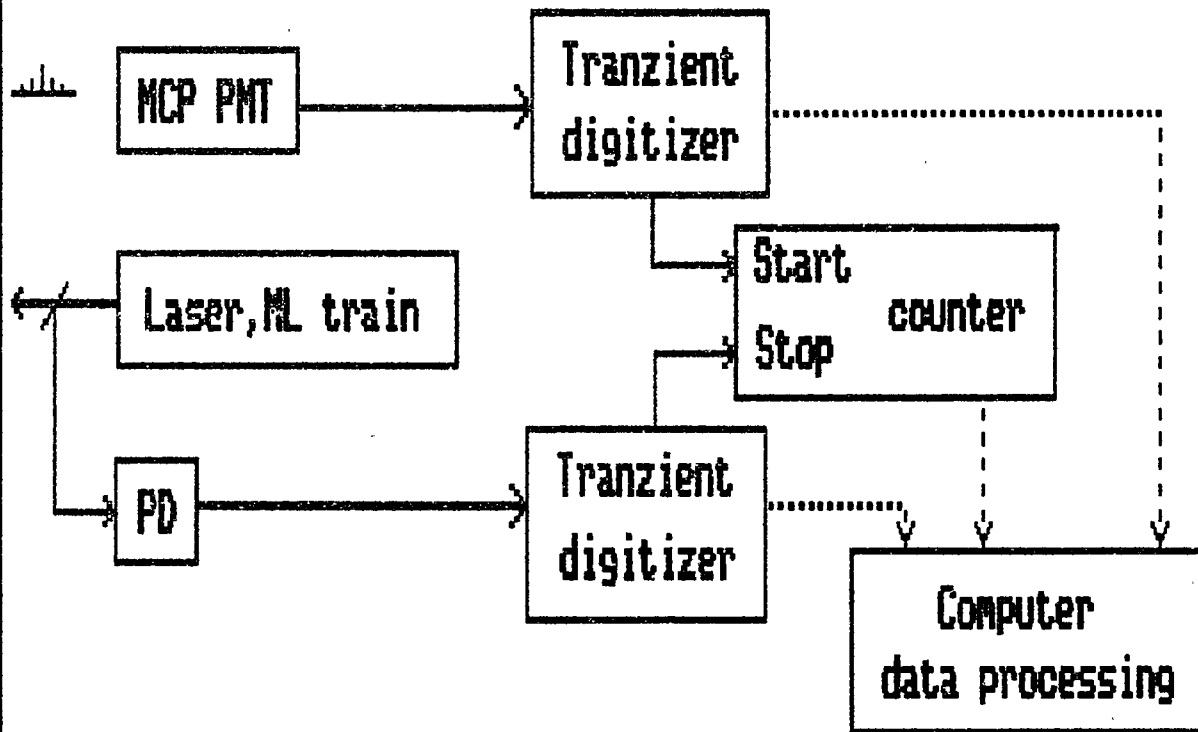
nonlinearities compensated

Start/Stop events data crosscorrelated

K. Haral, I. Prochazka  
3.Generation/version mode locked train/proposal

1

## Proposed block scheme



————— signal pass  
 ..... data flow

Jitter contributions:	multi PE	single PE
photomultiplier (MCP)	65 psec	100 psec
transient 2x + PD	30 psec	30 psec
counter (HP53700)	35 psec	35 psec
laser pulse (fwhm 30ps)	3 psec	12 psec
<b>RESULTING</b>	<b>80 psec</b>	<b>110 psec</b>

## Summary / conclusion

### PROPOSED SYSTEM ADVANTAGES: /in comparison to single pulse/

- \* LASER : simple / no slicer/
- \* AVERAGE POWER : 3-5 times higher for the same damage threshold, shorter pulses available
- \* SIGNAL PROCESSING : start/stop discriminators software modelled, the time walk, nonlinearity etc. software compensated
- \* CALIBRATION : both real time and pre/post pass possible, the signal strength is not critical
- \* AMBIGUITY : due to the ML train  
satellite / multi PE ranging / NO  
Moon /single PE, excellent ephemeris/ LOW/NO

### PROPOSED SYSTEM LIMITATIONS /in comparison to single pulse/

- \* DATA QUANTITY : additional 2 x 1 KBytes per shot
- \* SOFTWARE : more complex, data processing time consuming

K. Hanal, I. Prochazka  
3. Generation/version mode locked train/proposal

3

THE NEW SATELLITE LASER RANGING SYSTEM  
AT CAGLIARI OBSERVATORY

A. Banni  
International Astronomic Station of Latitude  
Cagliari - Italy

Telephone (39) 70 657657  
TWX 790326 OSSAST I

V. Capoccia  
Vitroselenia S.p.A.  
Cagliari

Telephone (39 70 99952  
TWX 791090

ABSTRACT

About one year ago the restructuring of our laser station was begun, with the technical assistance of the Vitroselenia Company of Cagliari.

The work consists of the total substitution of tracking, control and data acquisition equipment.

In carrying out the work the prime consideration was that of the reliability and precision of each single component.

The new station is expected to become operative in the first months of 1987.

## 1. TRANSMISSION-RECEPTION PULSES SYSTEM

At present we have available a first-generation Q-switched Ruby Laser that was custom-built for us by Apollo Lasers Inc.

This system remained inactive for about three years for various reasons, most of which of a technical nature.

Therefore we are now in the process of verifying the efficiency of the Pochels Cells assembly, the Q-switching system, the optical alignments, the electrical system and also the tracking system (fast diode, PMT, signal amplifiers).

The characteristics of our Ruby Laser Transmitter are given in Table 1.

For the transmission and reception of the laser shot we use a single reflector telescope of the Cassegrain-coude' type, the lenses of which were made in Florence.

In the previous system, transmission, reception and TV control were carried out by means of three distinct telescopes, with consequent problems of mechanical inertia, optical alignment and electromechanics.

We therefore designed an optical diagram that couples the three optical paths with the use of dichroic mirrors and beam splitters with minimum variations in the percentage of signal power loss.

As for mounting, we have available the base of a Contraves EOTVOS-B cinetheodolite the electromechanical components of which have been replaced, partly because they were obsolete and partly because they had deteriorated.

The characteristics of the telescope are given in Table 1 and the optical diagram is described in Figs 1a and 1b.

Table 1 .

### RUBY LASER SPECIFICATION

Oscillator Rod	1x7.5 cm AR coated ruby
Amplifier	1.3x15 cm AR coated ruby
Q-Switch	1 cm clear aperture, KD*P pockels cell
Cavity configuration	Flat-Flat, pulse-on switching
Wavelength	694.3 nm
Line width	0.3 A fwhm typical
Output Energy	1 Joule in 5 ns pulse width
Beam divergence	3 mrad
Repetition Rate	60 per minute, maximum
Main Mirror	50 cm Quartz and aluminium
Equivalent Focal Length	5 m
Field of View	0.0003-0.006 mrad



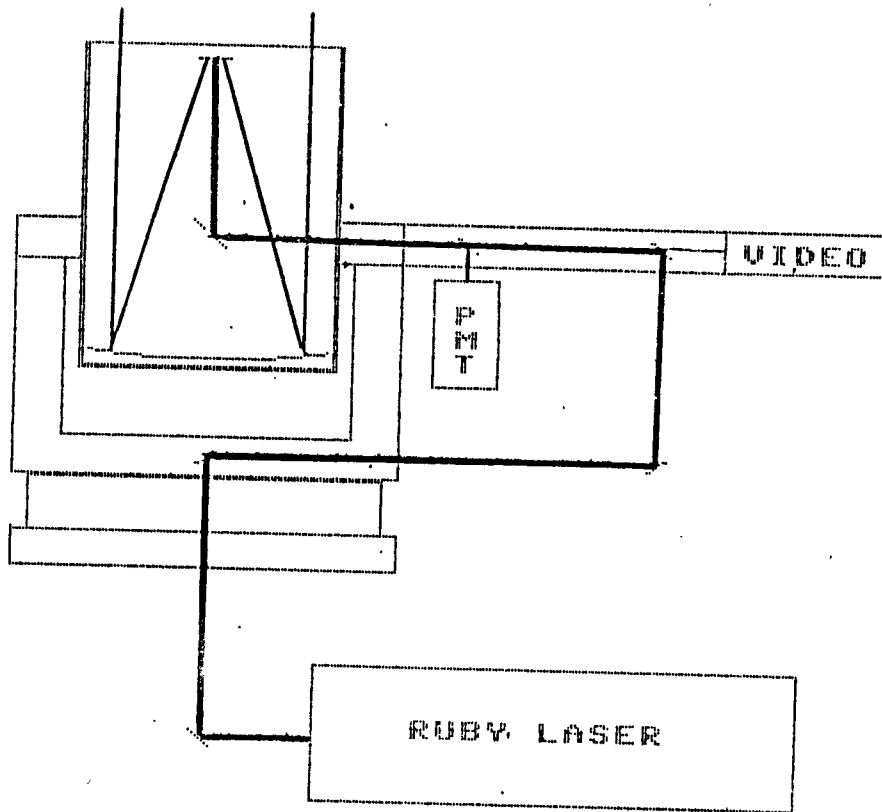


FIGURE 1a  
OPTICAL DIAGRAM

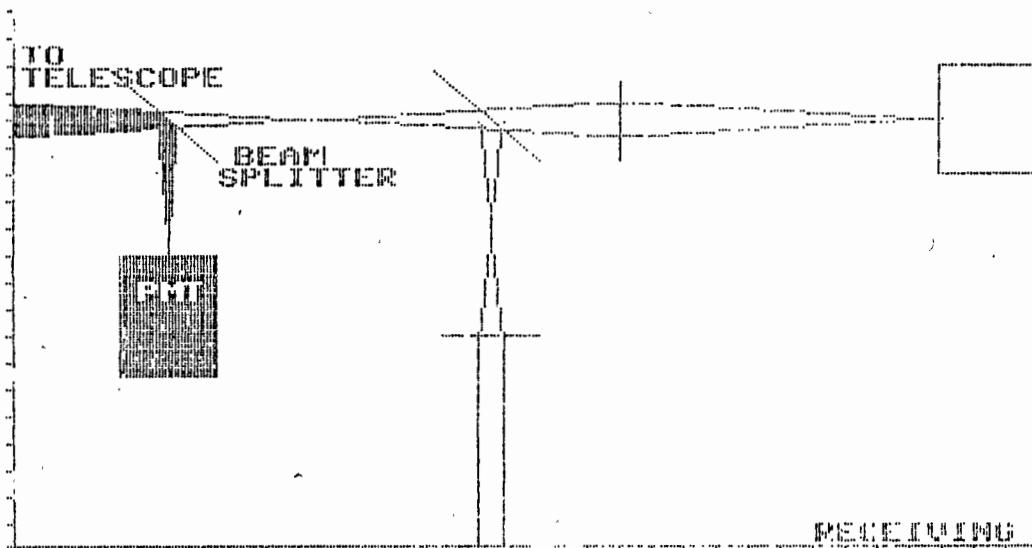
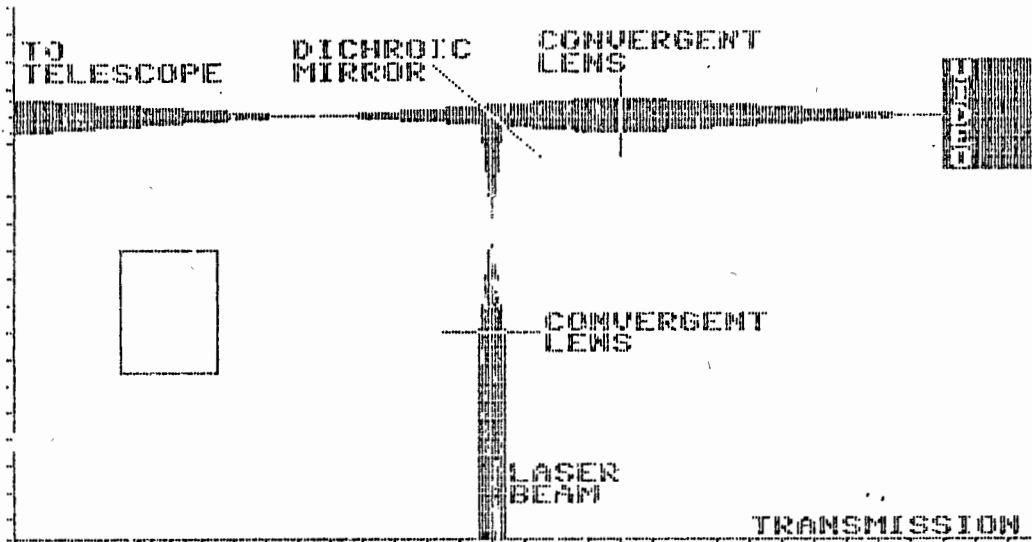


FIGURE 1b

## 2. FOLLOWING MOVEMENTS

For azimuth and elevation drives the cinetheodolite was equipped with servomotors of the type with direct current and low inertia which are coupled to the axes with gear wheel - worm screw couples.

The motors for following are driven by servoamplifiers and their speed is read by speedometer dynamos.

The speedometer dynamos, which make up the velocity feedback towards the servoamplifiers, are keyed on the same axis as the motors themselves.

The guiding servoamplifiers, built with LSI technology, are switching converters with bidirectional, high-speed response pulse wave modulation (PWM).

The controls are governed by a microprocessor which carries out the following duties:

- Control of the drive units
- Acquisition of angle data
- Closing of speed and position loops
- Limit switches
- Dialoguing with computer personnel

The microprocessor directly governs the function of following control by means of the position feedback supplied by the encoders.

The azimuth and elevation encoders used are of the absolute type with a 16 bit angular resolution; they consist of an optical-mechanical part and a card containing all the electronic interfacing to the data acquisition and control microprocessor.

In order to optimize the angle readings the encoders were installed close to the two rotational axes with a system for the taking up of mechanical play such as to guarantee aim accuracy with a tolerance of <0.1 degrees.

Table 2

### SERVOMOTOR AND ABSOLUTE ENCODER

NOMINAL TORQUE	77 Ncm
NOMINAL EFFECTIVE POWER	240 Watt
SPEEDOMETER DYNAMO LINEARITY	0.18%
ENCODER OUTPUT CODE	BINARY
NUMBER OF BIT	16
AIM ACCURACY	0.0017 rad
ZERO ADJUSTMENT	by dip switch

### 3. DATA ACQUISITION SYSTEM

As in the case of following control, the data acquisition sub-system is also governed by a microprocessor which carries out the following tasks:

- a). time reading at the instant it receives the stop signal from the PMT;
- b) telescope position reading;
- c) Reading of time interval recorded by the time interval counter;
- d) temperature, humidity and pressure sensor readings;
- e) Dialogue with computer personnel.

The clock is triggered by the 1 Mhz sample frequency of our Master Clock and therefore gives a resolution of 1 us.

Furthermore, the clock is equipped with an output at various frequencies for the laser control trigger.

Readings are carried out serially at the moment in which the stop signal is received from the photomultiplier in the order given above.

The entire system will be managed by an IBM or IBM compatible personal computer to facilitate the management of both the follow control and data acquisition sub-system and the files of data acquired during satellite rangings.

In Table 3 the salient characteristics of the system are described.

Table 3

#### DATA ACQUISITION SYSTEM FEATURES

CLOCK RESOLUTION	1 us
CLOCK PRECISION	not yet verified
PULSE TRIGGER FREQUENCY	1Hz-10Hz
HP COUNTER RESOLUTION	20 ps
HP COUNTER PRECISION	100 ps

Table 4

#### STATION SITE DATA

STATION NUMBER	9999 (Punta Sa Menta)
LATITUDE	39° 08' 32"
LONGITUDE	8° 58' 12"
ALTITUDE	202 m ssl
CAVU	Average 120 days an year

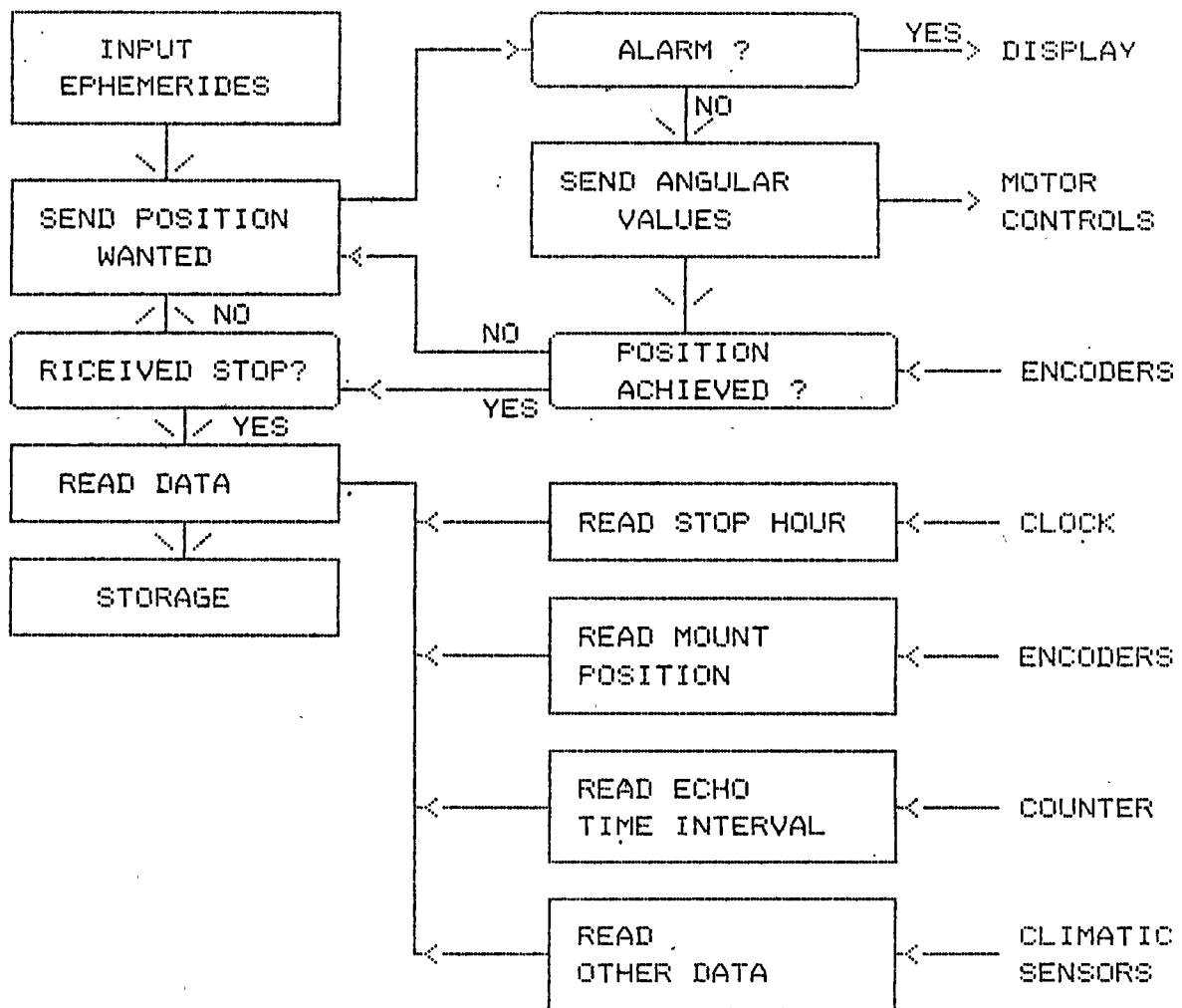


Figure 3  
CONTROL PROGRAM FLOW CHART

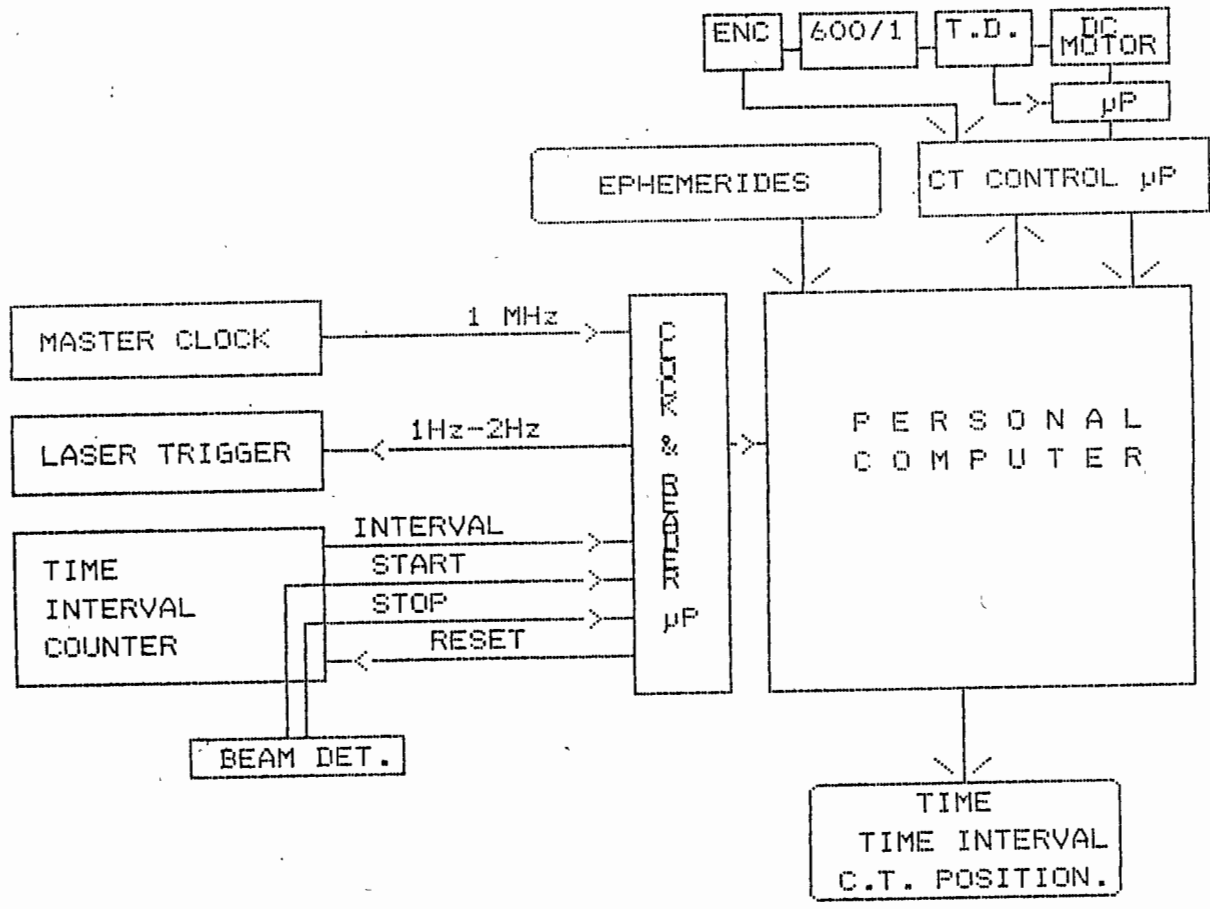
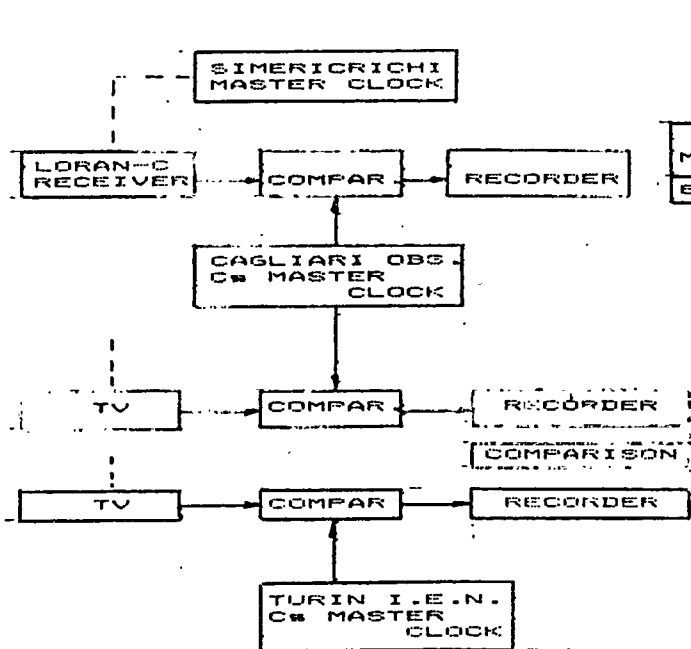


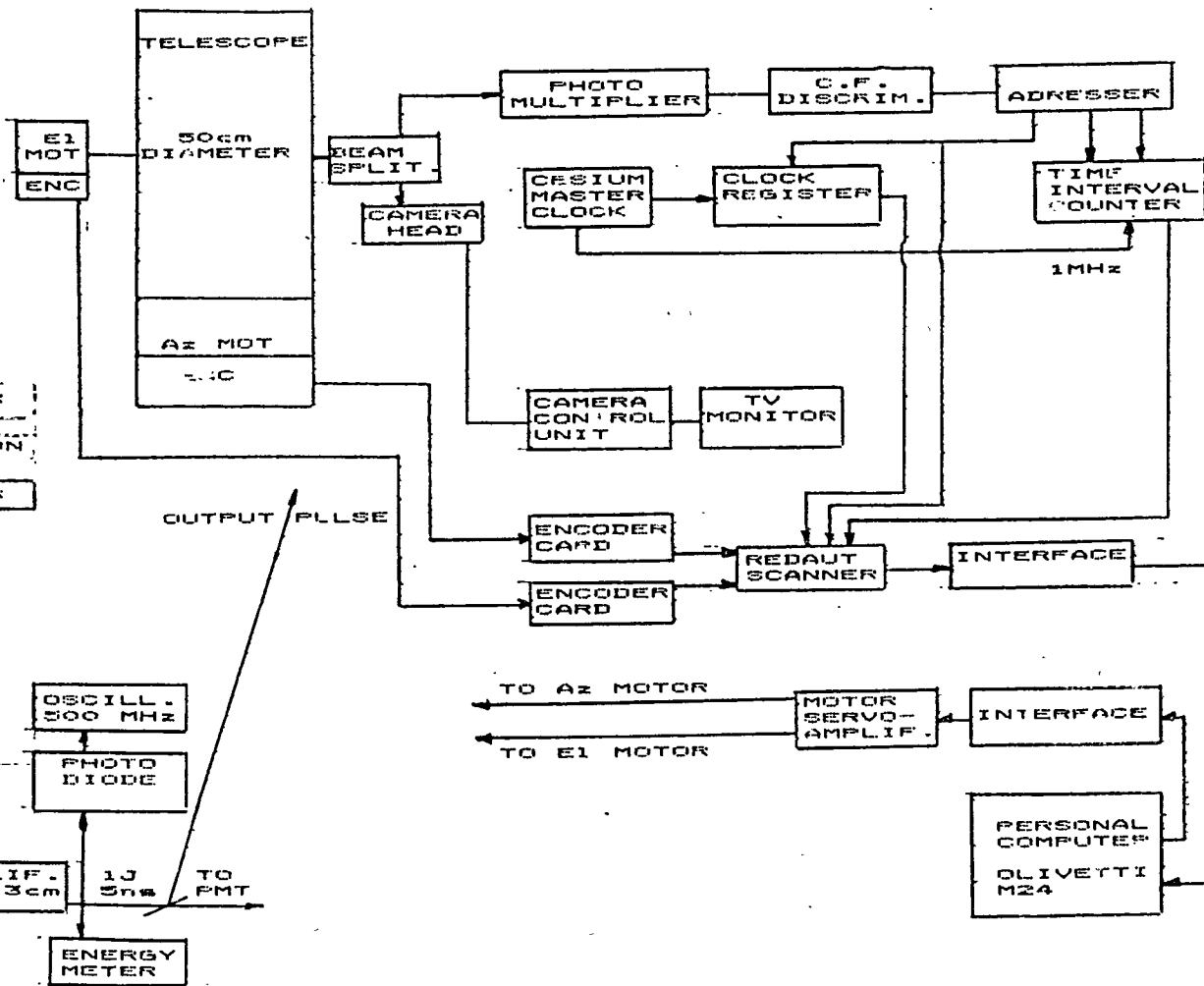
Figure 2  
CONTROL BLOCK DIAGRAM

# CAGLIARI LASER STATION

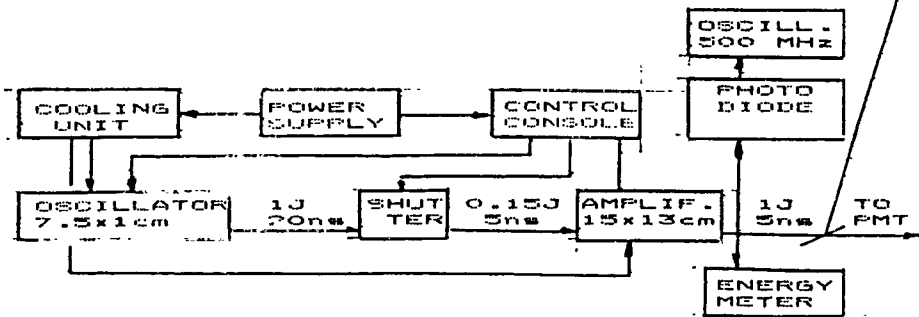
## TIME SYNCHRONIZATION



## ECHO RECEIVER AND DATA RECORDING SYSTEM



## LASER TRANSMITTER SYSTEM



## TRACKING SYSTEM

REFERENCE

Cugusi L., Messina F., Proverbio E.  
A LASER RANGE TRACKING STATION FOR GEODYNAMIC SATELLITES  
,Proceedings of the Second Workshop on Laser Tracking  
Instrumentation, Prague 1975

Cugusi L.  
THE SATELLITE LASER RANGING SYSTEM AT CAGLIARI OBSERVATORY  
Proceedings on Third Workshop on Laser Ranging  
Instrumentation, 1978



ZIMMERWALD SATELLITE OBSERVATION STATION

P. Kloeckler, Th. Schildknecht  
Astronomical Institute  
University of Berne  
Sidlerstrasse 5  
CH - 3012 Berne - Switzerland -

Telephone +4131 65 85 91  
Telex 912643 PIBE CH  
Mark-3/Quick-Com AIUB

1986 STATION REPORT AND ESTIMATE OF SYSTEMATIC ERRORS

## 1986 STATION REPORT AND ESTIMATE OF SYSTEMATIC ERRORS

### ZIMMERWALD SATELLITE OBSERVATION STATION

P. KLOECKLER AND TH. SCHILDKNECHT

ASTRONOMICAL INSTITUTE  
UNIVERSITY OF BERNE  
SIDLERSTRASSE 5  
CH - 3012 BERNE  
SWITZERLAND  
TELEPHONE: +4131/65 85 91  
TELEX: 912 643 pibe ch  
MARK-3/QUICK-COM: AIUB

#### 1. STATION REPORT AS PER SEPTEMBER 1, 1986

##### LASER

Measurements proved that the emitted laser energy in the mean was never above 5 millijoules, a fraction of the permitted energy with the Quantel 402 DP laser. Yet already at this output level the KD\*P doublers had to be reworked quite frequently. The reason for this is suspected insufficient mechanical stability, and possibly uneven energy profile of the beam.

The average frequency of the laser shots also was never up to the expected 9 Hz or so, but mostly lingered around 5 Hz. This in turn reduced data-yield. Active/passive mode-locking in the near future will improve this situation.

An unnoticed breakdown in primary laser cooling caused destruction of a ND-YAG window and consequently a break in observations between July and September 1985.

The pulse-selector (Krytron switch) proved unreliable and will be replaced by the end of this year.

##### TRANSMIT OPTICS

The lenses of the Galilei telescope were replaced by a more precise set with better coatings, thus affording better transmittance and far field.

##### RECEIVER

After the protective shutter had been installed, and 1 GHz bandwidth provided for the timing channel, the microchannel plate photomultiplier (Hamamatsu R1294U) was tried with some good results.

99% of the data, though, have been gathered with the conventional photomultiplier model D341B by EMI.

A HP5370A time interval counter was purchased in spring 1986 and added to the system. Due to the computer limitations mentioned

below, it could be used only for calibration purposes so far. Intercomparison with our time digitizer showed a small reduction in digitizing noise, but no noticeable difference in systematics.

### COMPUTER

The software was extended by some degree; most prominent extensions were the possibility of communicating via GE-Mk 3 (making telex transmission of QL data obsolete), improved tracking support and data screening.

The station computer PDP/11-40 under RT-11 and only 64 kbyte of RAM limited the program evolution, and many new concepts could not yet be implemented. Because of this, and the increasing failure rate, we decided to introduce a new computer, most possibly during 1987.

### TIME SYSTEM

The station was fitted with a BVA quartz oscillator as principal time-base. This type of oscillator is reported to yield the best short-time stability.

### OPERATIONS

Tracking efforts were considerable, but yields moderate. The weather limited observations, as well as the bad nocturnal coverage by LAGEOS in summer 1986. Much time was put into calibrations, to finally be able to specify an error budget.

Some special efforts were taking place in the fall of 1985, when the dutch MTLRS was visiting Mte. Generoso in southern Switzerland. SLR, terrestrial LR and GPS observations were gathered. Results are presently under review.

### FUTURE IMPROVEMENTS AND ADDITIONS

The modifications of the laser for active/passive mode-locking and spatial filtering are under way. The computer replacement (most probably by a DEC Microvax) and an exchange of angle-encoders will be the most prominent upgrades at the station in 1986/7. We also hope, by modification of the building structure, to gain space for a new laser table. The purpose is to rearrange the laser related equipment to facilitate a mechanically more stable setup, and to solve the radio interference problem into the electronic system.

## **2. PRECISION ESTIMATE OF ZIMMERWALD LRS**

This summary report covers the period September 1984 through August 1986. More detailed information is available on request.

### 2.1 MODELLING AND ENVIRONMENTAL ERRORS

The survey error is not being specified because we describe a stationary system.

Refraction corrections are especially sensitive to the pressure measurement. From barometer trips from the State Standards Laboratory, we conclude that the mercury barometer at our station is not beyond doubt. This situation is being cleared,

and for the reported period a worst case estimate used.<sup>1</sup> No measurements are made below 30°.

## 2.2 RANGING MACHINE ERRORS

### SPATIAL VARIATION

No test of this has been made due to the lack of external calibration. We trust that our mode-locked QUANTEL laser performs equal to those tested at GSFC. Any remaining spatial effect should tend to average out due to our rather erratic tracking.

### TEMPORAL VARIATION

As we perform in-pass calibration, temporal effects are minimized. However, the calibration measurements have been averaged over the whole pass so far. The mean has been rounded to 1/10 of a nanosecond, introducing a rounding error which should not introduce systematics.

### AMPLITUDE DEPENDENCE

The system was mostly operated in the 1-10 photon region (LAGEOS). Stronger returns were noticed on the display and the beam immediately widened, thus limiting time-walk. Any excess amplitudes could be detected after screening and appropriate measures taken.

### CALIBRATION PATH

The internal path geometry can be sufficiently well measured. On the other hand there is a piece of optical fibre for feedback, the delay of which has to be measured electro-optically. The method employed ensures an uncertainty of less than 100 picoseconds (a value which can be improved in the future.)

### CALIBRATION (METEOROLOGICAL CONDITIONS)

Not applicable because of internal calibration.

### MOUNT MODEL

Mount eccentricity is removed by the internal calibration.

### TIMING ERRORS

Daily TV comparisons ensure an accuracy of  $\pm 1$  microsecond; an additional allowance is made for the drift of the TV delay-constant, which is checked yearly by clock transport. Since this method allows only "a posteriori" time comparison, the QL data epochs are of LORAN accuracy. ( $\pm 5$   $\mu$ s worst case).

We finally wish to remark that we miss a specification of the short-time stability of the flight-time clock (scale factor) ! We urge that this issue be discussed at the next opportunity !

<sup>1</sup>Note: A fault in the mechanical readout of the barometer has been found meanwhile; no adjustment is made of the data because the error was judged negligible.

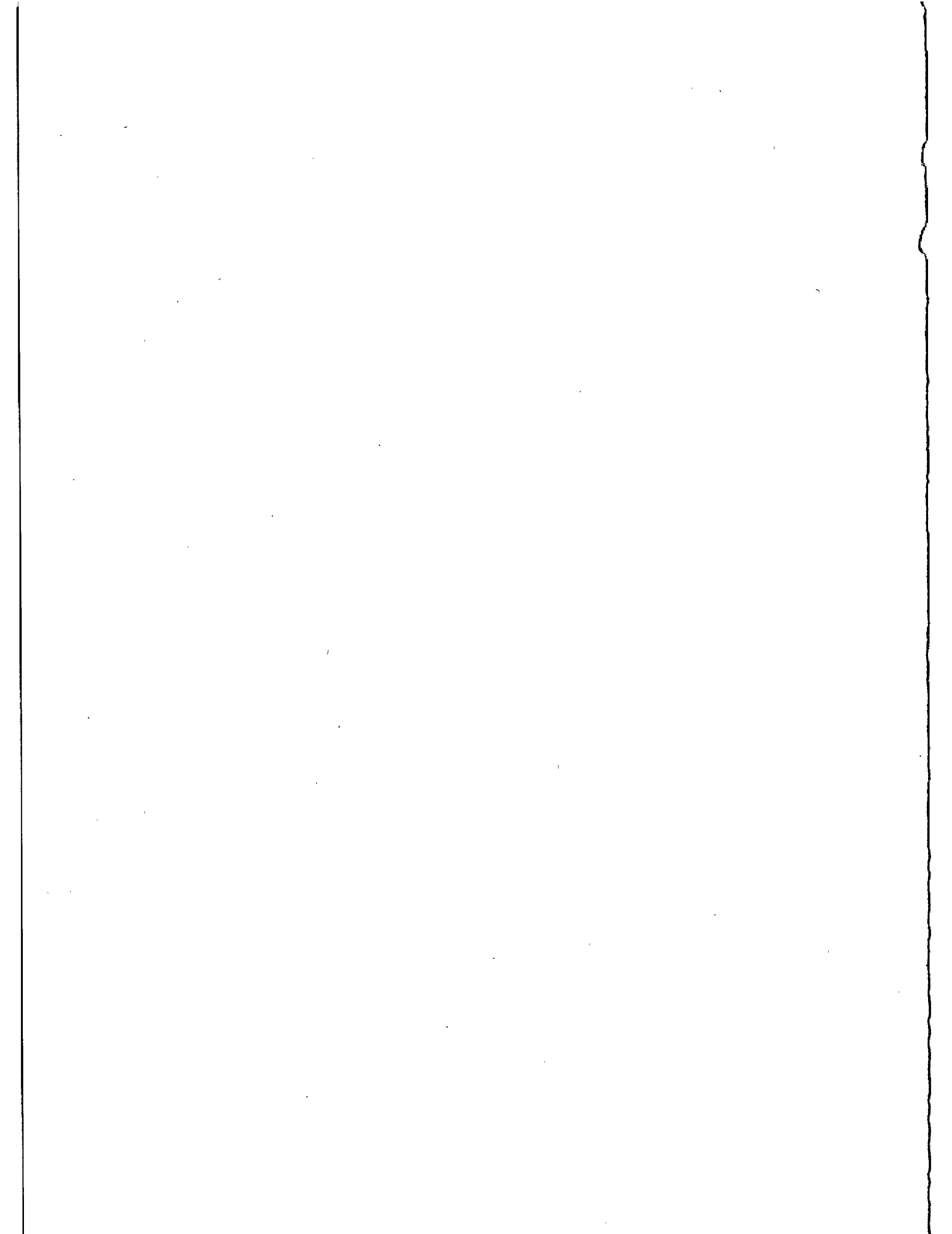
RANGING ERRORS (CM)

	PASS	DAY	MONTH	INDEF.
<b>MODELLING ENVIRONMENTAL ERRORS</b>				
ATMOSPHERIC PROPAGATION (MODEL)	.5	.5	.5	.5
ATMOSPHERIC PROPAGATION (METEOROLOGICAL MEASUREMENTS)	1.0	1.0	1.0	1.0
SPACECRAFT CENTER OF MASS	.2	.2	.2	.2
GROUND SURVEY OF LASER POSITION	-	-	-	-
DATA AGGREGATION	-	-	-	-
R.S.S.	1.2	1.2	1.2	1.2
<b>RANGING MACHINE ERRORS</b>				
SPATIAL VARIATION	1.0	.5	.5	.5
TEMPORAL VARIATION	1.0	.3	.1	.1
SIGNAL STRENGTH VARIATION	3.0	3.0	3.0	3.0
CALIBRATION PATH (SURVEY)	1.5	1.5	1.5	1.5
CALIBRATION PATH (METEOROLOGICAL CONDITIONS)	-	-	-	-
MOUNT ECCENTRICITIES	.1	.1	.1	.1
R.S.S.	3.70	3.50	3.40	3.40

RANGING ERRORS (CM)  
TIMING ERRORS (MICROSEC)

PORTABLE CLOCK SET	1.0	1.0	1.0	1.0
BROADCAST MONITORING	1.0	1.0	1.0	1.0
R.S.S.	1.5	1.5	1.5	1.5

ESTIMATED RANGING ERRORS FOR SATELLITE LASER RANGING SYSTEM  
ZIMMERWALD LRS (7810) 1984-1986



## THE NEW CERGA LLR STATION

Ch. Veillet, J.E. Chabaudie, Ch. Dumoulin, D. Feraudy  
J.G. Langlois, J.F. Mangin, J. Pham-Van, J.M. Torre  
C.E.R.G.A.  
Avenue Copernic  
06130 Grasse - France -

Telephone 93 36 58 49  
Telex 470865 F

### ABSTRACT

The new Cerga Lunar Laser Ranging station is presented with its main characteristics. The new YAG laser delivers at 10 Hz two beams 300mJ each in green with a 300 ps pulse. The new transmitting/receiving/pointing package is described as well as the computer environment. The first series on a single night (obtained after the workshop) are finally shown.

## 1/ Introduction

The CERGA LLR station has been operating for four years with results increasing both in quantity and quality. It used a ruby laser with a 3ns/3J pulse and 10 shots per minute. Fig. 1 shows the progression in data quantity and diversity (various reflectors ...). Since April 1984, the normal point accuracy has been stable around 16 cm on the Moon distance. The CERGA station has been the most productive in 1985, and more than 2/3 of the UT determinations made from LLR that year have used CERGA data.

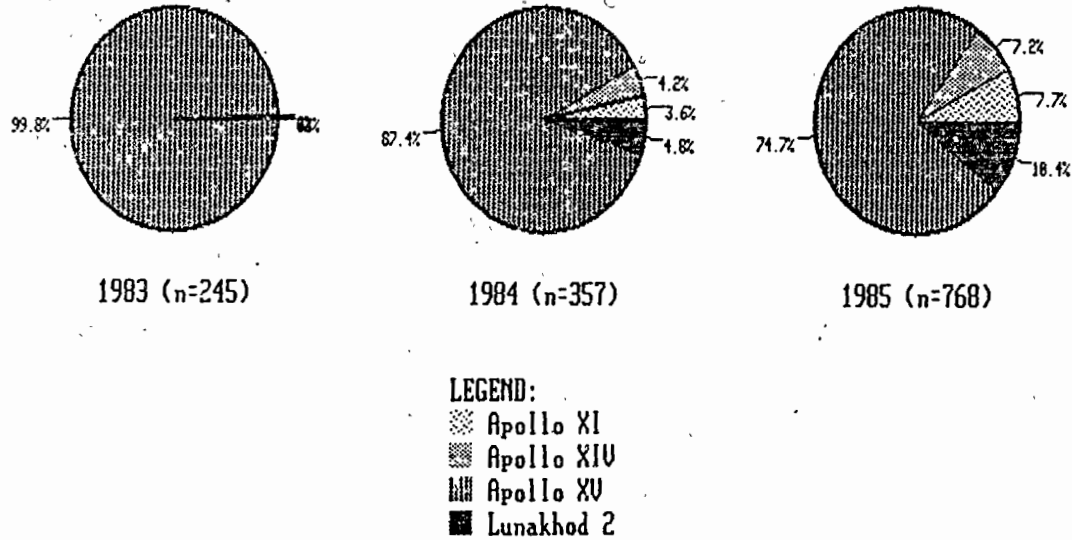


Fig. 1 - Normal point total number and repartition over reflectors - *n* is the number of normal points obtained with the old ruby laser at the CERGA LLR station for the given year.

In order to improve the accuracy of the data, an upgrade on two years has been planned for 1985 and 1986, including a new computer, a new laser and the new transmitting/receiving equipment linked to different laser rate and wavelength.

## 2/ The laser

Fig. 2 shows the implementation of the new Quantel Nd-YAG laser components on the granite. The oscillating cavity can work in both active/passive (dye cell) or active/active modes. After the slicer, each pulse is 1 mJ in 300 ps in active/active mode, or roughly .4 mJ in 200 ps in active/passive mode, both at a 10 Hz pulse rate and in infra-red. Two consecutive 7mm rod amplifiers permit to reach 200 mJ in active/active mode. This pulse is divided in two equal pulses, both of them being finally amplified on its own third amplifier (9mm rod), a delay line insuring a simultaneity of the start at the granite edge. The final energy is 600 mJ in infra-red per 300 ps pulse and per beam at 10 Hz.

By changing the Fabry-Perot glass at the cavity output edge, other pulse lengths in active/passive mode can be obtained down until 35 ps. They can be used for exemple for accuracy tests on the electronics. If the active/active mode is easier to work with (there is dye check and maintenance), it is less stable in energy. This mode has been used at the beginning till December 1986. The active/passive mode is now used due to a much better stability.



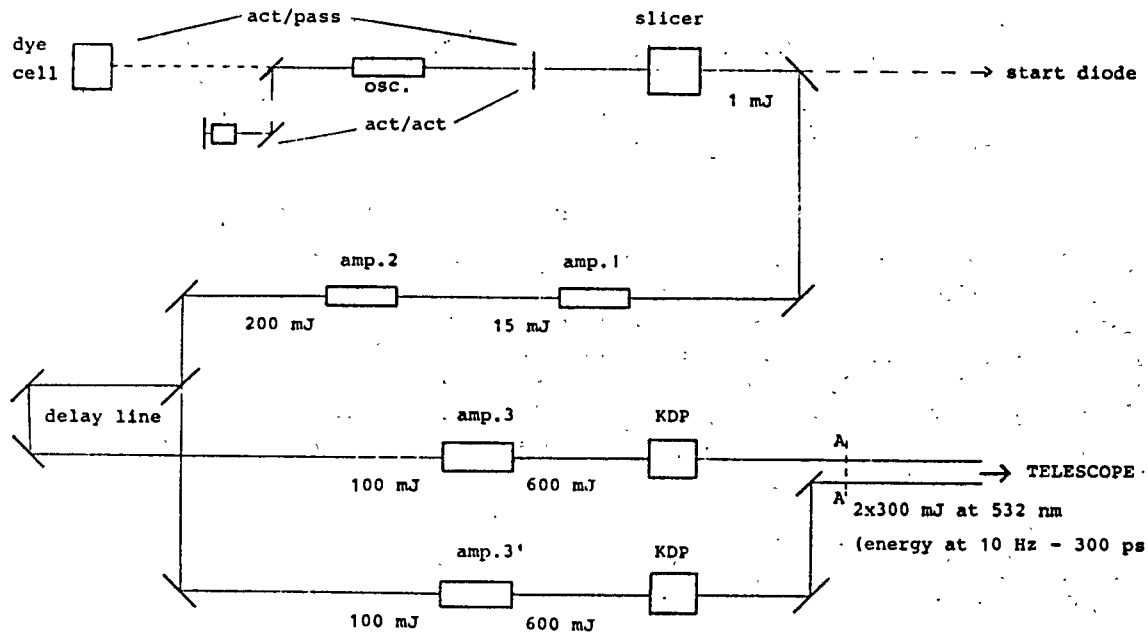


Fig. 2 - Laser configuration - Energies are given at 10 Hz rate for 300 ps pulses.

The shape of the two beams at the edge of the laser and on the telescope aperture can be seen on Fig. 3. Each beam has a 9 mm diameter after the last amplifier. The two beams are made parallel at the laser edge with a 9 mm separation. At the matching lens level, the laser spots are tangent and roughly 15 mm wide. This double beam configuration has been chosen in order to increase by a factor 2 the emitted energy without increasing the risks of damaging the optical components, and for only 20% of laser total cost.

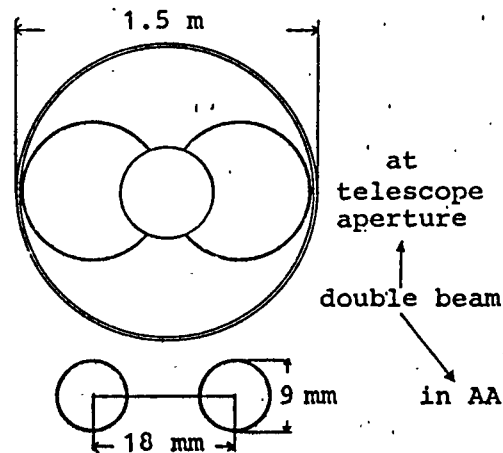


Fig.3 - Double beam configuration

### 3/ The transmitting/receiving/pointing package

The general design of this package is shown on Fig. 4. This system is mounted on the telescope and is moving with the telescope azimuthal motion. It has been designed in order to minimize the number of optical components encountered by the returns. The transmitted beam is entering the telescope after the matching lens (ML) and a reflection on a rotating mirror (RM1). This mirror itself starts the laser when in transmission position. Its speed is monitored by the computer in order to insure that the returns are entering the receiving path through the hole of the second rotating mirror, in fact a rotating hole (RM2). RM2 allows to send the pointed field on a COD camera and then to view the pointed area on a TV screen when RM1 is not transmitting nor RM2 receiving (most of the time).

A diaphragm adjustable from 5 to 60° is located at the telescope focus (F) on the return path. A dichroic glass (D) sends the green returns on the PMT through the filter wheel (FW) within an afocal system. The red way is free in R where an eye-piece can be used, waiting for a receiving package at 1.06 m.

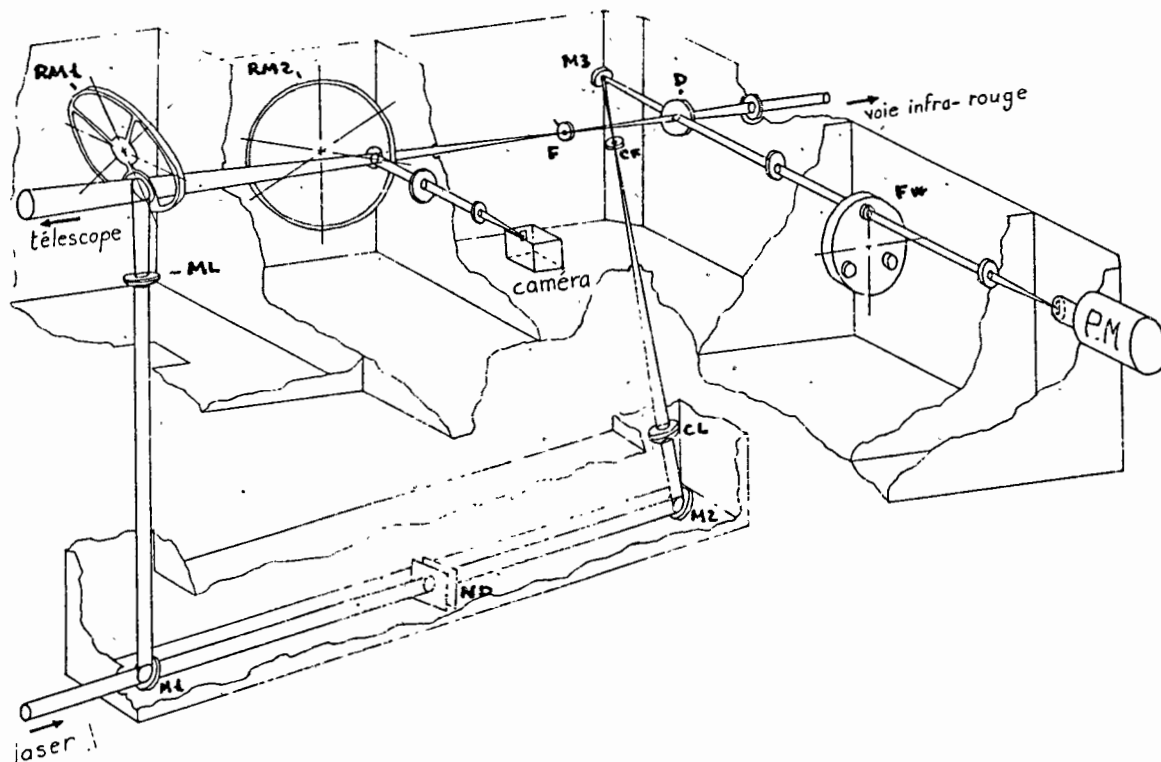


Fig. 4 - Transmitting/receiving/pointing package - See text for information.

The internal calibration path is shown on the same figure. The light transmitted by the first mirror M1 (lower left) is sent on the receiving package through neutral densities (ND) for attenuation, a second mirror M2 and a converging lens CL focusing the calibration in a point CF conjugate of the telescope focus. After M3, the calibration go through the dichroic glass (D) and follows the return path till the PMT.

#### 4/ The computer and its environment

The new computer (PDP 11/73) has been installed in September 1985 and has monitored the ruby station ten months before the laser change. Its environment is shown on Fig. 5. The main characteristics of the configuration is that the PDP is not concerned with telescope pointing and guiding. At the beginning of each observing session, the data needed for pointing the Moon (9 reference craters and the five reflectors) and close stars are sent from the PDP to a microcomputer Victor S1. This small computer is sufficient for running the telescope for all the night with a very friendly software.

The PDP is thus only busy with the real time monitoring of the station : rotating mirrors enslavement, event acquisition (laser starts, internal calibration and in gate events), gate commands, ... The event-timer has one channel for the laser start and three other for events (calibration or/and gate events). Its resolution is 50 ps. A link is planned between the PDP and a CCD camera used for pointing stars or features on the Moon. It could be used for an automatic pointing (planned for the end of 1987). A data processing is made at the end of each series providing with the normal point (if there are identified returns). At the end of the night, these data can be used for a UTO determination.

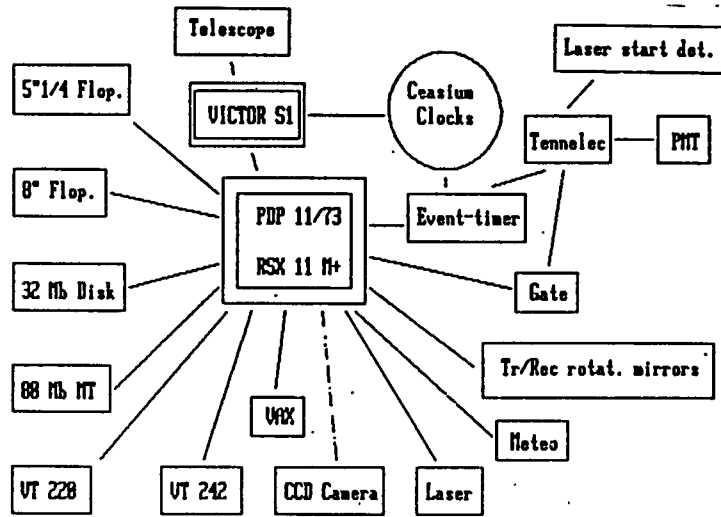


Fig.5 - Computer environment

The PDP is linked to the VAX computer located at the CERGA down and the normal points can be sent from the station on the VAX and from there on the CNES CDC computers.

#### 5/ Conclusion

The system described here is working since the end of September 1986. It is planned to spend 6 months to test and improve the various components of the station recently modified or changed (laser, electronics, mechanics and software). It is thus too early to give some conclusions on the efficiency of the new station. The next paragraph added after the workshop will show the first results, but no information on energy or error budgets can be extracted from these data. The PMT, the laser and the internal calibration were not at there normal efficiency ... and the timing electronics was not tuned at this time for minimal jitters and biases.

The year 1987 should proof the quality both in accuracy and in efficiency that we hope to have with this new LLR station.

## 6/ First results ...

Fig. 6 shows a plot of the residuals for four normal points obtained in November 1986 (ns on the round-trip). The dotted line shows the fit done to determine UT0 from the data. It can be seen that the prediction used for the observations was very poor. The value finally found using X and Y prediction from BIH is :

$$UT0 - UTC = -0.09024 \text{ s } (\sigma = .00127) \text{ at } JD = 2446759.673591$$

The weighted rms of the residuals is 4.5 cm on the Moon distance.

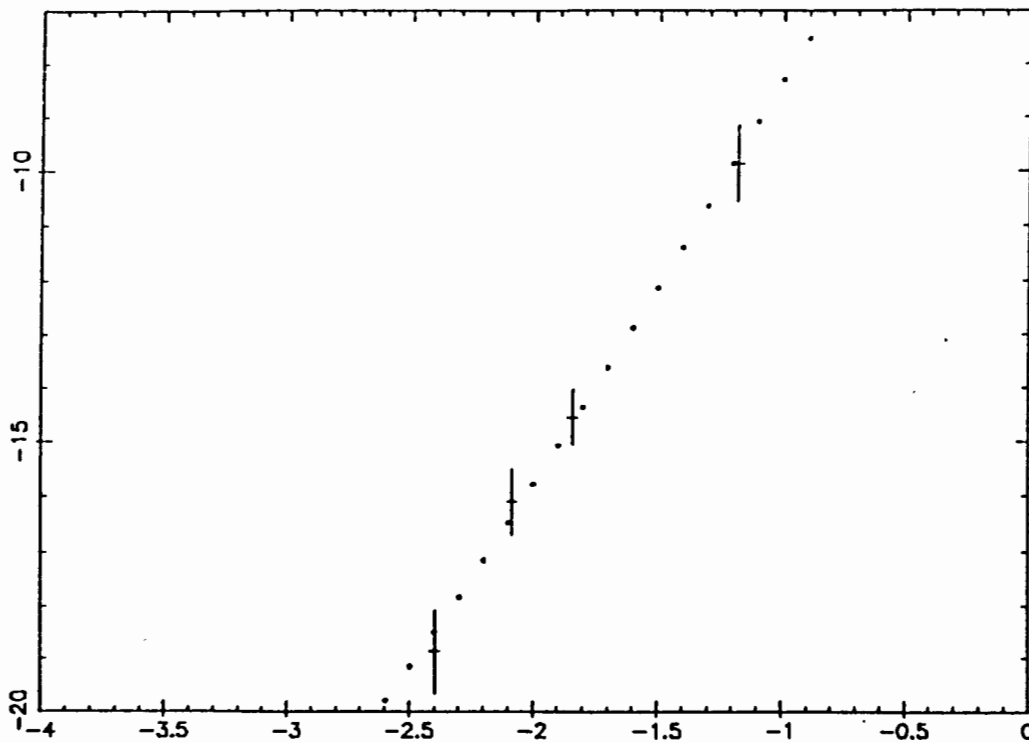


Fig. 6 - First normal point residuals - November 1986 - Residuals for four normal points in ns relative to the hour angle of the Moon (in hr). See text for more information

RECENT IMPROVEMENTS AND FUTURE PLANS AT THE UNIVERSITY OF HAWAII  
LUNAR AND SATELLITE RANGING STATION

M.L. White  
Lure Observatory  
Institute for Astronomy  
University of Hawaii  
Kula, HI 96790

Telephone (808) 878-1215  
Telex 7238459

ABSTRACT

Significant improvements have been made to the University of Hawaii laser ranging station during 1986. A new data processing and software development computer has been installed, and the real-time ranging computer has been upgraded. The ranging electronics and optical systems have been improved. These improvements and future station plans are discussed in this paper.

## RECENT IMPROVEMENTS AND FUTURE PLANS AT THE UNIVERSITY OF HAWAII LUNAR AND SATELLITE LASER RANGING STATION

### I. Computer Hardware Improvements

During 1986 at Hawaii, major improvements have been made to the computer hardware. Due to the increased demand on the ranging computer by lunar operations, and the necessity for on site lunar data analysis, a new Micro PDP-11 computer was purchased and installed at the observatory's administrative office in Waikoa. The new computer will free up the real-time ranging computer for operations, while allowing the majority of software development and lunar data analysis to be done at Waikoa. Future lunar data analysis requires near real-time normal point formation. The operation's crew will hand carry lunar data on a removable 26 megabyte disk cartridge to the Waikoa data processing center where the Micro PDP-11 will be used create normal points and earth rotation/polar motion solutions. The lunar data products will be entered on the G.E. Mark 111 system the morning after the data is acquired.

Concurrently, plans were developed and hardware purchased to expand the real-time operating computer backplane from 18 to 22 bits, increase the virtual memory to 1.25 megabytes and increase the data storage capacity to 52 megabytes. These changes will significantly speedup real-time execution and streamline operational procedures.

### II. Optical Improvements

A new receive package was installed in the Multi-Lens-Telescope (MLT), greatly improving lunar ranging efficiency. During normal lunar operation the MLT alignment must be routinely compared to a guide camera to insure correct telescope pointing. The new receive package allows the operator to verify the telescope pointing and alignment by the electro-mechanical movement of a movie camera into the same location as the photo multiplier tube. The new receive package allows one operator to perform a task in several minutes which previously took two operators nearly 30 minutes.

The MLT has 160 individual turning mirrors which direct incoming light to a common focus. These turning mirrors were refastened after the epoxy, previously used to hold the mirrors in place, deteriorated. The deterioration of the epoxy caused the mirrors to become loose and unstable. The old epoxy was not as moisture resistant as expected. The new epoxy was applied in large quantities and is moisture resistant. A dramatic improvement in MLT alignment stability was observed as a result of applying the new epoxy. A complete MLT alignment is now required every 2 months rather than every 2 weeks.

A 1 angstrom bandpass filter was purchased and successfully tested in the lunar receiver. The double peak, polarized interference filter substantially improved the signal-to-noise ratio on illuminated lunar targets and during daylight lunar ranging.

Due to the unique design of the MLT, which consists of 80 individual light paths of varying lengths, a light pathlength compensator is needed. The compensator consists of 3 cylinders of solid glass that fit in the optical path of the MLT, delaying the longer path lengths. As is often the case with unique optical components, substantial fabrication time is required. After nearly two years since placing the order for the compensator, it is expected to be delivered by the end of 1986.

### III. Ranging Machine Improvements

Plans to install a new Micro-Channel Plate (MCP) detector in the satellite and lunar systems have been approved. As part of the MCP package, new Tennelec discriminators will replace the currently used Ortec 934 discriminators. The new detectors are likely to be installed and acceptance tested by early 1987. Other future ranging machine improvements include new 50 pico-second vernier cards for the University of Maryland event timer currently used in the lunar system.

### IV. Calibration

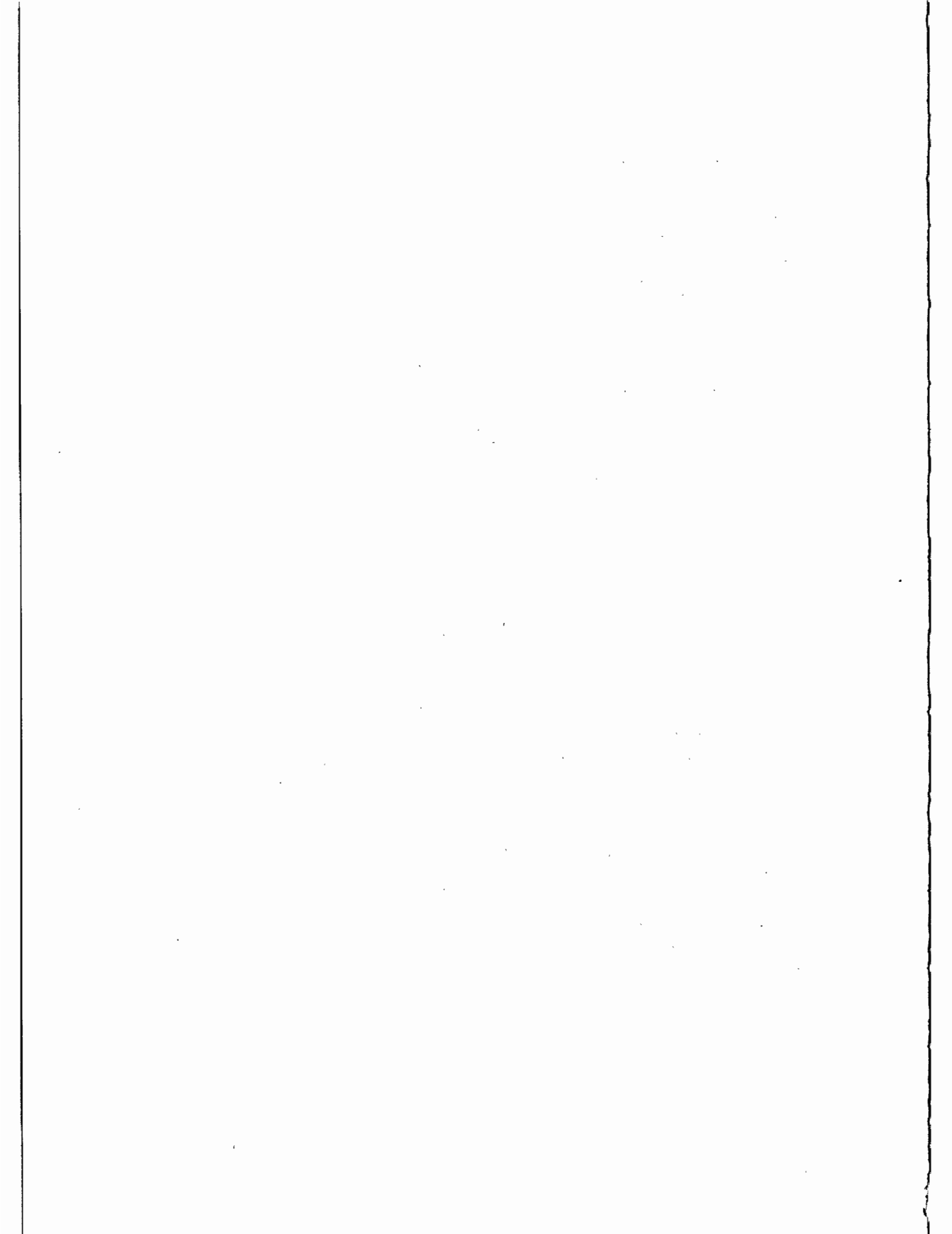
Currently, both the the lunar and satellite calibration are accomplished by ranging to an external calibration board located approximately 1 kilometer from the station. Internal calibration will be implemented by early 1987. The satellite system internal calibration will be easily accomplished due to the uniquely, simple design of the transmit/receive optics. The lunar system however, has a separate transmit and receive telescope making internal calibration more difficult. The use of a lengthy, single mode fiber optic cable will be required, and considerable testing will be necessary to verify calibration accuracy. Unlike the satellite system which uses a single stop epoch timer, the lunar system uses a multi-channel event timer, making real-time calibration possible. In both the satellite and lunar system the external calibration board will continue to be used as a verification of the internal calibration.

### V. Observing Schedule

Over the past 2 years, the Hawaii ranging station has generally scheduled 2 observing shifts, back to back during the evening, Monday through Friday. The 2 shifts range to LAGEOS and the moon with LAGEOS as the first priority. This schedule resulted in a considerable loss of lunar data when optimal ranging times occurred over the weekend, and occasional loss of LAGEOS data, when LAGEOS moved out of the night-time window. As of August 1986, the station began scheduling one shift during optimal lunar ranging periods (including weekends), and scheduling the second shift to maximize lageos coverage. This new scheduling scheme, though sometimes complicated in the case of lunar scheduling, has greatly improved lunar coverage and contributed to increased lageos tracking efficiency.

### VI. Conclusion

The University of Hawaii laser ranging station has provided very consistent state-of-the-art satellite ranging measurements to the scientific community for the past six years. During the past 3 years, the station has regularly provided lunar ranging data in quantities previously unobtained, and with normal point accuracies of less than 2 centimeters. The improvements discussed in this paper will allow the station to maintain state-of-the-art status by improving the ranging system accuracy and precision by a factor of 2 to 3, providing increased satellite and lunar coverage, and providing real-time earth rotation/polar motion solutions.





THE McDONALD OBSERVATORY LASER RANGING STATION : MLRS

J.R. Wiant, P.J. Shelus  
McDonald Observatory and Department of Astronomy  
University of Texas at Austin  
Austin, Texas 78712-1083 - USA -

Telephone (512) 471 4461  
TWX 910874 1351

ABSTRACT

Since the last Workshop of this type, which had been held in England some two years ago, a number of changes have been made with respect to laser ranging operations at McDonald Observatory near Fort Davis, Texas. First and foremost is the fact that all lunar operations on the 2.7 m (107") McDonald reflector have been discontinued and our entire operations, both lunar and LAGEOS, have been totally assumed by the stand-alone, dedicated 76 cm (30") based system now known as the McDonald Laser Ranging Station, MLRS. Since the MLRS system has been the subject of many reports in the past, this paper will only summarize the up-grades and improvements which have been made to that system over the past two years. These improvements include, but are not limited to, a new high-energy, short-pulse Quantel Nd-YAG laser capable of ranging both to the moon and to LAGEOS, a second Data General NOVA-based computer and Winchester-type hard-disk system providing for improved observing capabilities as well as for data pre-processing and analysis, the installation of 21-bit encoders and a new telescope bearing for improved tracking and pointing, as well as new timing and photomultiplier equipment. All of the relevant changes will be presented and discussed together with the impact of those improvements on the MLRS data yield, both with respect to the moon and to LAGEOS.

This work is being supported by the National Aeronautics and Space Administration under Contract NAS5-29404 to McDonald Observatory and the University of Texas at Austin from the Goddard Space Flight Center in Greenbelt, Maryland.

## Introduction

The McDonald Observatory and Department of Astronomy of the University of Texas at Austin continues to operate the McDonald Laser Ranging Station (MLRS) for the NASA Crustal Dynamics Program under contract to Goddard Space Flight Center. The MLRS is a dual purpose installation designed for laser ranging operations to both lunar and artificial satellite targets. The station is located on the grounds of the Observatory, about 17 miles north of Fort Davis, Texas. Various operational, programmatic, and logistical support is also provided by several personnel associated with the Department of Astronomy on campus at the University of Texas in Austin. Since the MLRS system and its operations have been the subject of so many reports in the past, this paper will only summarize the up-grades and improvements which have been made to that system over the past two years (since the last laser ranging workshop).

## Hardware Changes

The 18-bit absolute encoders on both axes of the alt-alt telescope were removed and replaced with 21-bit encoders. Only minimal software changes were required to take full advantage of the increased angular resolution and the expected pointing and tracking improvement was recognized immediately. The full extent of MLRS pointing and tracking capabilities has still not been fully realized however because of suspected bearing problems (especially for the telescope yoke). Work on this sub-project continues.

A single, short-pulse, dual-power laser was supplied to us by NASA/Goddard to replace the original two-laser system of the MLRS. With the help of Grant Moule, from the Australian laser ranging station at Ororral, this new laser went from shipping crate to operational status at the MLRS within nine calendar days. The advantages of the new laser system over the old are numerous. Alignment and calibrations need now only be performed for a single laser. There is possible a very rapid changeover from lunar to LAGEOS operations and vice-versa (~20 seconds). A more convenient physical arrangement allows for easier maintenance. And, of course, the ability to range the moon with a 200 picosecond pulse (instead of the 3 nanosecond pulse of the former system) has not been lost on the LLR analysts.

The Varian "super-tube" photomultiplier was recovered from the TLRS, when that system was up-graded to a more powerful laser, and this new tube was then incorporated within the MLRS. This new PMT has been observed to reduce the RMS of both the internal calibration and the data themselves by a factor approaching two over their former values. Further, the Varian is considerably less "noisy" than the previous tube used. A cloud on the horizon is the possible contamination of data quality caused by a potential time-dependent "beam-walk" problem across the face of the tube.

In order to establish the capability of performing simultaneous data acquisition and data reduction at the MLRS, some additional funding provided to us by the U. S. Naval Observatory allowed us to purchase and install an entire second Data General Nova computer system within the MLRS operating environment. In addition to a new CPU, there were two 160 M-Byte Winchester disk systems (with associated dual-controllers), an additional 9-track magnetic tape deck, and various communications peripherals purchased. As an additional benefit of this new computer system is the fact that two data streams can be simultaneously processed (when no observing is being performed) and we can temporarily share equipment to retain full observational capability (at the expense of data reduction) if there is an equipment failure. An IBM PC/AT Microcomputer was purchased with various peripheral hardware and software items as we seek to do "smart" terminal emulation in anticipation of the eventual "death" of our old and venerable Tektronix 4025 graphics terminals. Finally, an Apple Macintosh PC microcomputer was purchased for documentation preparation, the making of schematic

drawings, monthly reporting, and direct file transfers between the Austin and the Observatory portions of this project.

In an attempt to alleviate as many seeing-related problems as possible at the MLRS, an air conditioning unit was purchased and installed in the MLRS telescope room. This unit provides active temperature and humidity control during non-operating hours. Operations have been streamlined since this installation because far less time need now be spent in waiting for the telescope to come to thermal equilibrium with its surroundings after the dome has been opened in anticipation of ranging operations.

Finally, after 15 years of faithful service, our LORAN-C receiver has been retired. Its role in providing accurate epoch monitoring at the station has been taken over by a Global Positioning System (GPS) receiver. Also, we have abandoned our attempts to incorporate the computer controlled narrow-pulse filter in the MLRS receive system.

### Software and Logistical Changes

As might be expected, a myriad of software changes were incorporated into the MLRS computing systems in concert with most of the hardware changes mentioned above. Fortunately, because the MLRS was originally designed to be a software intensive one, these software changes could be designed, coded, and debugged "off-line", well before the implementation of the actual hardware changes. Thus, in most instances, they could be incorporated into the system without requiring additional station down-time except for that which was required for the actual hardware changes themselves. Further, many routine changes were made in the data processing systems to accommodate data format and electronic communications up-dates and up-grades. Again, each of these was completed and implemented with a minimum of difficulty, all the time maintaining active communications with the outside world.

As far as MLRS observing operations go, it is safe to say that since December 1985, the station has finally realized a large percentage of its original observational potential. Day-time LAGEOS ranging is now accomplished with the same ease as night-time ranging and the lunar system has become as reliable as the 2.7-m system was. In reality, over the past year or so, only the weather has been our major problem (see the illustration of MLRS data statistics for both the moon and LAGEOS). With that in mind, a great deal of time and effort has been expended to examine the trade-offs between cost and data throughput to provide for the most cost effective operation of the dual lunar and artificial satellite capabilities of the MLRS. To that end we have strongly recommended that a minimum of two-shift operation always be present at a dual-capable station like the MLRS. In that scenario, one of the shifts is relatively fixed in an eight hour per day, five day per week schedule to concentrate on the LAGEOS target. The second shift is quite variable and "chases the moon" as efficiently as possible, in concert with whatever physical and personnel constraints may exist. Each shift, wherever possible, attempts to take the other crew's target as a "target of opportunity". To the best of our ability and within the constraints of our budget, those are the procedures which we try to emulate at the MLRS.

Using this scenario for our observing operations, it is easy to see that the scheduling of the LAGEOS crew is quite straightforward and can be implemented with little difficulty. For maximum lunar data throughput things get a bit more difficult. We attempt to maximize our coverage at the lunar quarters (completely ignoring week-ends). During a lunar ranging session we attempt to obtain a minimum of three Apollo 15 reflector observations with as wide an hour angle spread as possible; all remaining time is spent on observing the other three accessible lunar targets and/or observing any potential LAGEOS "targets of opportunity". At the present time, a successful lunar observation is considered to be made when a total of 25 photon returns have been identified (in real-time) by the observing crew.

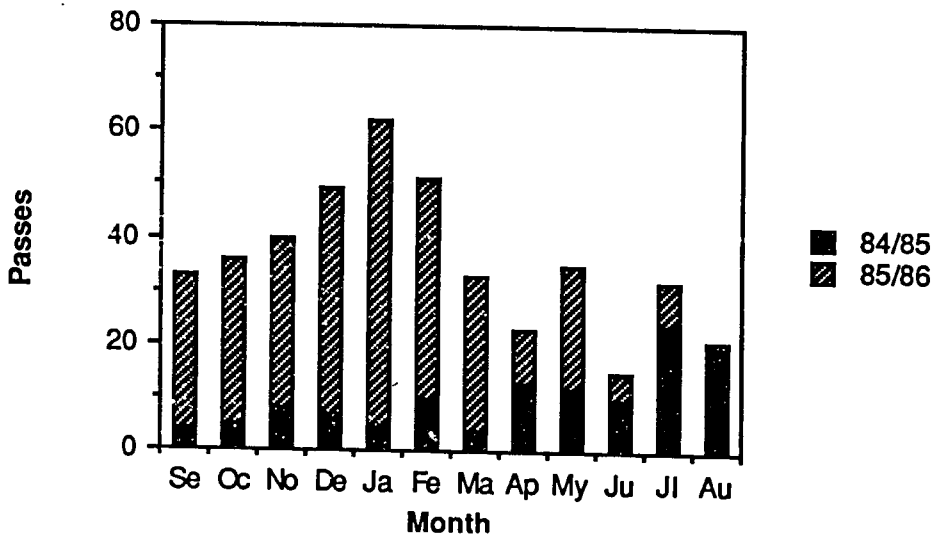
On other matters, as reported elsewhere in these workshop proceedings, we have established real-time Earth orientation computations at the MLRS, using lunar data. Normal lunar laser ranging data is identified, filtered, compressed, formatted, and analyzed on-site, and when sufficient data exists, an Earth orientation reduction is performed. The results are electronically transmitted to the U. S. Naval Observatory (and to other interested parties), usually within hours of the data taking.

Finally, the MLRS Operational Readiness Review was satisfactorily completed in the summer of 1985, testifying to the fact that the MLRS has indeed taken its place in the world among the other fine stations in the international laser ranging network. The road to the completion of the MLRS was a long and a hard one and, at times, many of us had our doubts as to whether or not it would ever come up to the standards which were set by our old 2.7-m system. To the future, we look forward to the time when the MLRS might be moved from its present "saddle-site" to one which is much more favorable, in order that it might be truly raised to its full observational potential.

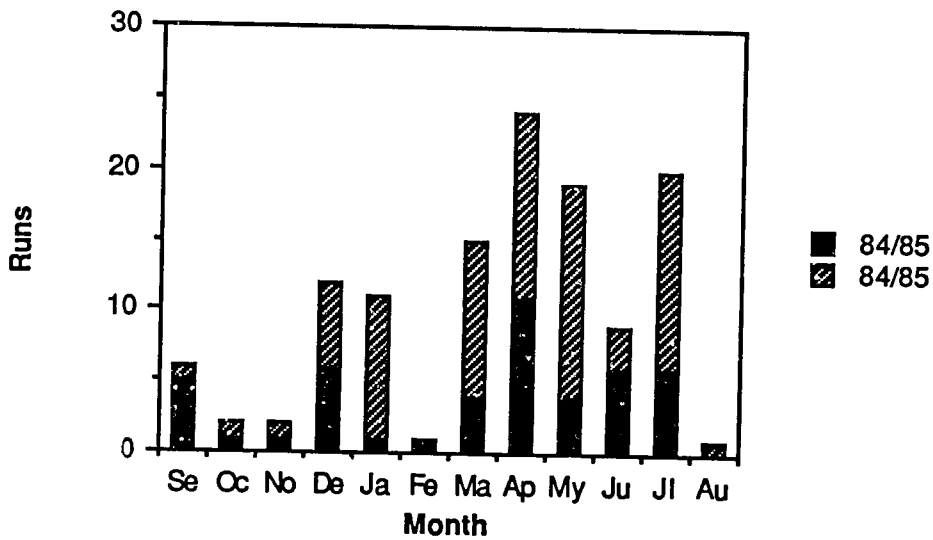
### **Acknowledgements**

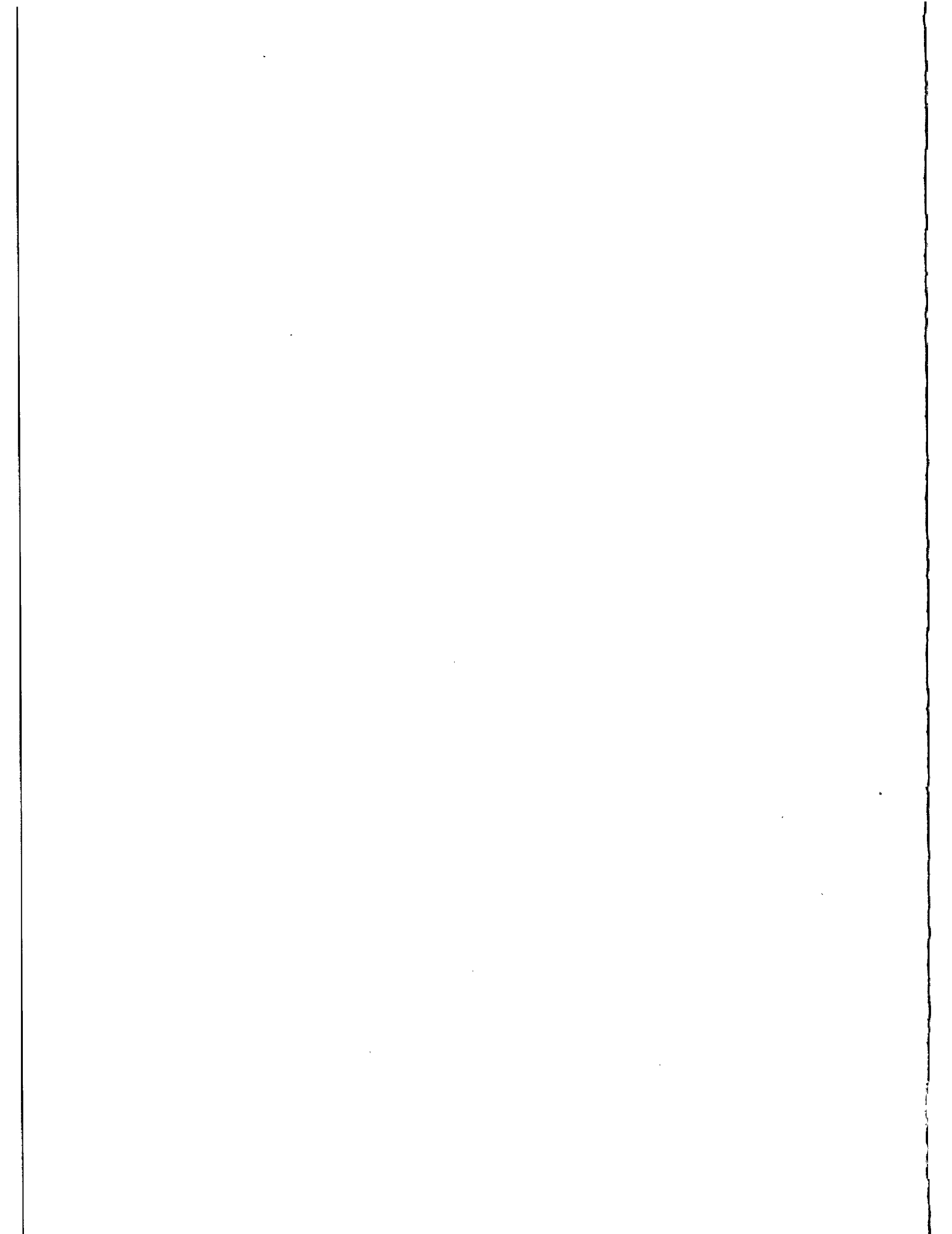
The authors acknowledge that this work is being supported at McDonald Observatory and the University of Texas at Austin by National Aeronautics and Space Administration Contract NAS5-29404 out of Goddard Space Flight Center, Technical Officer Mr. Robert L. Appler.

### MLRS/LAGEOS Statistics



### MLRS/Lunar Statistics





## START DETECTOR FOR THE MODE LOCKED TRAIN LASER RADAR

I. Prochazka  
Czech Technical University  
Faculty of Nuclear Science and Physical Eng.  
Brehova 7, 115 19 Prague - Czechoslovakia -

Telephone 848 840  
TWX 121254 FJFI C

### ABSTRACT

The start detector + discriminator for the mode locked train laser radar is described. The device is based on the semiconductor optical switch. The jitter test experiment using streak camera and the optical sampling application of the detector is described.

# START DETECTOR FOR THE MODE LOCKED TRAIN LASER RADAR

I. Procházka

The Interkosmos laser radar is using the mode locked train transmitter since 1983 /1/. The laser emits the train of pulses HAFW<30psec, spaced at 2.00 nanoseconds (see fig.1). To start the ranging electronics channel, the appropriate detector/discriminator capable of responding to the train of pulses was to be developed. The most common set up consisting of fast photodiode followed by constant fraction discriminator is far from optimum, because no discriminator available is able to respond to a single pulse from a narrow spacing train with low jitter. A special type of a fast fixed threshold detector/discriminator was developed by Cech /2/ and applied 1983-85. It was based on the fast photodiode followed by tunnel diode monostable circuit and pulse forming circuit. The jitter and time walk 150psec at the dynamical range 1:2 was achieved. To meet the high requirements of picosecond ranging using the train, the new principle of detector/discriminator was developed.

Its electrical scheme is on fig.2. The circuit is based on the in house built semiconductor opto switch (OS). The switch is working in the avalanche regime generating on its output the uniform signal (see fig.3) of several volts with fast leading edge 10mV/picosec. The OS switches at the fixed signal level, thus the first pulse higher than this level is causing generation of the electrical output pulse. Taking into account the pulse duration <30psec, the fixed threshold discriminator technique is no drawback for the application.

The jitter of the device was tested and the circuit optimised using the train of 10-30psec laser pulses and a streak camera (Hamamatsu 979) as a detector. The camera was triggered by the circuit output, the laser pulse was displayed. The digitised data from the camera were processed in the on line computer. The jitter of the device may be determined from fluctuations of the pulse position on the streak screen taking into account the trigger jitter of the camera itself (18psec measured by the manufacturer). On fig.5 there is a plot of consequent streak records. The excellent overlap of the pulses/trains may be seen. Using a streak camera, the jitter ranging 10-40picosecond was measured. The actual value of the jitter depends on the laser pulse length and amplitude fluctuations. Using pulses longer than 50picoseconds, the trigger jitter was about 0.4 times the pulse length.

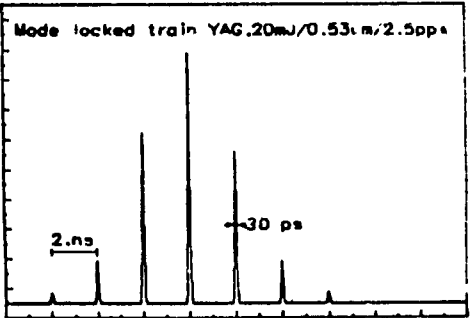
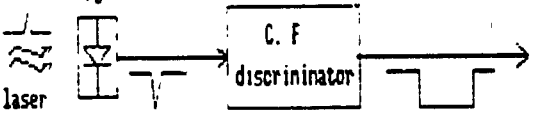
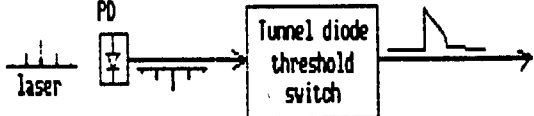
Using two identical circuits set to different trigger levels and a high resolution time interval meter, the simple sampling scheme may be constructed. One detector starts the counter the second it stops. On fig. 6 there is a histogram of measured times. The peaks separation corresponds to the laser resonator round trip, the peaks width determines the jitter  $(2 \times \text{Start} + \text{counter})$  typ. 50-70psec. The quality of mode locking may be estimated from the background. For comparison, on fig.7 there is the analogical histogram of measurements taken on the passively



mode locked laser oscillator incorrectly adjusted, transmitting multiple pulses. The laser output was monitored simultaneously on the streak camera. The background is of order higher. Thus, the pair of the START circuits may be used for quick check of the mode locked train transmitter in the quasi sampling mode with effective bandwidth of 5GHz. The possibility to monitor the mode locking quality is attractive especially in connection with passively mode locked laser for picosecond pulses generation.

Literature

- 1/ K.Hamal et all, Interkosmos laser radar, version mode locked train proceedings of 5-WLRI, Herstmonceux, Sept. 1984, edited by J. Caignebet
- 2/ M.Cech, Start discriminator for the mode locked train laser, in /1/

Start detector requirements	Available start detector/discriminator schemes
<p style="text-align: center;">SLR Transmitter output pulse</p>  <p style="text-align: right;">Fig. 1</p> <p><b>Requirements:</b></p> <ul style="list-style-type: none"> <li>- process train of psec pulses with few (1..6)nsec spacing</li> <li>- low jitter &lt; 50 psec</li> <li>- dynamical range &gt; 10 : 1</li> <li>- rugged and simple</li> <li>- simple adjustment/test procedures</li> </ul>	<p>1/ Standard scheme :</p>  <ul style="list-style-type: none"> <li>- not applicable for mode locked train of pulses with nsec spacing because of C.F. discriminator time response</li> </ul> <p>2/ Scheme by M.Cech (5-th WLRI, Herstmonceux, 1984)</p>  <ul style="list-style-type: none"> <li>- applied in Helwan, 1983..1985 nissions</li> <li>- jitter/time walk 150 psec / dyn.ratio 2:1 only</li> <li>- delicate set up</li> </ul>
<p>I.Prochazka Start Detector For Mode Locked Train Laser Radar</p> <p style="text-align: center;">1</p>	<p>I.Prochazka Start Detector For Mode Locked Train Laser Radar</p> <p style="text-align: center;">2</p>

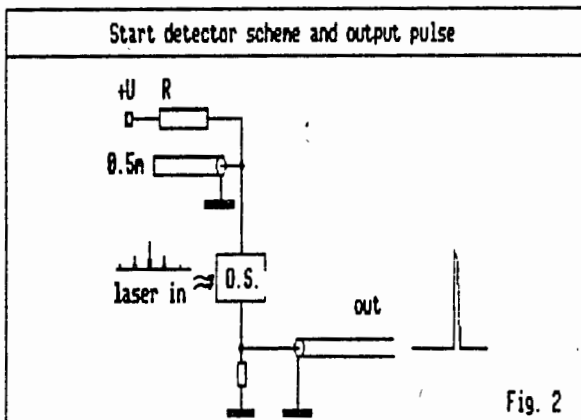


Fig. 2

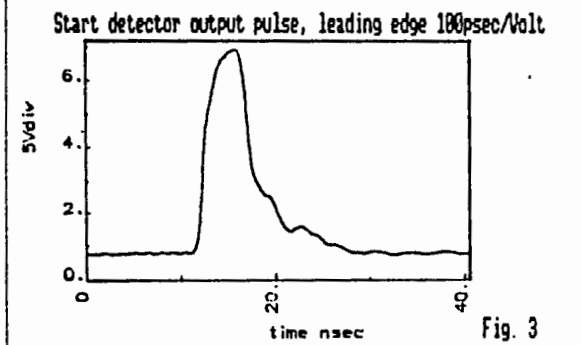


Fig. 3

I. Prochazka  
Start Detector For Mode Locked Train Laser Radar

3

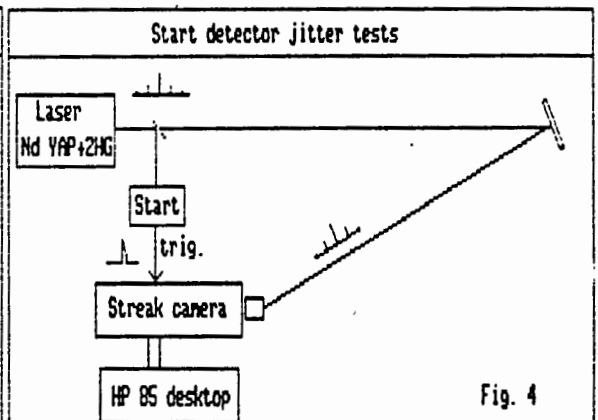


Fig. 4

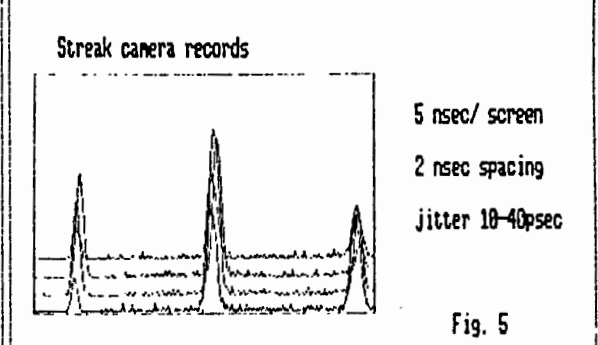


Fig. 5

I. Prochazka  
Start Detector For Mode Locked Train Laser Radar

4

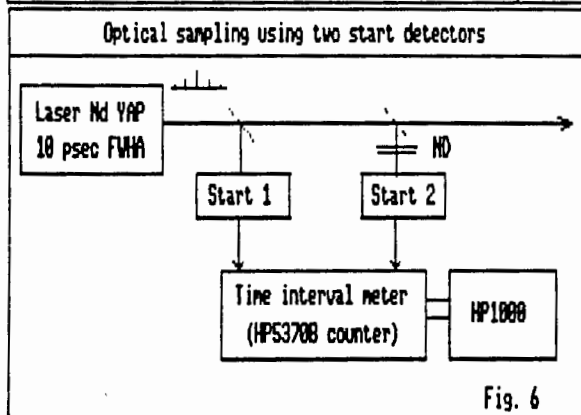


Fig. 6

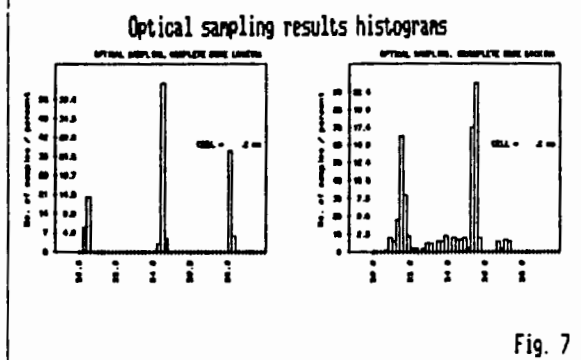


Fig. 7

I. Prochazka  
Start Detector For Mode Locked Train Laser Radar

5

**Start detector summary**

Start detector/discriminator performance:

- process train of picosecond ML pulses with nsec spacing
- fast fixed threshold discrimination
- uniform, high amplitude output
- internal delay ( 1 nsec
- jitter ( 40 psec
- dynamic range ) 20 : 1
- optical sampling capability :

\* passive mode locking check  
\* equivalent bandwidth 5 GHz

- changing bias voltage, serves as a laser monitoring PD  
- applied in Helwan 1986,  
calibration ranging jitter before 520ps after 300 ps  
system stability before 150ps after 120 ps

I. Prochazka  
Start Detector For Mode Locked Train Laser Radar

6

· AMBIGUITY AND RESOLUTION OF A MODE-LOCKED  
PULSE TRAIN LASER RADAR

R. Neubert, B. Ritschel, L. Grunwaldt  
Academy of Sciences of G.D.R.  
Central Institute for Physics of the Earth  
Telegrafenberg A 17, Postdam 1500 - G.D.R. -

Telephone  
Telex 15305

ABSTRACT

The accuracy of a multipulse laser radar has been studied with indoor experiments and computer simulation. For the experiments a mode-locked Nd-YAG laser producing 7 to 9 pulses of 4.6 ns spacing at 10 Hz repetition rate is used. The frequency-doubled pulses are divided by a beamsplitter and recombined at the photomultiplier which is working at the single photoelectron level. The time-of-flight data are treated by cross-correlating the empirical distributions corresponding to the two light paths. This leads to an estimate of the time-of-flight difference. Using a large amount of data sets the following parameters are determined :

- a) The percentage of estimates shifted by more than half a pulse spacing.
- b) The standard deviation of the unshifted estimates.

For the parameters of our system, the percentage of "good" estimates is higher than 90 % if more than 200 measurements are used. A standard deviation of about 100 ps is obtained under the same conditions. These results are obtained using electrostatic PMT's with about 500 ps jitter. Good agreement between the experiments and computer simulations is found. Thus the simulation method is used to determine the system performance in a wider parameter range.

The use of the full mode-locked pulse train for laser radar is advantageous because of laser simplicity and efficient use of its energy. However, because of the ambiguity problem, this concept found only limited applications as yet [1], [2]. The ambiguity of such a laser was discussed in an earlier paper [3] on the basis of computer simulation. In the following we report on comparison of the simulation results with laboratory experiments.

### Experimental setup

The simplified optical diagram of the setup is shown in Fig.1. The signal of the mode-locked Nd-YAG laser is split into three parts. A first part is reflected by a beam splitter (BS) to a silicon photodiode (PD) which is connected to the start input of the PS-500 time interval counter via a leading edge trigger. The stop receiver (usually a PMT) is illuminated with very weak signals reaching it along two different ray paths:

- the short calibration path 1
- the longer ranging path 2

The attenuation to the single-photoelectron level is achieved by neutral density filters (F). By choice of the filters, the signal level is adjusted in such a way, that 10 to 50% of the laser shots are causing the emission of one electron from the PMT photocathode. Thus, the stop of the counter occurs randomly by a photon arriving along path 1 or path 2. The single-photoelectron pulses from the PMT are detected by a constant-fraction discriminator [4] to reduce the timing noise caused by PMT gain fluctuations.

The main specifications of the passively mode-locked Nd-YAG laser, which has been designed in our laboratory, are given in Table 1.

Table 1: Specifications of the Nd-YAG laser

Energy of pulse train ( $\lambda = 1.06 \mu\text{m}$ )	3 mJ
Number of pulses per train	7-9
Pulse separation	4.6 ns
Pulse width	68 ps *)
Repetition rate	10 Hz
Laser rod dimensions	5 x 75 mm.
Optical resonator type	large radius mirrors
Resonator length	69 cm
Modelocker	Soviet dyes 3955 or 3274 in methanol

\*) Average value for  $\lambda = 1.06 \mu\text{m}$ , estimated by the two-photon fluorescence method

For second harmonic generation, a KDP crystal is used. To

have definite polarization of the laser, Brewster plates are introduced into the optical resonator.

#### Time resolution tests

Starting point for the analysis of the measurements is the frequency distribution (histogram) of the time-of-flight values. This distribution is calculated usually from 1000 measurements. A typical example is shown in Fig.2. To determine the resolution of the system, the part of the distribution corresponding to one ray path is necessary only. As an example the left-hand part of Fig.2 is plotted in Fig.3 with higher resolution of the abscissa. The pulse structure of the laser is well resolved, but to take into account the partial overlap of the individual pulses, the distribution is analyzed using a least-square fit of a sum of Gaussian functions. To reduce the number of free parameters, the separation and width of the peaks have been assumed to be equal. The RMS width of the peaks obtained in this way can be used as a measure of the overall time resolution. The most important contribution to the timing noise is the fluctuation of the PMT delay (jitter). This quantity depends on PMT type and sample and its working conditions (voltage divider, illuminated area). Some contributions are also given by the amplitude fluctuations. This effect depends on the discriminator performance. Some results of resolution tests for different PMT tubes obtained in earlier experiments are shown in Table 2.

Table 2: Time resolution of the system

PMT type	Sample No.	RMS - Jitter (ps) *)	
		No diaphragm	1 mm diaphragm
RCA C 31034A	47105	540	370
FEU 79	4665	530	530
FEU 136	2053	600	470

\*) Overall jitter including start, i.e. no deconvolution applied. Start photodiode type SP 109 directly connected to the counter (HP 5370 in these experiments).

It can be seen that the restriction of the illuminated area has some effect on the resolution, especially for the RCA C 31034A tested. The best resolution was obtained with this tube as yet, but with selected samples of other electrostatic PMT even better results might be attained. To determine the contribution of the start-time noise, some experiments were carried out using a silicon photodiode for the stop too. Using the HP 5082-4220 type in both channels, a RMS resolution of 300 ps was obtained. This value could be improved to 150-200 ps using the fast SP 109 photodiode (VEB Werk fuer

Fernsehelektronik Berlin). Assuming that the start- and stop-time fluctuations are equ. and independent in this case, the RMS start-time noise can be calculated to be 100-140 ps. For the experiments with PMT receiver, the SP 109 was always used. Thus, the jitter of the RCA C 31034A can be estimated by quadratic subtraction of the start noise to be around 350 ps. From this example it can be seen, that the start-time noise has only small influence on the overall resolution in our experiments.

The precision of the cross-correlation method

The generally adopted method for treating the data of a mode-locked train laser radar is to calculate first the frequency distributions of the calibration- and the ranging-measurements separately, and then to determine the time shift for maximum correlation of the two distributions. An example distribution is shown in Fig.2. The two subdistributions according to path 1 and 2 are well separated from each other by roughly 60 ns. Convolutin<sup>r</sup> both distributions, Fig.4 was obtained. In this figure the convolution sum is plotted like a polygon linking the points separated by the bin width of 250 ps. The maximum can be determined very accurately using some interpolation method. In our case we obtain for the time shift of maximum correlation  $(61.16 \pm 0.1)$ ns.

To investigate the precision of the method, the measurements of this and several other experiments were arranged into groups. Then the cross-correlation method was applied to each group so that an ensemble of time shifts is obtained from which statistical estimates for the precision can be gained. The parameters under consideration are:

1. the percentage of time shift results deviating from the real value not more than half a pulse separation (this quantity called "uniqueness")
2. the RMS error of the results deviating not more than half a pulse separation

These parameters are plotted in Fig. 5 and 6 in dependence of the quantity of measurements. As a normalized measure of the data quantity we are using  $(1/n_1 + 1/n_2)^{1/2}$ , where  $n_1$  and  $n_2$  are the number of measurements for path 1 and path 2, respectively. This is just the probable error of the ranging average for a single pulse system, expressed in terms of the standard deviation of a single time interval measurement. To estimate the uniqueness (resp. ambiguity) and precision from the measurements, 10 runs of 1000 points each are used. The total ensemble of 10000 measurements is arranged into groups of  $n_1 + n_2 = 60, 120, 240, 480$  individual measurements. For each group the cross-correlation method is applied resulting in the generation of an ensemble of ranges from which the interesting average parameters are estimated. The return rates for the two light paths are slightly changing

from run to run. Therefore averages for the parameter  $(1/n_1 + 1/n_2)^{1/2}$  have to be determined also. The resulting experimental values for the uniqueness and precision are plotted with the symbol "+" in Fig. 5 and 6.

For comparison with theoretical values and to obtain more general results (including different shapes of the laser signal like reduced pulse numbers), computer simulations were carried out assuming the photodetection process to be described by Poisson statistics and the timing jitter to have a Gaussian distribution. The simulator is a pseudo random number generator which outputs two possible numbers: 0 (corresponding to no detection) and 1 (detection). The probabilities of the two states are determined by the average number of photoelectrons ( $s$ ) of the pulse according to:

$$P(0) = \exp(-s); \quad P(1) = 1 - \exp(-s)$$

The simulator is called for each consecutive pulse of the group using the pulse intensities as input parameters. When the first positive answer occurs, the corresponding pulse number is stored together with some added Gaussian timing noise. By repeating this process, 5000 simulated time intervals for both the calibration and the ranging channel are generated and stored into the memory. In this process, the average return rate for the calibration is set to be 50% and for the other channel 25%.

To estimate now the performance parameters of the system in dependence on the amount of measurements, example realizations are selected from simulated measurements and then treated by the cross-correlation method in the same way as is done with the real measurements. The selection of the individual values from the memory is done by calling an equally distributed pseudo random number generator to determine the addresses. 500 example realizations are used to estimate the performance parameters, i.e. the uniqueness and the RMS error of a cross-correlation result.

To compare the experimental values with the simulations, the average shape of the time interval histogram is needed. It has been approximated by 9 Gaussian peaks with Gaussian envelope according to

$$h = a_0 \sum_{k=-4}^4 \exp(k^2/U) \cdot \exp((t - t_k)^2 / 2\sigma^2) \quad (1)$$

The average experimental parameters are  $U = 4.61$ ,  $\sigma = 386$  ps. The separation of consecutive pulses is

$$\Delta t = t_{k+1} - t_k = 4.55 \text{ ns.}$$

So the relative resolution is  $C = \sigma / \Delta t = 0.0848$ . Using these parameters the results marked in Fig. 5 and 6 by "\*" are generated. They agree reasonably well with the experimental points, especially for the uniqueness (Fig.5). This

agreement is somewhat surprising because the laser pulse shape fluctuations are not directly modelled in the simulations. Instead, the pulse shape is chosen in agreement with the observed histograms. Note further that the simulated results showed almost no dependence from  $n_1 / n_2$  if the above introduced parameter  $(1/n_1 + 1/n_2)^{1/2}$  is kept constant. This is proved in the range  $n_1/n_2 = 1 \dots 10$ .

For the conditions used in our experiments, the following conclusions can be drawn:

- the performance of the system can be reasonably well determined by the described simulation method
- 200 measurements for both calibration and ranging are required to have 90 per cent probability of correct assignment of the data (not shifted by a multiple of the pulse separation)
- the standard deviation of a result generated from 200 measurements is in the order of 100 ps.

The good representation of the experiments by the simulation encouraged us to study the dependence of the system performance from the laser pulse shape and the timing resolution more detailed. Some of the results are graphically represented in Fig.7 and 8. In these figures, both the uniqueness parameter (broken lines, 1 at the vertical scale corresponds to 100%) and the ratio of the RMS error of the cross-correlation result to the single-shot timing jitter (full lines) are plotted in dependence on the amount of measurements. The relative RMS error as defined describes the effect of averaging.

In Fig.7 for a fixed laser pulse shape the influence of the timing resolution is represented. As a measure of the resolution, the parameter C (defined as the ratio of the overall RMS jitter of the timing system to the pulse separation of the laser pulses) is used. The time resolution is visualized by the probability distributions of the time intervals, i.e. the shapes of the histograms for very large amounts of measurements.

As can be seen from Fig.7, the timing resolution has a very small influence on the uniqueness (resp. ambiguity) but some effect on the relative RMS error. This behaviour is to be expected. We conclude from Fig.7 that the resolution parameter C should be smaller than 0.2. Note that for a given resolution of the timing system, the parameter C can be adjusted by the separation of the laser pulses which is possible by choosing the laser resonator length.

The number of pulses in a laser pulse group is represented by the parameter U. More precisely, this is the overall width of the probability distribution of the time intervals according to equ.(1). The parameter U is chosen to be  $U = 6$  in Fig.7.

The dependence of the system performance on the parameter U



for a fixed resolution ( $C = 0.1$ ) is shown in Fig.8. As expected, the parameter  $U$  has almost no effect on the error, but strong influence on the ambiguity. Fig.8 may be used to determine the amount of data to reach a given uniqueness level. A uniqueness of 90% in connection with  $U = 2$  is reached for  $n_1 = n_2 \approx 50$ . For  $U = 1$  only 20 measurements are needed in both channels to reach 90% uniqueness. There are some methods to minimize the parameter  $U$  including laser design, the combined use of nonlinear optical effects and well matched start detectors. With generally available technology,  $U = 1..2$  should be a realistic value.

### Conclusion

From the results of this study we conclude that the mode-locked train laser radar remains to be an attractive variant. Its main limitation, the ambiguity, can be reasonably overcome using a sufficient data quantity. The minimum data amount for a given probability of correct assignment can be gained from this paper. As a guide to good performance, one should restrict the number of pulses per group to a minimum and adjust the pulse separation to roughly 10 times the timing jitter. A special advantage of the rigorous use of single photoelectron detection is the low level of systematic errors. This gives the possibility to attain normal point errors near 1 cm even by using conventional electrostatic photomultiplier tubes.

### REFERENCES

- [1] Silverberg, E.C.: The Feedback Calibration of the TLRS Ranging System  
Proc. 4th Intern. Workshop on Laser Ranging Instr.,  
Austin 1981  
Edt. P. Wilson, Bonn 1982, p. 331-37
- [2] Hamal, K. et al.: INTERKOSMOS Laser Radar, Version Mode-Locked Train  
Proc. 5th Intern. Workshop on Laser Ranging Instr., vol. II  
Herstmonceux 1984  
Edt. J. Gaignebet, Bonn 1985, p. 214-18
- [3] Neubert, R.: Simulation Studies on the Statistics of a Multipulse Laser Radar Working at the Single Photoelectron Level  
Nabl. Isk. Sput. Zemli, Prague 23 (1984), p.93-102
- [4] Fischer, H.: Empfangsdiskriminator fuer Satellitenentfernungsmessung mit verbessertem Zeitverhalten  
Radio Fernsehen Elektronik, Berlin 31 (1982) 8, p.491-92

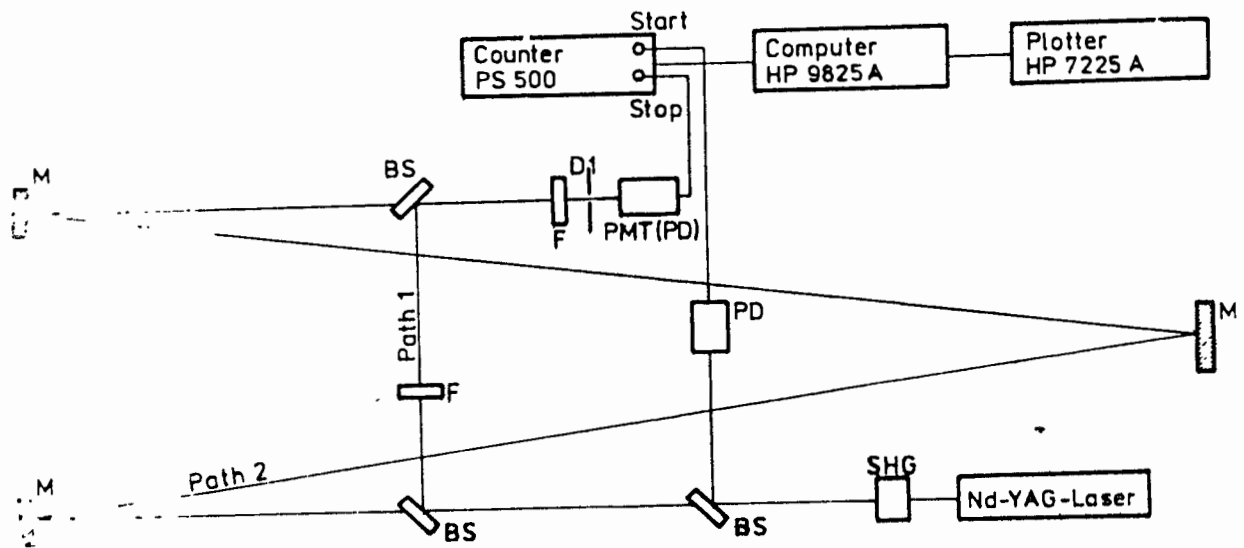


Fig. 1: Scheme of the experimental setup

BS - beam splitter, D - diaphragm  
 F - neutral density filter, M - mirror  
 PD - photo diode

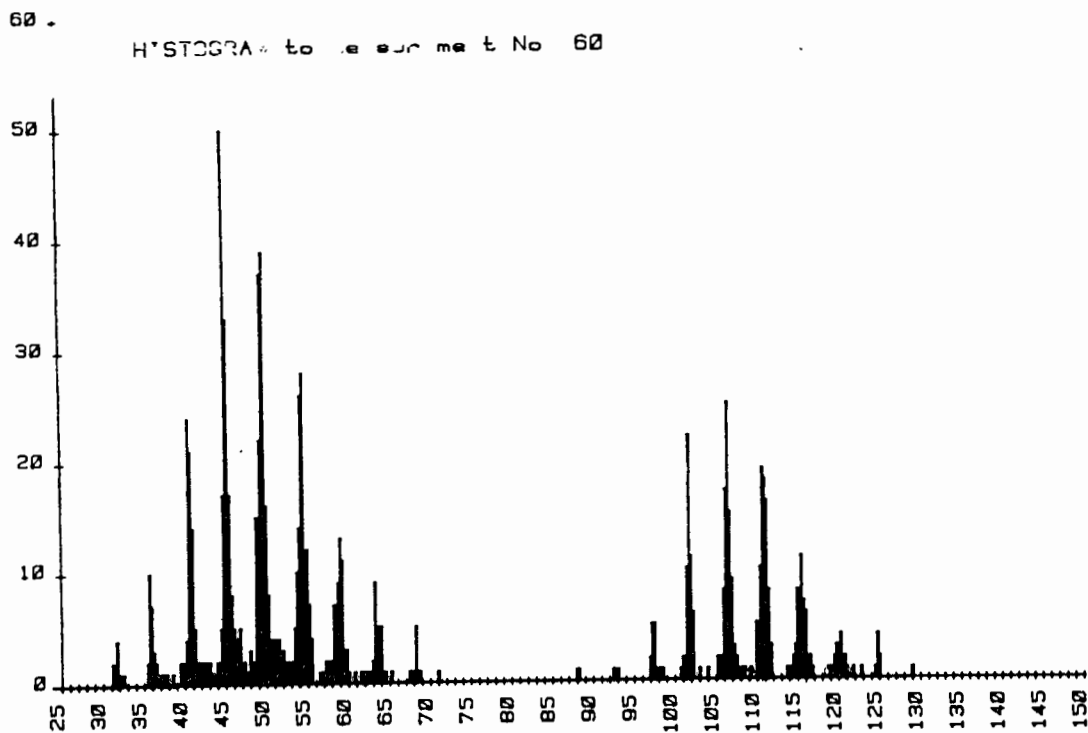


Fig. 2: Histogram of the time of flight values for a typical ranging experiment  
 Abscissa: Time interval in ns  
 ordinate: Number of measurements

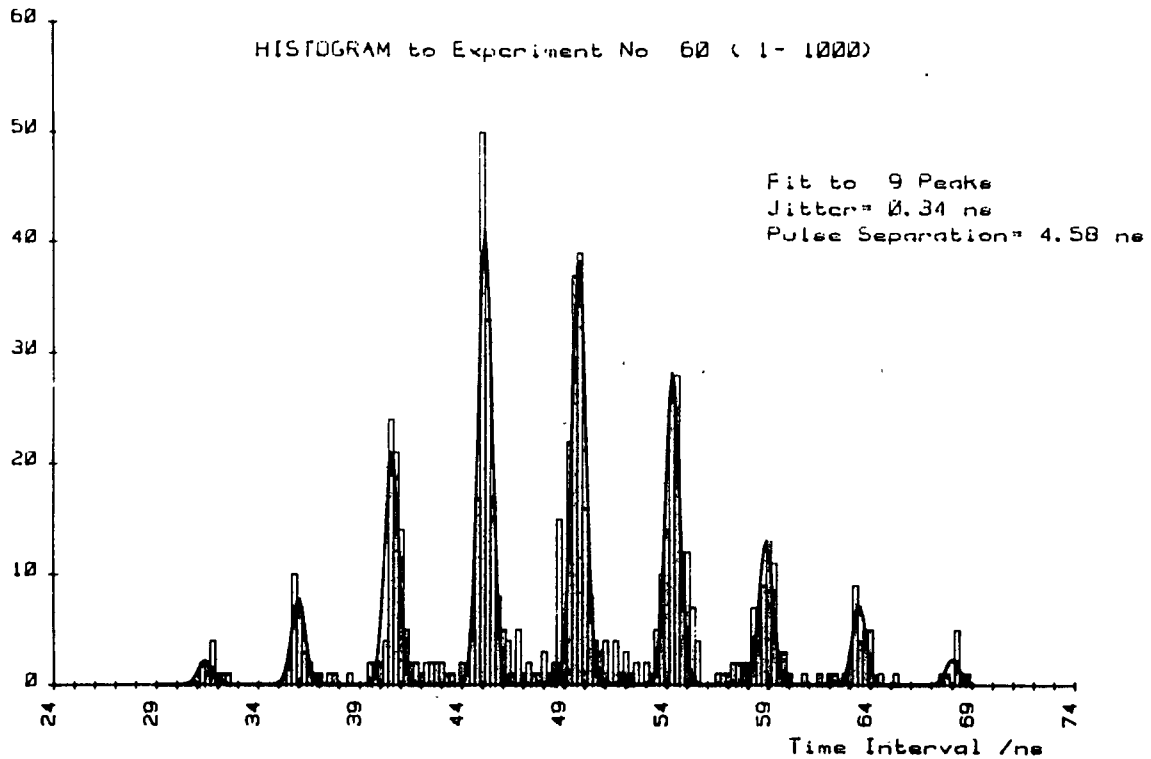


Fig. 3: Least square fit of a sum of Gaussian functions to the calibration part of experiment No. 60 (Fig. 2) bin width: 0.25 ns, RMS resolution: 0.34 ns, peak separation: 4.58 ns

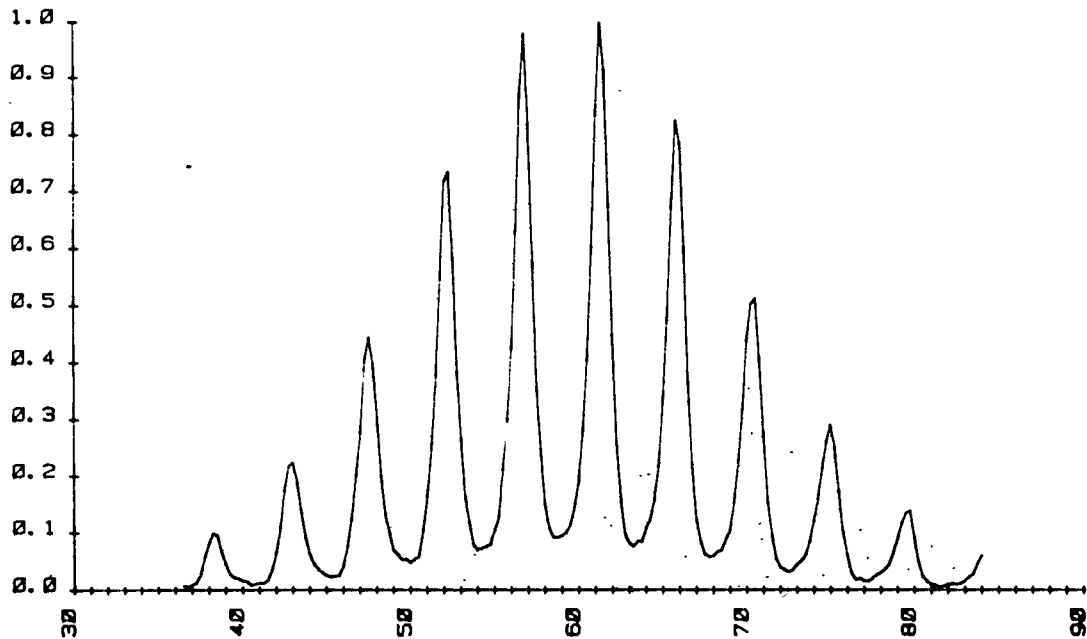


Fig. 4: Empirical cross-correlation to experiment No. 60 (convolution sum of the histograms corresponding to ray path 1 and 2 resp.)

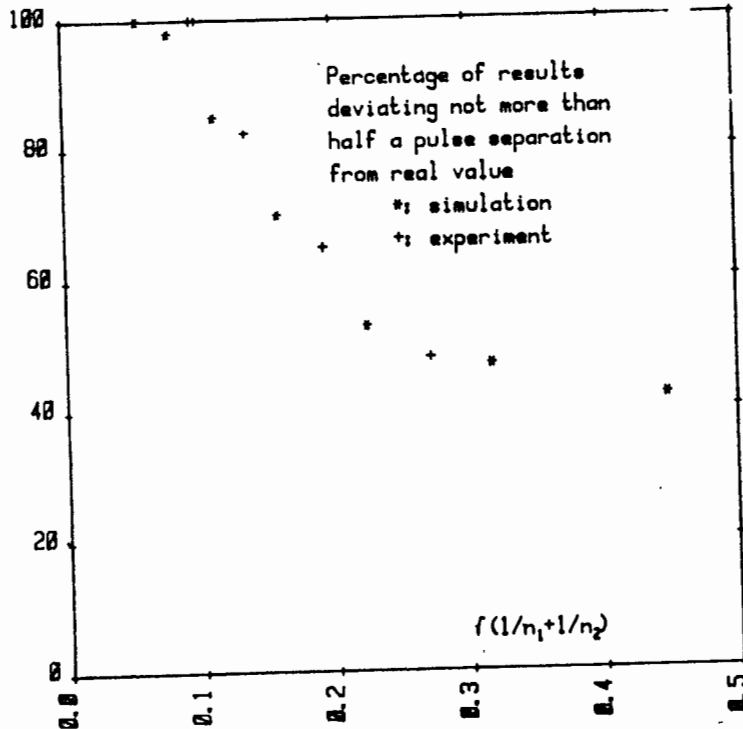


Fig. 5: Uniqueness in dependence of the amount of measurements: comparison of experiment and simulation.  
 $n_1$  - number of measurements for path 1  
 $n_2$  - number of measurements for path 2

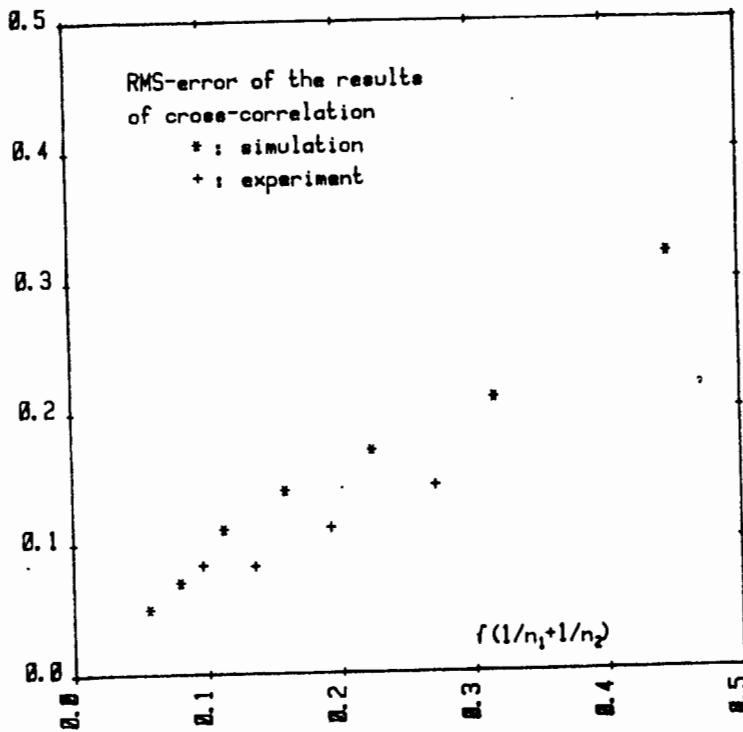
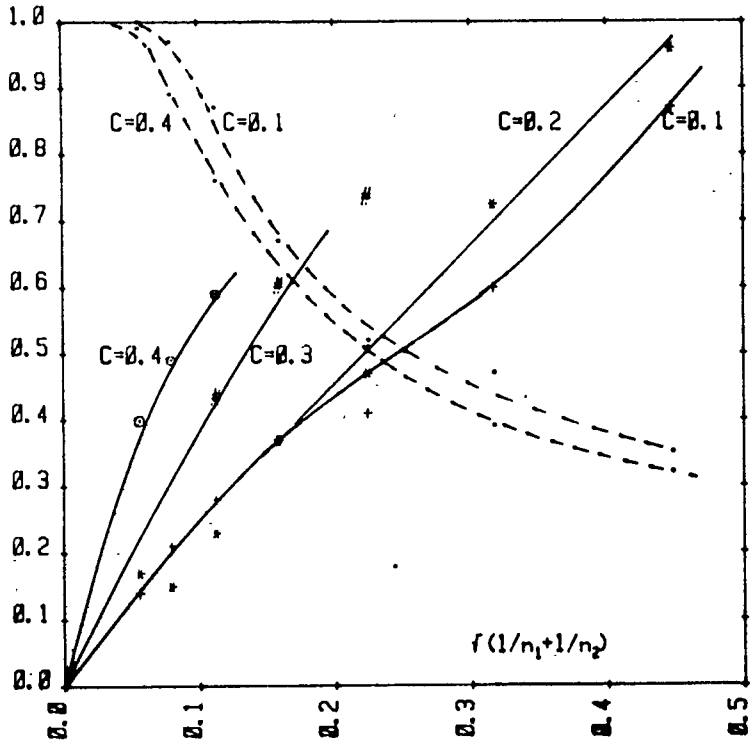


Fig. 6: RMS-error of the time shift corresponding to maximum cross-correlation: comparison of experiment and simulation



Laser radar performance  
for different probability  
distributions of the  
time intervals  
--- uniqueness  
— rms/Jitter  
Envelope Param. U=6

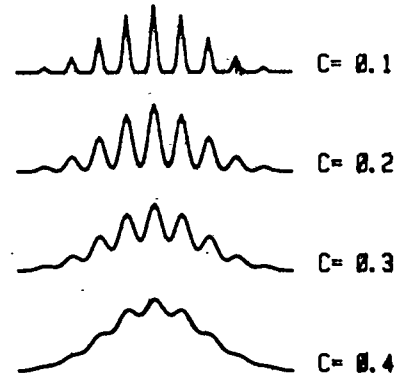
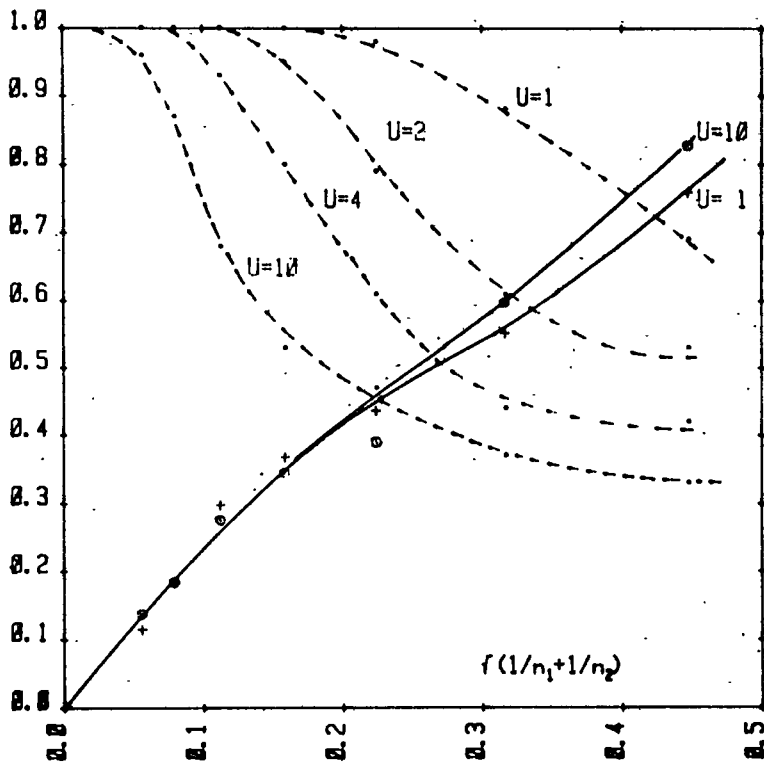


Fig. 7: Uniqueness and error obtained from simulations:  
dependence from timing resolution



Laser radar performance  
for different probability  
distributions of the  
time intervals  
--- uniqueness  
— rms/Jitter  
Jitter: C=0.1

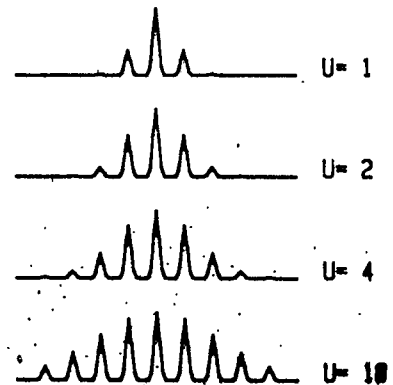
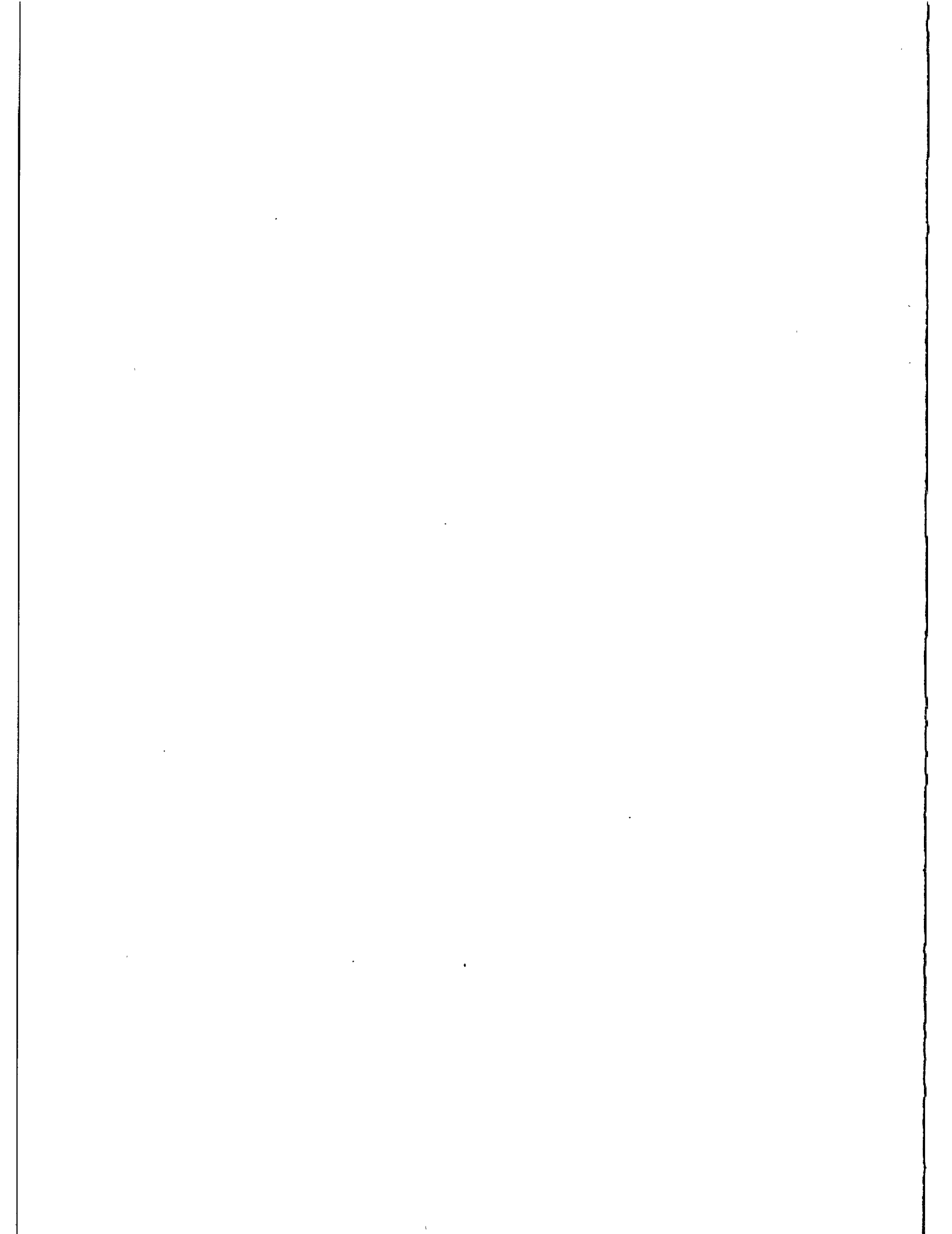


Fig. 8: Uniqueness and error obtained from simulations:  
dependence from the number of peaks



## MICROCHANNEL/DYNODE PHOTOMULTIPLIERS COMPARISON EXPERIMENT

I. Prochazka, K. Hamal  
Czech Technical University  
Faculty of Nuclear Science and Physical Eng.  
Brehova 7, 115 19 Prague - Czechoslovakia -

Telephone 848840  
TWX 121254 FJFI C

J. Gaignebet  
C.E.R.G.A.  
Avenue Nicolas Copernic  
06130 Grasse - France -

Telephone 93 36 58 49  
Telex 470865 CERGA F

### ABSTRACT

The calibration/comparison experiment for PMTs jitter measurement is described. The Tranzient digitizer interfaced to a minicomputer together with the powerful software package is used as a high performance discriminator and time interval meter with jitter typ. 23 psec. The transit time jitter and time walk for single PE and multi PE response of the MCP PMT Varian and dynode PHT RCA 8852 were measured.

## MICROCHANNEL/DYNODE PHOTOMULTIPLIER COMPARISON EXPERIMENT

I.Procházka, K.Hamal, J.Gaignebet

Analysing the 2G or 3G laser ranging system jitter budget one may conclude, that the photomultiplier contribution is the most significant. The transit time jitter and the time walk (transit time versus amplitude dependence) are the dominant parameters. The goal of this work was to measure the transit time jitter and the time walk of the microchannel and the dynode PMT. Although these parameters have been measured by several authors before (/1/,/2/ and others), the discrepancies between them and between the experience from the field was existing. That is why this measurement/comparison experiment was carried out.

The experimental set up is on fig. 1. The single pulse from Nd YAG, frequency doubled laser, FWHM of 90psec is illuminating the fast vacuum photodiode and /after an appropriate attenuation/ the PMT photocathode. To reduce the effect of transit time dependence on the illumination spot position /1/, the light spot size on the dynode PMT photocathode was reduced to 3mm. Using the ND filters, the PMT input signal was set to 1 to 50 photoelectrons. The outputs of the photodiode and the PMT were added and fed to the Transient digitizer Y-input. The optional amplifier 1000MHz/30dB was used for MCP photomultiplier at low signals. The Transient digitizer Tektronix, bandwidth 400MHz, min. 10mV/div, 512x512 pixels array is interfaced to the HP1000 computer system. The Transient together with the computer hardware/software package are used as a high performance discriminator and short intervals meter. The recording speed exceeds 10frames per second. The records are off-line processed and data analysed. The example of the Transient output is on fig. 2. The first pulse corresponds to the photodiode, the second to the PMT output. The PMT output pulse amplitude  $A_2$  and the pulses mutual distance  $T$  are the main process output parameters. The fluctuation of  $T$  is caused by the Transient, photodiode and PMT jitters. The Transient and photodiode jitter contributions were calibrated /3/ and found to be 23psec. The constant fraction (1/2) discriminator (software modelled) was used for all the measurements.

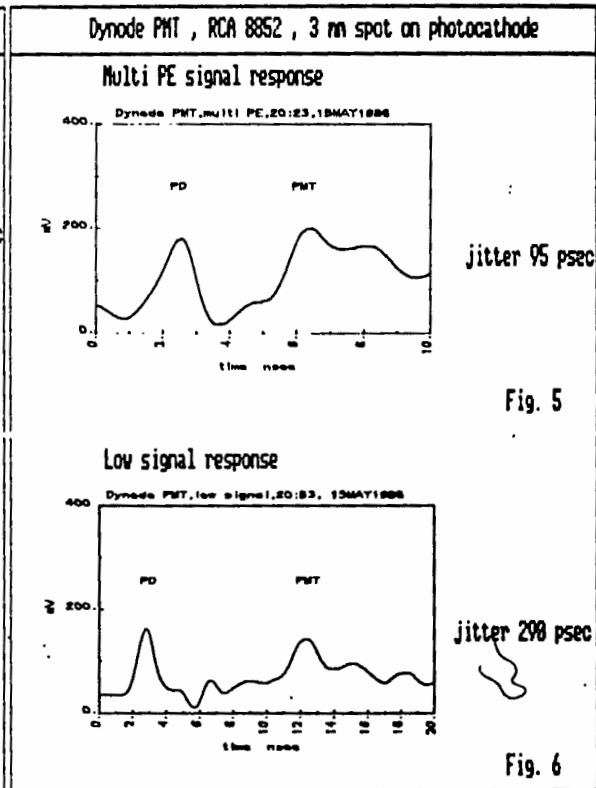
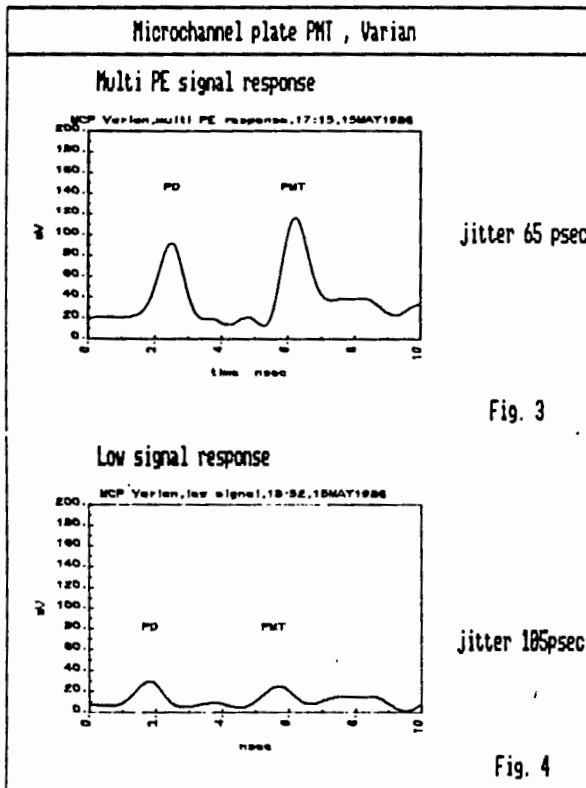
The examples of the records are on the figures 3 to 6 for the microchannel and dynode and multi PE and low signal, respectively. The results are plotted on fig.7 and 8 where is a graph of a photomultiplier transit time difference as a function of signal strength. The vertical bars represent the jitter for given signal strength.

### Literature:

- 1/ S.K.Poultney, Single photon detection and timing, experiments and techniques, Advanced electronics and electron physics, Vol.31, 1972
- 2/ J.J.Degnan, Satellite laser ranging, current status and future prospects, IEEE, Geoscience nad remote sensing, Vol.GE-23, No.4
- 3/ I.Prochazka, Picosecond laser ranging using photodiode in this proceedings

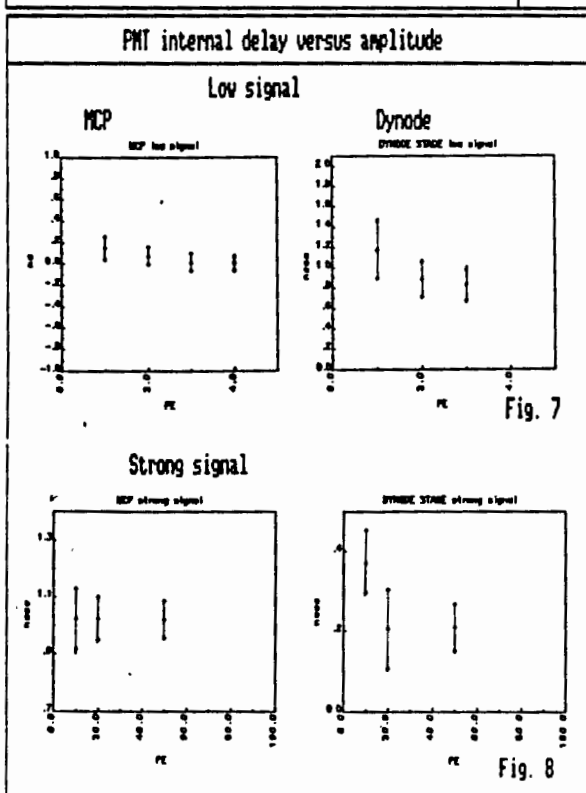


INTERKOSMOS SATELLITE LASER RADAR NETWORK		PMT measurement goals	
<p><b>MICROCHANNEL/DYNODE PHOTOMULTIPLIERS COMPARISON EXPERIMENT</b></p> <p>I. Prochazka, K. Hanal Czech Technical University Faculty of Nuclear Science and Physical Engineering Brehova 7, 115 19 Prague, Czechoslovakia</p> <p>J. Gaignebet C.E.R.G.A, Grasse France</p>		<p><b>Goals</b></p> <p>- measurements :</p> <ul style="list-style-type: none"> <li>* jitter at single/multi PE signal level</li> <li>* time walk (int. delay/amplitude) dependence</li> <li>* ultimate jitter limits</li> </ul> <p>- comparison :</p> <ul style="list-style-type: none"> <li>* microchannel plate PMT      Varian</li> <li>* dynode type      PMT      RCA8852 (3mm spot)</li> </ul>	
I. Prochazka, K. Hanal, J. Gaignebet Microchannel/Dynode Photomultiplier Comparison Exper.		0	I. Prochazka, K. Hanal Microchannel/Dynode Photomultiplier Comparison Exper.
PMT test experiment		PMT test chain characteristics	
<p style="text-align: center;">Fig. 1</p>		<p>Laser - Nd YAG + 2HG, 90 psec FWHM</p> <p>Transient - 400MHz, 10 nV / div</p> <p>T7912AD - sweep speed 20 psec/pixel (MCP) 40 psec/pixel (dynode)</p> <p>- amplitude resolution 512 levels</p> <p>jitter - Pd (vacuum) + Transient 23 psec</p>	
<p>Transient record processing :</p> <p style="text-align: center;">Fig. 2</p>		<p>Limitation - dynamic range 5 : 1</p>	
I. Prochazka, K. Hanal J. Gaignebet Microchannel/Dynode Photomultiplier Comparison Exper.		2	I. Prochazka, K. Hanal J. Gaignebet Microchannel/Dynode Photomultiplier Comparison Exper.



I. Prochazka, K. Hanal J. Gaignebet  
Microchannel/Dynode Photomultiplier Comparison Exper. 4

I. Prochazka, K. Hanal J. Gaignebet  
Microchannel/Dynode Photomultiplier Comparison Exper. 5



PMT jitter comparison summary

		PMT type	
		M C P	Dynode
		Varian	RCA8852
Jitter	1 PE	185 psec	298 psec
	10 PE	100 psec	150 psec
	100 PE	65 psec	95 psec

I. Prochazka, K. Hanal J. Gaignebet  
Microchannel/Dynode Photomultiplier Comparison Exper. 6

I. Prochazka, K. Hanal J. Gaignebet  
Microchannel/Dynode Photomultiplier Comparison Exper. 7

DETECTORS FOR III.GENERATION LASER RANGING SYSTEMS

Z. Neumann  
Astronomical Institute  
Czechoslovakia Academy of Sciences  
Telephone (0204) 999201

ABSTRACT

Possible detectors are described and their properties jitter, gain, spectral response and noise are considered. The avalanche photodiodes are described in some detail.

The accuracy of transit time depends on - laser pulse width, accuracy of time counter, time property of photodetecting element, frequency properties of cables, type of discriminator, time properties of electronic circuits.

It is possible to generate a pulse width below 100 ps by mode-locking, it influences the detection accuracy ( at one photoelectron level ) by 40 ps approximately ( see lit./1/, relation 2.14 ). In case of one photoelectron detection level, the accuracy almost does not depend on the type of the discriminator used ( see lit./3/ table 1 ). The top time counters reach the accuracy level better than 40 ps ( HP 5370 ). There are cables for frequencies over 10 GHz and with a convenient arrangement ( discriminator as near as possible to the detector ) the influence of cables is below 10 ps. It is possible make electronic circuits with jitter below 20 ps. Thus, the transformation of light pulse into the electric one by a photodetector is the main effect that determinates the transit time accuracy.

The case of a photodetector for a start impulse is relatively simple. It is possible to use an intensive light pulse so that no amplification is necessary. The absorption process is fast enough and it implies that the time properties depend on passive elements ( encasing, parasitic capacity, inductance etc. ). It is possible realize photodetectors, see lit./10/,/11/, such as having a jitter below 10 ps. For the start impulse we can use photoresistor, PIN photodiode, Schottky photodiode etc.

The case of a photodetector for the stop impulse is more difficult. One photoelectron or some photoelectron detection level implies the need of a high subsequent amplification (  $10^6 - 10^7$  ). Up today solution by the usage of photomultipliers is limited. The photomultipliers reach a sufficient gain, however, the principle of photomultiplier activity causes the best photomultipliers having the jitter of approximately 500 ps ( see lit./3/,/4/ ). Therefore, the photomultiplier limits the resultant accuracy to a value of appro-

ximately 7 cm.

What are the possibilities of improving ? The usage of microchannel plate photomultipliers is one solution. They reach a sufficient gain of  $10^7$  and maybe also a convenient jitter with regard to their time response of approximately 250 ps ( FWHM ). The comparison of this value with the time response of best photomultipliers ( approximately 5 ns ) and with their jitter ( see lit./3/,/4/ ) shows the probable jitter of microchannel photomultipliers being of about 30 ps.

The other possibility is to look for some other devices acting on an other principles. The need to detect a single photon implies the necessity of amplifying in the same device where the photon is detected. So, main attention among semiconductor devices is directed to the avalanche photodiode.

The amplifying effect of avalanche photodiodes is based on the knocking-out the electrons from a valence in to a conduction band by high energetic electrons and holes. Heterogeneous photodiodes, instead of homogeneous ones, are used to decrease the dark current. They consist of absorption and avalanche regions, see fig. 1 . Photon is detected in the

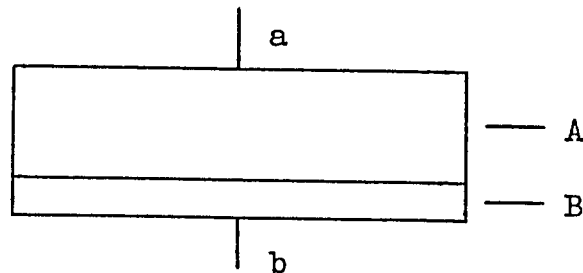


Fig. 1 Schematic illustration of an avalanche photodiode  
A - absorption region, B - avalanche region, a - negative outlet, b - positive outlet

absorption region ( A ). The free electron penetrates into the avalanche region ( B ) where it induces an avalanche propagation. Arise free electrons get out by the b outlet, the holes penetrate through absorption region to the a outlet.

Avalanche photodiodes from germanium, silicon or  $A^3B^5$  semiconductor ( mainly  $In_xGa_{1-x}As_yP_{1-y}$  ) are under consideration from technology point of view.

Avalanche photodiode, as an amplifier, can operate in two modes - linear amplifier mode and photon counting mode. In the first case, it reaches the gain of approximately 10 to 100 which is a very small value for usage in laser ranging system. In the other case, an avalanche photodiode operates either nearly below breakdown voltage or ( a short time ) over breakdown voltage. In this mode, the gain reaches a value of  $10^6$  or higher ( for silicon see lit./6/,/9/ ). This is sufficient for a one photoelectron detection level, too.

The type of the semiconductor used implies a spectral response, see fig. 2 . We can see that all materials are able

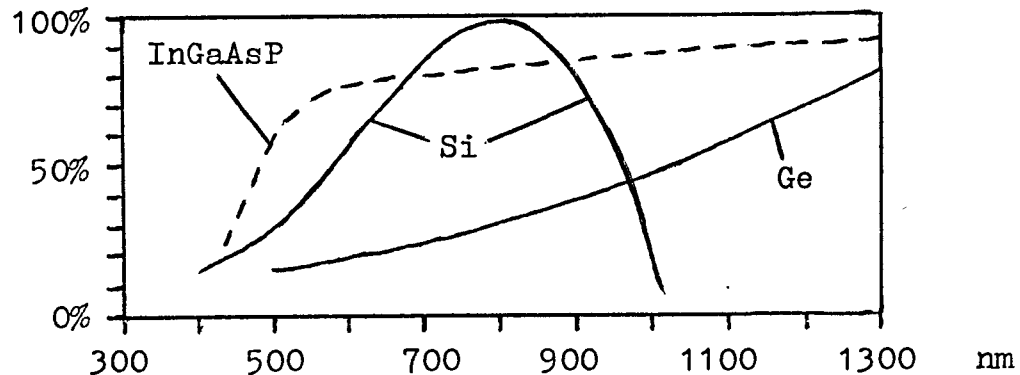


Fig. 2 Spectral response of semiconductor materials  
 Comment spectral response of InGaAsP changes according to the relation of components

to detect the radiation with 532 nm wavelength as well as with 1064 nm wavelength.

Total photodiode quantum efficiency at concrete wavelength is determined mainly by the value of absorption coefficient at this wavelength and by the thickness of the absorption layer ( and also by antireflection improvement etc. ). To obtain a reasonable quantum efficiency ( over 10% ), a minimal thickness of the absorption layer ought to be of 10  $\mu m$

( for 532 nm ) and 5 um ( for 1064 nm ) in case of germanium, of 20 um ( for 532 nm ) and 100 um ( for 1064 nm ) in case of silicon and of 1 um ( for both wavelength ) in case of InGaAsP.

The jitter of an avalanche photodiode is determined mainly by the thickness of the absorption layer. A photon is absorbed randomly on any place of the absorption layer. Due to the different speed of light ( approximately  $10^8 \text{ m.s}^{-1}$  ) and electron ( approximately  $10^5 \text{ m.s}^{-1}$  ), the delay between a photon coming into the photodiode and the electrical pulse leaving out the photodiode changes according to the place of photon absorption. The jitter implying from this effect reaches approximately 50 ps ( 10 um layer ) and 25 ps ( 5 um layer ) for germanium, 100 ps ( 20 um layer ) and 500 ps ( 100 um layer ) for silicon and 5 ps ( 1 um layer ) for InGaAsP.

The signal-to-noise ratio is not constant ( depending on gain ) at avalanche photodiodes, as it is in the case of photomultipliers, but it decreases as the gain increases. This dependence is shown on the equation /1/ ( according lit./7/ )

$$s:n = \frac{K_1 \cdot P^2 \cdot M^2}{(K_2 \cdot P + 2 \cdot e \cdot I_d) \cdot M^2 \cdot F \cdot K_3 + K_4}, \quad /1/$$

where  $K_1$  to  $K_4$  are constants,  $M$  is the gain,  $P$  is the optical power,  $I_d$  is the dark current,  $e$  is the electronic charge and  $F$  is the excess noise factor depending on the semiconductor material. If the ionization coefficients of electrons and holes are equal, the noise power increases as  $M^3$  but the signal one only as  $M^2$ . When the ionization coefficients are very different, the noise power increases also as  $M^2$ . The biggest difference between the ionization coefficients reveals silicon. In the case of InGaAsP the difference depends on the ratio between the components.

It is reasonable to describe the noise properties of a

photodetector for laser ranging instruments by the frequency of noise pulses instead by its noise power. According to data from lit./6/ - the dark current 18 nA and a gain of  $2 \cdot 10^4$  ( at temperature  $25^\circ \text{C}$  ) - it is possible to compute the frequency of noise pulses of 5 MHz. According to data from lit./9/ - the dark current  $10^{-13}$  A and the gain 250 ( at the temperature  $-22^\circ \text{C}$  ) - the frequency is equal to 2500 Hz. It is possible to compute, according to data from lit./8/ - dark current  $3 \cdot 10^{-10}$  A and the gain 100 - the frequency of noise pulses 20 MHz for InGaAsP .

Conclusion : The microchannel photomultipliers and silicon avalanche photodiodes with an approximately 20  $\mu\text{m}$  thick absorption layer ( and probably cooled ) are convenient for stop impulse detection of 2. harmonic of the Nd:YAG laser for III. generation laser ranging instruments.

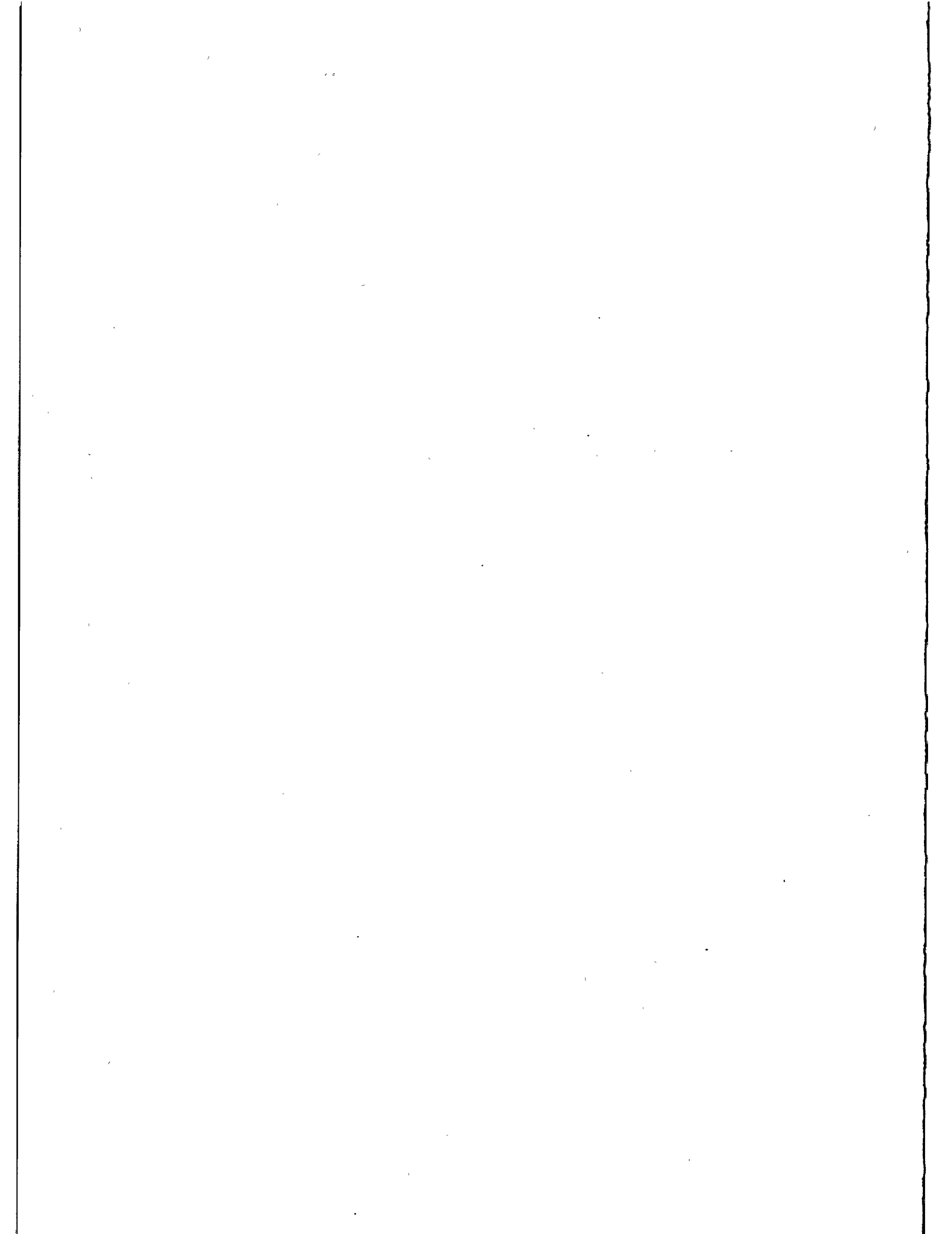
Only silicon avalanche photodiodes with approximately 20  $\mu\text{m}$  thick absorption layer ( for small jitter ) in the photon counting mode seem to be convenient for stop impulse detection of 1064 nm wavelength. The quantum efficiency ( due to thin absorption layer and small absorption coefficient ) is small, of about 2 to 3%.

For the future, after improving the technology, the InGaAsP avalanche photodiodes seem to be most perspective photodetectors ( see lit./7/ pages 413-414 ). A detection of not only 532 nm, but also of 1064 nm wavelength radiation with high quantum efficiency and a very small jitter will be probably possible in the case of convenient ratio between the components. The jitter will be probably so small to make it reasonable to consider their usage in a two-colour laser instruments ( instead of streak camera ). Different ionization coefficients enable to reach small noise. The gain  $10^6$  or more will be probably reached in the photon counting mode.



Literature

- /1/ Matti Paunonen : Studies on the Metsáhovi Satellite Laser Ranging System
- /2/ Centre National D'Études Spatiales, GRGS : Starlette
- /3/ K. Hamal, I. Procházka, J. Gaignebet : Mode Locked Train YAG Laser Calibration Experiment, Observations of Artificial Earth Satellites 23/1984
- /4/ R. Neubert, B. Ritschel, L. Grunwald : Ambiquity and Resolution of a Mode-locked Train Laser Radar, paper on the International Scientific Seminar "Laser Satellite II<sup>nd</sup> and III<sup>d</sup> generation ", 26-30 May 1986, Sofia
- /5/ Specification VPM-221D ( 2 MCP's ) Photo Plate Detector, Varian
- /6/ private information
- /7/ T.P. Pearsall : GaInAsP Alloy Semiconductors, John Wiley and Sons, 1982
- /8/ Kishi, Y and others : Liquid-phase-epitaxial growth of InP/InGaAsP/InGaAs Buried-structure avalanche photodiodes, Electronic Letters, Vol.20, page 165
- /9/ Photonics Spectra, June 1986, page 52
- /10/ Roth, W., Schumacher H., Beneking H. : Fast Photoconductive GaAs detectors made by laser stimulated MOCVD, Electronic Letters, Vol.19, nom.4, page 142
- /11/ Wang S, Y., Bloom D. M. : 100 GHz Bandwidth Planar GaAs Schottky Photodiode, Electronics Letters, Vol.19, nom.14. page 554



THE USE OF GEIGER MODE AVALANCHE PHOTODIODES FOR PRECISE  
LASER RANGING AT VERY LOW LIGHT LEVELS :  
AN EXPERIMENTAL EVALUATION

S.R. Bowman, Y.H. Shih, C.O. Alley  
Department of Physics and Astronomy  
University of Maryland  
College Park, Maryland 20740 - USA -

Telephone (301) 454 - 3405  
Telex 908787

ABSTRACT

Measurements have been conducted to determine the utility of commercially available silicon avalanche photodiodes as detectors in single photon ranging systems. When cooled and operated in a gated Geiger mode these detectors offer an attractive alternative to photomultipliers.

Seven different types of diodes were evaluated for Geiger mode operation. Characteristics such as dark noise and temporal response were used to select the best diode types. Response time studies were conducted on the selected diodes at very low light levels using a mode-locked frequency doubled Nd-YAG laser and a picosecond resolution streak camera system. Single photon response time distributions with standard deviations as small as 90 picoseconds were observed.

Detection efficiency at the singles level was also studied. Using a parametric down conversion process to generate a source of correlated photon pairs, the absolute single photon detection efficiency was measured at 532 nanometers. Efficiencies of 28 % were observed and changes in the detection efficiency with gating voltage were studied.

Results from low and moderate intensity laser ranging with Geiger mode diodes are discussed. The ranging results acquired at the Goddard Optical Test Facility include both terrestrial targets and the Laser Geodynamics Satellite, LAGEOS.

measurements. In this application "echo" pulses are not a significant problem.

Qualitatively the theory of Geiger mode operation is quite simple. The combination of low temperature and a high reversed biasing potential produces an essentially carrier-free region in the junction and depleted intrinsic region of a P<sup>n</sup>N diode, Figure 1. When a carrier is produced in the depleted region it will move into the high field region of the junction and undergo avalanche amplification as large as  $10^9$ . The resulting current pulse will continue until voltage across the diode falls to below the breakdown voltage.

Geiger mode operation is easy to observe. The circuit in Figure 2 is cooled to  $-60^{\circ}\text{C}$  using dry ice. Reverse bias is applied through a current limiting resistor to bring the diode to within a few volts of breakdown. An additional gating voltage pulse is capacitively coupled onto the diode. In this way the diode can be overvoltaged by as much as several hundred volts during the time of an expected signal. (If the diode is kept in almost total darkness the full voltage can be applied continuously. Most of the silicon diodes tried exhibited dark count rates of less than 100 Hertz at this temperature.) When the diode does break down the resulting pulse is large, usually several volts. This is a great advantage when working with lasers or other electrically noisy devices.

#### DETECTION EFFICIENCY

To determine their usefulness as laser ranging detectors, several different avalanche photodiodes were purchased. They were selected for large active area, high responsivity, and low cost. Each was tested for Geiger mode operation. Diodes that either failed to exhibit Geiger mode or had dark count rates above one kilohertz were rejected. Figure 3 illustrates relative measurements made to determine the optimum diode operating conditions. Measurements were made to determine detection efficiency and temporal response.

Accurate measurements of the detection efficiency of silicon Geiger diodes were made using a technique first described by D.N. Klyshko.<sup>5</sup> Conceptually, this is a very simple technique. A single weak laser beam passes through a nonlinear crystal that is phase matched for non-collinear parametric frequency halving. With proper spectral filtering, the result will be two very weak beams having the same wavelength. In fact, energy conservation requires that an equal number of photons,  $N$ , are simultaneously created in each beam. Two very sensitive detectors are used to count photons in each beam. The number of counts in each beam,  $N_1$  and  $N_2$ , are recorded. Also, the number of coincidence counts,  $N_c$ , is recorded. The absolute detection efficiencies,  $\eta_1$  and  $\eta_2$  can then be calculated from the simple relations:

$$N_1 = \eta_1 N \quad N_2 = \eta_2 N \quad N_c = \eta_1 \eta_2 N.$$

Figure 4 details the actual device set up to realize the Klyshko technique at the wavelength of interest, 532 nanometers. The results of measurements using two RCA C30902E diodes were maximum single photon detection efficiencies of 21

$\pm 3\%$  and  $28 \pm 3\%$ .

#### TEMPORAL RESPONSE

In addition to detection efficiency, the temporal response of the diodes was studied. Three important properties of the Geiger pulse were measured. They were amplitude stability, pulse risetime, and internal delay time jitter.

Amplitude fluctuations are a potential source of timing error in any ranging system.<sup>6</sup> Fortunately, the amplitude of the Geiger pulse is very stable. Under normal conditions "good" diodes have only a few percent variation in pulse amplitude, Figure 5. If the diode is operated at high count rates (greater than 5 kilohertz for d.c. biasing), it will not recharge completely before each firing. The result is a wide spectrum of pulse heights. Some diodes, particularly the RCA C30954E, exhibited frequent echo pulses within  $10^{-4}$  seconds of the leading pulse. The amplitudes of the echo pulses varied substantially again, probably due to lack of charging time.

Rise time measurements on the Geiger diode pulses are summarized in Table 1. All were measured with a load impedance of 50 ohms. A weak dependence of the risetime on temperature and voltage was observed. Lowering the temperature or raising the voltage could shorten the risetime by as much as a factor of two. The fastest rise attained was 1.0 nanosecond. This may be limited by the impedance of the diode packaging, a TO-18 can and socket.

Internal delay jitter was measured in two different ways. The first was to trigger a Hamamatsu C1000 Streak Camera System with the output of a Geiger diode. This system incorporates a C1583 streak camera with a streak trigger jitter of 5 picosecond as measured by the company. After a thousand laser firings, the width of the distribution of camera streaks was measured. Comparing this with the distribution produced by triggering from an ultrafast PIN diode, the internal jitter in the Geiger diode can be found. For the single photon intensity level, the standard deviation of the distribution was 90 picoseconds. These distributions clearly show an increase in the 10% full width trigger jitter from 190 to 360 picoseconds when the moderate intensity was reduced by  $10^7$  to the single quanta level. This increase in the internal delay jitter at low light levels can be explained in terms of the carrier transit time of the depleted region. At very low intensities the carriers which start the avalanche in the junction are formed throughout the depleted region. The structure of the RCA C30902E diode on which these measurement were made is such that the depletion region and junction are 15 and 2 microns thick, respectively.<sup>7</sup>

Similar results were obtained when the detector was used for terrestrial ranging. Figures 6 and 7 show histograms of the timing spread for ranges to a terrestrial corner cube reflector. With only a factor of 10 difference in the intensities used, the broadening of the distribution is clear. In addition to a 39% increase in the standard deviation, the mean value shifted later by 200 picoseconds. These measurement have 40 picosecond uncertainty associated with the timing electronics used.

Although Geiger mode photodiodes offer many advantages to photomultipliers in the measurement of weak light pulse epochs, they do have a serious drawback. After the avalanche pulse occurs, the diodes experience a relatively long deadtime associated with the carrier lifetimes in silicon. The minimal recovery time was not studied here but is thought to be of the order of  $10^{-7}$  seconds. In this research the recovery time was limited by the RC time constant of the biasing circuit,  $10^{-4}$  seconds. As a result the GM diodes used here were basically single stop detectors. This leads to significant noise blanking when the diodes are used in the presence of high background lighting, photon flux rates above  $10^5$  Hz. To resolve this problem work is currently under way on a multiple diode detecting package.

#### RANGING RESULTS

As a final test of utility of the GM photodiodes, laser ranging sessions were conducted using a single RCA C30902E diode as detector. The ranging test were conducted at the 1.2 meter precision tracking telescope on the Goddard Optical Test Site in Greenbelt Maryland. Strong return rates were achieved from the Laser Geodynamics Satellite (LAGEOS) using only two millijoules of transmitted laser energy. The LAGEOS satellite is in a nearly circular orbit with an altitude 6000 kilometers. For ranging at the single photon level, a chi squared fit to a second order polynomial using a typical two minute sample of the resulting timing residuals gave a standard deviation of 192 picoseconds. Figure 8 shows ranging residuals from a typical LAGEOS ranging session where higher laser energies are used to get a nearly one to one signal rate.

Lunar ranging data has also been acquired using the GM photodiode receiver. The results shown in Figure 9 were obtained in five minutes using 100 millijoule pulses under marginal atmospheric conditions. JPL analysis of this data gave a standard deviation of 168 picoseconds or a range uncertainty of 2.8 centimeters.

#### CONCLUSION

Measurements were conducted with silicon avalanche photodiodes used in a cooled Geiger mode to determine their usefulness in satellite laser ranging systems. Single photon detection efficiencies were measured to be 28% for 532 nanometers. Timing jitters of the single photon responses were found to have a standard deviation of 90 picoseconds. The high quality lunar and satellite ranging results obtained here prove the commercially available GM photodiodes to be an excellent alternative to photomultipliers both in terms of cost and performance.

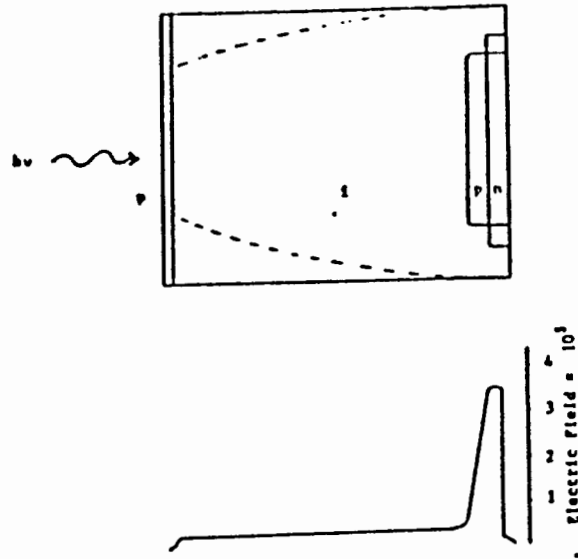
### ACKNOWLEDGMENT

The authors would like to thank Bob Hyde for his initial suggestion of this research topic. Thanks also go to John Rayner, Jack Bufton, and Liming Ding for their assistance during this work.

TABLE 1  
TYPICAL GEIGER MODE PROPERTIES OF APD'S TESTED  
T = +60°C

RCA C309021S	$V_{Brk} = 165 \text{ V}$ , $T_{Rise} = 3 \text{ ns}$ Dark count = 16 Hz @ $V_{Brk} + 20 \text{ V}$
RCA C30902E	$V_{Brk} = 170 \text{ V}$ , $T_{Rise} = 1.2 \text{ ns}$ Dark count = 100 Hz @ $V_{Brk} + 40 \text{ V}$
RCA C30948E	$V_{Brk} = 192 \text{ V}$ , $T_{Rise} = 1.7 \text{ ns}$ Dark count = 50 Hz
RCA C30954E	$V_{Brk} = 140 \text{ V}$ , $T_{Rise} = 3 \text{ ns}$ Dark count = 70 Hz @ $V_{Brk} + 20 \text{ V}$
RCA C30955E	No Geiger mode
NDL 1202	$V_{Brk} = 135 \text{ V}$ , $T_{Rise} = 1 \text{ ns}$ Dark Count = 2 kHz @ $V_{Brk} + 15 \text{ V}$
NDL 5100 (Germanium)	$V_{Brk} = 30 \text{ V}$ , $T_{Rise} = 5 \text{ ns}$ very noisy, triggered immediately, amplitude only 10mV

### REACH-THROUGH APD STRUCTURE



From P.P. Webb et al. "Properties of Avalanche Photodiodes,  
R.C.A. Review 35, (1974), 251.

FIGURE 1

### GEIGER MODE PHOTODIODE BIASING CIRCUIT

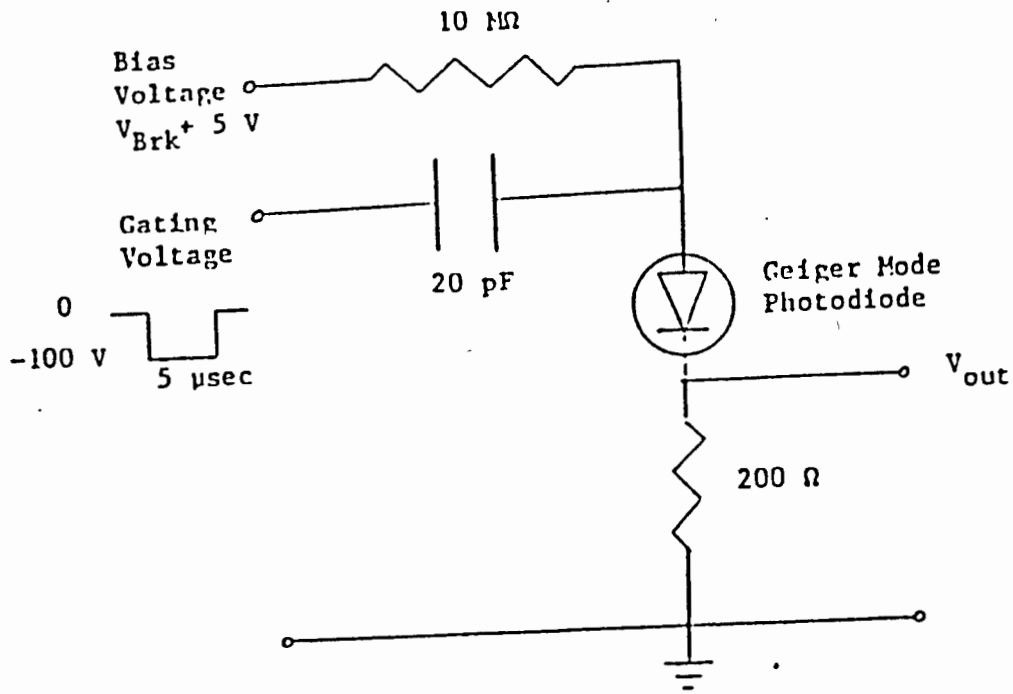


FIGURE 2



GEIGER MODE PHOTODIODE PERFORMANCE VS. VOLTAGE

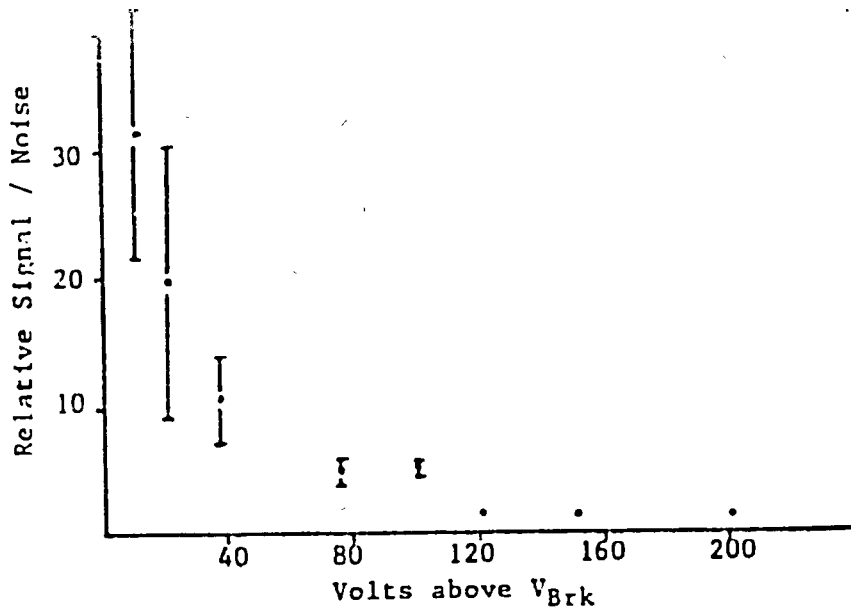
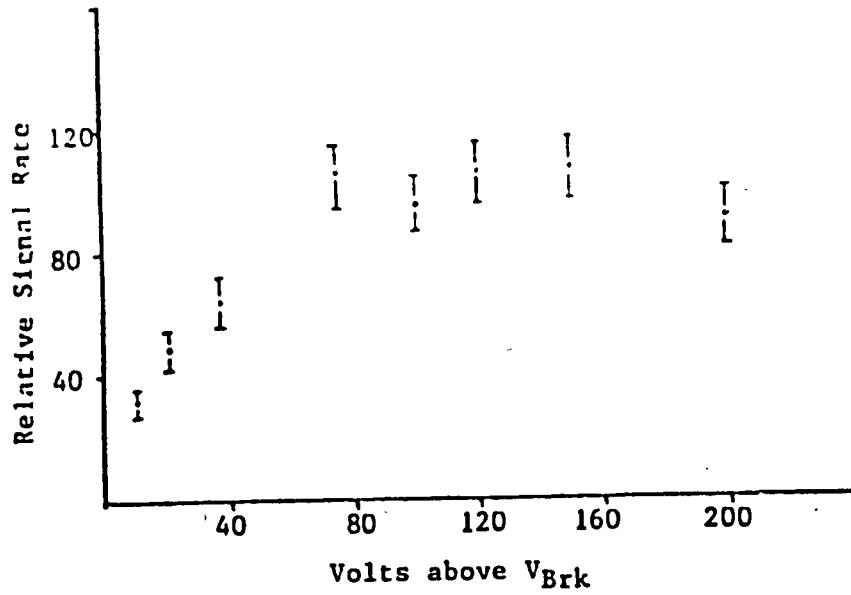


FIGURE 3

# KLYSHKO DETECTION EFFICIENCY MEASUREMENT

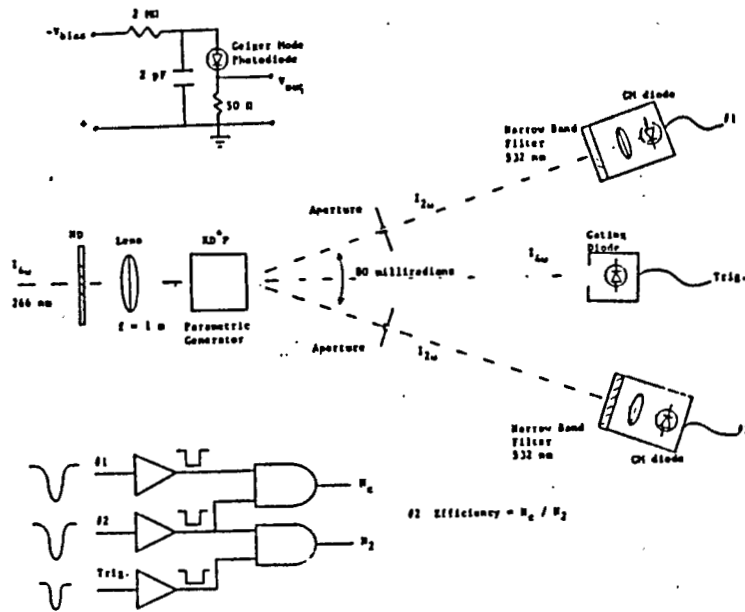
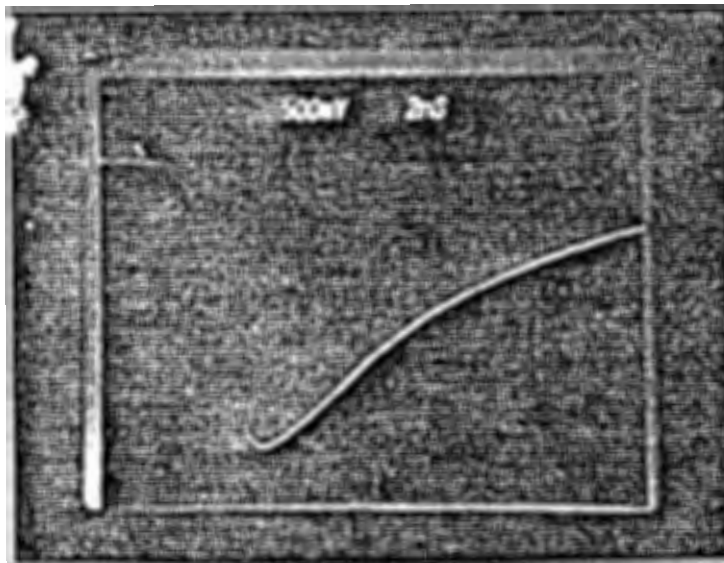


FIGURE 4



RCA30902E DIODE SN 40889,  $V_{\text{gate}} = +50 \text{ V}$ ,  $V_{\text{bias}} = -160 \text{ V}$   
 Three Pulses, Risetime = 1.2 ns (10% to 90%)  
 measured with Tektronics 7104 Oscilloscope

FIGURE 5

TERRESTRIAL RANGING WITH GM PHOTODIODE, ND = 9

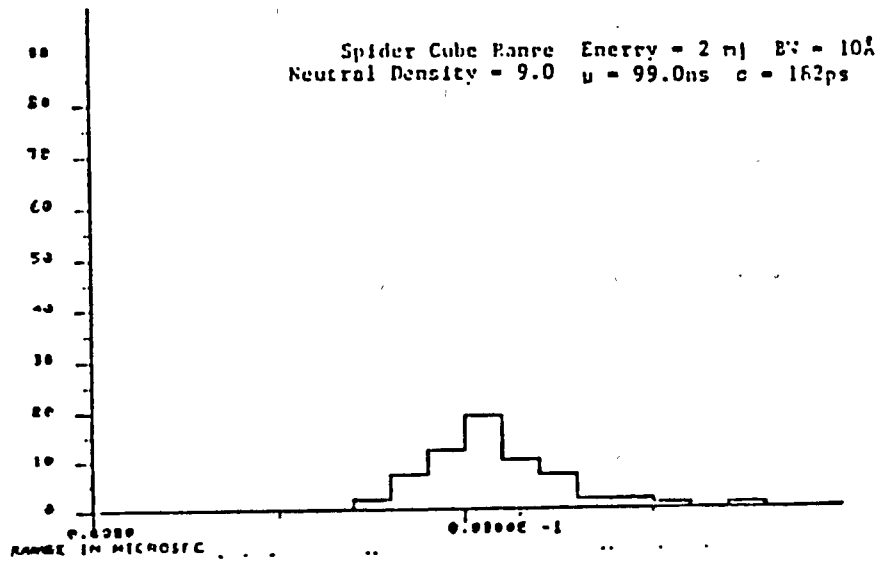


FIGURE 6

TERRESTRIAL RANGING WITH GM PHOTODIODE, ND = 10

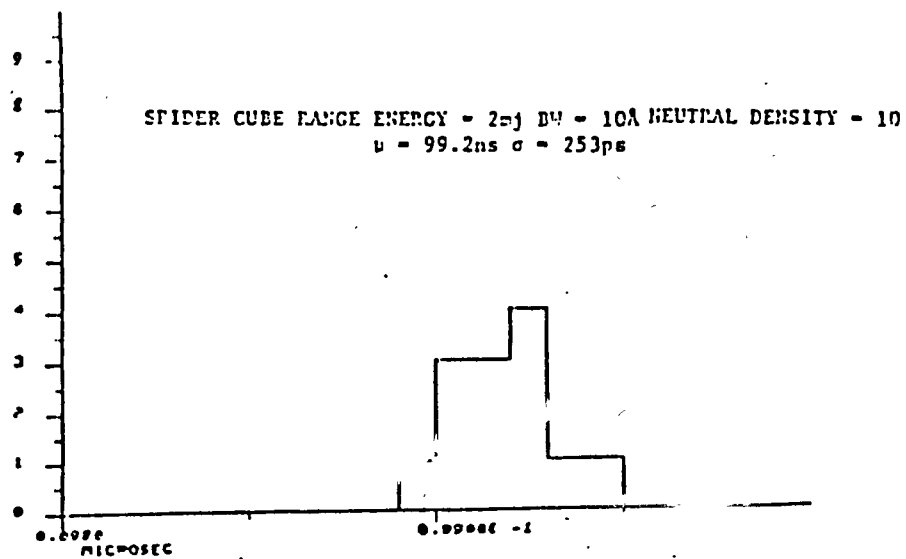


FIGURE 7

SATELLITE RANGING RETURNS

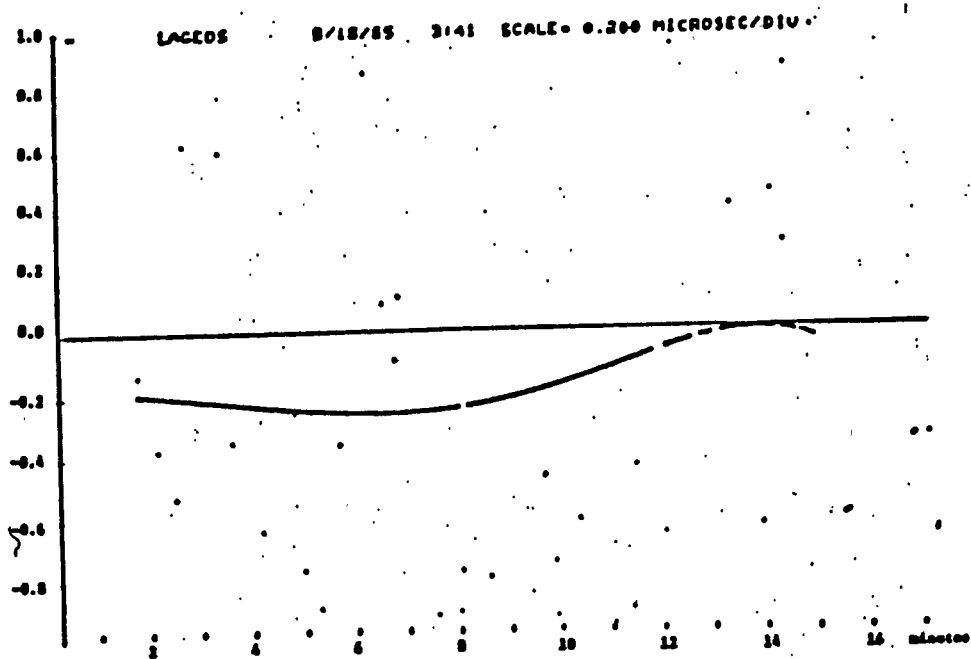


FIGURE 8

LUNAR RANGING RETURNS

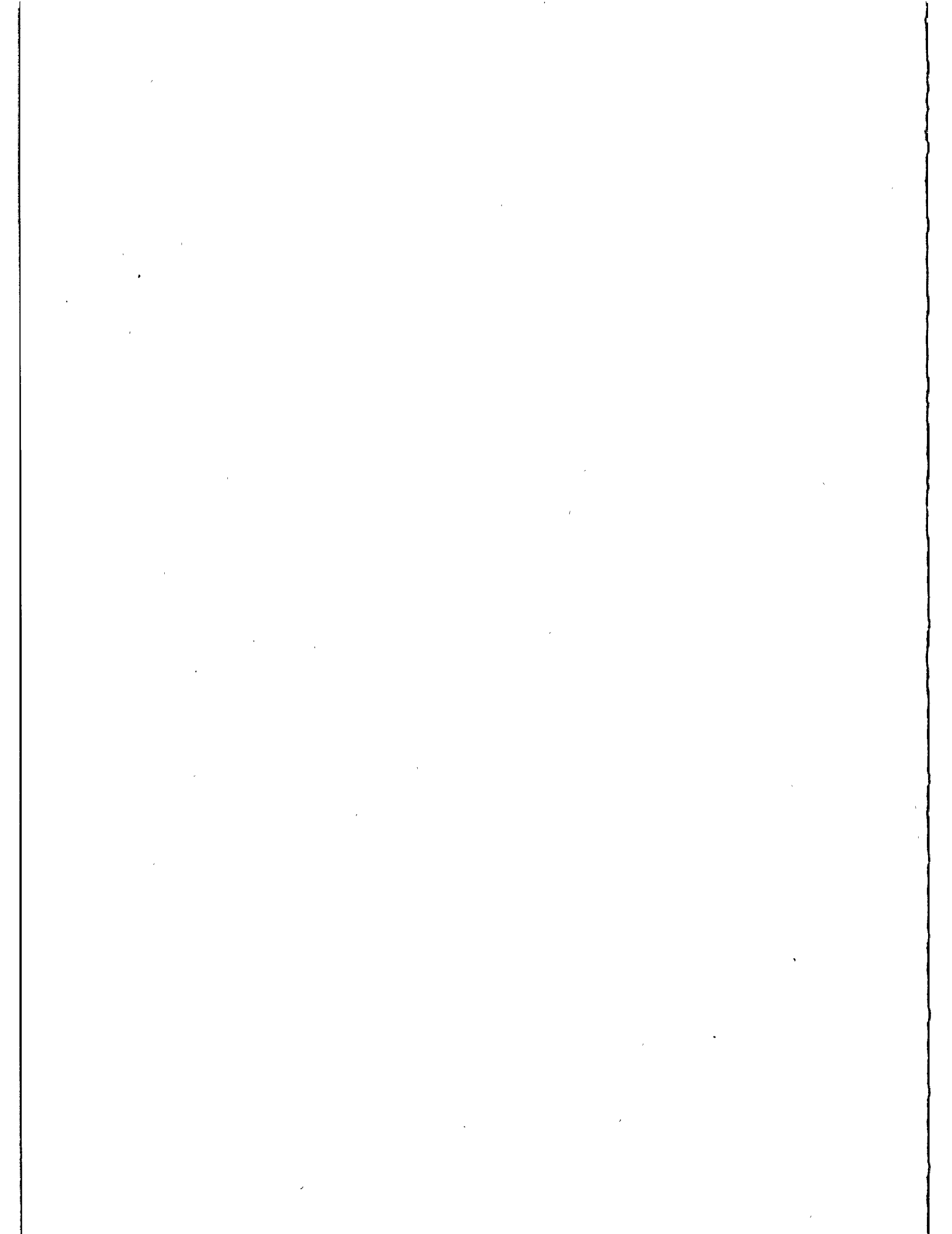
HADLEY 8143 8/26/86



FIGURE 9

#### REFERENCES

1. R.J. McIntyre, "The Distribution in Gains in Uniformly Multiplying Avalanche Photodiodes : Theory," IEEE Transactions on Electron Devices, ED-19 (1972), 703.
2. T.E. Ingerson, et al., "Photon counting with photodiodes," Applied Optics, 22 (1983), 2013.
3. P.A. Ekstrom, "Triggered avalanche detection of optical photons," J. Appl. Phys., 52 (1981), 6974.
4. P.P. Webb and R.J. McIntyre, "Recent developments in silicon avalanche photodiodes," RCA Engineer, 27-3 (1982), 96.
5. D.N. Klyshko, "Use of Two Photon Light for Absolute Calibration of Photoelectric Detectors," Sov. J. Quantum Electron. 10 (1980), 1112.
6. T.M. Zagwodzki, Test Techniques for Determining Laser Ranging System Performance, NASA Technical Memorandum TM82061 (Goddard Space Flight Center, Greenbelt, MD. Jan. 1981).
7. Webb and McIntyre, p.100.



SINGLE PHOTON SOLID STATE DETECTOR  
FOR RANGING AT ROOM TEMPERATURE

K. Hamal, H. Jelinkova, I. Prochazka, B. Sopko  
Czech Technical University  
Faculty of Nuclear Science and Physical Eng.  
Brehova 7, 115 19 Prague, Czechoslovakia

Telephone 848 840  
Telex 121254 FJFI C

ABSTRACT


To detect return signal at satellite/lunar laser ranging stations, mostly photomultipliers are exploited. There is a strong interest to exploit solid state detector. We developed a solid state detector operating at single and multiphoton level at room temperature. The quantum efficiency is 10/2% at 0.53/1.06 $\mu$ m. The timing jitter at single photon detection is 100/220 psec at 0.53/1.06 $\mu$ m. Two modes of operation: active and passive quenching have been exploited.

**Photodiode for ranging**

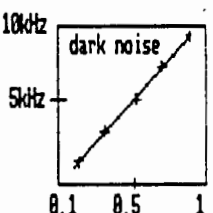
**RANGING DETECTOR - REQUIREMENTS**

JITTER	LOW
QUANTUM EFFICIENCY	HIGH
WAVELENGTH	0.4 - 1.08 $\mu\text{m}$

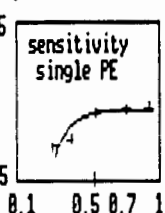
**DESIGN**



R. H. HAITZ, J. APPL. PHYS., 35, 1964, 1370  
 BREAKDOWN VOLTAGE CCA 26V,  $-20\text{mV}/^\circ\text{C}$



dark noise



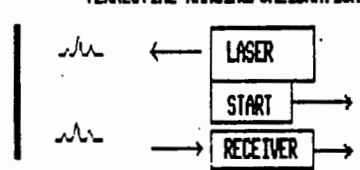
sensitivity single PE

Volts above break

K. Hana, H. Jelinkova, I. Prochazka, B. Sopko  
 Single Photon Solid State Detector For Ranging ...

**Optical scheme/laser**


**TERRESTRIAL RANGING/CALIBRATION**



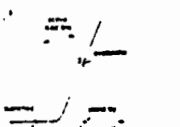
diffused target

YAG LASER/SHG  
 MODE LOCK TRAIN 2-3 PULSE  
 PULSE DURATION 30 ps  
 ROUND TRIP TIME 2ns

**MODES OF OPERATION**



PASSIVE/GEIGER

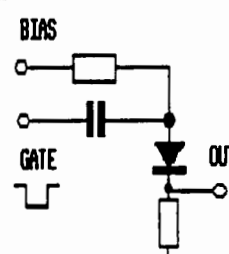


ACTIVE/SPAD

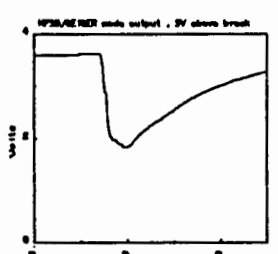
S. Gova, JQE-19, 1983, 630

K. Hana, H. Jelinkova, I. Prochazka, B. Sopko  
 Single Photon Solid State Detector For Ranging ...

**Passive Quenching/Geiger mode 0.53  $\mu\text{m}$**



BIAS  
GATE  
OUT

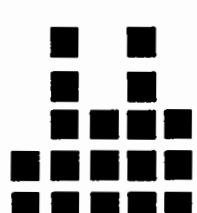


SPAD/GEIGER mode output, 2V above break

PD/GEIGER — ORTEC — COUNTER — COMPUTER

**SINGLE PHOTON DETECTION JITTER**

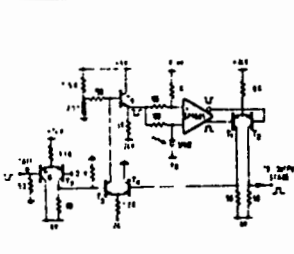
RAW	112ps
START	30ps
COUNTER	36ps
LASER	10ps
ORTEC	20ps
TARGET	30ps

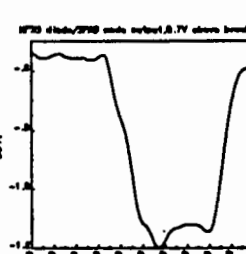


DECONVOLUTED 90ps      .80 90 100 110 120 ps

K. Hana, H. Jelinkova, I. Prochazka, B. Sopko  
 Single Photon Solid State Detector For Ranging ...

**Active Quenching/Spad mode 0.53  $\mu\text{m}$**





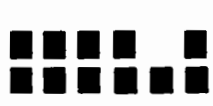
SPAD mode output, 0.7V above break

S. Gova, JQE-19, 1983, 630

PD/SPAD — COUNTER — COMPUTER

**SINGLE DETECTION JITTER**

RAW	125ps
START	30ps
LASER	10ps
COUNTER	36ps
TARGET	30ps



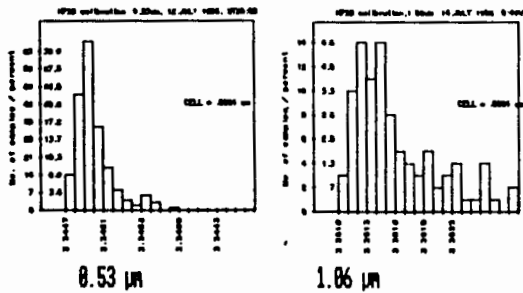
DECONVOLUTED 110ps      90 100 110 120 130 140 ps

K. Hana, H. Jelinkova, I. Prochazka, B. Sopko  
 Single Photon Solid State Detector For Ranging ...



Active Quenching: 0.86  $\mu\text{m}$

SINGLE PHOTOELECTRON RANGING

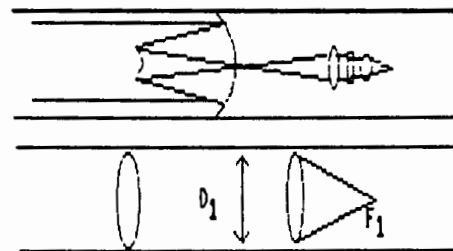


1.06 PHOTON PENETRATES NEUTRAL REGION

RAW	225ps
START	30ps
LASER	18ps
ORTEC	20ps
COUNTER	36ps
TARGET	30ps
DECONVOLUTED	220ps

Field of View / Max. Beam Divergence

RECEIVER OPTICS



TRANSMISSION EFFICIENCY

$$\eta = \frac{\beta_{\text{diode}}^2 (f_1/D_1)^2}{\beta_R^2 \cdot D^2}$$

IF  $\beta=45\mu\text{m}$ ,  $f_1/D_1=1$ ,  $\eta=1$        $\beta_R \text{ LIMIT} = \frac{45 \cdot 10^{-3}}{D}$

TELESCOPE DIAMETR	1.5M	1M	0.6M	0.3M
MAX. FIELD OF VIEW	6°	9°	15°	30°

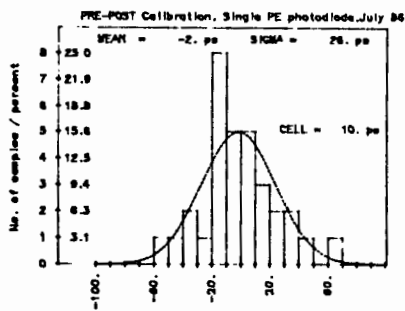
K. Hanal, H. Jelinkova, I. Prochazka, B. Sopko  
Single Photon Solid State Detector For Ranging ...

5

K. Hanal, H. Jelinkova, I. Prochazka, B. Sopko  
Single Photon Solid State Detector For Ranging ...

6

System Stability



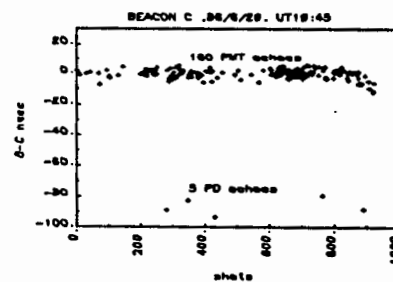
PERIOD      JULY 1986  
SERIES      100-200 ECHOES  
WAVELENGTH      0.53  $\mu\text{m}$   
SINGLE PHOTOELECTRON

K. Hanal, H. Jelinkova, I. Prochazka, B. Sopko  
Single Photon Solid State Detector For Ranging

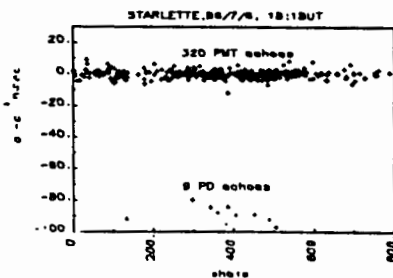
7

Satellite Ranging

BEACON-C




STARLETTE



K. Hanal, H. Jelinkova, I. Prochazka, B. Sopko  
Single Photon Solid State Detector For Ranging

8

HPSS diode ruggedness	
<p>Diode used as a SLR experimental receiver detector, the system was alligned using corner cube at 100n, accidentally, the MD were nissing lasing with the full power</p> <p>total energy 70 nJ power flux density 7.000 GW/cm<sup>2</sup></p>  <p><b>NO DAMAGE</b></p>	
<p>K. Hanal, H. Jelinkova, I. Prochazka, B. Sopko Single Photon Solid State Detector For Ranging ...</p>	

Summary / Single Photon Detectors Review				
	Hanal et al		PMT dyn./MCP	Bowman et al
	Geig	SPAD		
JITTER psec	0.53	98	118	298 185 253/162/98
	1.06	220	220	
QUANTUM EFFICIENCY %	0.53	10	10	10-30 28
	1.06	2	2	0.3
DARK COUNT kHz		6	6	< 0.1
DEAD TIME incl. discrim			150ns	60ns 100 μs
OUTPUT PULSE per Photoel.	2 V	NIM		2-50mV 3 V
RUGGEDNESS	excellent		low/very low	excellent
FIELD OF VIEW	9"/1n		no limit	
TEMPERATURE	room		room	-68°C
DISCRIMINATOR	yes	no	yes	yes
POWER SUPPLY	30V		2.5kV/5kV	160 V
GATE	TTL	NIM	HV/HV	50 V
<p>K. Hanal, I. Prochazka, H. Jelinkova, B. Sopko Single Photon Solid State Detector for Ranging at Room.</p>				9

"CONSTANT FRACTION" DISCRIMINATORS IN FEW  
AND MULTIPHOTOELECTRON LASER RANGING

W.A. Kielek  
Departement of Electronics  
Institute of Radioelectronics  
Warsaw University of Technology  
Nowowiejska str. 15/19 00-665 Warsaw - Poland -

Telephone 21007653 or 253929  
Telex 813 307

ABSTRACT

The report explains some not widely known properties of c.f. discriminators used in nuclear techniques when using in laser ranging, as for instance mean value of timing point walk with signal energy, and the possibility of jumps in results in some conditions. Accuracy optimization methods are given for the case of the absence of jumps.

"CONSTANT FRACTION" DISCRIMINATORS IN FEW-  
AND MULTIPHOTOELECTRON LASER RANGING

W.A. Kielek  
Department of Electronics  
Institute of Radioelectronics  
Warsaw University of Technology  
Nowowiejska str. 15/19 00-665 WARSAW, POLAND

Telephone 21007653 or 253929  
Telex 813 307

ABSTRACT

The report explains some not widely known properties of c.f. discriminators used in nuclear techniques when using in laser ranging, as for instance mean value of timing point walk with signal energy, and the possibility of jumps in results in some conditions. Accuracy optimization methods are given for the case of the absence of jumps.

1. GENERALITIES

Almost all so called "constant fraction" discriminators use the principle of work as follows [1], [2], [3], [4]: from the input signal attenuated in accordance with fraction value, the input signal unattenuated but properly delayed is subtracted, and resulting signal is examined for zero - crossing. After that subtraction, one obtains the signal

$$\psi(t) = f \cdot f(t) - f(t - T_d) \quad (1)$$

where:  $f$  - fraction,  $T_d$  - delay,  $f(t)$  - input signal.

This operation is done using for instance block schemes as at Fig. 1. All ORTEC, TENNELEC 454 and 455, EC&G and almost all other c.f. discriminators used in nuclear technics follow this principle of work. The independence of timing point on the amplitude of incoming pulses is preserved in case of constant deterministic shape of them. This situation is illustrated at the Fig. 2. There is the single zero - crossing only in case of that deterministic pulse signal case.

The signal at the PMT output, it is the sum of random Poisson number of PMT single-photoelectron responses, each of deterministic shape, but of random amplitude. The single realisation of that signal can be described by the formula:

$$f(t) = \sum_{i=1}^K g_i f_{SER}(t - t_i - \tau_i) \quad (2)$$

where:  $K$  - Poissonian number of photoelectrons realised,  $g_i$ ,

$t_i$ ,  $\tau_i$  - random variables: PMT gain, times of PE generation at the photocathode, and delay in PMT, respectively;  $f_{SER}(t)$  - deterministic shape of single PE (photoelectron) response of PMT. Due to existence of the sum  $t_i + \tau_i$  in parentheses of formula (2), it is clear that probability density of PMT delay curve has got the same effect on the accuracy as the laser pulse shape, and the "equivalent" laser pulse can be introduced, of the shape of the convolution of laser pulse and PMT delay density curve. In case of single - photoelectron signal the shape of the signal is the same in each realisation. It is also true when the signal is composed of few or many PE but the length of the laser pulse and PMT delay density curve is very short in comparison with the single electron response pulse of the PMT tube.

## 2. POSSIBILITY OF JUMPS

When it is not the case, the shape of the input signal is random, not the same in each realisation. For few PE in realisation of the signal, and sufficiently small relation between widths of  $f_{SER}$  and convolution of the laser pulse and PMT delay density curve, the width of  $f_{SER}$  is not enough to make one smooth pulse signal. There is the group of separated  $f_{SER}$  pulses with breaks between them. The signal can be also of the form of the multi - top single pulse. In both such cases the resulting signal at the input of the zero - crossing sensitive trigger can have more than one zero - crossing (Fig. 3). The time position of work of the discriminator jumps from the right position to the first zero - crossing. This effect produces the increase in standard deviation and decrease in the mean value of results.

Especially severe influence on the results can have this effect, when the laser signal is not well limited in time, for instance when the main signal pulse stands at some pedestal of weaker radiation (e.g. when using pulse chopper), or when laser pulse is a Gaussian pulse. For such signal, in few - and multi - PE work there exists the possibility to obtain the jumps in results in the direction to decrease the result by few nanoseconds.

This phenomenon is illustrated at the Fig. 4 (Gaussian signal pulse). Single photoelectrons generated by the weak laser radiation before main part of the signal can move in some realizations the time point of work of zero - crossing trigger from the right position to the wrong position few ns before the right one.

At low energies, there is no this effect due to small probability of generation of photoelectrons far before the central part of the laser pulse. At higher energies, when the photoelectron number is high, there exists the high probability of compensation of the influence of the first photoelectrons by the subsequent ones. The probability to obtain false zero - crossing at the summing point in the circuit is again small. The max. probability lies in the medium energy region, between 20 and 1000 PE, dependent on parameters such as fraction, filtration and delay.

It can be deduced from signal model and formula (1) that

probability of jumps should be smaller when: increasing the delay of delay line, or / and the filtration F, or / and the fraction value f. These statements are confirmed by simulations and experiment in laboratory and at the 1-st generation laser stations. Simulation results are given at Figs. 5 and 6.

### 3. WALK IN THE CASE OF ABSENCE OF THE JUMPS

But also when the jumps are absent, there is no possibility to obtain no delay walk with energy when using c.f. or fixed threshold discriminators. Suppose the symmetrical shape of the "equivalent" laser pulse. In case of the single photoelectron in the signal, the mean position of this photoelectron is in the centre of this pulse, say zero, due to equal probabilities of negative and positive values of PE position. But in case of two photoelectrons, the probability of positive value of position of both photoelectrons is 25% only. Then, the probability of existence of at least 1 PE on the left side from the zero position is 75% (50% for single PE). For very high PE number, the PMT output signal has got the shape of the  $f_{SER}$  convolution with the "equivalent" laser pulse shape, and the timing point goes to the negative position in accordance with the fraction value. Then, for the signal following (2), the walk is unavoidable even in the ideal case of no walk for deterministic signal shape. Some results for walk obtained from simulations are given at Fig. 5.

### 4. STANDARD DEVIATION

There exists the proof, that normalised to the pulse half-width random error, approximately, for large PE number, follows the formula:

$$\sigma_{\Delta}/T = g_1 \alpha^{1/2} N^{-1/2} \quad (3)$$

where  $\alpha$  is the mean square of the normalised to unity PMT gain, N is the mean PE number, T - half of width of the pulse, or  $\sigma$  parameter of Gaussian pulse.

The  $g_1$  coefficient obtained by simulations is given at the Fig. 6.<sup>1</sup> Fortunately, no jumps are present up to 20 PE energy level. Well limited in time (for instance trapezoidal) waveforms without wide pedestal do not produce the jumps. In case of absence of jumps, this discriminator is quite good, especially for the random error.

The theoretical formula I obtained (remarks about method in [5]) for  $g_1$  coeff. dependent on f, F and w (fraction, filtration and  $g_1$  normalised delay respectively) when the signal and filter (PMT) response is of the form of Gaussian pulse is as follows:

$$g_1^2 = \left\{ f^2 \exp \left[ - \frac{z+1}{2z+1} A^2 \right] + \exp \left[ - \frac{z+1}{2z+1} B^2 \right] + \right. \\ \left. - 2f \exp \left[ - \frac{z+1}{2z+1} \left\{ \frac{w^2}{2} \left( z + \frac{1}{2} \right) + \left( \frac{\ln \frac{1}{f}}{w} \right)^2 \right\} \right] \right\} \cdot \\ \cdot \frac{z+1}{z \sqrt{2z+1}} \cdot \left\{ B \exp \left[ - \frac{B^2}{2} \right] - f A \exp \left[ - \frac{A^2}{2} \right] \right\}^{-2} \quad (4)$$

where:  $w^2 = \frac{T_d^2}{\sigma^2 + \sigma_F^2}$ ,  $T_d$  - delay time at Fig. 1,  $z = (\sigma/\sigma_F)^2$   
 $F = (8 \ln 2)^{1/2} \cdot \sigma_F/\sigma$

$$A = \frac{w}{2} - \frac{\ln \frac{1}{f}}{w}, \quad B = -\frac{w}{2} - \frac{\ln \frac{1}{f}}{w}, \quad \sigma, \sigma_F - \text{parameters}$$

of Gaussian signal and filter response, respectively. Computations from formula give the results as at the Figs. 7, 8, 9.

The case of  $f$  equals 1, there is also the case of Short Circuited Delay Line shaping and zero crossing detection. The results indicate that proper choice of parameters can give the same standard deviation as for max. likelihood estimation [6].

## 5. CONCLUSIONS

- A. The mean value change is unavoidable when using C.F. timing in case of changing the energy level from 1 to few PE. That change is proportional to the width of the convolution of laser pulse and PMT delay density curve.
- B. Above 10-20 PE energy jumps in results can exist. This effect is absent for laser pulse waveforms well limited in time.
- C. Probability of jumps decreases when increasing the filtration ( $f_{SER}$  width), fraction, delay, and charge sensitivity of zero-crossing trigger or comparator.
- D. In the absence of jumps, for proper values of  $F$ ,  $T_d$ ,  $f$  parameters, Gedcke-Mc Donald type c.f. discriminator is good, especially for standard deviation, and is only slightly poorer in mean value walk than the c.f. discriminator with peak value memorization [5].
- E. Standard deviation reaches the minimum for much higher delay values than the value which is needed to obtain constant fraction work for the deterministic signal.

REFERENCES

1. D.A.Gedcke, W.J. Mc Donald. Nucl. Instr. Methods 55, 1 (1967).
2. M.R.Maier, P.Sperr. Nucl. Instr. Methods 87, 13 (1970).
3. T.J.Paulus, M.O.Bedwell. "High Speed Timing Electronics and Applications of Hybrid Electronics in Nuclear Instrumentation". ORTEC Inc.
4. Instructions and data sheets for ORTEC and other c.f. discriminators.
5. W.Kielek. V-th Workshop on Laser Ranging Instrumentation, Proceedings, p. 112-118.
6. I.Bar David. IEEE Trans. on Information Theory, IT-15, 31 (1969).

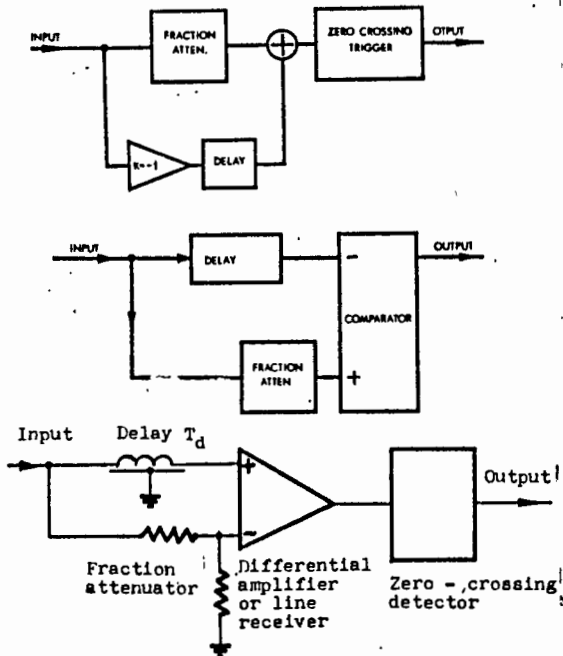


Fig. 1 Variants of principal scheme of nuclear "c.f." discriminators

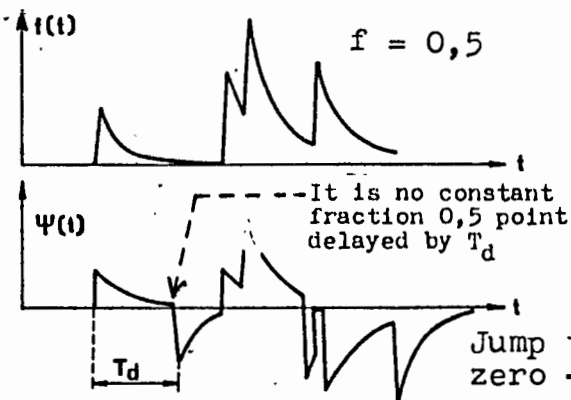


Fig.3 Illustration of work of the circuits from Fig.1, few PE, stochastic signal

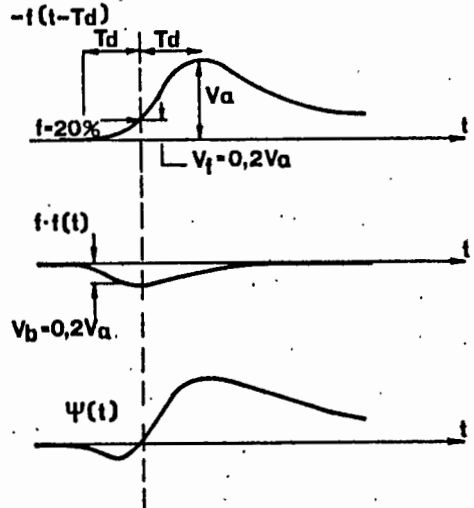


Fig.2 Illustration of work of the circuits from Fig.1, deterministic in shape single signal pulse

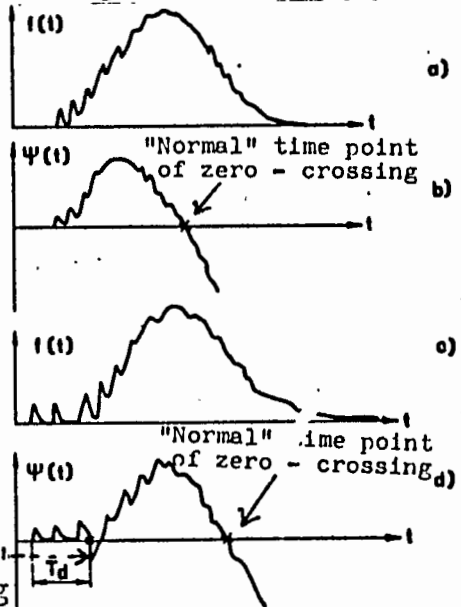


Fig.4 The same as at Fig. 3, 50+1000 PE, small filtration F(f<sub>SER</sub> width divided by half-width of the laser pulse)



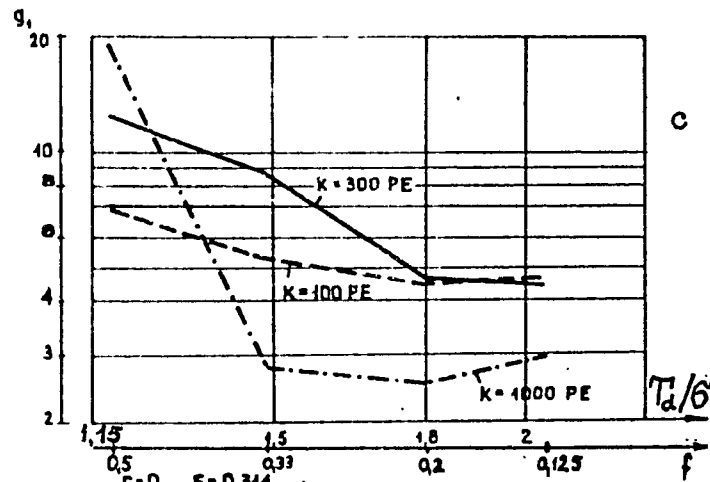
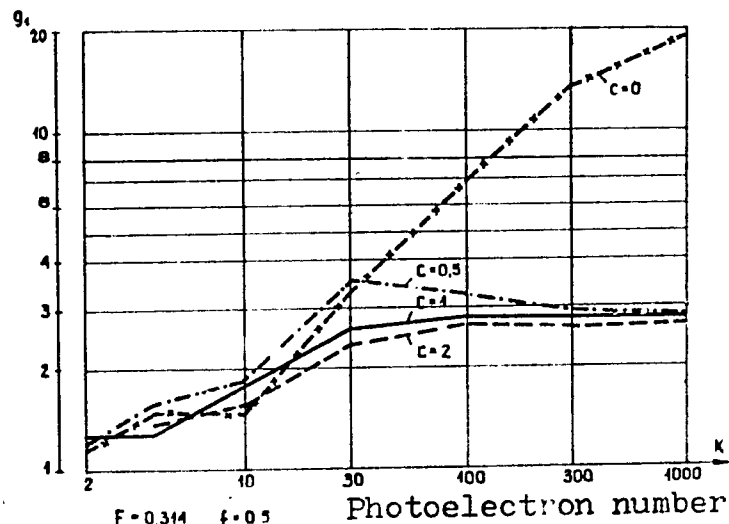
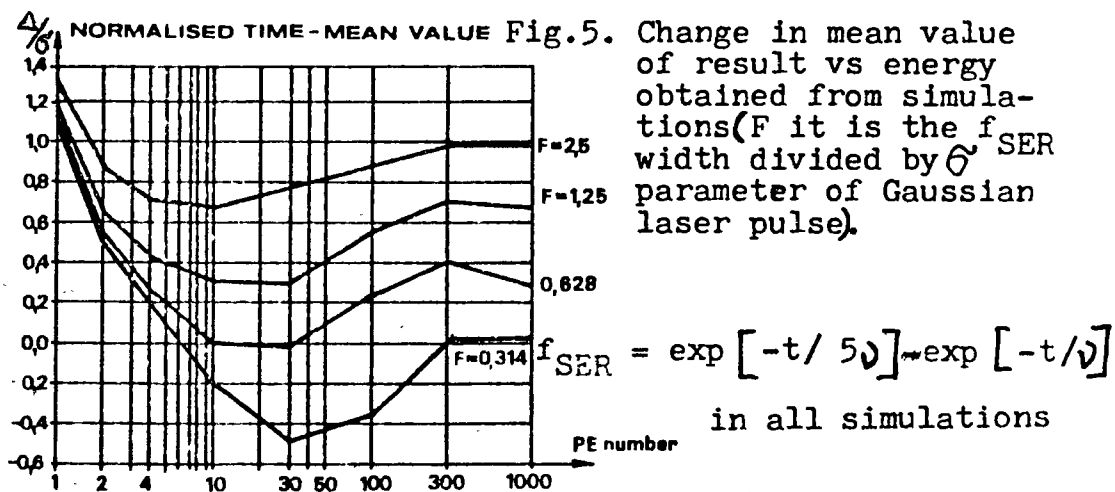
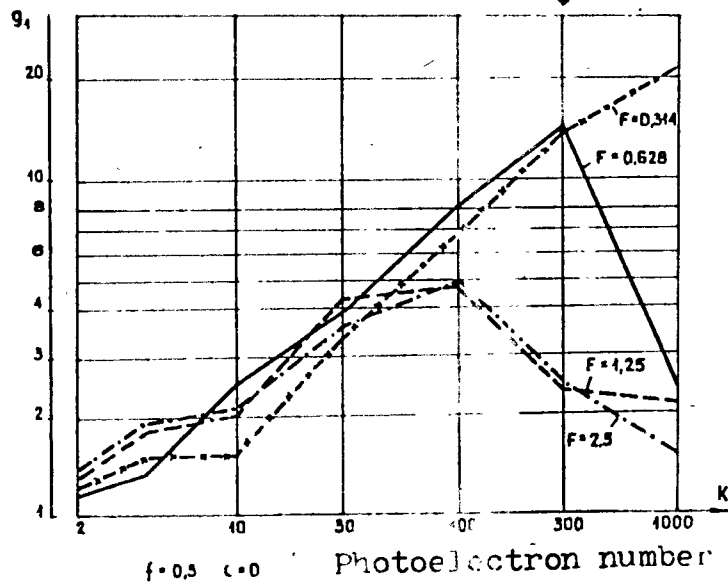


Fig.6.  $g_1$  values obtained from simul. a/ vs energy and charge sensitivity, b/ vs energy and filtration, c/ vs energy and normalised delay  $T_d/\sigma$  (fraction value changes also)



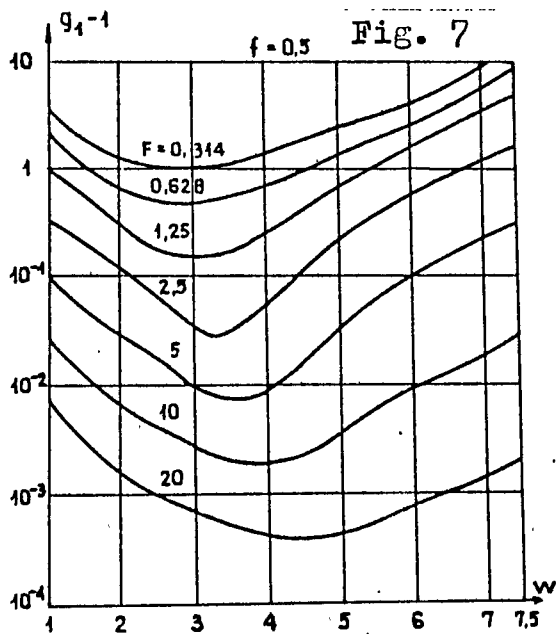
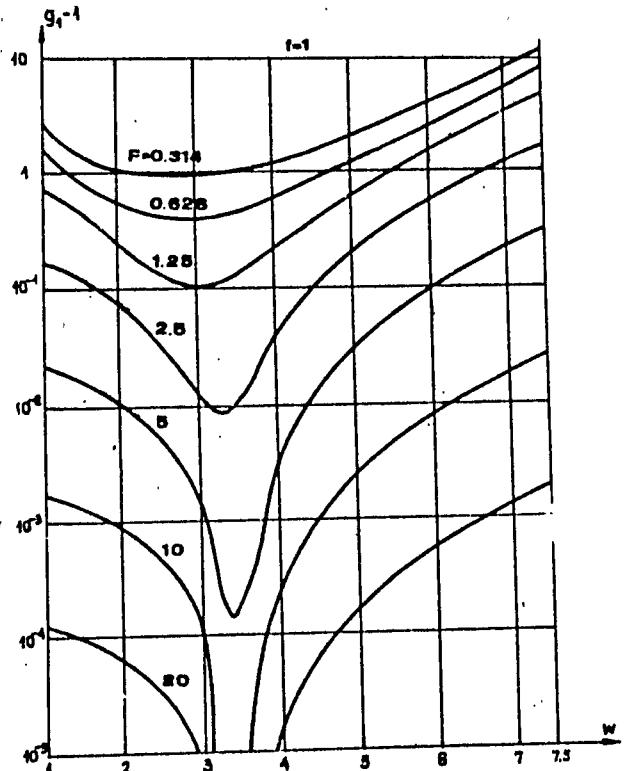
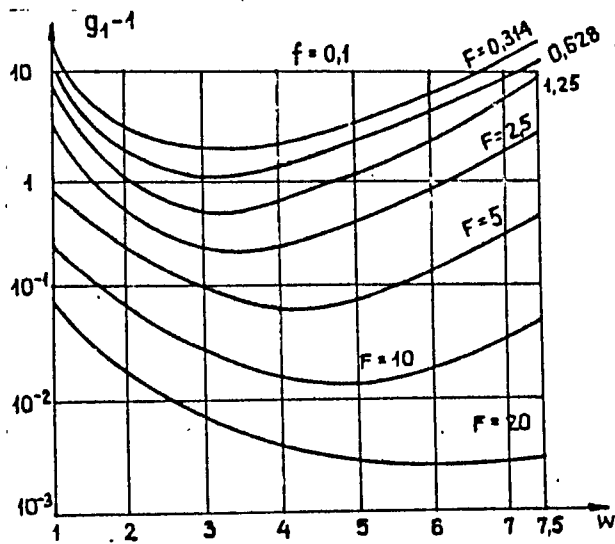


Fig. 7.  $g_1-1$  values vs delay  $W$  and filtration  $F$  for 3 values of fraction  $f$ .

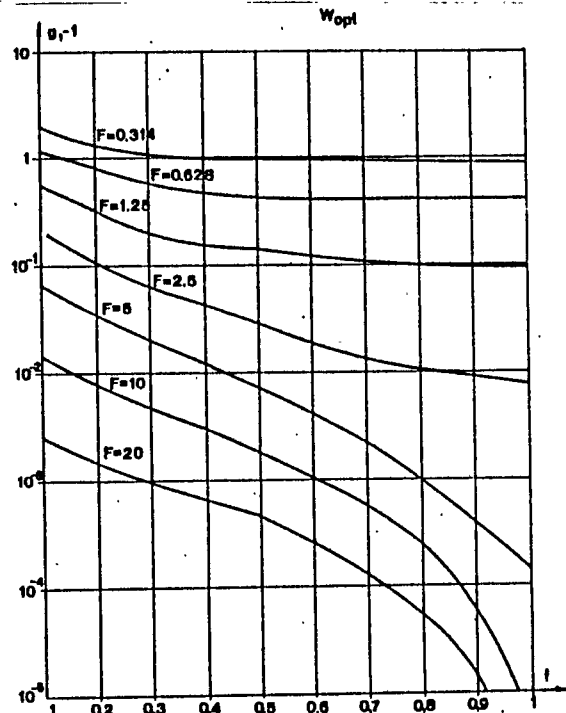
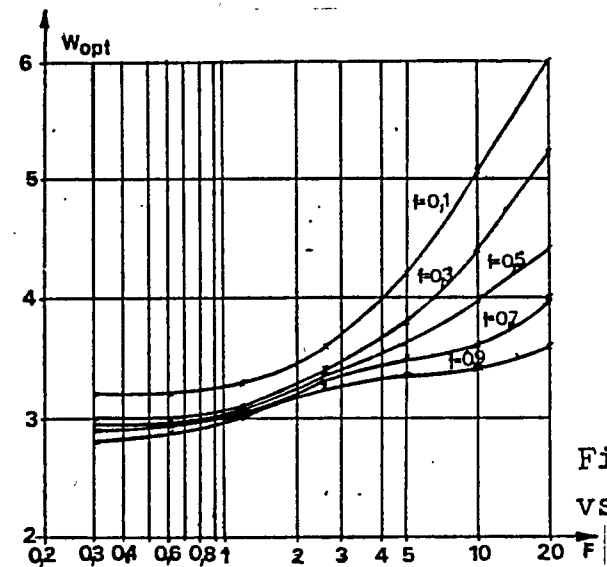


Fig. 9.  $g_1-1$  values for  $W_{opt}$  vs fraction  $f$  and filtration  $F$

Fig. 8. Optimum delay  $w_{opt}$  values vs filtration  $F$  and fraction  $f$ .

## CALIBRATION OF SUB-PICOSECOND TIMING SYSTEMS

B.A. Greene  
Division of National Mapping  
P.O. Box 31  
Belconnen ACT 2616 - Australia -

Telephone (6162) 525095  
Telex AA 62230

### ABSTRACT

The difficulties of calibrating picosecond precision timing systems are discussed. A wide range of techniques are considered, and a minimum configuration for rigorous calibration is described. High speed techniques that lend themselves to full automation are evaluated in the context of a fully operational system.

# CALIBRATION OF SUB-PICOSECOND TIMING SYSTEMS

B.A. Greene

## 1. Introduction

The recent development of timing systems with picosecond and even sub-picosecond accuracy has stimulated a requirement to calibrate such systems. In SLR systems the systematic errors are of overriding importance, and even if real time surveillance of the absolute accuracy [1] of the SLR system as a whole is maintained, it is still essential to be able to calibrate the timing sub-system independently. Once calibrated, it is a tool which can then be used to characterise the errors, systematic and otherwise, in other sub-systems.

The principal requirements for timing system calibration are to establish

- . stability
- . continuity ('smoothness')
- . linearity

If these characteristics are properly established, then the absolute accuracy of the timing system is rigorously proven.

In the context of a time interval measurement system, stability can be defined as the RMS error associated with a straight line fit of zero slope against time for a constant (not necessarily known) time interval.

Linearity is defined as the degree to which system error is proportional to length of time interval measured.

Continuity is defined as the degree to which linearity and stability are maintained as the time interval between test (calibration) points is reduced continuously.

A rigorous calibration procedure must examine all of these parameters.

In this paper we discuss several calibration techniques, and the role they can play in establishing system accuracy in terms of which of the above criteria are adequately tested.

## 2. Delay Line Calibrations

An established calibration technique for nanosecond timing systems utilizes an array of switchable coaxial delay lines, which have been pre-measured and are thus of 'known' delay. Even if it is assumed that the original calibration of each delay line was accurate without limit, this technique is unsuitable for picosecond calibrations because

- . cable ageing causes delay changes
- . cable flexing causes delay changes
- . typical switch repeatability is only 3 ps RMS
- . cable delays are temperature dependent
- . coaxial connect-reconnect repeatability is only 3 ps RMS

This technique can be adapted to produce sub-picosecond tests of stability only. If the cable temperature is controlled such that the delay is stable to 0.5 ps RMS, then long term stability tests can be conducted on the timing system. A typical temperature sensitivity for coaxial cable is 0.03% per degree (C). Although temperature servos have been developed which can offer .001°C temperature control, it is in practice difficult to control coaxial cable to better than 0.1°C for each 50 ns of delay. That is, 0.5 ps stability can be readily obtained up to about 17 ns of delay. This is of little use if time interval units (TIUs) are used directly (i.e. in time interval mode) to measure satellite range. However, if precision TIU's are used as the high precision vernier of an epoch timing system, it is not necessary for them to count beyond 20 ns. Thus temperature stabilised delay lines can be used for 0.5 ps stability tests throughout the range of use of the TIU.

### 3. Variable Delay Lines

Rigid coaxial delay lines have been manufactured for calibrating the linearity and continuity of timing systems. These systems proliferated during a period when 100 ps timing system accuracy was the achievable limit, and could be expected to be inadequate for picosecond calibrations. This is the case, although some well constructed variable (rigid) coaxial delays can produce 3 ps RMS linearity and repeatability. Their stability will depend on delay length chosen, heat sources and sinks attached to the delay, and mechanical wear.

### 4. Dual Oscillator Techniques

It is now possible to obtain crystal oscillators which have sub-picosecond stability over 1 second, and ageing rates which are undetectable over 20 minutes with present instrumentation. The relative phase of two such oscillators provides a very slowly and linearly time varying delay for calibration purposes. This calibration technique is in everyday use at some SLR sites [2,3], using less stable oscillators for coarser (50 ps) calibrations. Provided that care is taken in generating the pulses to the timing system from the crystal output frequencies, this technique can give 1 ps linearity and accuracy, and sub-picosecond continuity checks.

### 5. Phase Locked Loop Method

An alternative oscillator phase technique utilises a single high stability oscillator and another oscillator phase-locked to it. The phase angle is programmable allowing selection of the relative phase of the crystals and thus a time interval. This technique gives linearity and continuity test capability, but is inherently noisier than the dual oscillator technique (above).

The noise attributable to the phase locking process can be brought down to around 5 ps if great care is taken with the circuit design. In addition, several picoseconds of systematic error arise from non-linearities in state-of-the-art phase angle programming circuits.

## 6. Optical Delay Line (ODL)

The time required for light to travel up to 10 m in air is virtually independent of environmental parameters [4]. To effect a 0.5 ps change in observed optical delay, environmental changes of the following order would be required:

$$\begin{array}{l} P = 30 \text{ mb} \\ \text{or} \\ P_w = 200 \text{ mb} \\ \text{or} \\ T = 10^\circ\text{C} \end{array}$$

[where P is atmospheric pressure,  $P_w$  is water vapour pressure, and T is air temperature]

The use of an optical delay line provides excellent linearity, accuracy, continuity, and stability. For example, if the delay elements are used to form a one-way light path, 100 microns of displacement of either end will cause a 0.33 ps change in the delay. Since the delay path can be very accurately controlled, to within a few microns, femtosecond resolution and accuracy can be obtained for differential delays.

For a two-way (folded path) calibration range, only 1.5 m of travel is required to produce a delay change of 10 ns. Such a path length is both simple to control environmentally and quite simple to automate for translation with 0.1 mm accuracy. Thus high resolution verniers with up to 10 ns full scale count can be absolutely calibrated to 0.66 ps under program control.

The technique is usually limited by the characteristics of the optical transmitter and receiver used to generate and detect the light pulse which transits the delay so accurately formed. Using a 30 ps FWHM diode laser transmitter, and a 30 ps risetime detector, sub-picosecond relative accuracy, stability, and resolution can be achieved, provided environmental parameters are controlled.

## 7. Ensemble Techniques

The process of refining the accurate determination of time interval is analagous to that of defining time itself. The well established technique of using clock ensembles and optimised algorithms for manufacturing a timescale can be readily adapted to the time interval problem.

The use of as large an ensemble as possible of time interval counters is suggested by two factors arising from a very limited development program for TIUs for the Natmap Laser Ranging System (NLRS) at Orroral:

- . no single TIU was ever constructed or tested which had better than 8 ps RMS single-estimate uncertainty for time interval.
- . even the very best units ever tested at Orroral would exhibit occasional and inexplicable short term (minute) systematic excursions of up to 4 standard errors of a single estimate as measured from the long term average. Over a long period (20 mins) these units would produce sub-picosecond (averaged) stability of a mean estimate.

Since the Orroral program goal was to produce 5 ps RMS single estimate random errors with 0.5 ps systematic error, it was necessary to aggregate the performance of many TIUs to damp out excursions and to statistically reduce time interval errors.

A feature of the ensemble technique is that it requires very compact TIU design, so that a large number of TIUs can be fed an electronic signal over short paths, and so that complete environmental control of the ensemble is possible.

It has been found that the ensemble techniques are very effective in improving the resolution and linearity of TIU systems. Ensemble techniques do not yield absolute accuracy, but do facilitate absolute accuracy calibration of systems by improving linearity. The decay of accuracy of an ensemble is also significantly slower than that of individual TIUs, allowing less frequent resort to absolute accuracy calibrations, which can be tedious to execute rigorously.

The ensemble techniques can be used to calibrate individual TIUs simply by examining the performance of the unit in comparison to the ensemble mean. In general, if the ensemble is well behaved, errors in the individual TIUs can be readily identified. The technique lends itself very well for total automation, but is clearly not rigorous.

## 8. Calibration Techniques for the NLRS

Although the NLRS has the capability to apply any of the above calibration techniques, in practice the only techniques routinely used are:

- . optical delay line
- . fixed (stable) cable delays
- . ensemble

The NLRS is constrained to operate almost totally automated. Thus only techniques which can lend themselves to total automation can be routinely used. The optical delay line method, which is the only rigorous technique listed above, is used very infrequently because it is not totally automated (here defined as requiring no user intervention whatsoever).

The timing system philosophy for the NLRS uses a large ensemble to reduce random error and give momentum to the system (the ensemble characteristics change more slowly than those of its elements). These ensembles can then be monitored very infrequently using a primary (rigorous) test such as ODL.

Such a complex calibration technique is not required to monitor the ensembles for accuracy. In practice a very simple approach is used, called fixed delay epoch measurement (FDEM).

For FDEM, two electronic pulses are obtained from a fixed, stable, delay cable built into the timing system. One NLRs timing ensemble measures the epoch of the first pulse, whilst a second ensemble measures the epoch of the second. The pulses are sourced such that they are totally random in phase with respect to the time base of the epoch timing system. Thus the full count range of the ensembles will be sampled if many measurements are taken. The delay is obtained by subtracting epochs. An error in either ensemble, at any point in its range, will cause the distribution of delay estimates to depart from the ideal. This is most easily seen as an increase in the spread of the distribution.

Because the delay is fixed, the error space of the ensemble measuring the second epoch is not sampled randomly. That is, the point in its range which is sampled is 100% correlated with the sample point of the first ensemble. Thus it is possible for errors to compensate and go undetected. The probability of this is reduced significantly if more than one delay is used.

The utility of this technique, which is used before every tracking operation, has been borne out by occasional applications of rigorous tests such as ODL.

The three techniques in routine use at Orroal are thus applied in the following way:

- (a) On every shot. On each shot, at least 34 estimates of epoch are made. The ensemble size is large enough to give a good reduction in systematic drift and random error over individual TIU elements. Individual TIU readings are processed through a double-pass filter which utilises the recent performance history of a TIU to adjust its reading before comparing it to the ensemble mean in the filter process. Units may be 'accepted' or 'rejected'. Consistent rejection implies a need for repair or recalibration.

Also on each shot, a real-time calibration of system delay is made. This is essentially an ODL calibration in which the delay is not known a priori to better than 200 ps, because of long term drift in the apparatus. However, the system delay so measured can be and is used in an FDEM sense. The calibration curve is displayed, shot by shot, in real time, with picosecond resolution, so that the operator (if present) can monitor the overall system performance, including timing. The data is continuously analysed in real time, and statistics presented to the operator. Only gross errors of over 40 ps would be detected at this stage because the detector used (MCP-PMT) has around 40 ps RMS error itself, and can walk 40 ps during a typical SLR pass.

- (b) Before each pass.

Before each pass, over 3000 samples of timing system performance are taken in FDEM mode, under total software control. The FDEM algorithm in use calculates the signal delays to each ensemble, and trims them into equality before the pass commences (usually only a few ps adjustment).



- (c) Occasionally the granularity and accuracy of the timing system are checked independently. A good test for continuity of the timing system is obtained by taking a delay line and heating it for 1 minute and then allowing it to cool. The thermal relaxation produces a delay continuum. If the delay is sampled at 50 Hz, delay changes of 20 fs can be sampled. Figure 1 shows a typical result from a continuum test of this kind, showing individual delay measurements. Strong structure at the picosecond level is evident, but the results show very good performance overall.

The accuracy calibration used is the ODL technique, applied infrequently because of its need for operator intervention.

Finally, system stability checks are carried out periodically. A typical stability plot for the NLRS timing system is shown in Figure 2. Each point plotted is a normal point of 400 ensemble estimates of a fixed and stable delay. The RMS error of a straight line fit to the data shown is around 0.6 ps, which is a typical result. The suggestion of a cyclic systematic error is present in the data. This has been seen in ODL tests also, so it is likely to be attributable to the timing system.

## 9. Comments

The electronic measurement of time interval to the picosecond level is exceedingly complex. The NLRS timing system can only approach picosecond performance on a statistical basis. That is, it is beyond our present technology to adjust a delay by 5 picoseconds and be 100% confident that the TIU single sample reading, or even that of a TIU ensemble, will change by 5 picoseconds. However, if many hundreds of estimates are made, delay changes of less than 1 ps can be accurately determined by TIU ensembles.

## REFERENCES

1. Greene, B.A., "Calibration of Sub-Millimetre Precision Satellite Laser Ranging Systems", proc. Sixth International Workshop on Laser Ranging Instrumentation, to be published.
2. Sinclair, A., Royal Greenwich Observatory, UK, Private Communication.
3. Steggerda, C. University of Maryland, USA, Private Communication.
4. Owens, J.C., "Optical refractive index of air dependence on pressure temperature and composition", Appl. Opt., Vol 6, No 51, 1967.

Figure 1  
TIMING CONTINUUM TEST

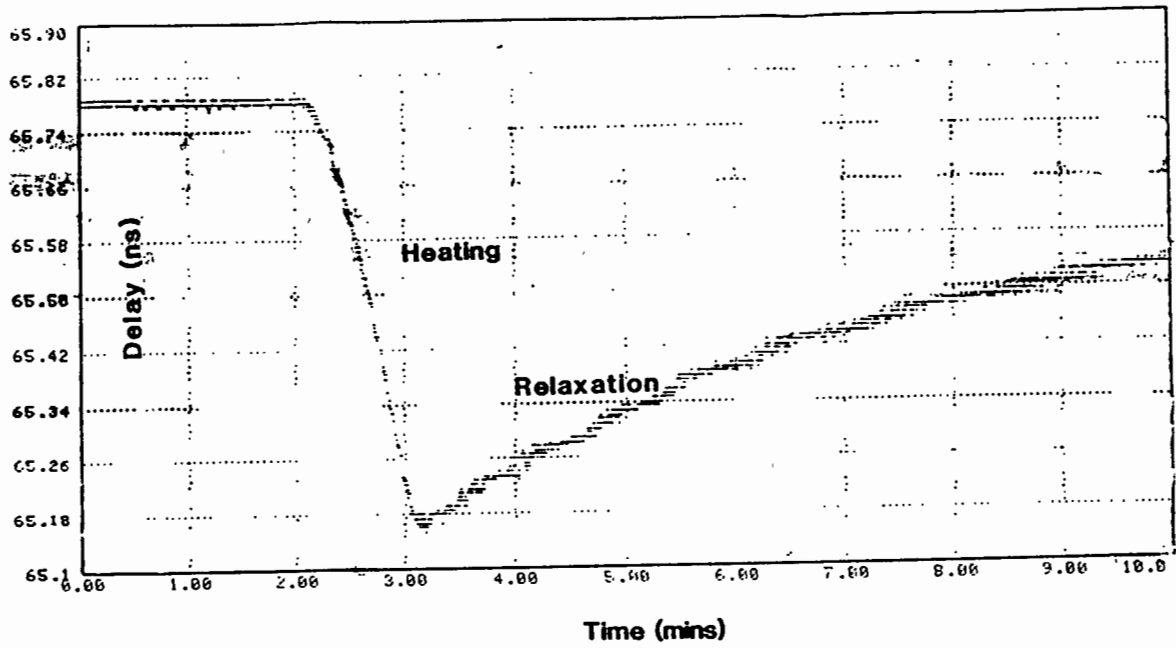
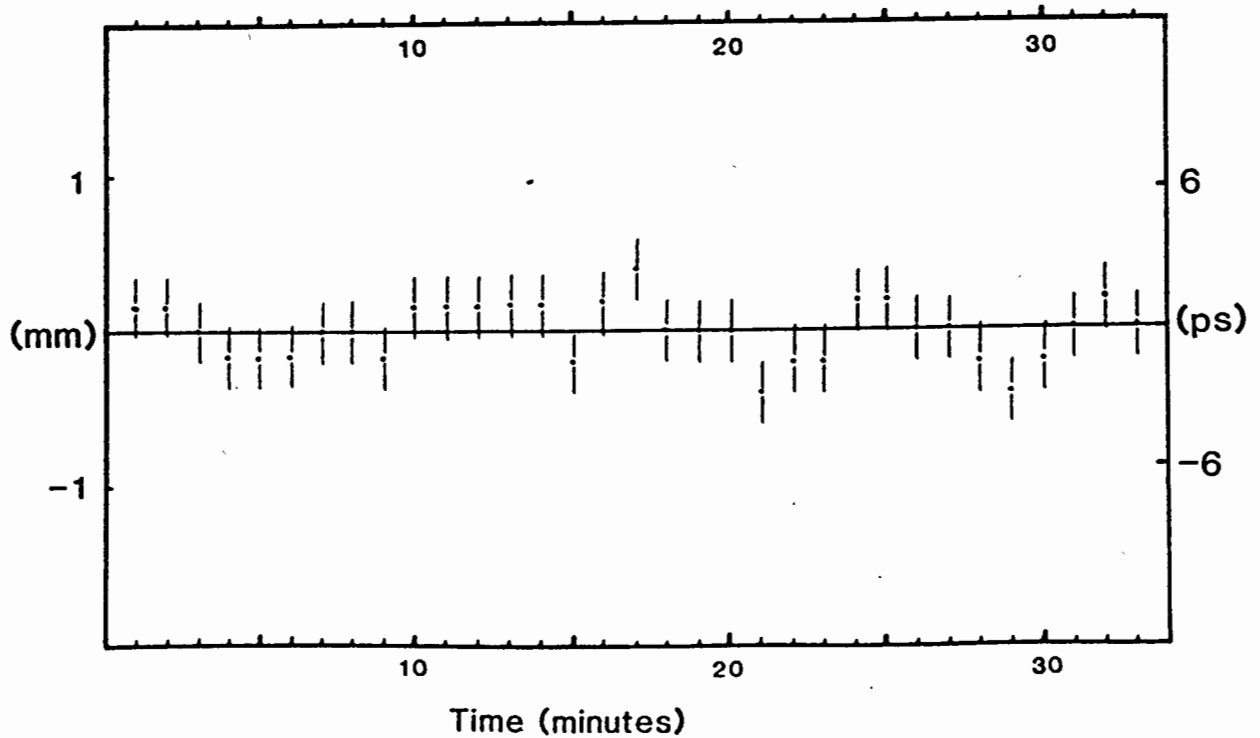


Figure 2  
NLRS TIMING STABILITY



RECENT ADVANCES IN THE GLTN TIMING AND  
FREQUENCY INSTRUMENTATION

P. Dachel, and A1  
Bendix Field Engineering Corporation  
One Bendix Road  
Columbia, Maryland 21045 - USA -

Telephone (301) 964 7189  
TWX 198120 BENFLD COLB

ABSTRACT

The stringent epoch time requirements necessary for the Goddard Laser Tracking Network to satisfy its global geodetic survey programs have consistently pushed the state of the art. As geophysical baseline accuracy requirements have approached the sub centimeter level, new time and frequency technologies have been sought.

This paper will describe the early Global Positioning Satellite (GPS) time transfer receiver development. The GPS receiver development program at the Naval Research Laboratory for NASA was the forerunner of many commercial efforts which have led to unitized construction and firmware controlled receivers. Along with the GPS receiver development, NASA worked with other U.S. and international timing organizations to develop strategies to optimize the use of these receivers by forming a global timing network for geophysical measurements. Through the use of "common look" techniques a laser tracking site may observe a GPS satellite simultaneously with the data reduction center which is in turn synchronized to UTC via USNO. Using this common look technique, orbital & spacecraft clock systematic errors may be minimized.

With a need for greater synchronization accuracy also grew the need for improved short term frequency stabilities. In the past, where less accurate geodetic measurements were being performed, much of the low level phase noise and frequency instabilities were seen as random processes. Recent investigation has shown that many of these frequency instabilities have systematic signatures which contribute to measurement error. To meet the sub centimeter accuracy goal of the Crustal Dynamics Program the need for picosecond short term stabilities in generation, distribution and monitoring systems is becoming a necessity. System options are described which will allow a spectrally pure crystal oscillator (better than 2 picoseconds over a 50 millisecond interval) to be frequency locked and steered to epoch time accuracies of 100 nanoseconds via the GPS system.

Prior to the inception of the Goddard Laser Tracking Network (GLTN) ten years ago, NASA required that satellite support stations be synchronized within  $\pm 25$  microseconds. The GLTN need for  $\pm 1$  microsecond world-wide time synchronization required the development of new methods for maintaining time synchronization.

Recognizing that conventional means of timekeeping using LORAN-C, HF and VLF could not practically achieve the required  $\pm 1$  microsecond global clock synchronization, the cesium portable clock was used to provide time synchronization. Periodic portable clock trips were made to each station to determine the station's nominal LORAN-C value. Each station's cesium clock offset from U.S. Naval Observatory (USNO) time was plotted from daily LORAN-C values, time steps were calculated to synchronize station time to USNO time, and the station was directed to make the proper equipment adjustments to achieve the recommended time step.

With the improvement of laser equipment and the demand for more accurate ranging, the need for sub-microsecond timing has become a valid requirement.

This need prompted investigation and development of satellite timing receivers in a combined effort between the Naval Research Laboratory and NASA.

The Navigational Technology Satellite receiver was developed as a forerunner to the GPS Time Transfer Receiver now being used for sub-microsecond time transfer.

## GPS TIMING

Techniques are being developed to utilize GPS timing for the GLTN, with a goal of world-wide time synchronization to the greatest feasible accuracy.

To utilize the time transfer capability of the GPS, a timing receiver was developed by the Naval Research Laboratory (NRL) for NASA, was tested at field sites, and was used in time transfer experiments (References 1 and 2). The first commercial GPS time transfer receiver was built by Stanford Telecommunications Incorporated (STI). This receiver was evaluated for possible use in the GLTN. The STI and the NRL receivers are operated from a keyboard similar to that of a personal computer. The cost of the STI receiver was approximately one half that of the NRL receiver and it was more suitable for mobile installations. More recently a third receiver, the Frequency and Time Systems (FTS) Model 8400 was evaluated and found to be the best suited for GLTN operations because of its smaller size, unit construction and lower cost.

Figures 1 and 2 compare time transfer data obtained with an FTS 8400 GPS receiver or the identical Trimble 5000A and a cesium portable clock at several timing installations. Portable clock time was compared to USNO time before and after these trips. The measurements were supplemented by TV Line 10 measurements which were accurate to +/- 50 nanoseconds with respect to USNO.

Figure 3 lists current deployments of FTS 8400 GPS timing receivers in the GLTN.

## GLTN GPS DATA COLLECTION

GPS time position measurements are made daily at the GLTN stations. The stations collect GPS data twice a day for each visible satellite. The raw time position reading is recorded during the 10-minute satellite observation pass. This data point along with the date, time, and satellite vehicle number are recorded for each measurement. The measurement data are transmitted to the NASA Communications Center in the daily Laser Operations Report (LOR). Also transmitted in the LOR is information concerning station time steps, frequency changes, power outages, equipment problems, etc.

## AUTOMATED TIME POSITION SYSTEM (ATPS)

The Automated Time Position System is the means by which station time is monitored and analyzed for the GLTN. The ATPS

- o provides daily time position determination
- o calculates long term cesium frequency drift
- o predicts the date the station tolerances exceed 1 microsecond
- o evaluates the validity of data and data analysis methods

The System includes several computer programs that (1) read the LOR data into the ATPS data bases, (2) permit the manual entry, editing, deletion, and listing of data files and (3) perform the analysis of the timing measurements. The system is coded in FORTRAN and runs on a VAX computer

cluster. The cluster consists of two VAX-11/780 computers and one VAX 8600 computer. The analysis program is operator inactive and produces a printed data output. The data output consists of the source listing data from the data files used in the analysis, a least-squares calculation of the original source data, and a line printer graph of the original and least-squares data plot.

#### GPS COMMON VIEW

Utilizing the GPS common view technique described in Reference 3, orbital and spacecraft clock systematic errors can be minimized.

A common view/near common view GPS time transfer experiment was conducted in 1983 to determine the accuracy of GPS time transfer receivers for the GLTN (Reference 4). The experiment was conducted between the Bureau International de l'Heure (BIH), Paris, France, the Institute Fur Angewandte Geodasie (IFAG), Wettzel, Germany and the GLTN data reduction center at Columbia, Maryland. The local time bases incorporated HP5061 (Option 004) Cesium standards or hydrogen masers. Results of the experiment showed the overall accuracy to be consistently better than 100 nanoseconds. Recent improvements in the GPS system have permitted common view accuracies approaching 10 to 20 nanoseconds. (Reference 5).

Efforts are underway to utilize GPS common view techniques on a day-to-day operational basis in the GLTN (Figure 4).

## TIME INTERVAL MEASUREMENT ERRORS

The GLTN utilizes Hewlett Packard 5370 time interval counters with an atomic standard for the time base. The 5370 has a 20 picosecond single shot resolution, however, the accuracy is typically +/- 40 picoseconds. The accuracy of the time interval measurement is influenced by the summation of:

- o trigger level
- o input signal noise
- o interval timing jitter
- o time base short term stability

Event timers developed by the University of Maryland and by the Division of National Mapping (Australia) reduce the internal timing jitter and improve the short term stability. The University of Maryland unit uses a 200 MHz oscillator phase locked to the atomic standard.

## IMPROVEMENTS IN SHORT TERM STABILITY

Improved short term stability oscillators that can be steered to UTC via the GPS are being developed.

Austron, Inc. and the GLTN are developing a low noise disciplined frequency standard (Reference 6) that utilizes a microprocessor controlled system which automatically locks the frequency of a precision BVA crystal oscillator to an atomic standard having superior long term stability.



With the use of a third-order servo technique, the instrument is able to correct the frequency offset and aging of the internal BVA oscillator. If the frequency of the atomic standard is altered (due to loss of lock, loss of signal or failure) the unit will continue to apply corrections to the internal BVA oscillator. These corrections are calculated from data accumulated while the atomic standard is stable. These corrections are automatic and do not disturb the phase. This technique minimizes the effect of aging of the BVA oscillator and holds the unit to within +/- 3 parts in  $10^{12}$  per day.

The short term stability (50 milliseconds to 100 seconds) of the low noise disciplined frequency standard is represented in Figure 5. The internal BVA oscillator has a short term stability  $\sigma$  ( $\tau = 0.2$  to 30 seconds)  $\approx 5 \times 10^{-13}$  and an aging rate of  $1 \times 10^{-11}$  per day. Frequency steering of the low noise disciplined oscillator by the atomic standard to epoch time accuracies of 100 nanoseconds via the GPS system can be achieved.

#### REFERENCES

1. J. Oaks, J. Buisson, C. Wardrip, "GPS Time Transfer Receivers for the NASA Transportable Laser Ranging Network", NASA/GSFC x-814-82-6, April, 1982.
2. J. Oaks, A. Franks, S. Falvey, M. Lister, J. Buisson, S. Wardrip and H. Warren, "Prototype Design and Initial Test Evaluation of a GPS Time Transfer Receiver", NRL report 8608, July 27, 1982.
3. D. W. Allan and M. A. Weiss, "Accurate Time and Frequency Transfer during Common-View of a GPS Satellite", Proceedings of 34th Annual Frequency Control Symposium, 1980.
4. C. Wardrip, J. Buisson, J. Oaks, et al., "An International Time Transfer Experiment", Proceedings of the 37th Annual Frequency Control Symposium, 1983.
5. M. A. Weiss, "Weighting and Smoothing of Data in GPS Common View Time Transfer", Proceedings of the 17th Annual Precise Time and Time Interval Applications and Planning Meeting, 1985.
6. B. Bourke and B. Penrod, "An Analysis of a Microprocessor Controlled Disciplined Frequency Standard", Proceedings of the 37th Annual Frequency Control Symposium, 1983.

<u>FEB 5 1985</u>	<u>MOBLAS 1 TAHITI</u>	<u>GPS SV</u>	<u>PC VS USNO USING GPS</u>	<u>PC VS USNO CALCULATED</u>	<u>(GPS-USNO)-(PC-USNO)</u>
		06	2.003	1.991	+0.012 *
		08	1.996	1.991	+0.005
		09	2.009	1.991	+0.018
		11	2.012	1.991	+0.021
		13	1.999	1.994	+0.005
		12	1.995	1.997	-0.002

ALL VALUES IN MICROSECONDS

TIMES VERIFIED BY PORTABLE CLOCK CLOSURES WITH USNO.

\*  $\pm 200$  NANoseconds DUE TO SATELLITE AND PORTABLE CLOCK ERRORS.

FIGURE 1 - GPS VS PORTABLE CLOCK TIME TRANSFER.

<u>DATE</u>	<u>LOCATION</u>	<u>(PC VS USNO) USING GPS</u>	<u>(PC VS USNO) CALCULATED</u>	<u>(GPS-USNO) - (PC-USNO)</u>
FEB 12 1985	CSIRO, AUSTRALIA	2.087	1.989	0.098 *
FEB 13 1985	NATMAP, AUSTRALIA	2.050	2.030	0.020
FEB 14 1985	TIDBINBILLA, AUSTRALIA	2.160	2.068	0.092
FEB 16 1985	MOBLAS 5, AUSTRALIA	2.243	2.159	0.084
FEB 19 1985	TELCOM, AUSTRALIA	2.262	2.262	0.000
FEB 20 1985	CSIRO, AUSTRALIA	2.275	2.296	-0.021
FEB 22 1985	HOLLAS, HAWAII	2.395	2.406	-0.011

ALL VALUES IN MICROSECONDS

USNO CLOSURE ON FEB 8 AND FEB 27, 1985

\* ±200 NANoseconds DUE TO SATELLITE AND PORTABLE CLOCK ERRORS.

FIGURE 2 - GPS VS PORTABLE CLOCK TIME TRANSFER

<u>STATION</u>	<u>DATE OF INSTALLATION</u>
MOBLAS-2 ISRAEL	SEPTEMBER 85
MOBLAS-5 WESTERN AUSTRALIA	OCTOBER 85
MOBLAS-6 MEXICO	MAY 86
HOLLAS HAWAII	APRIL 86
SAO-2 PERU	AUGUST 86
NATMAP AUSTRALIA	OCTOBER 85
MLRS TEXAS	JUNE 86
TLRS-1 GORF	NOVEMBER 85
TLRS-2 GORF	NOVEMBER 85
MATERA	NOVEMBER 86 (PROPOSED)

FIGURE 3 - DEPLOYMENT OF FTS-8400 GPS TIME TRANSFER MONITORS

# FREQUENCY COMPARISON OF VARIOUS STANDARDS

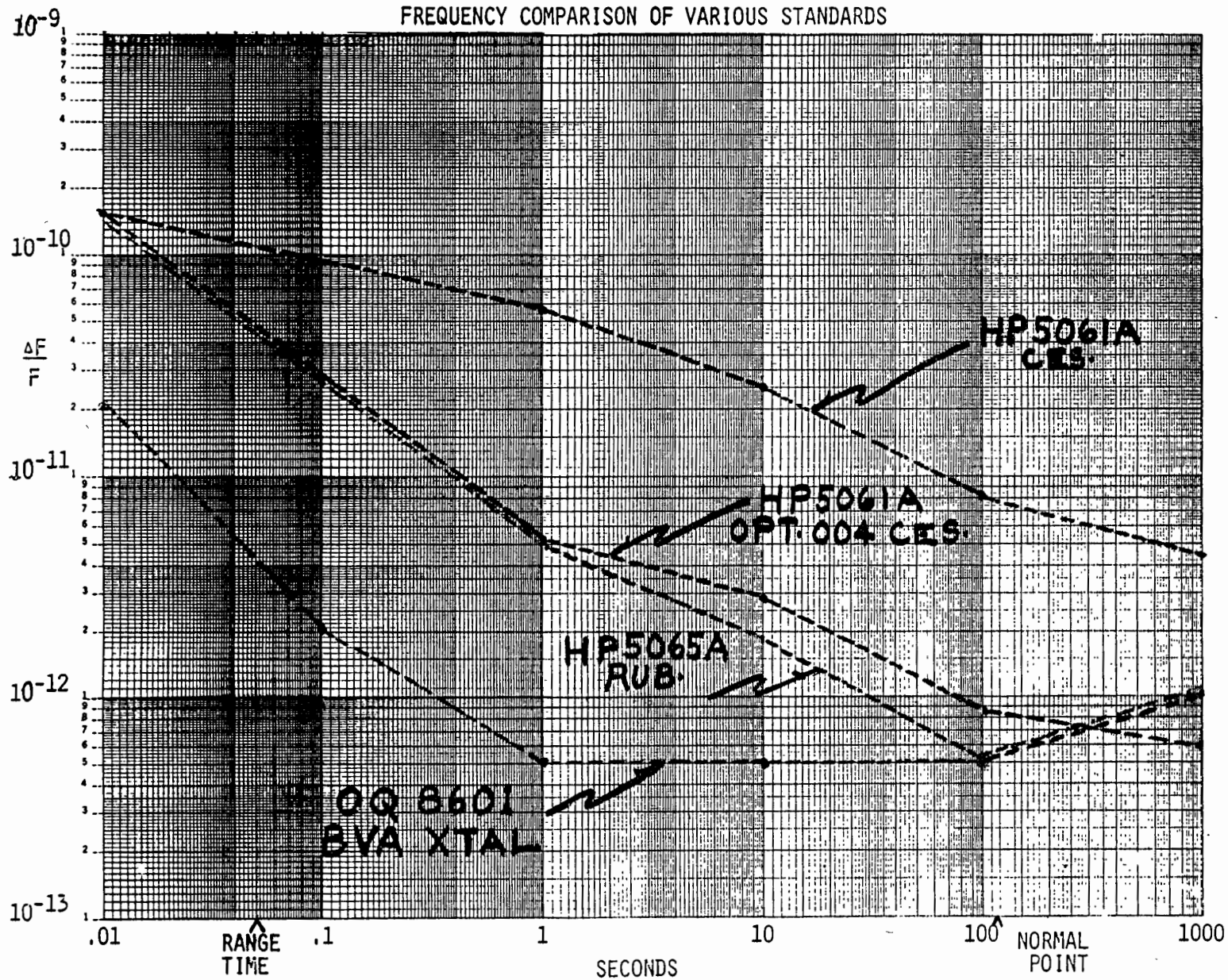
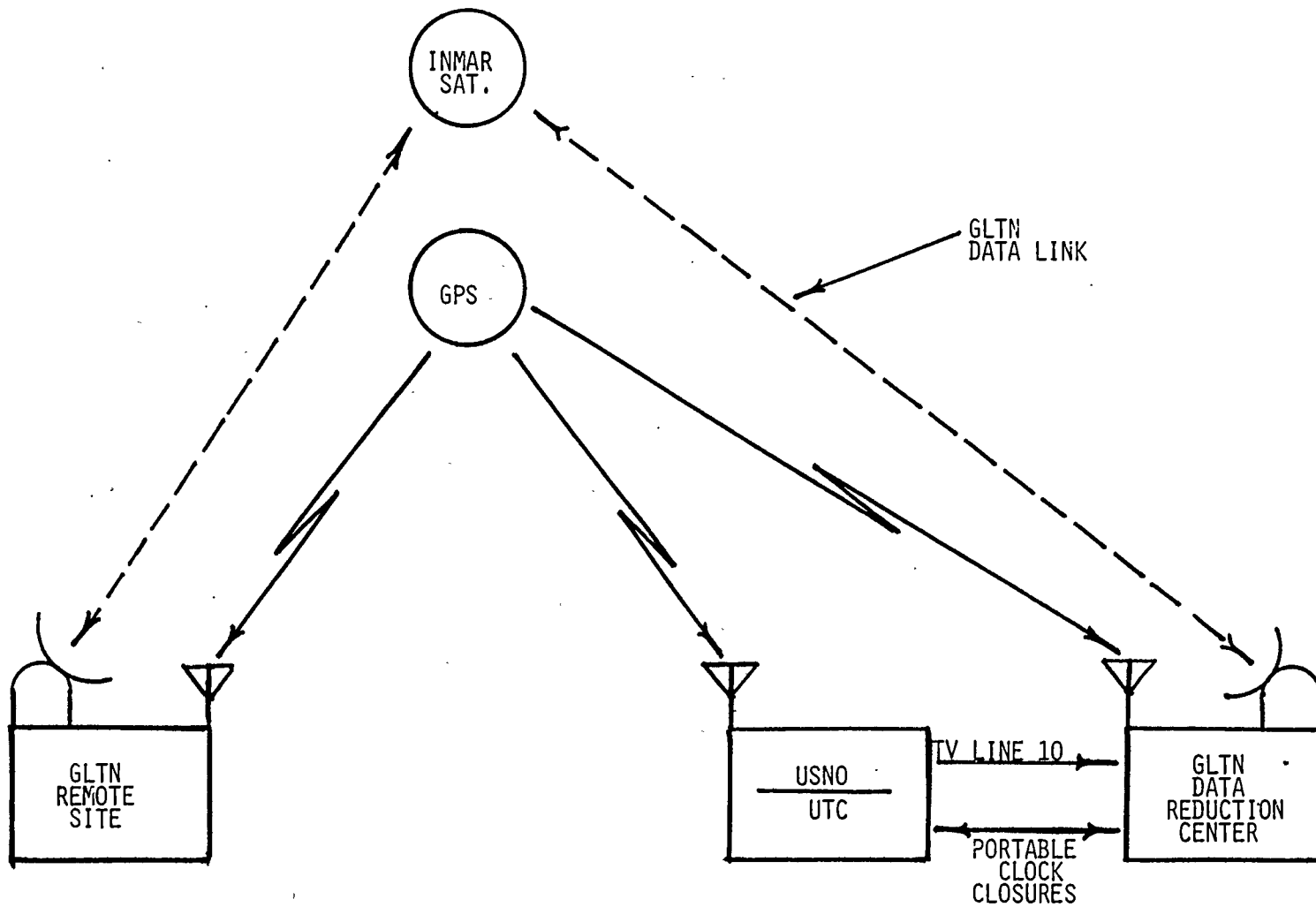


FIGURE 5

FIGURE 4



GPS "COMMON LOOK" &  
GLTN DATA TRANSFER METHODS

Prior to the inception of the Goddard Laser Tracking Network (GLTN) ten years ago, NASA required that satellite support stations be synchronized within  $\pm 25$  microseconds. The GLTN need for  $\pm 1$  microsecond world-wide time synchronization required the development of new methods for maintaining time synchronization.

Recognizing that conventional means of timekeeping using LORAN-C, HF and VLF could not practically achieve the required  $\pm 1$  microsecond global clock synchronization, the cesium portable clock was used to provide time synchronization. Periodic portable clock trips were made to each station to determine the station's nominal LORAN-C value. Each station's cesium clock offset from U.S. Naval Observatory (USNO) time was plotted from daily LORAN-C values, time steps were calculated to synchronize station time to USNO time, and the station was directed to make the proper equipment adjustments to achieve the recommended time step.

With the improvement of laser equipment and the demand for more accurate ranging, the need for sub-microsecond timing has become a valid requirement.

This need prompted investigation and development of satellite timing receivers in a combined effort between the Naval Research Laboratory and NASA.

The Navigational Technology Satellite receiver was developed as a forerunner to the GPS Time Transfer Receiver now being used for sub-microsecond time transfer.

#### GPS TIMING

Techniques are being developed to utilize GPS timing for the GLTN, with a goal of world-wide time synchronization to the greatest feasible accuracy.

To utilize the time transfer capability of the GPS, a timing receiver was developed by the Naval Research Laboratory (NRL) for NASA, was tested at field sites, and was used in time transfer experiments (References 1 and 2). The first commercial GPS time transfer receiver was built by Stanford Telecommunications Incorporated (STI). This receiver was evaluated for possible use in the GLTN. The STI and the NRL receivers are operated from a keyboard similar to that of a personal computer. The cost of the STI receiver was approximately one half that of the NRL receiver and it was more suitable for mobile installations. More recently a third receiver, the Frequency and Time Systems (FTS) Model 8400 was evaluated and found to be the best suited for GLTN operations because of its smaller size, unit construction and lower cost.

Figures 1 and 2 compare time transfer data obtained with an FTS 8400 GPS receiver or the identical Trimble 5000A and a cesium portable clock at several timing installations. Portable clock time was compared to USNO time before and after these trips. The measurements were supplemented by TV Line 10 measurements which were accurate to  $\pm 50$  nanoseconds with respect to USNO.

Figure 3 lists current deployments of FTS 8400 GPS timing receivers in the GLTN.



## GLTN GPS DATA COLLECTION

GPS time position measurements are made daily at the GLTN stations. The stations collect GPS data twice a day for each visible satellite. The raw time position reading is recorded during the 10-minute satellite observation pass. This data point along with the date, time, and satellite vehicle number are recorded for each measurement. The measurement data are transmitted to the NASA Communications Center in the daily Laser Operations Report (LOR). Also transmitted in the LOR is information concerning station time steps, frequency changes, power outages, equipment problems, etc.

## AUTOMATED TIME POSITION SYSTEM (ATPS)

The Automated Time Position System is the means by which station time is monitored and analyzed for the GLTN. The ATPS

- o provides daily time position determination
- o calculates long term cesium frequency drift
- o predicts the date the station tolerances exceed 1 microsecond
- o evaluates the validity of data and data analysis methods

The System includes several computer programs that (1) read the LOR data into the ATPS data bases, (2) permit the manual entry, editing, deletion, and listing of data files and (3) perform the analysis of the timing measurements. The system is coded in FORTRAN and runs on a VAX computer cluster. The cluster consists of two VAX-11/780 computers and one VAX 8600 computer. The analysis program is operator inactive and produces a printed data output. The data output consists of the source listing data from the data files used in the analysis, a least-squares calculation of the original source data, and a line printer graph of the original and least-squares data plot.

## GPS COMMON VIEW

Utilizing the GPS common view technique described in Reference 3, orbital and spacecraft clock systematic errors can be minimized.

A common view/near common view GPS time transfer experiment was conducted in 1983 to determine the accuracy of GPS time transfer receivers for the GLTN (Reference 4). The experiment was conducted between the Bureau International de l'Heure (BIH), Paris, France, the Institute Fur Angewandte Geodasie (IFAG), Wettzel, Germany and the GLTN data reduction center at Columbia, Maryland. The local time bases incorporated HP5061 (Option 004) Cesium standards or hydrogen masers. Results of the experiment showed the overall accuracy to be consistently better than 100 nanoseconds. Recent improvements in the GPS system have permitted common view accuracies approaching 10 to 20 nanoseconds. (Reference 5).

Efforts are underway to utilize GPS common view techniques on a day-to-day operational basis in the GLTN (Figure 4).

## TIME INTERVAL MEASUREMENT ERRORS

The GLTN utilizes Hewlett Packard 5370 time interval counters with an atomic standard for the time base. The 5370 has a 20 picosecond single shot resolution, however, the accuracy is typically +/- 40 picoseconds. The accuracy of the time interval measurement is influenced by the summation of:

- o trigger level
- o input signal noise
- o interval timing jitter
- o time base short term stability

Event timers developed by the University of Maryland and by the Division of National Mapping (Australia) reduce the internal timing jitter and improve the short term stability. The University of Maryland unit uses a 200 MHZ oscillator phase locked to the atomic standard.

## IMPROVEMENTS IN SHORT TERM STABILITY

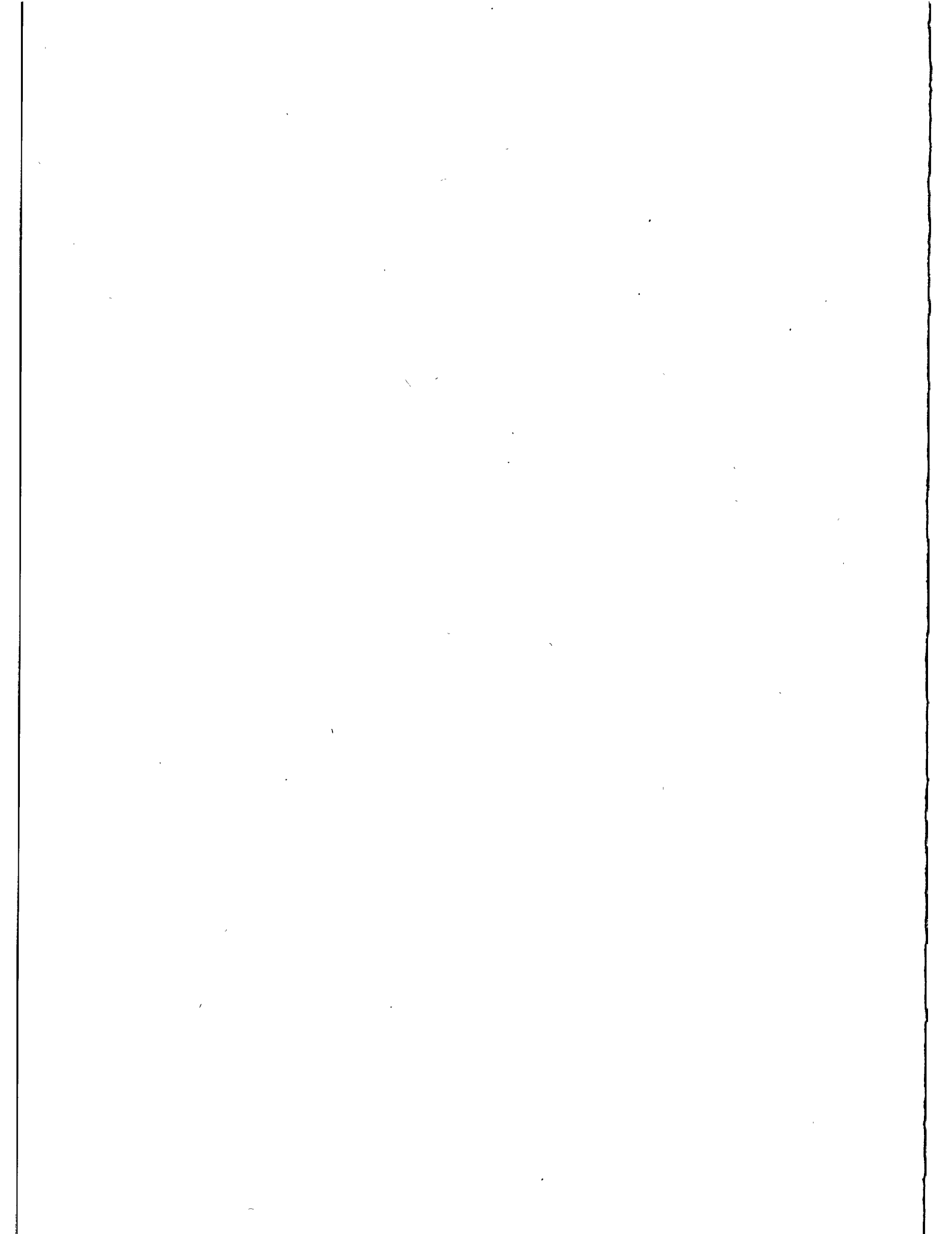
Improved short term stability oscillators that can be steered to UTC via the GPS are being developed.

Austron, Inc. and the GLTN are developing a low noise disciplined frequency standard (Reference 6) that utilizes a microprocessor controlled system which automatically locks the frequency of a precision BVA crystal oscillator to an atomic standard having superior long term stability. With the use of a third-order servo technique, the instrument is able to correct the frequency offset and aging of the internal BVA oscillator. If the frequency of the atomic standard is altered (due to loss of lock, loss of signal or failure) the unit will continue to apply corrections to the internal BVA oscillator. These corrections are calculated from data accumulated while the atomic standard is stable. These corrections are automatic and do not disturb the phase. This technique minimizes the effect of aging of the BVA oscillator and holds the unit to within +/- 3 parts in  $10^{12}$  per day.

The short term stability (50 milliseconds to 100 seconds) of the low noise disciplined frequency standard is represented in Figure 5. The internal BVA oscillator has a short term stability  $\sigma$  ( $\tau = 0.2$  to 30 seconds)  $\cong 5 \times 10^{-13}$  and an aging rate of  $1 \times 10^{-11}$  per day. Frequency steering of the low noise disciplined oscillator by the atomic standard to epoch time accuracies of 100 nanoseconds via the GPS system can be achieved.

#### REFERENCES

1. J. Oaks, J. Buisson, C. Wardrip, "GPS Time Transfer Receivers for the NASA Transportable Laser Ranging Network", NASA/GSFC x-814-82-6, April, 1982.
2. J. Oaks, A. Franks, S. Falvey, M. Lister, J. Buisson, S. Wardrip and H. Warren, "Prototype Design and Initial Test Evaluation of a GPS Time Transfer Receiver", NRL report 8608, July 27, 1982.
3. D. W. Allan and M. A. Weiss, "Accurate Time and Frequency Transfer during Common-View of a GPS Satellite", Proceedings of 34th Annual Frequency Control Symposium, 1980.
4. C. Wardrip, J. Buisson, J. Oaks, et al., "An International Time Transfer Experiment", Proceedings of the 37th Annual Frequency Control Symposium, 1983.
5. M. A. Weiss, "Weighting and Smoothing of Data in GPS Common View Time Transfer", Proceedings of the 17th Annual Precise Time and Time Interval Applications and Planning Meeting, 1985.
6. B. Bourke and B. Penrod, "An Analysis of a Microprocessor Controlled Disciplined Frequency Standard", Proceedings of the 37th Annual Frequency Control Symposium, 1983.



## THE DEVELOPMENT OF A DUAL FREQUENCY EVENT TIMER

C.A. Steggerda  
Department of Physics and Astronomy  
University of Maryland  
College Park, Maryland 20742

Telephone (301) 454 3406  
Telex 908787

### ABSTRACT

The fundamental concepts and equations of the Event Timer are discussed. The evolution of the Event Timer since the Herstmonceux conference and the specifications are stated. New circuits are described which reduce the RMS jitter to the range of 15 picoseconds. Under ideal conditions, over a period of one hour, the stability and the RMS variation of 1000 point mean points is in the order of one picosecond. Plans for a 5 picosecond resolution Timer are presented.

## INTRODUCTION

About five years ago I started developing an Event Timer or chronograph, using the dual frequency vernier system. Described two years ago at the Herstmonceux conference, the Event Timer is near completion and I hope to have at least two Timers built by the end of this year. One of the Event Timers will go to the Yunnan Observatory of the Peoples Republic of China when Mr. Wang Ben-Chun returns to China. Others will be used by Dr. Alley for time synchronization experiments and satellite and lunar ranging.

This paper is organized into three parts. The first part is a description of the fundamental concepts and the equations of the Event Timer. The second part describes the specifications and describes how the Event Timer has evolved since the Herstmonceux conference. The third part concerns the measurement of jitter and a new circuit which improves the jitter characteristics. Final concluding remarks describe a possible new next Event Timer.

## Part 1      Fundamental Concepts of the Event Timer

Figure 1 shows the essence of the dual frequency Event Timer concept. One of the dual frequencies,  $F_1$ , is produced by a 200 MHz tunable crystal oscillator which is synchronized to a 5 or 10 MHz standard. The 200 MHz oscillator runs continuously to drive a 26 bit synchronous counter which is the time generator. The time generator has exactly 50,000,000 states so it repeats every  $\frac{1}{4}$  second.

The second of the dual frequencies,  $F_2$ , is produced by a delay line oscillator which is tuned by other circuits to operate at 199.2217899 MHz called 199\* MHz.  $F_1$  and  $F_2$  come into synchronization every 257 cycles of  $F_1$  and 256 cycles of  $F_2$ .  $F_2$  is derived from  $F_1$  by the equation  $F_1 - F_2 = F_2/256$ .

An event, either from the test circuit or an outside source, stops, then restarts the 199\* MHz restartable oscillator to drive a 9 bit counter called the A register. Constantly monitoring the two frequencies is a comparator which reacts to the rising edges of  $F_2$  and transitions in state of  $F_1$ . The result of this operation is that the comparator reacts to the nearest co-incidence of the rising edges of  $F_1$  and  $F_2$ . When the  $F_1$  and  $F_2$  rising edges are in closest synchronization, the comparator gives a Sync. pulse which latches or stores the state of the 26 bit time generator and stops the 9 bit A counter.

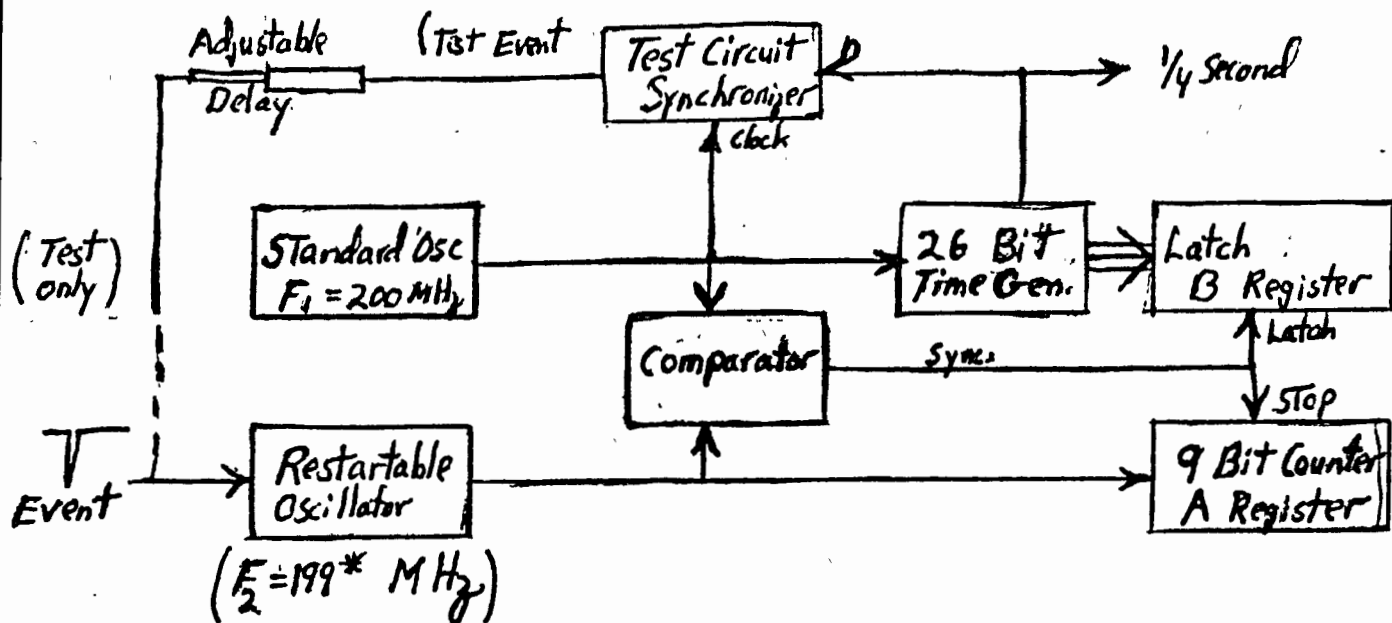
From the contents of the A and B registers, the epoch of the event can be computed within a  $\frac{1}{4}$  second interval. The epoch of the event is = Time of Sync. (represented by the number latched in the B register) - the A register count times 5.01953125 n.s.. (5.01953125 n.s. is the period of 199\* MHz.)

The vernier action occurs because the period of  $F_1$  and  $F_2$  differ by 19.53125 p.s.. Using the test circuit, which produces an event synchronized to the 200 MHz standard every  $\frac{1}{4}$  second, we find that A and B repeat every  $\frac{1}{4}$  second. In figure 2, if the event is delayed by 19.53125 p.s., the Sync condition occurs one cycle sooner, A and B are both decreased by 1.

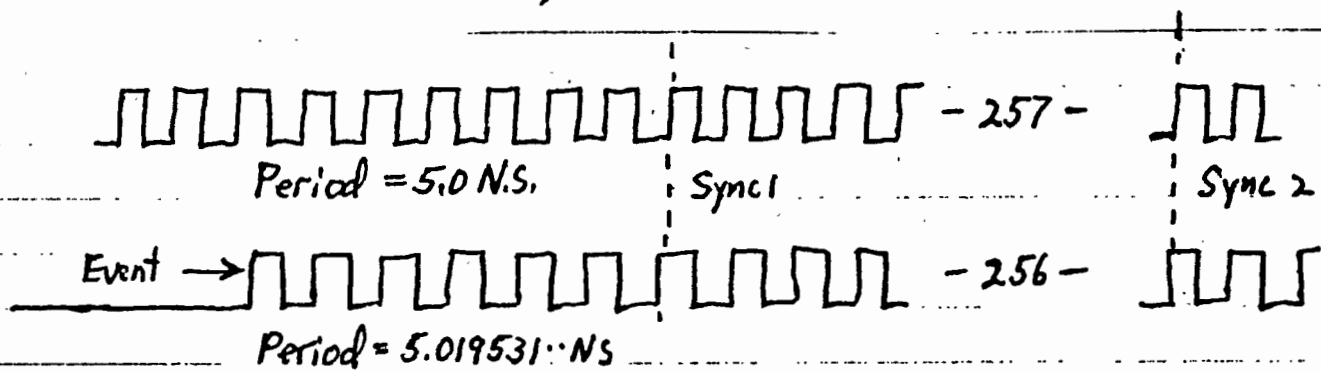
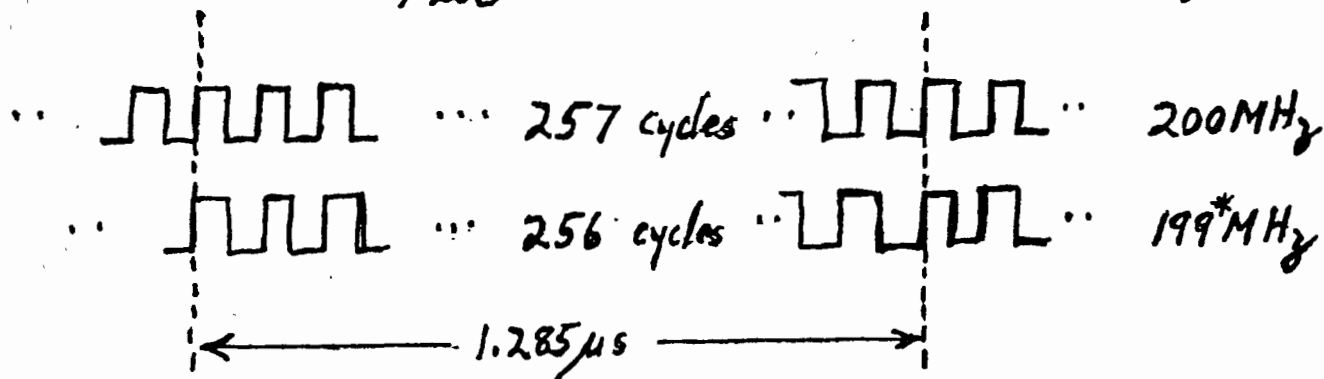
The equation Epoch =  $(B-A)(5.0 - A(19.531 \times 10^{-3})$  n.s.  
and Epoch' =  $[(B-1)-(A-1)] 5.0 - (A-1)(19.531 \times 10^{-3})$  n.s.  
give Epoch' = Epoch + 19.53125 p.s.

# Fundamental Concepts of the Event Timer

Figure 1



$$F_1 - F_2 = F_2 / 256 \quad \therefore \quad F_2 = 199.2217899 \text{ MHz}$$



$$\text{Epoch} = \text{Time at Synchronization} - A (5.01953125) \text{ N.S.}$$

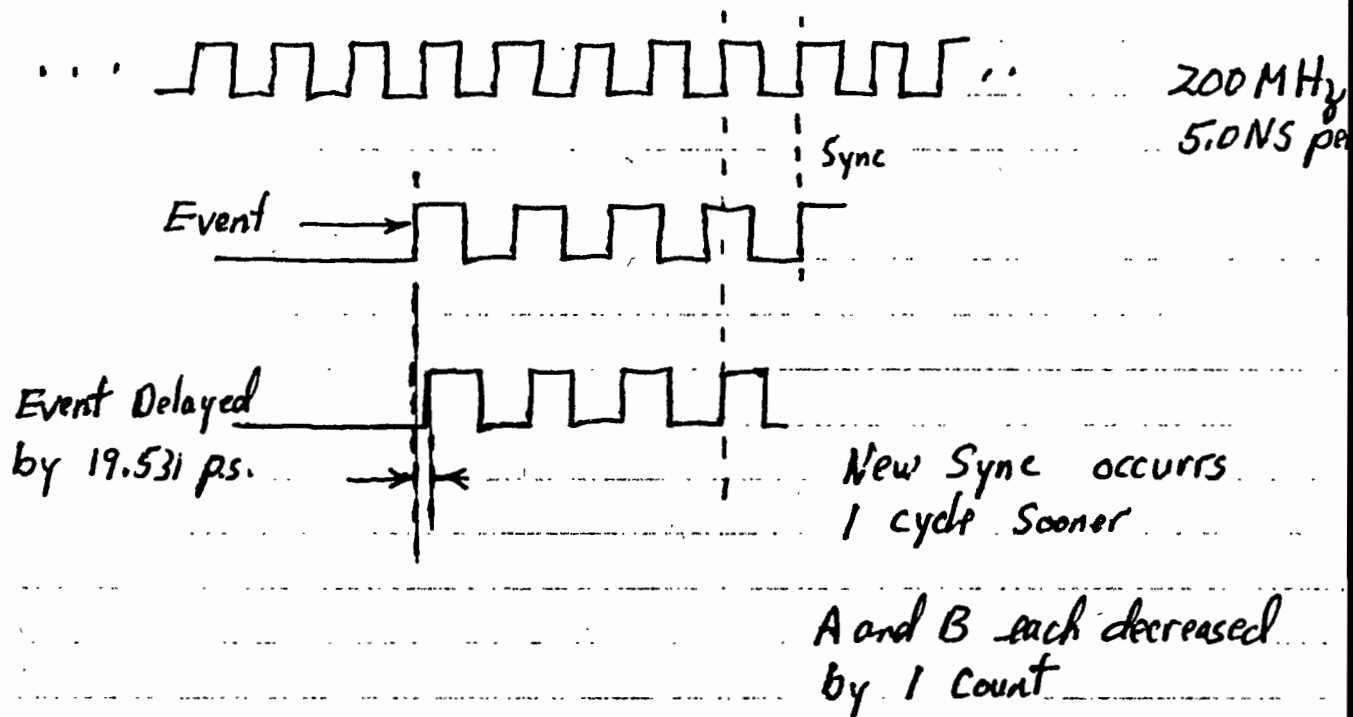
$$\text{Epoch} = B(5.0) - A(5.01953125) \text{ N.S.}$$

$$\text{Epoch} = (B - A)5.0 - A(19.531 \times 10^{-3}) \text{ N.S.}$$



Fundamental Concepts Continued

figure 2



$$\text{Epoch}' = [(B-1) - (A-1)] 5.0 - (A-1)(19.531 \cdot 10^{-3}) \text{ N.S.}$$

$$\text{Epoch}' = (B-A) 5.0 - A(19.531 \cdot 10^{-3}) + 19.531 \cdot 10^{-3} \text{ N.S.}$$

$$\text{Epoch}' = \text{Epoch} + 19.531 \cdot 10^{-3} \text{ N.S.}$$

In General

$$\text{Epoch} = [(B+257N) - (A+256N)] 5.0 - (A+256N)(19.531 \cdot 10^{-3})$$

$$\text{Epoch} = (B-A)(5.0) - A(19.531 \cdot 10^{-3}) + [5.0 - 256(19.53125 \cdot 10^{-3})] N$$

" 0

$$\text{Epoch} = (B-A)(5.0) - A(19.531 \cdot 10^{-3})$$

If we can continue increasing the delay of the test event, the Sync. point will come closer and closer to the event. The actual Event Timer is built such that when A becomes equal to about 15, the first Sync. is ignored whereby the next Sync. point 1.285 u.s. later is used. At this time, the A register jumps 256 counts and the B register jumps 257 counts. In fact, any Sync point can be used to compute epoch. In fact, for the Nth synchronization point

$$\text{Epoch} = [(B + 257N) - (A + 256N)] 5.0 - (A + 256N)(19.531 \times 10^{-3})$$

$$\text{Epoch} = (B - A)5.0 - A(19.531 \times 10^{-3}) + N(5.0 - 256(19.531 \times 10^{-3}))$$

but  $5.0 - 256(19.531 \times 10^{-3}) = 0$

$$\text{Epoch} = (B - A)5.0 - A(19.531 \times 10^{-3}) \quad \text{n.s.}$$

Thus the epoch of the test pulse may be moved about in the 1/4 second interval. Either the first or second Sync. point is used to generate A and B from which the epoch can be computed.

## Part 2

## Block Diagram and Specifications

Figure 2 shows a partial block diagram of the Event Timer. This diagram is useful primarily to show input and output functions.

The Event Timer has been expanded to have two independent verniers. It is thus possible to measure the epoch of two events up to and including co-incidence. Each event can arrive on its own cable, or, the events may be combined to feed both verniers in which case the first vernier arms the second.

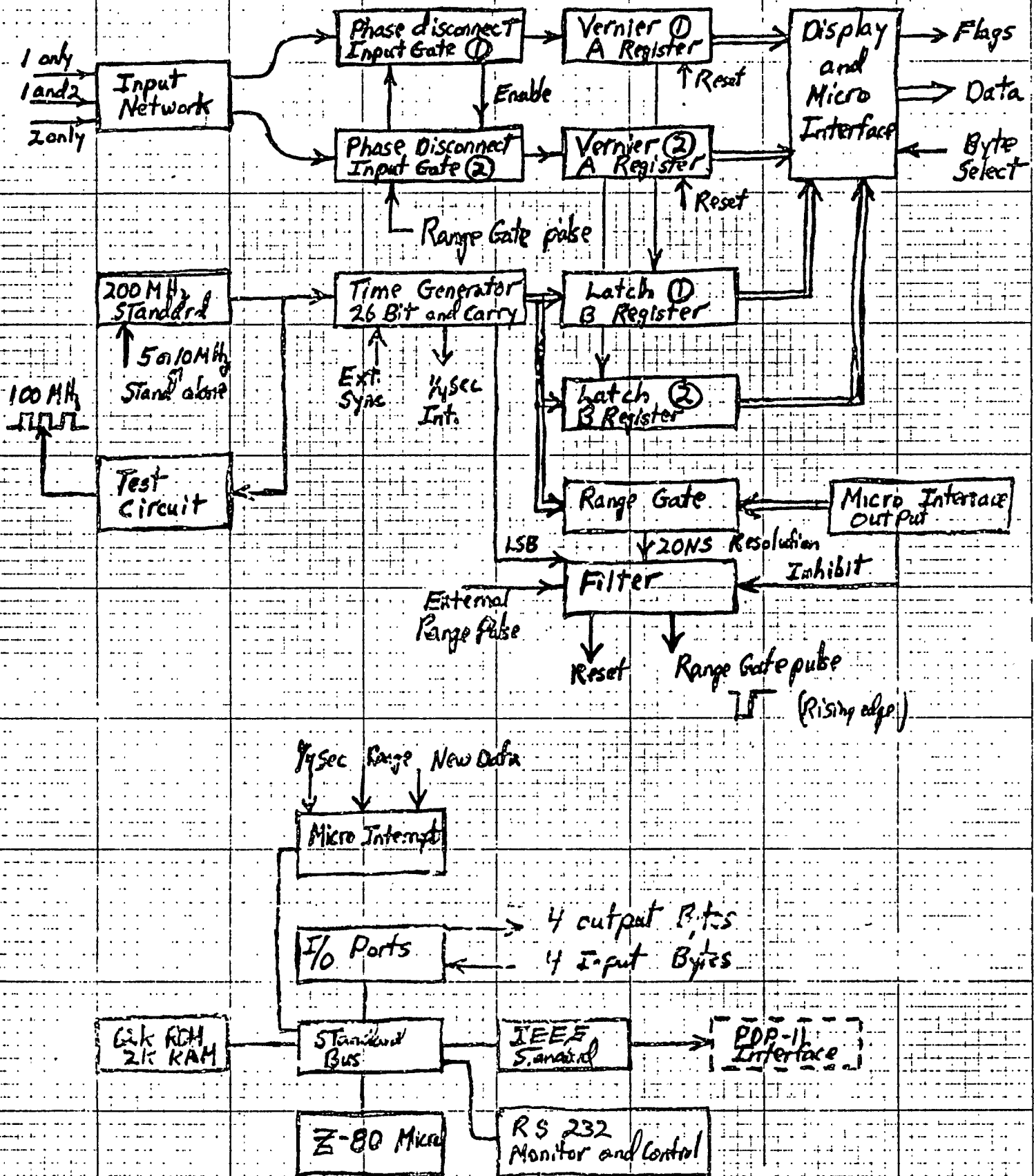
There are three inputs, each terminated in 50 ohms. In one mode, input 1 drives vernier 1 only, and input 2 drives vernier 2 only. In the second mode, input 3 drives both verniers. The input networks accept negative NIM type pulses going from an initial value of 0 volts to an amplitude of  $-.5$  to  $-1.0$  volts. Verniers respond to leading edges, so the pulses may be any width greater than 1 n.s..

The 200 MHz standard is a  $66.66\cdots$  Mhz voltage controlled crystal oscillator with a times 3 multiplier and a very narrow band filter. The oscillator is phase locked to either 5 or 10 Mhz standards, or, the oscillator may be operated without a standard at a frequency very close to 200 Mhz..

The time generator consists of a 24 bit synchronous counter and two  $\div 2$  prescalers adjusted so that the rising edges of all bits are synchronous. A 27th bit carry is provided to prevent ambiguity problems if events occur near the  $1/4$  second point. The 26 bits and 27th bit carry are supplied to latches 1 and 2. The 24 bit synchronous counter number is compared with a 24 bit number supplied by the microprocessor to form a range gate to enable the Event Timer. The output of the comparator is filtered by a glitch suppressor to form both a reset pulse for the A registers and a rising edge to enable the input gate portions of the phase disconnect circuits. The microprocessor supplies an inhibit pulse to the glitch suppressor to prevent false range gate pulses while the numbers are being updated in the comparator. The range gate may be opened on the next 20 n.s. clock pulse following an external NIM type pulse.

Partial Block Diagram of Event Timer

figure 3



The phase disconnect circuit ① is enabled by the trailing edge of the range gate pulse. Phase disconnect circuit ② is enabled by either the same range gate pulse if the verniers are to be enabled simultaneously, or, phase disconnect circuit ② may be enabled when circuit ① has received an event to allow operation in the serial mode.

The outputs from the A and B registers are displayed with LED readouts and are stored in two 40 bit storage registers. The Z-80 microprocessor receives program interrupts when new data is available, when the range gate goes off, and when the 1/4 second pulses are generated from the time generator. The microprocessor reads in the data one byte at a time and can tell how much data is available by reading data status flags. Because the A and B registers act as storage registers along with the two 40 bit storage registers of the interface, it is possible to store four epochs, two from each vernier before the data must be read out. This feature provides for very rapid acquisition of data for very close targets.

The micro computer has 62K of ROM and 2K of RAM. The system operates the IEEE bus and RS-232 type monitors. Programs have been developed in FORTH language to calculate epoch and time of day and various tests for the Event Timer.

The Event Timer in conjunction with the Z-80 can give range data to the mainframe system computer at a rate of 172 ranges per second or every 5.8 milliseconds. However, the Event Timer can operate by itself every 7 microseconds or at a rate exceeding 100,000 ranges per second for each vernier.

Through the kindness of Messieurs Dachel and Ingold of the Bendix Corporation, the Allen Variance and the harmonic content of the 200 MHz standard were measured. Jeff Ingold's report is shown in figure 4.

CHARLES A. STEGGERDA

figure 4

9-4-86

200 MHz PHASE LOCKED OSCILLATOR

VECTRON S/N 628441 PHASE LOCKED TO NP 2 VS NP 4

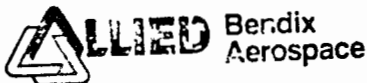
TAU	ALLAN VARIANCE ( $\sigma_y^2$ )	FLOOR
0.1 second	1.00 E-11      500 samples	6.49 E-12
1.0	2.39 E-12      500	8.43 E-13
10	2.08 E-13      100	1.00 E-13
100	3.30 E-14      5	1.53 E-14

#### HARMONICS

2<sup>ND</sup> (400 MHz) > 56 dB down from CARRIER  
3<sup>RD</sup> (600 MHz) > 60 dB down from CARRIER  
4<sup>TH</sup> (800 MHz) > 60 dB down from CARRIER

SUB HARMONICS & SPURIOUS RESPONSE

> 70 dB down from CARRIER



9-4-86

JEFF INGOLD

964-7188

### Part 3      Jitter Measurements and a New Phase Disconnect Circuit

Consider again the basic block diagram of figure 1. If an event is generated precisely every  $1/4$  second and this event is synchronized to the 200 MHz standard, then the A counter and B latch will repeat the same numbers every  $1/4$  second. This in fact does happen, the same epoch being calculated for 10 to 20 minutes at a time with no jitter.

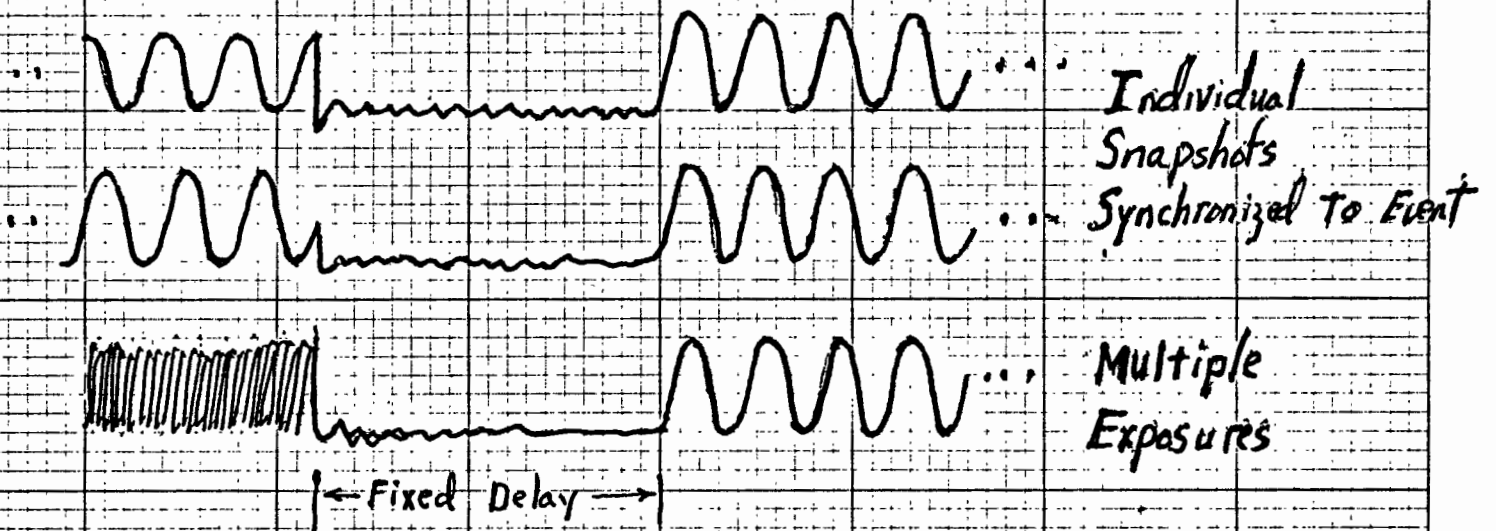
This test mode is not however the way the Event Timer is to be used. In operation the range gate operates 10 to 100 times a second in varying patterns according to the laser firing and the expected return time. A more valid test would replace the  $1/4$  second period pulse with a pulse from an ordinary free running pulse generator running at 30 pps.. In this mode an event is generated that is synchronized to the 200 MHz standard but comes at a random time in the  $1/4$  second interval. In this mode the A counter value should be constant and the B latch value should constantly change. The Event Timer of 6 months ago however had a jitter of up to 8 counts on the A counter when the range gate was moved randomly yet the A count was very stable if the range gate was opened at precise intervals as generated by the time generator. Measurement of the interpolator assembly of the Hewlett Packard 5370 universal counter revealed the same problem, which is understandable since the Event Timer verniers are directly related to H.P. interpolators.

It appears that an improvement can be made in the system jitter if  $F_2$ , the 199\* MHz oscillator, is stopped and restarted in a controlled manner. In the original fixed delay phase disconnect circuit, a 10 n.s. pulse synchronized to the event to be measured, stops and restarts  $F_2$ . Before this synchronization process, the event is in no way synchronized to  $F_2$ , and so the oscillator is stopped at any point in its cycle as shown in figure 5. When the oscillator is restarted, the initial conditions vary depending on what part of the cycle the oscillator was stopped. The changing initial conditions cause a phase jitter in  $F_2$  relative to the event which then is measured as a system jitter.

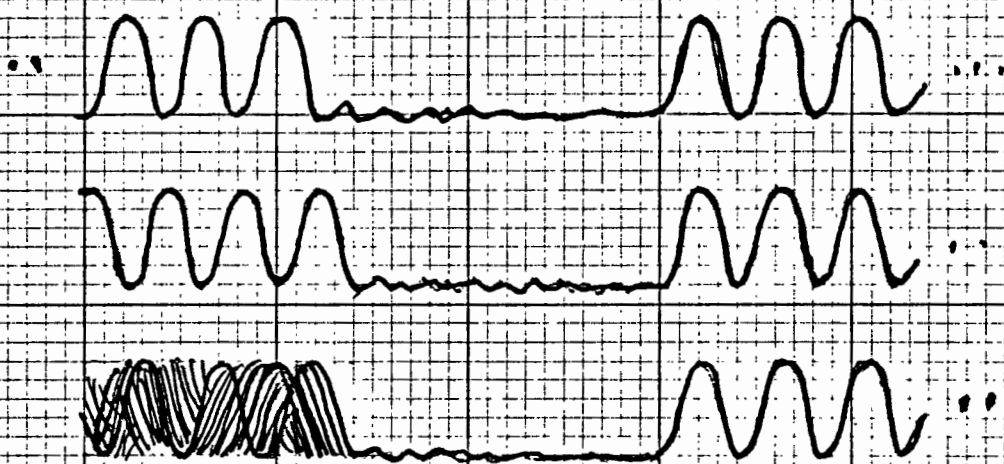
The Action of Phase Disconnect Circuits

Figure 5

A. Fixed Delay Phase Disconnect  $F_2$  Waveforms (Pin 11)



B. Variable Delay Phase Disconnect  $F_2$  Waveforms





A different way to stop  $F_2$  would be to allow the oscillator to complete its current cycle and always stop at the same minimum voltage. Then, after the transients have subsided, restart the oscillator synchronized to the event. This variable delay phase disconnect technique has the same conditions at turnoff but a variable delay time for the transients to subside. The fixed delay phase disconnect technique has differing energies stored in the oscillator at turn off but a fixed delay time for the transients to subside. The variable delay seems to result in less phase noise. Further improvements can be made by increasing the delay before restart.

Jitter measurement have been made on five H.P. restartable oscillators in the Event Timer. The test event was a 100 MHz square wave synchronized to the 200 MHz standard. The range gate was opened randomly on the next 20 n.s. window by a free running pulser running at about 30 p.p.s.. The range gate opening is synchronized by the 50MHz least significant bit of the time generator to prevent slicing of the event pulse. 100 sample runs were made for all values of the vernier and the RMS jitter was calculated. The results are shown in figures 6,7, and 8.

Use of this variable delay phase disconnect circuit has resulted in a reduction of jitter from perhaps 35 p.s. RMS to the order of 15 p.s. RMS at this time. Further improvements may be possible. While this reduction may not be important in Lageos tracking where there is an abundance of data to smooth out the jitter, this should be a decided advantage in Lunar ranging where every data point is precious.

Again, using the above described test of measuring a 100 MHz square wave at random times, a test was made over a period of one hour of the stability of the system. During the test, the delay line was not changed, the temperature was held constant at 22.5 C., and 1000 measurements were made and averaged every two minutes. The mean value of each 1000 measurements is plotted in figure 9.

Further tests, which have not been done as yet, would measure the linearity of the vernier. In this linearity test, the standard used to generate the test signal would be allowed to slowly drift with respect to the standard of the Event Timer. If measurements were made at precisely known times, the rate of drift could be measured and a projected ideal vernier could be formulated. The deviation from this ideal vernier would measure the linearity error.

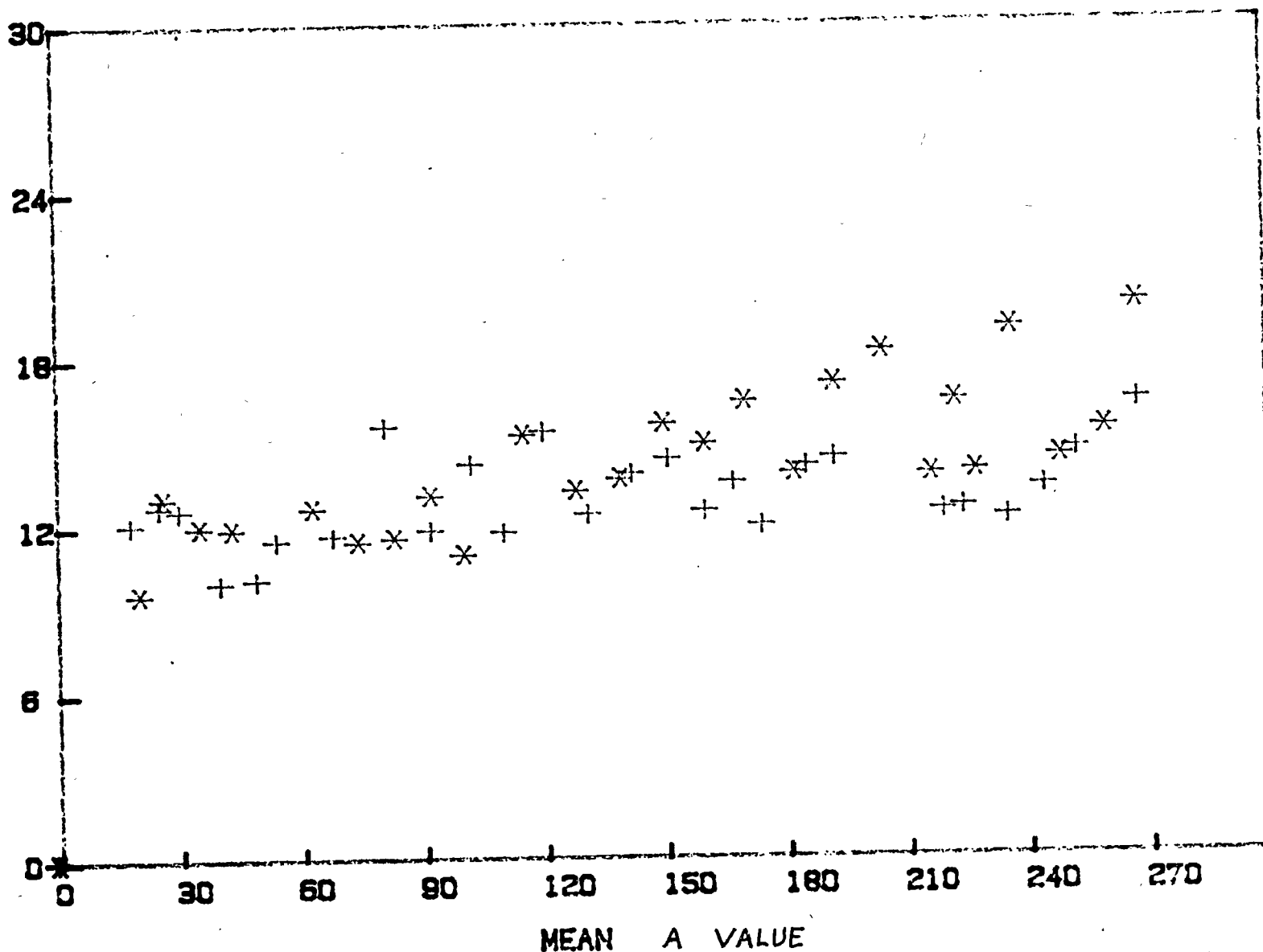
# EVENT TIMER RMS JITTER

+ - Chip 2  
\* - Chip 5

RMS PS.

CHIP#1 CHIP#2 CHIP#3 CHIP#4 CHIP#5 CHIP#6

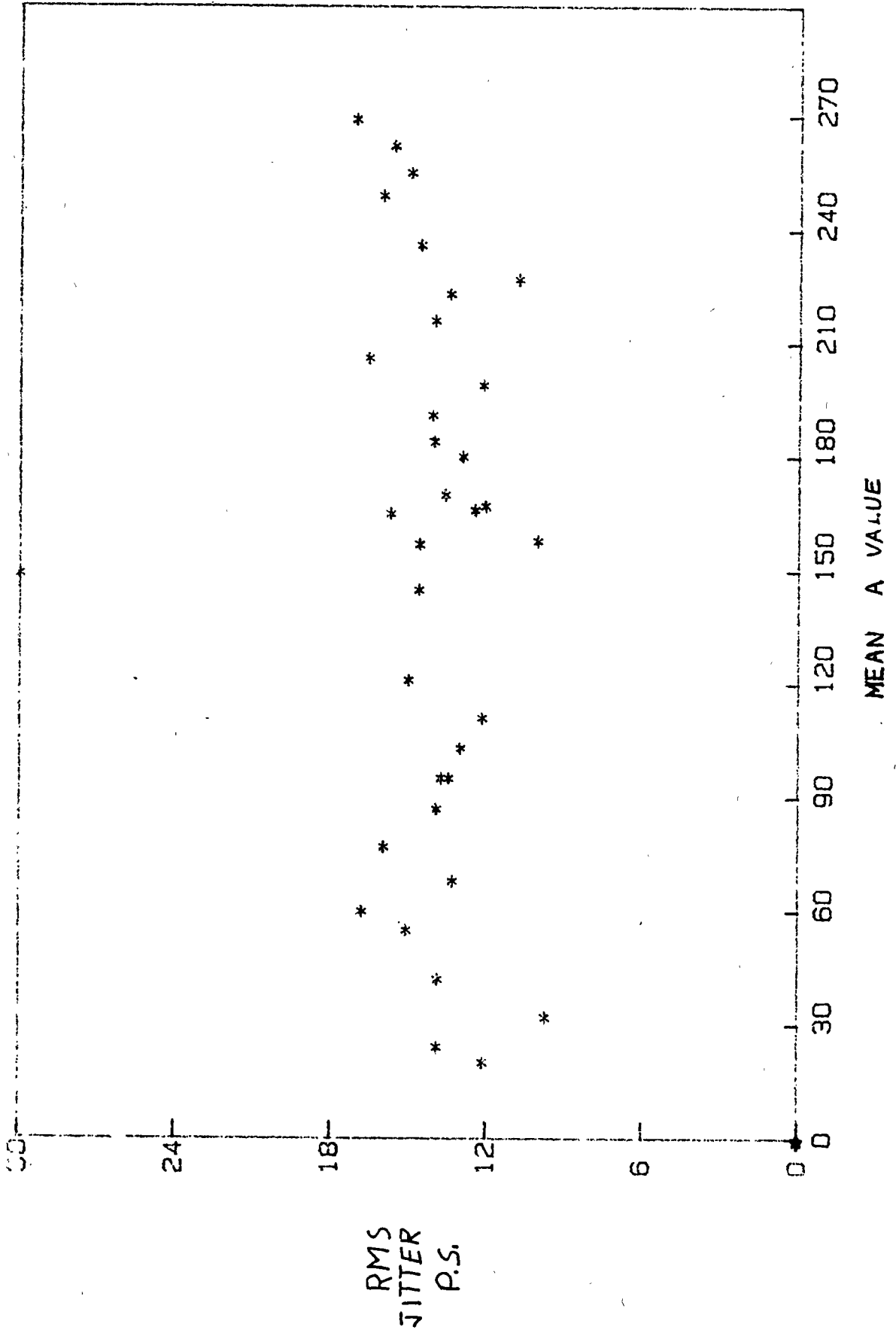
figure 6



# EVENT TIMER RMS JITTER

figure 7

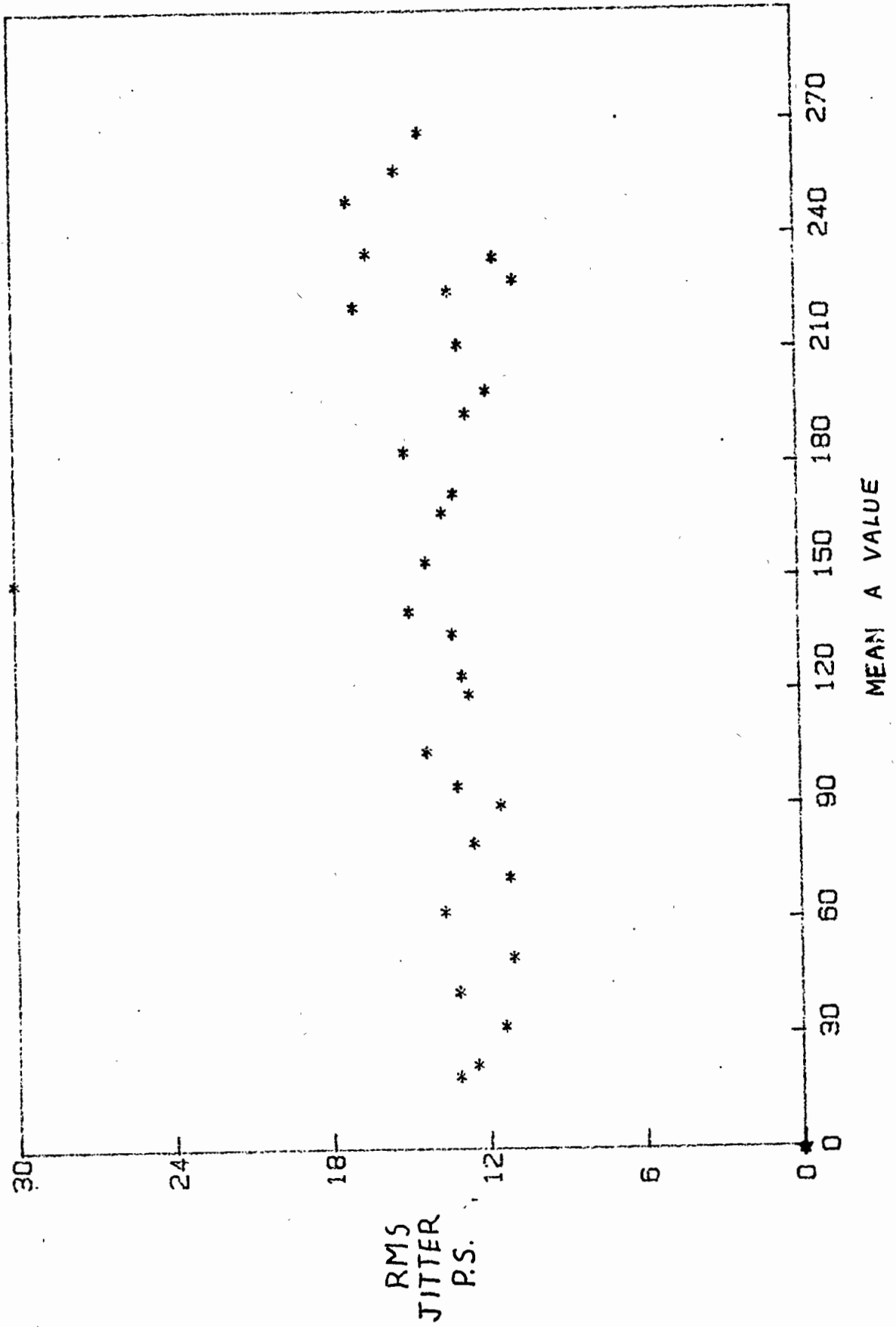
CHIP #1A



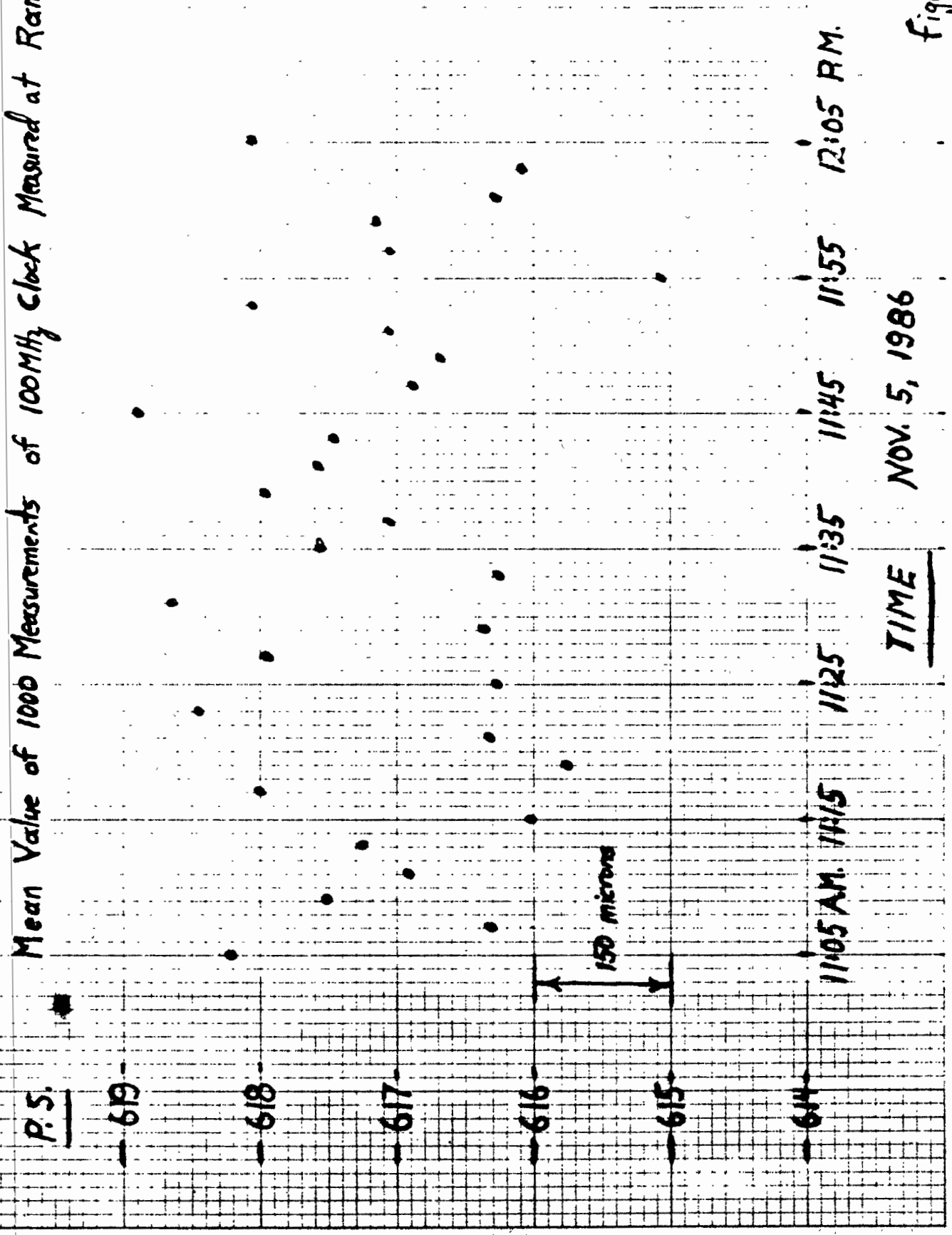
# EVENT TIMER RMS JITTER

Figure 8

CHIP4A



Mean Value of 1000 Measurements of 100MHz Clock Measured at Random



TIME

NOV. 5, 1986

Figure 9

Finally, I have been asked whether a 10 p.s. resolution Event Timer could be made using the H.P. restartable oscillator. It is not practical to use the H.P. chip in its present form because the transmission line oscillator cannot be stably tuned to the required 199.610136.. MHz. In this mode of operation there would be 513 of the 200 MHz. cycles for 512 of the offset frequency giving a resolution of 9.76 p.s.

If, as is shown in figure 10, an entirely new restartable oscillator were to be made, I believe that it is possible to design an Event Timer based of the standard frequency of 400 MHz. Using 512 as the offset frequency divider instead of 256, the restartable oscillator frequency becomes 399.2202729 MHz with a period of 2504.882813 p.s.. The resolution of the Event Timer is 4.88 picoseconds. Hopefully, the RMS jitter could be less than 5 p.s..

## Design of 400 MHz Event Timer

Figure 10

- 1)  $F_1 = 400 \text{ MHz}$
- 2) Time generator is a 27 Bit Synchronous Counter consisting of 3  $\div 2$  prescalers and the present 24 Bit counter.
- 3) Resolution of Range Gate 20 N.S.

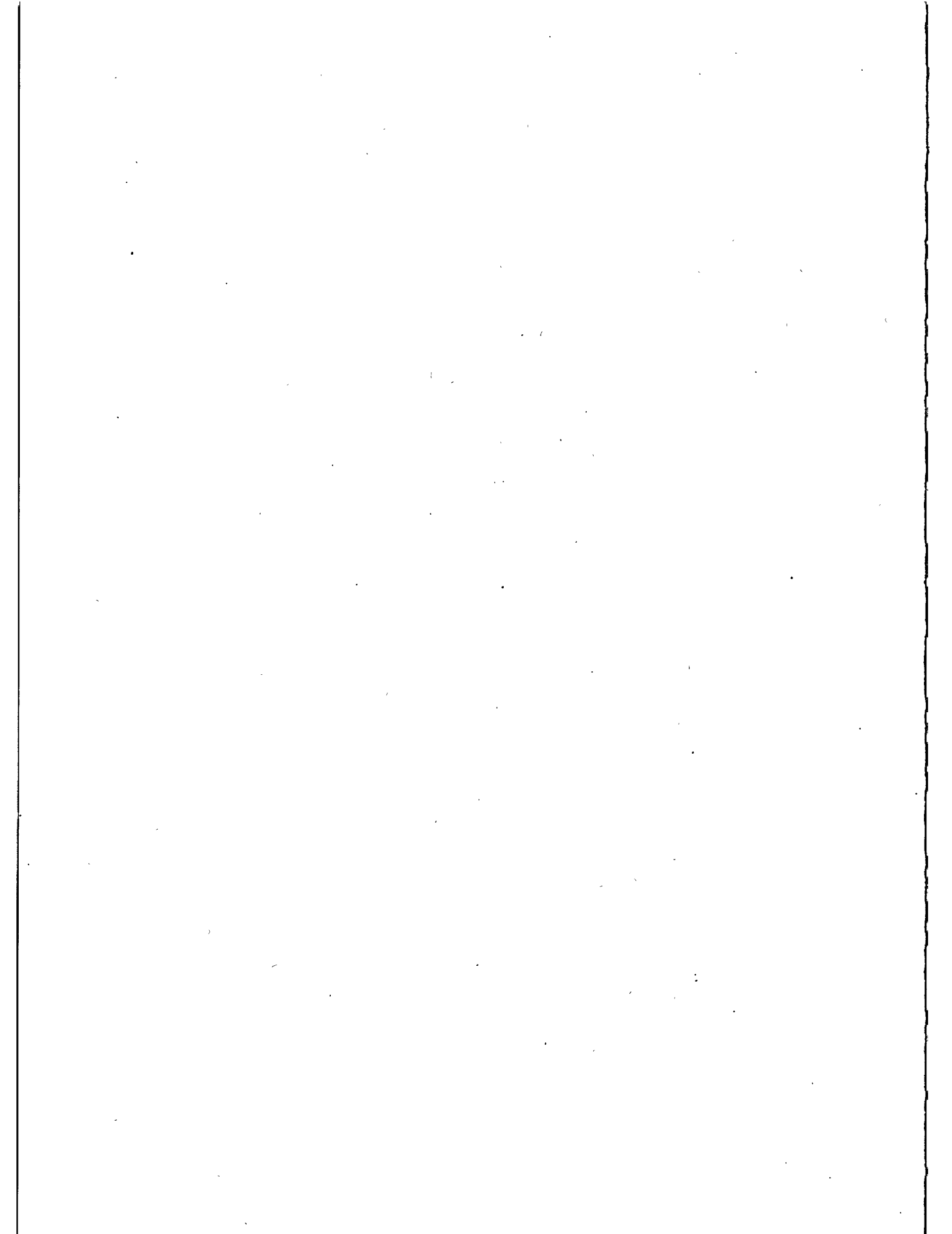
$$F_1 - F_2 = F_2 / 512 \quad F_2 = 399.2202729 \text{ MHz}$$

$$\frac{400 \text{ MHz}}{513} = .77972 \dots \text{ MHz Beat Frequency}$$

$$2500 \left( \frac{513}{512} \right) = 2504.882813 \dots = \text{period of } F_2 \text{ P.S.}$$

$$\text{Period of } F_1 = 2500 \text{ P.S.}$$

- 4) Resolution of Vernier = 4.8828 p.s.





## STABLE SATURABLE DYE FOR 1.06 $\mu\text{M}$

K. Hamal, H. Jelinkova  
Czech Technical University  
Faculty of Nuclear Science and Physical Eng.  
Brehova 7, 115 19 Prague 1 - Czechoslovakia -

Telephone 848840  
TWX 121254 FJFI C

### ABSTRACT

Most of the second generation Satellite and Lunar ranging stations and practically all of the 3. generation ones exploit pico-second pulses to ensure the required accuracy. To synchronize the modes and to Qswitch the resonator, either an active or passive modulator or combination of them, may be used. To apply a passive modelocker/Qswitch, some characteristics of the saturable modulator (bleacher) are required.

## STABLE SATURABLE DYE FOR 1.06 $\mu\text{m}$

Karel Hamal, Helena Jelinkova

Most of the second generation Satellite and Lunar ranging stations and practically all of the 3. generation ones exploit picosecond pulses to ensure the required accuracy. To synchronize the modes and to Qswitch the resonator, either an active or passive modulator or combination of them, may be used. To apply a passive modelocker/Qswitch, some characteristics of the saturable modulator (bleacher) are required:

- compatibility with the Nd transition and host (YAG, YAP, Nd glass, etc) (wavelength, absorption cross-section, lifetime, saturation intensity)
- short/long term stability
- acceptable solvent
- to range Satellites/Moon, the desirable pulse duration is 30-100 psec (3. generation) and 30 psec or less for 4. generation /1/.

We have worked to develop saturable dye having performances closed the mentioned ones above. The parameters of the resulting saturable dye ML51 /2/ are summarized in the table 1. Some other dyes are mentioned for comparison.

The photostability has been estimated from the following experiment: the sample of the dye was illuminated by the cw high pressure xenon flash lamp XBO500 /3/. The exposure time of the photodecomposition was measured and the slope was compared for different dyes (Fig.1.).

To investigate modelock/Qswitch properties, we have used different laser configuration:

(1) /4/ The YAG rod was cut at 1 deg near the back mirror, the perpendicular surface on the opposite side acted as the output mirror. A 5 mm cell, containing 2 cc of no flowing dye, was placed at the Brewster angle between the back mirror and the YAG crystal. The optical length of the resonator was 30 cm. The single mode operation was accomplished by an iris 1 mm in diameter. The output energy was 3 mJ in a train of two or three pulses, the replate was 2.5 Hz. The pulse duration and the output energy fluctuation were detected and statistically processed using a diagnostics chain consisting of the second harmonic generator, the streak camera Hamamatsu C-979 (10 psec resolution) interfaced with the SIT camera and temporal analyzer, the HP85 console and

the computer HP 1000. The resulted pulse duration at 0.53  $\mu\text{m}$  was 30 psec RMS, the output energy 3mJ,  $RMS = 3\%$  (Fig.2A). The corresponding power density is 3 GW/cm<sup>2</sup>. To examine the output spatial structure of the beam, the detection chain /5/, consisting of the CCD Fairchild camera, Quantex singleframe memory and HP 1000 has been used. The beam profile is closed to the Gaussian. (Fig.3.) The divergence is 1 mrad, close to the diffraction limit. The corresponding brightness is  $3.10^{15}$  W/cm<sup>2</sup> sr.

(2) To prove the saturable dye in the active/passive arrangement, we put it to Quantel laser system at CERGA (fall 1983). The oscillator contains a dye cell and a active modelocker. The records of the output pulse train and selected pulses are on Fig.4. The transmission of the bleacher has been set to obtain required 5-7 pulses within FWHM envelope. The replate was 10 Hz. A similar experiment was carried out at U. of Maryland /10/ using Kodak 9740 and ML51. Pulse widths were between 20-50 psec, however the shot to shot energy stability of the cavity dumped single pulse was poor.

(3) The ML51 was applied in two wavelength experiment /6/. To obtain picosecond ranging accuracy, the pulse duration should be minimized. The oscillator consisted of the concave 5m, 100%, back mirror in contact with 2 mm flowing dye cell. The YAG rod 3 mm in diameter 2deg/2deg AR coated was pumped in Quantel head. The front mirror was a quartz plate 0.25 mm thick. The duration was 14 psec at 0.53  $\mu\text{m}$ , when deconvoluted. The pumping energy was varying up to 2.3 times above the modelock threshold and no change in the pulse duration or stability has been observed.

(4) The saturable dye was used to modelock the YAP laser /7/. The laser setup was similar to the experiment in (1). The raw value of the pulse duration was 10 psec, actually equal to the temporal resolution of the streak camera.

Generally, we did not observed any damage of any optical element throughout all experiments and during long term exploitations in different laser configurations. The saturable dye ML51 has been used at the INTERKOSMOS satellite laser station in Egypt since 1982 /1/, for two wavelength experiment /9/, for the ophthalmology and in several other lasers, occasionally, the dye lasts in the cell for several months.

LITERATURE

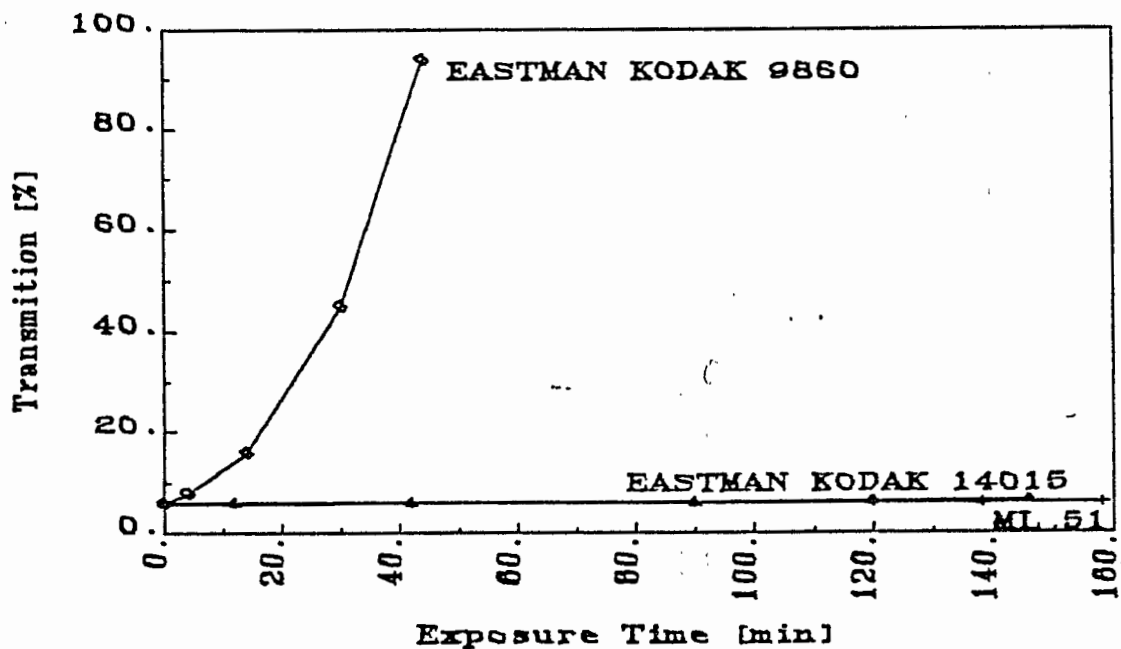
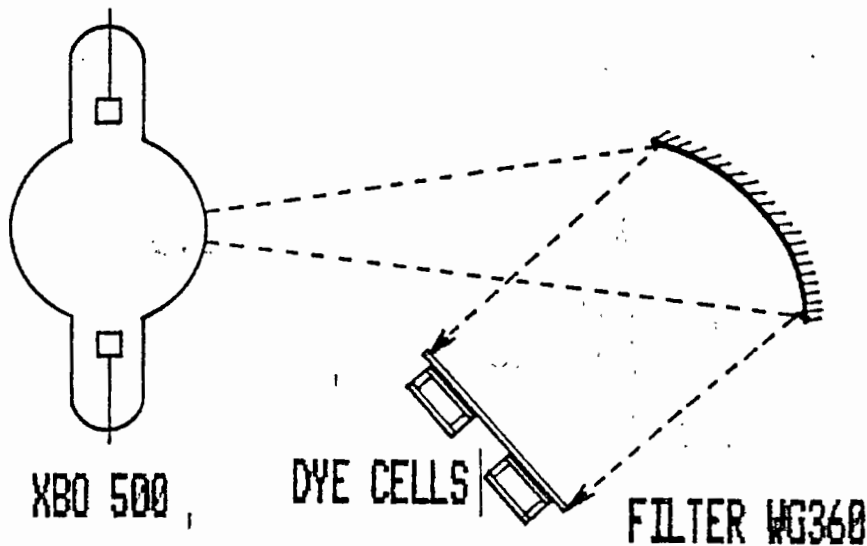
- /1/ Proceedings of the V. International Workshop on the Laser Ranging Instrumentation, Greenwich, 1984.
- /2/ K. Hamal, H. Jelinkova, V. Hruskova, CLEO, Baltimore, May, 1985
- /3/ B. Kopański et al, Appl. Phys., 15, 1982, p. 29.
- /4/ H. Jelinkova, in /1/
- /5/ H. Jelinkova, in this Proceedings.
- /6/ J. Gaignebet et al, in this Proceedings.
- /7/ K. Hamal, to be published.
- /8/ K. Hamal et al, in /1/.
- /9/ V. A. Babenko et al, Quantum Electronics, 7, 1980, p. 1796, (in Russian).
- /10/ W. Koechner, Solid-State Laser Engineering, Springer-NY, 1986
- /11/ I. Prochazka, in this Proceedings.
- /12/ M. Košelja, MS thesis.

Parameters of saturable dyes				
	ML51 /2/	3955	Kodak 9740	Kodak 9860
Solvent	dichloethane	etylalcohol	chlorbenzen	dichloethane
Molec. weight	631	688	762	
$\lambda_{MAX}$ (nm)	1010	1040 /9/	1049	
$\sigma_{MAX}$ ( $10^{-10}$ cm <sup>2</sup> )	5.54		6.2	
$\sigma_{1000}$ ( $10^{-10}$ cm <sup>2</sup> )	0.45	3.2 /9/	5.7	3.5
$\tau$ (ps)	37+/-2	40 /9/	8.3 /10/	9.3 /10/
$I_s$ (MW/cm <sup>2</sup> )	.112	7.3 /9/	40 /10/	56 /10/

Tab. 1.

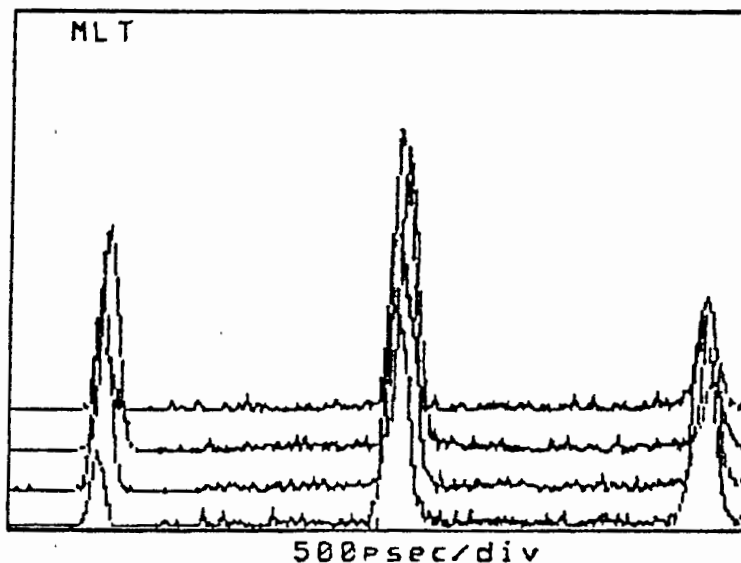
# PHOTOSTABILITY TEST

## EXPERIMENTAL ARRANGEMENT

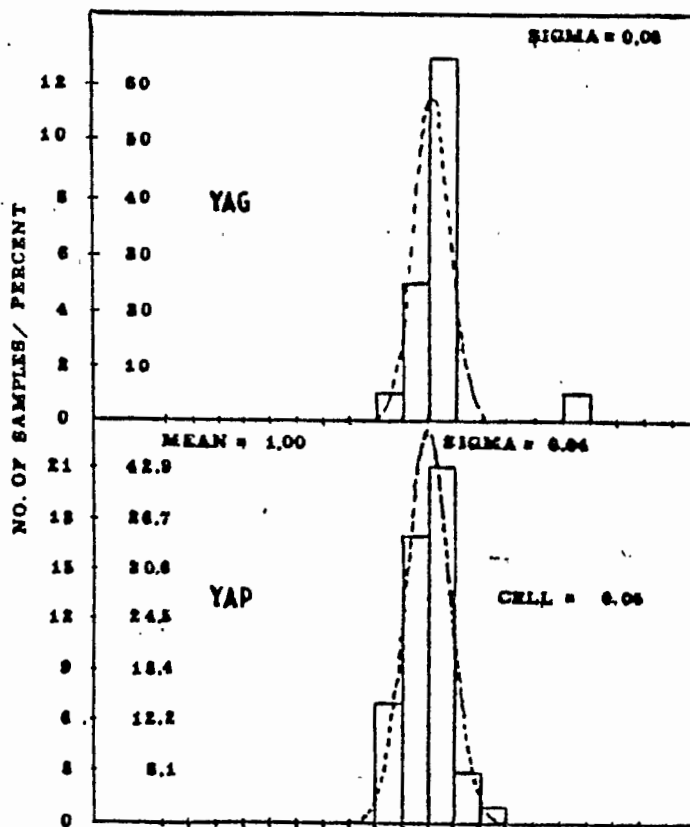


K. Hanal, H. Jelinkova  
Stable Saturable Dye For 1.06 $\mu$ m

# LASER OUTPUT



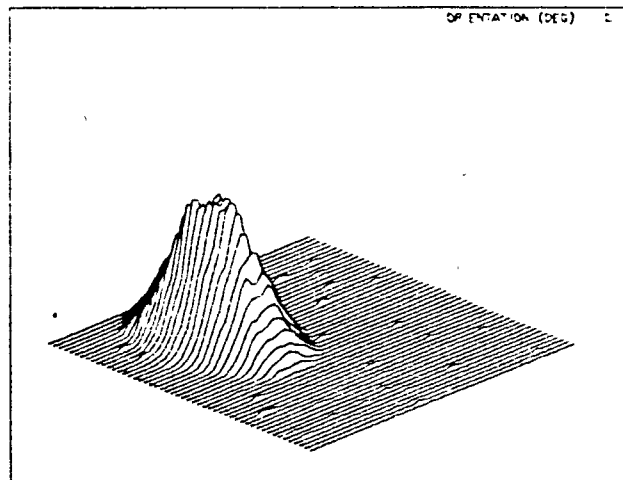
MODELOCKED TRAIN  
(STREAK)



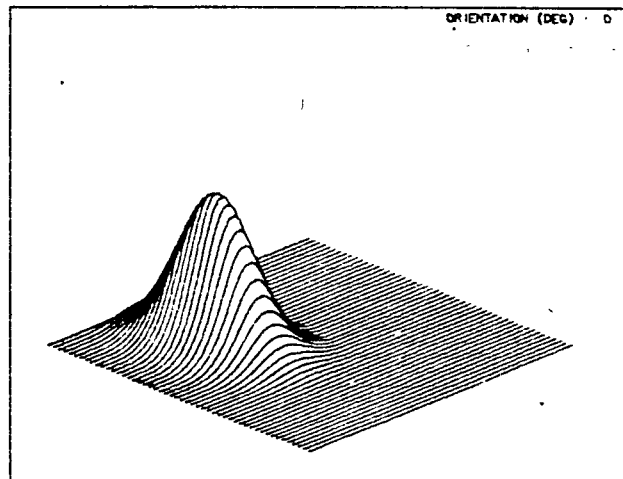
ENERGY STABILITY  
HISTOGRAM

# SPATIAL STRUCTURE OF THE OUTPUT BEAM

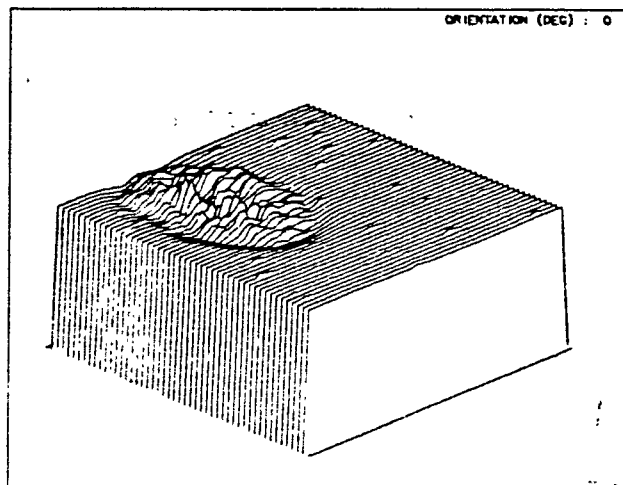
OSCILLATOR BEAM  
DIVERGENCE 1 MRAD



GAUSS PROFILE  
(THEORY)

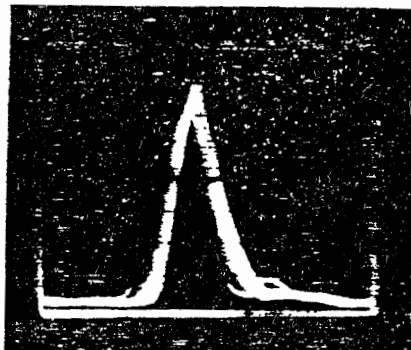
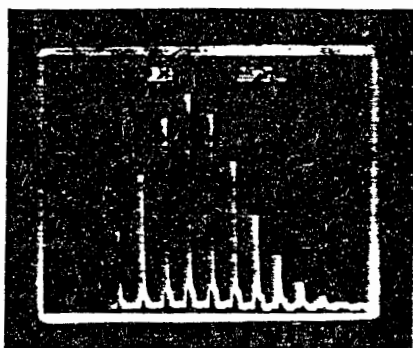


DIFFERENCE ~ 8%



# INTERKOSMOS SATELITE LASER RADAR NETWORK

## ACTIVE/PASSIVE MODE LOCKED LASER OUTPUT TRAIN



K. Hamal, H. Jelinkova  
Stable Saturable Dye For  $1.06\mu\text{m}$



SPATIAL STRUCTURE OF THE DOUBLED Nd : YAG  
LASER TRANSMITTER BEAM

H. Jelinkova, P. Valach  
Czech Technical University  
Faculty of Nuclear Science and Physical Eng.  
Brehova 7, 11519 Prague 1 - Czechoslovakia -

Telephone 848840  
TWX 121254 FJFI C

J. Del Pino  
Cuban Academy of Sciences  
Institute for Geophysics and Astronomy  
Santiago de Cuba

ABSTRACT

The beam spatial structure of the passively mode-locked Nd : YAG oscillator/amplifier/SHG laser radar transmitter has been examined.

To analyze the laser beam structure, an on line diagnostic chain, giving a three-dimensional graphic display, the contours and the two dimensional Fourier transformation of the output pattern was implemented at the Interkosmos indoor calibration facilities.

The beam was studied in every point of the laser transmitter and the IR Gaussian beam structure changes due to the outside oscillator optical elements were eliminated from the system. The SH beam profile was investigated from the point of view of temperature dependent efficiency and the pointing stability. The difference between the spatial shape of pulse IR and SH was found and the changes between them were tried to be compensated by the help of the tandem scheme of two SHG crystals.

# SPATIAL STRUCTURE OF THE DOUBLED Nd:YAG LASER TRANSMITTER BEAM

H.Jelinkova, P.Valach, J.del Pino

## INTRODUCTION

A Nd:YAG laser (YAG, YAP, etc.) allows to generate picosecond pulses for laser ranging. However, up to now, a lack of detectors in the near IR requires the radiated frequency to be multiplied into the second resp.third harmonics. To apply a second harmonic generator (SHG) into the laser transmitter scheme, the homogeneous, Gaussian IR output beam is required. Every change of the laser system configurations (resonator readjustement, active or passive elements temperature dependence, pumping inhomogeneity, etc.) causes significant changes of the Gaussian beam structure. Applying the new technology giving the fast accurate response, we have got the possibility to optimize the laser system performance. Consequently, the spatial structure of the transmitter output SH beam has been investigated.

## EXPERIMENTAL ARRANGEMENT

The laser system configuration /1,2,3/, we employed, consists of passively mode-locked Nd:YAG oscillator, isolation saturable dye cell, expanding telescope, single pass amplifier and KDP doubling crystal (Fig.1.). According to /4/ the image in the focal plane of a well corrected lens coincides with the beam far field pattern (in Fraunhofer region). Therefore, in the laboratory, the beam farfield was observed in the focus of the 2.5 m thin lens by the help of the CCD array (Fairchild 320 x 489 cells). The CCD output signal was digitized using Quantex image memory (256 x 256 cells, 8 bits, 100 MHz) and stored on line on the magnetic disc of the host computer (Fig.2.).

## IR BEAM

To understand the beam distortion through the laser transmitter, the beam was examined at different points (Fig.1, Fig.3) (behind the oscillator (A), the isolation cell (B), the expanding telescope (C), the amplifier (D)). The oscillator output beam structure was clean, near Gaussian, with the divergence of the one mrad (Fig.3A). The greater increment to the distortion was made by the isolation 5 mm thick Brewster angled dye cell (Fig.3B). The improvement was

obtained by tilting the dye cell to 1 degree. Resultant divergences in every measured points are summarized in Tab.1.

#### SH BEAM

In general case, the index of refraction of the negative nonlinear crystal, which is mostly used in SHG, depends on the incidence angle  $\theta$ , the temperature  $T$  and the basic radiation wavelength  $\lambda$ . Every change of these parameters causes the index matching condition modification.

In our experiment, the temperature dependence of the SHG was investigated in detail.

1) The temperature of the SH crystal was varied from the 16°C to 37°C and the index matching angle was found for every examined temperature. From Fig.4 it can be seen that there is no variation in the efficiency within the experimental limit and therefore in the measured temperature interval the optimal thermal region for dominating SH output does not exist.

2) The index matching angle was alligned for the 24°C and the temperature dependence of the efficiency and the spatial structure was investigated. For the KDP crystal type II the temperature dependence is expressed by /5/:

$$\Delta T = \frac{0,44\lambda}{L} \cdot \left( \frac{\partial n_e^{2\omega}}{\partial T} - \frac{\partial n_o^{\omega}}{\partial T} \right)^{-1}$$

where  $\lambda$  is the wavelength of the incident wave,  $L$  is the crystal length,  $T$  is the temperature. For the KDP crystal (10x10x30 mm) which was used to SH conversion  $\Delta T_{CALC} = 5.8^\circ\text{C}$ . ( $\Delta T$  is the interval in which the efficiency is more than 1/2 of maximum value). This calculated value coincides with the experimental measured data plotted on Fig.5 from which follows  $\Delta T_{EXP} = 6.2^\circ\text{C}$ . The independent experimental determination was done by the integration of the CCD output spatial structure.

From the measuring of the temperature dependence of the far field SH beam spatial structure (Fig.6) follows that inside the temperature range 24°C-32°C, the SH beam has mostly clean profile and due to the diffraction aperture effect, the contour has a little elliptical form. Within the range 10°C-22°C, the beam profile was deformed and in the temperature range 36°C-52°C, the most significant feature observed was the appearance of a double spot alternating regularly with the homogeneous elliptical one. In all cases, the center of the beam has been shifted with changing temperature.

In Fig.6. it is seen that the far field beam structure of the SH beam has the elliptical form. This distortion of the spatial structure in one direction follows from the fact that due to the double refraction of the nonlinear crystals, the extraordinary ray deviates in the anisotropy or walk off angle. The beam of the SH radiation is therefore deviated from the original (IR beam) direction and from this fact the aperture effect follows which decreases the efficiency of the SHG and changes the shape of the pulse (Fig.7.B). We try to use the tandem scheme /7/ for the compensation of this deviation. The resulted spatial beam structure is on Fig.7.C.

#### SUMMARY

The laser transmitter system was designed to have an optimum farfield beam spatial structure what implies a good farfield and a higher efficiency of the SH radiation beam. The measurement of the temperature dependence of the SH crystal showed the strong dependence of the efficiency, of the spatial structure and of the pointing accuracy on temperature changes.

#### LITERATURE

- /1/ Jelinkova H., Proceedings of the Vth International Workshop on Laser Ranging Instrumentation, Greenwich, England, 1984.
- /2/ Hamal K., Hruskova V., Jelinkova H., Proceedings of CLEO 1985, Baltimore, USA.
- /3/ Hamal K., Jelinkova H., "Stable Saturable Dye for 1.06  $\mu\text{m}$ ", in this Proceeding.
- /4/ Born M., Volf E., "Principles of Optics", Pergamon Press, 1964.
- /5/ Koechner W., "Solid-State Laser Engineering", New York, Springer Verlag, 1976.
- /6/ Tarasov L.V., Dmitrijev V.G., "Prikladnaja Nelinejnaja Optika", Moskva, Radio i Svjaz, 1982 (in Russian).
- /7/ Volosov V.D. et al., Sov. J. Quantum Electron., 6, p.1163, 1976.

Tab.1. Laser System Divergence

A) Isolation cell - Brewster angle

Measured point	X [mrad]	Y [mrad]
A	1	0.9
B	1.7	1.1
C	0.8	0.6
D	0.7	0.6

B) Isolation cell - 1 deg angle

Measured point	X [mrad]	Y [mrad]
A	1	0.9
B	1.1	0.9
C	0.6	0.6
D	0.6	0.6

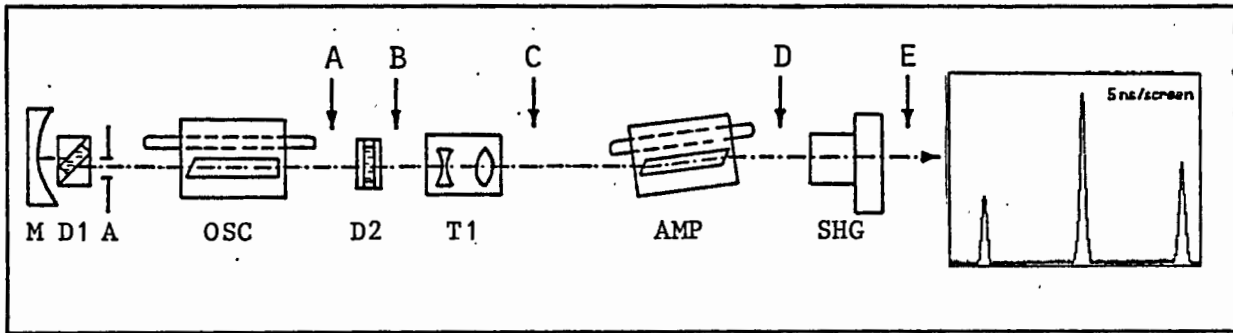


Fig.1. Block diagram of the optical lay-out of the Nd:YAG laser transmitter.

M	End mirror	D2	Dye cell
D1	Dye cell	T1	Telescope
A	Aperture	AMP	Amplifier head
OSC	Oscillator head	SHG	KDP II Frequency doubler

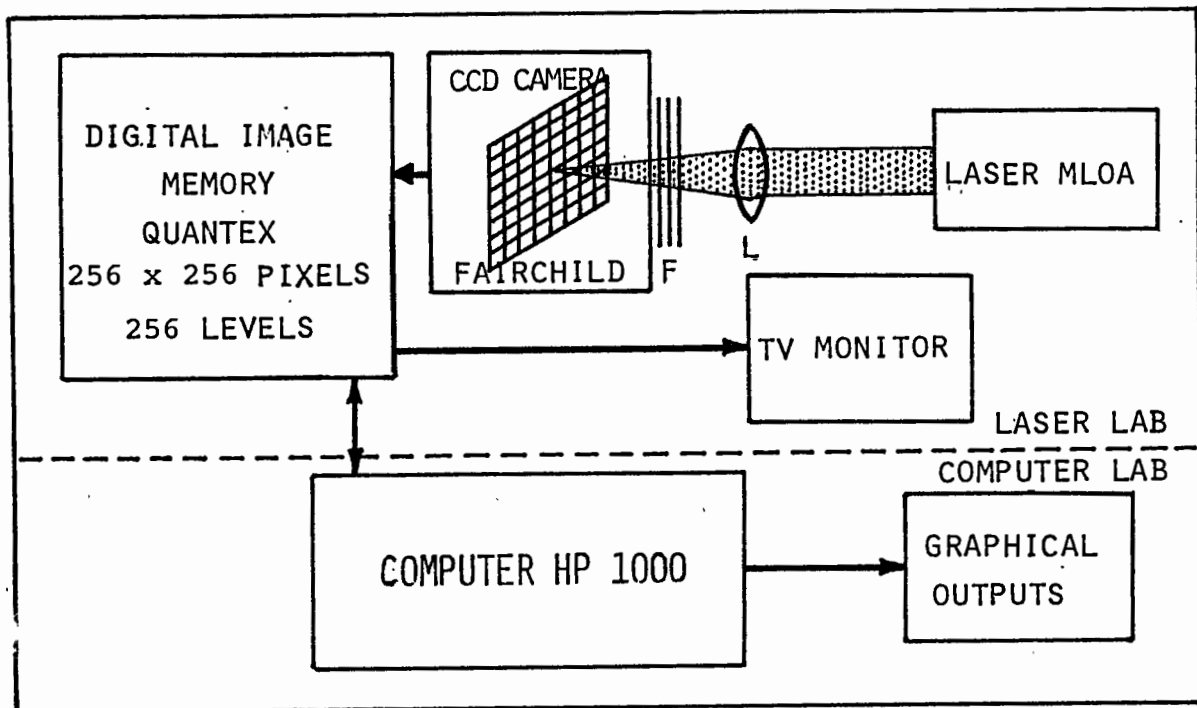


Fig.2. The experimental set up of the farfield beam spatial structure measurements. (F - neutral density filters, L - 2.5 m lens.)

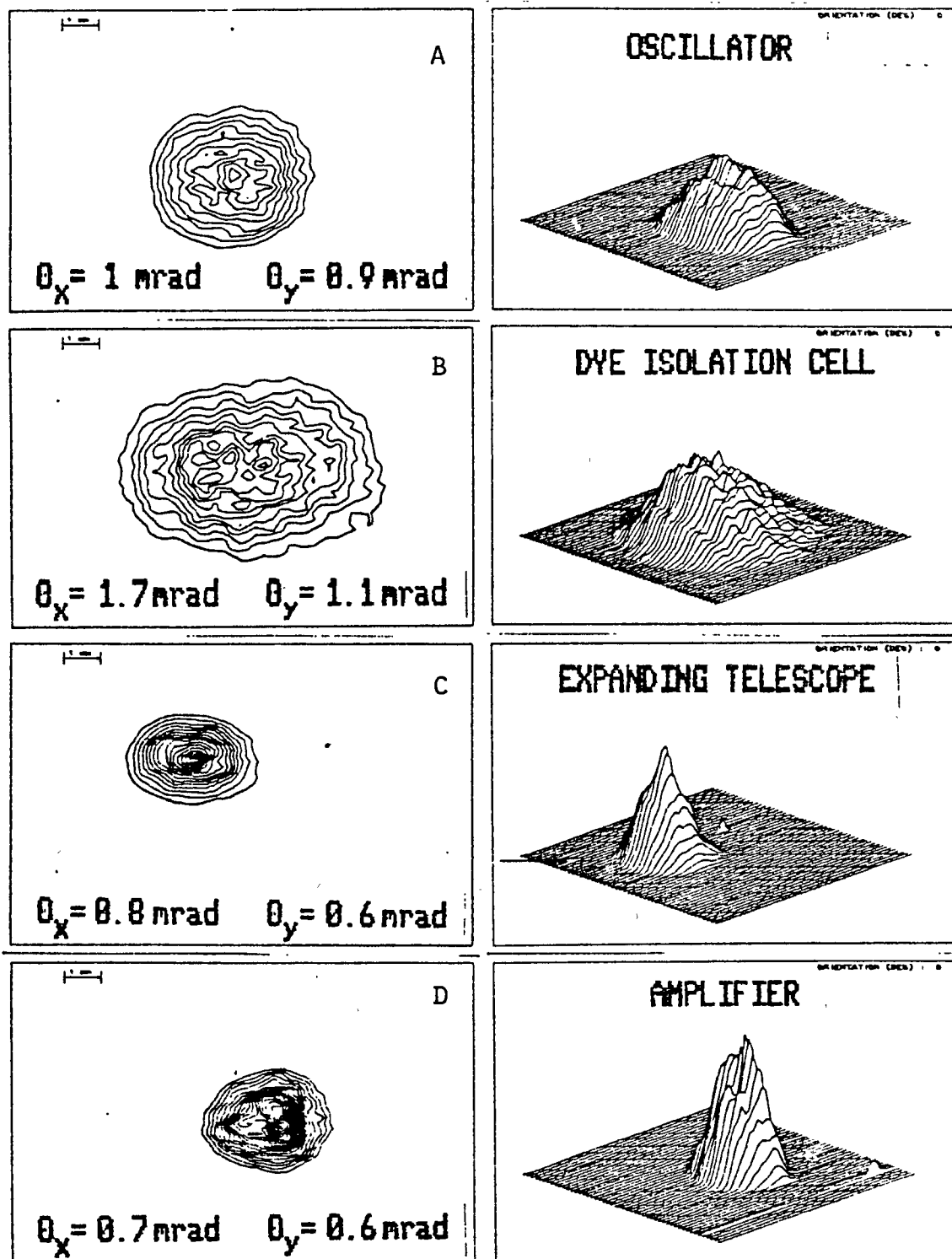


Fig.3. The IR far field beam spatial structure.

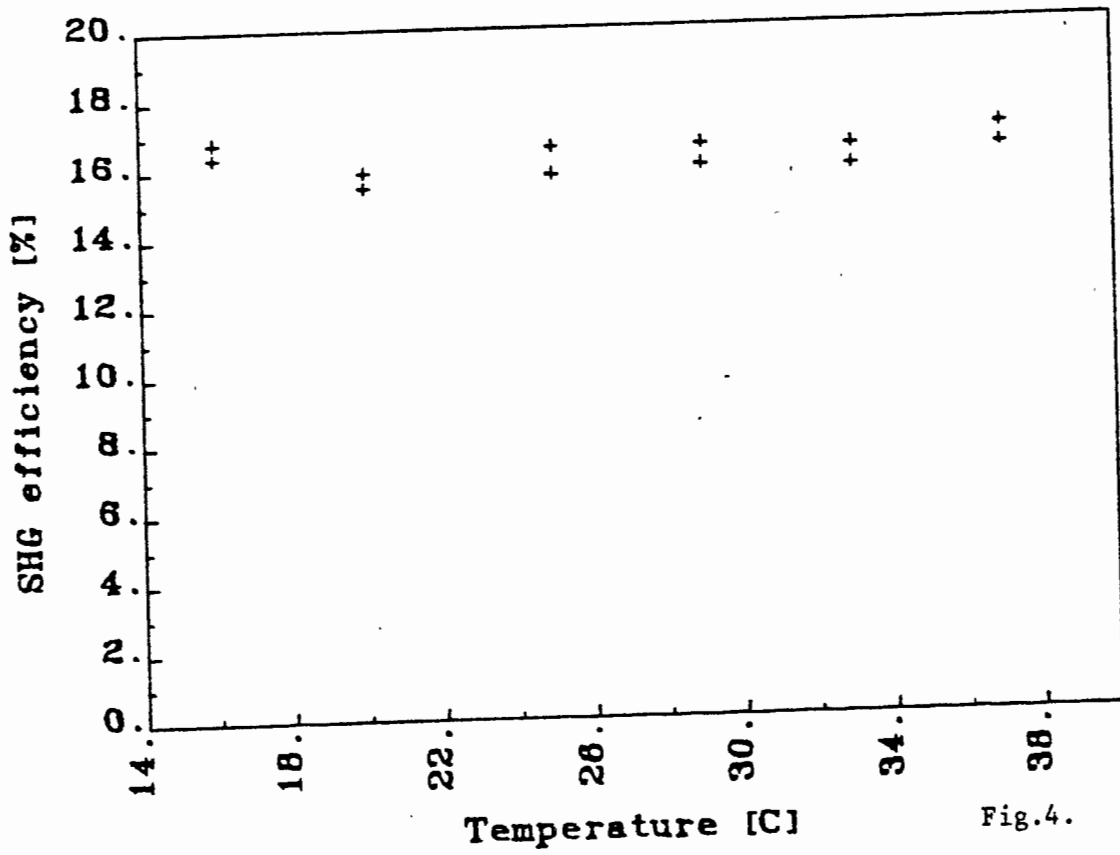


Fig.4.

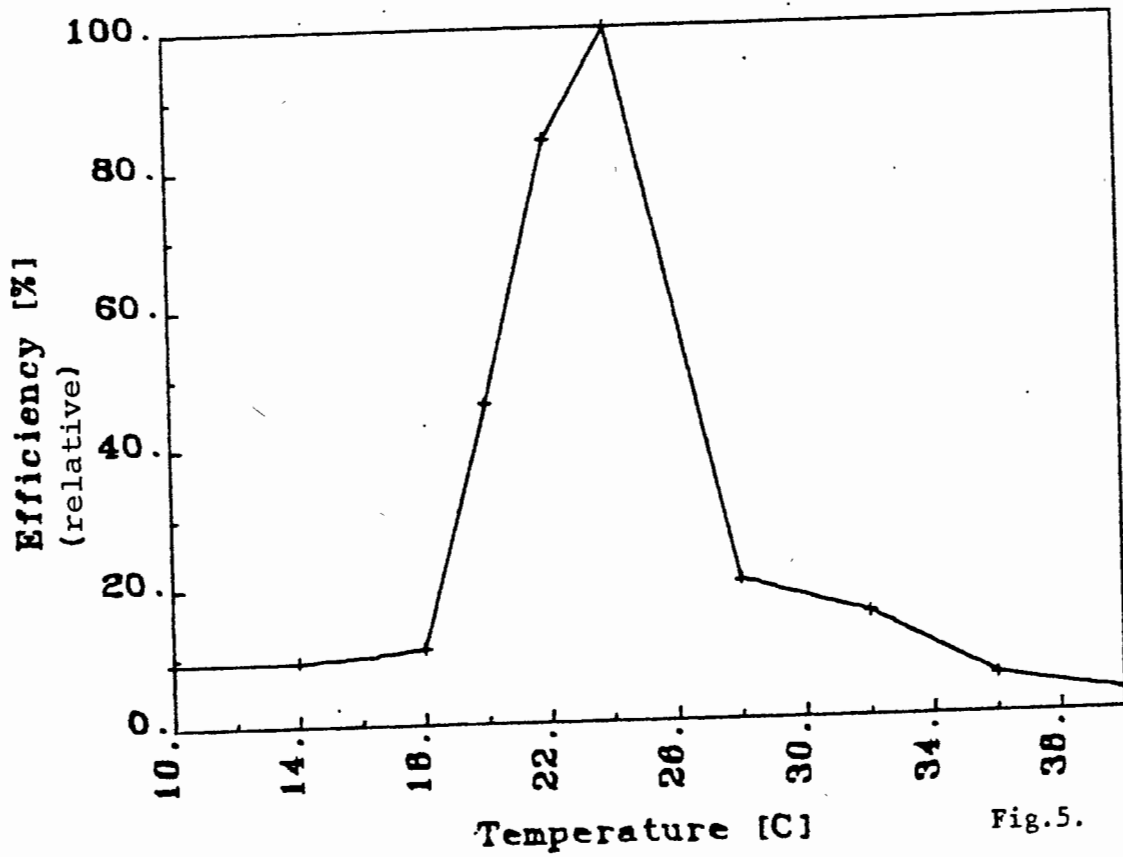


Fig.5.



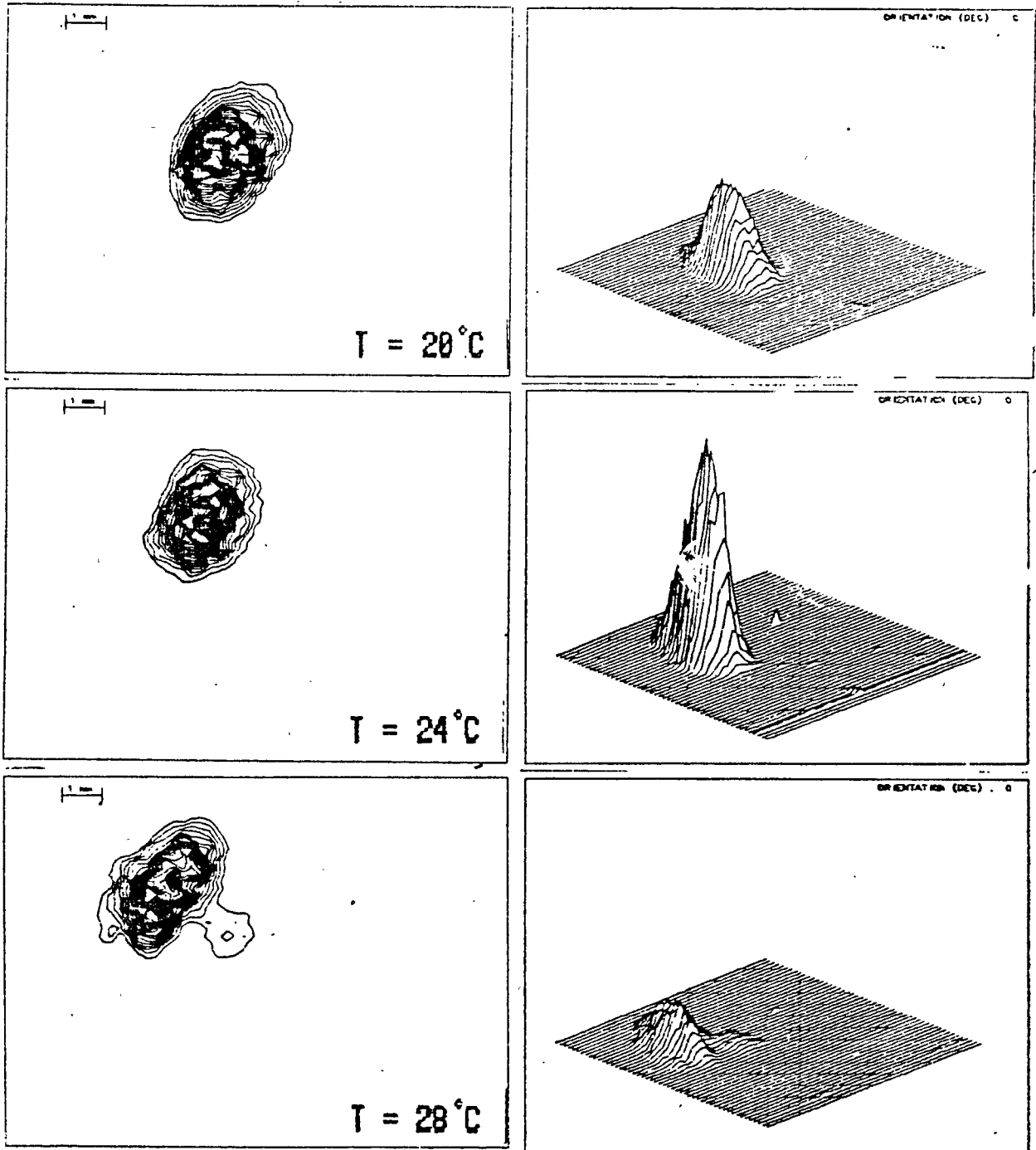


Fig.6. Temperature dependence of the far field SH beam structure.

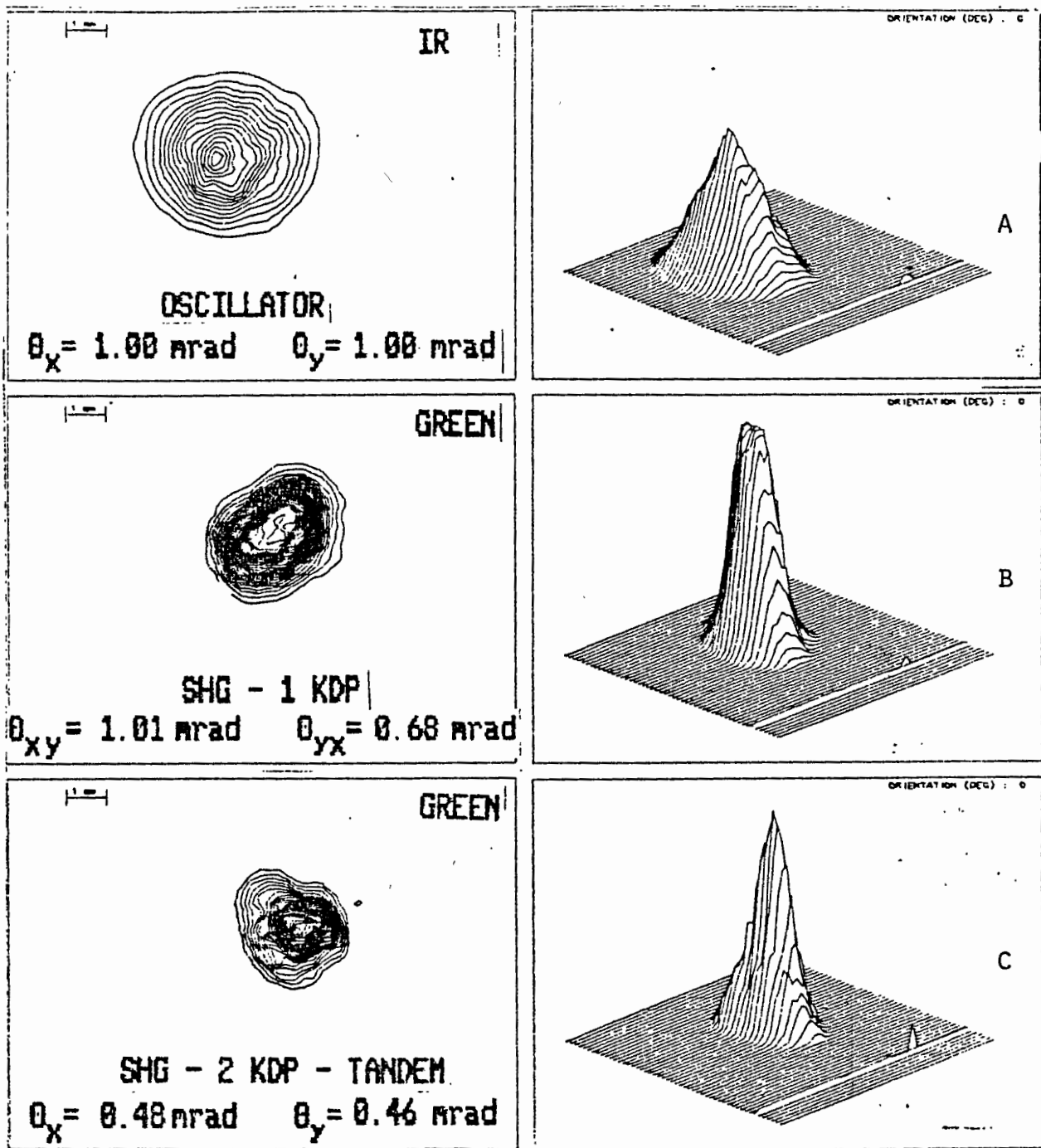


Fig.7. Aperture effect compensation

SOME SPECIAL REQUIREMENTS  
TO LASERS FOR SATELLITE LASER RANGING

L. Jiyu  
Wuhan Technical University of  
Surveying and Mapping  
23 Lo-yu Road, Wuhan  
The People's Republic of China

ABSTRACT

When designing or improving an SLR system it will be necessary to take into consideration that which laser should be selected. This paper has given an outline of some special requirements to select a suitable laser.

At present solid-state lasers are used to measure the distances not only between a ground station and the satellite specially equipped with retroreflectors far off several thousand kilometers, but also between a ground station and the moon set by five retroreflectors arrays far off about 380 thousand kilometers. Laser pulses generated by a solid-state laser are not modulated with any way, but used directly to measure the distances. In this case, what requirements are proposed for lasers? This paper will try to discuss them.

# Some Special Requirements to lasers for Satellite Laser Ranging

Liu JiYu  
Wuhan Technical University of  
Surveying and Mapping  
23 Lo-yu Road, Wuhan  
The People's Republic of China

## Abstract

When designing or improving an SLR system it will be necessary to take into consideration that which laser should be selected. This paper has given an outline of some special requirements to select a suitable laser.

At present solid-state lasers are used to measure the distances not only between a ground station and the satellite specially equipped with retroreflectors far off several thousand kilometers, but also between a ground station and the moon set by five retro-reflector arrays far off about 380 thousand kilometers. Laser pulses generated by a solid-state laser are not modulated with any way, but used directly to measure the distances. In this case, what requirements are proposed for Lasers? This paper will try to discuss them.

It is known that the received photons per pulse for SLR systems,  $N$  are given as follows:

$$N = \frac{16E\lambda A_s A_r \tau_t \tau_r \tau_y^2}{\pi^2 h c \delta_t^2 \delta_s^2 D^4} \quad (1)$$

Where,

- E = transmitted energy per pulse, in joule;
- $\lambda$  = laser wavelength, in meter;
- $A_s$  = effective area of Satellite-borne retroreflectors, in  $\text{cm}^2$ ;
- $A_r$  = effective area of the received objective of a received telescope, in  $\text{cm}^2$ ;
- $\tau_t$  = transmitter optical transmission;
- $\tau_r$  = receiver optical transmission;
- $\tau$  = one-way atmospheric transmission which is a function of zenith distance, site altitude, locality, visibility and wavelength;
- $\gamma$  = reflectivity of the satellite-borne retroreflectors, generally  $\gamma = 0.8$ ;
- $h$  = Planck's constant,  $h = 6.625 \times 10^{-27}$  erg second;
- $c$  = light velocity, in meters/second;
- $\delta_t$  = full angular divergence of a transmitted laser beam, in arc;
- $\delta_s$  = reflected laser beam divergence by the satellite-borne retroreflectors, in arc;
- D = distance between the ground station and the laser satellite, in cm.

It is seen from the above equation that the parameters,  $E\lambda\delta_t$  are dealt with the lasers. How their magnitudes are selected is a problem which laser is designed to satisfy some requirements for an SLR system. Therefore it is very useful to discuss their selections.

Table 1: Lasers used by worldwide SLR systems

country	wavelength	pulsewidth	transmitted power	Repetition rate	Detector type
Australia	532 nm	5-7 nsec	250 mJ	1 pps	2233 Amperex
"	694.3 nm	6 nsec	350 MW	8 ppm	RCA 7265
"	694.3 nm	6 nsec	1 J	12 ppm	RCA 31034
Austria	530 nm	100 ps	100 mJ	up to 10 Hz	
"	694.3 nm	3 ns, 6 ns	2.5 J, 4 J	up to 0.25 Hz	
Brazil	694.3 nm	6 nsec	350 MW	8 ppm	RCA 7265
China	532 nm	5 nsec	20 MW	1 Hz	GDB 49
"	694.3 nm	20 nsec	80 MW	30 ppm	
Cuba	694 nm	30 nsec	50 MW	15 ppm	RCA 8852
Ecuador	694.3 nm	35 nsec	1 J	0.25 pps	FEU-84
Egypt	694 nm	30 nsec	50 MW	15 ppm	RCA 8852
"	694 nm	4 nsec	200 MW	15 ppm	RCA 8852
W-Germany	532 nm	200 pps	0.25 J	4 pps	Varian Static Crossed Field 154
"	539 nm	400 pps	10 mJ	10 Hz	RCA 8850
Finland	694.3 nm	20 nsec	50 MW	4 ppm	RCA C 31034
France	694.3 nm	3 nsec	1.5 J	6 ppm	RCA 31034
"	694 nm	3.5 nsec	3 J	10 ppm	centroid detection
DDR	694.3 nm	20 nsec	0.5 to 1 J	10 ppm	RCAC 34034A
Greece	694.3 nm	25 nsec	4.5 J	8 ppm	RCA 7265
Hungary	694 nm	20 nsec	0.5 J	0.5 Hz	FEU-84
India	694.3 nm	20 nsec	1 J	1 pps	RCA 8852
Japan	694.3 nm	15 ns, 4 ns (with slicer)	0.3 J	0.1 pps	RCA 7265
"	532 nm	200 ps	250 mJ	4 pps	static crossed field
Netherla.	694.3 nm	1.8 nsec	700 mJ	15 ppm	RCA 8852
"	539 nm	400 ps	10 mJ	10 Hz	RCA 8852
Peru	694.3 nm	6 nsec	350 MW	8 ppm	RCA 7265
Poland	694 nm	25 nsec	1.5 J	7 ppm	RCA 8852 with CFD

Table 1 (Continuous)

country	wavelength	pulsewidth	transmitted power	Repetition rate	Detector type
Spain	694 nm	27 nsec	0.7 J	6 ppm	RCA 31034A
Switzerla.	694 nm	17 nsec	1.5 J	0.25 Hz	RCA 7265
United Kingdom	532 nm	150 ps	30 MJ	10 Hz	Varian VPM 152S
USA (Texas)	694.3 nm	3 nsec	0.4 J	20 ppm	RCA 31034A
" "	532 nm	100 ps	0.4 J	10 Hz	RCA 8852
" "	532 nm	100 ps	35 MW	10 Hz	Varian 152S
" (Hawaii)	694 nm	5 nsec	750 mJ	1 pps	56 TVP
" (Colorado)	694 nm	5 nsec	750 mJ	1 pps	56 TVP
" (CA)	694 nm	5 nsec	750 mJ	1 pps	56 TVP
" (GSFC)	532 nm	varied	varied	1 pps	56 TVP
" "	532 nm	5-7 nsec	250 mJ	1 pps	56 TVP
" "	532 nm	0.2-0.4 nsec	250 mJ	1 pps	56 TVP
" (CA)	532 nm	5-7 nsec	250 mJ	1 pps	Amperex 56 TVP
" (GSFC)	532 nm	0.2-0.4 nsec	250 mJ	1 pps	Amperex 56 TVP
" (Maui)	532 nm	500 ps	0-6 J	3 Hz	Amperex XP2233
USSR	694.3 nm	20 nsec	50 MW	0.7 Hz	FEU-79
"	694.3 nm	25 nsec	1 J	0.33 Hz	FEU-84

On the basis of the materials published by the Fourth International Workshop on Laser Ranging Instrumentation held at the University of Texas in Austin, Texas USA, October 12-16, 1981 the essential specifications of the lasers operating in worldwide SLR systems are shown in the Table 1. The used laser wavelengths are of three types of 6943 Å, 5320 Å and 5390 Å, corresponding with three laser medium of ruby, Nd:YAG and Nd:YAP crystal. The longer laser wavelength used is to the benefit of detections with the view of the transmission traveled in the atmospheric layer (see Table 2). Under the condition of the smallest zenith distance there is not greater difference between

Table 2: Atmospheric transmission at different wavelengths and zenith distances, from Mastrocinque

$\lambda$ (nm)	$\tau(0^\circ)$	$\tau(60^\circ)$	$\tau(70^\circ)$
760	0.79	0.63	0.50
694.3	0.77	0.58	0.45
532	0.67	0.45	0.30
380	0.44	0.20	0.09

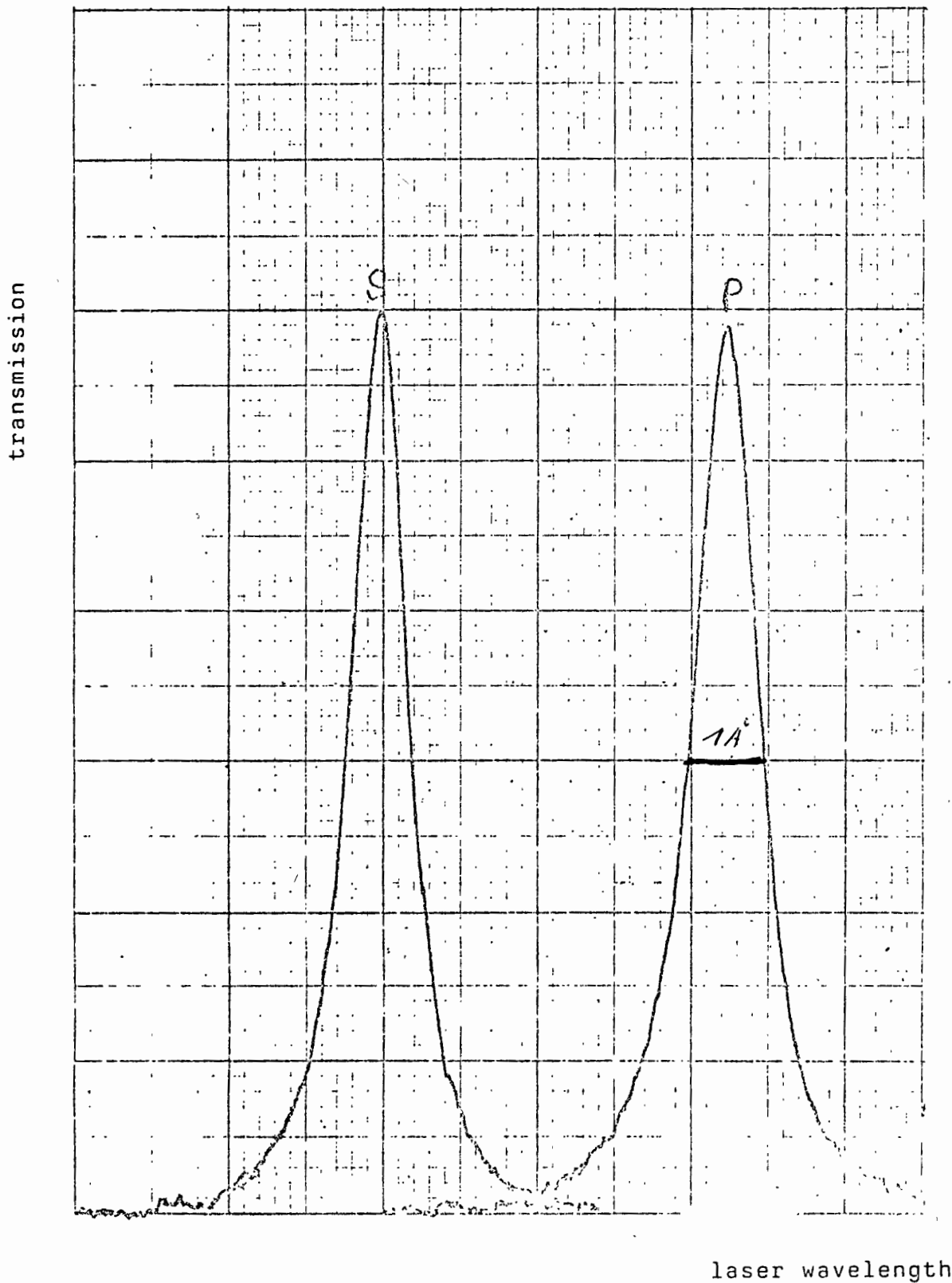
atmospheric transmission at different wavelengths. However, the smaller the elevation is, the greater the transmission difference gets. For example, the atmospheric transmission of 6943 Å laser will be 50 % higher than that of 5320 Å laser obtained with a second harmonic generator (SHG) when the elevation is equal to 20°. It is known that the SHG halves the wavelength of 1064 nanometers generated by Nd:YAG laser to 532 nanometers which is in the visible region of the spectrum. If there should be any photoelectronic conversion device which is of higher efficiency of quantum for a infrared laser it would be of great advantage for SLR systems to directly use the laser beam generated by the laser system without



SHG, such as 1064 nm laser falling within an atmospheric window. When omitting the SHG for which maximum conversion efficiency is up to 30 percent (energy) the latter is equivalent to increase the transmitted energy of about 70 percent. On the other hand, it will be seen from equation (1) that the received photons varies as the laser wavelengths. Under the condition of the same parameters the number of the received photons is increased with an increased wavelength. It will be possible to execute normal SLR with the smaller transmitted energy produced by a simplified laser.

If there is any significant drift for the laser wavelengths this will produce three bad effects. First is a transmission decrease for a telescope. It is known that the coatings of all optical components are compatible with a certain operation wavelength. The greater the drift of the laser wavelength is, the smaller the transmission for a transmitted laser beam gets. Second is an attenuation increase for a narrowband filter. In order to heighten the signal-to-noise ratio a narrowband filter is used in a receiver based on PMT. Due to a very narrow FWHM, such as that of  $1 \pm 0.2 \text{ \AA}$ , the attenuation of the narrowband filter for the returned laser will be greatly increased when there is any greater drift (see Fig.). For example, when the drift of laser wavelengths is equal to  $\pm 0.5 \text{ \AA}$  the transmission gotten through the narrowband filter will be decreased to 50 percent. Third is a reduction of the conversion efficiency from a light pulse to an electronic one. The peak conversion for a photocathode is compatible with a certain wavelength. Due to the drifted wavelength the conversion efficiency can not be impinged in the peak region. It will be seen from these that the stability of the laser wavelength is very important to insure the optimal operation for SLR systems. The spectral line stability should be better than a few subangstroms.

It will be seen from Table 1 that in 44 lasers used by worldwide SLR systems the minimal transmitted energy is 10 millijoules, the maximum 4.5 joules; the minimal pulsewidth is 100 picoseconds,



Transmission of double peak polarized interference filters produced by DayStar Filter corporation, California, USA

the maximum 35 nanoseconds. It was pointed out that the more narrow the laser pulsewidth, the smaller the pulsewidth error [Liu, 1985]. In practice the relationship was also found with constraining the laser pulsewidth. For example, the pulsewidth was constrained from 25 nsec to 6 nsec by means of a pulse chopper in an SAO SLR system so that the ranging accuracies increased to at least 50 percent [Tapley, et al, 1982]. From the following equation it can be demonstrated:

$$M_w = \frac{k_p \tau_p}{\sqrt{N_r}} \quad (2)$$

Where,

$M_w$  = pulsewidth error;

$\tau_p$  = FWHM of a laser pulse;

$N_r$  = number of received photoelectrons;

$k_p$  = coefficient depending on different detection.

However, to use the pulse chopper for a narrow laser pulsewidth is a temporary improvement means. Due to its reject for a sizable fraction of the laser energy it is not efficient. An essential and efficient means is to employ the new laser which can not only generate laser pulses as short as 30 psec, but also operate in a pure fundamental TEM<sub>00</sub> mode. The latter can produce the smallest beam divergence, the highest power density, and, hence, the highest brightness. Furthermore, the radial intensity profile is uniform and uniphase [Koechner, 1976]. The experiment by GSFC demonstrated that the requirements can be satisfied essentially when using modelocked Nd:YAG lasers. Their repeatability and rangemap measurements have shown less than 2 cm peak-to-peak variation in 100 point mean. The repeatability and rangemap measurements for PTM Q-switched and Q-switched lasers were of more than 6 cm peak-to-peak variation in 100 point mean [Degnan and Zagwodzki, 1982]. It will be seen from the above

that modelocked Nd:YAG (or YAP) lasers should be substituted for Q-switched ones. The latter has also other problem leading to a wavefront error. Its source and magnitude have been discussed in another paper [Liu, 1985]. For at least decreasing the wavefront error SLR systems do not employ also the Q-switched lasers, but the modelocked ones.

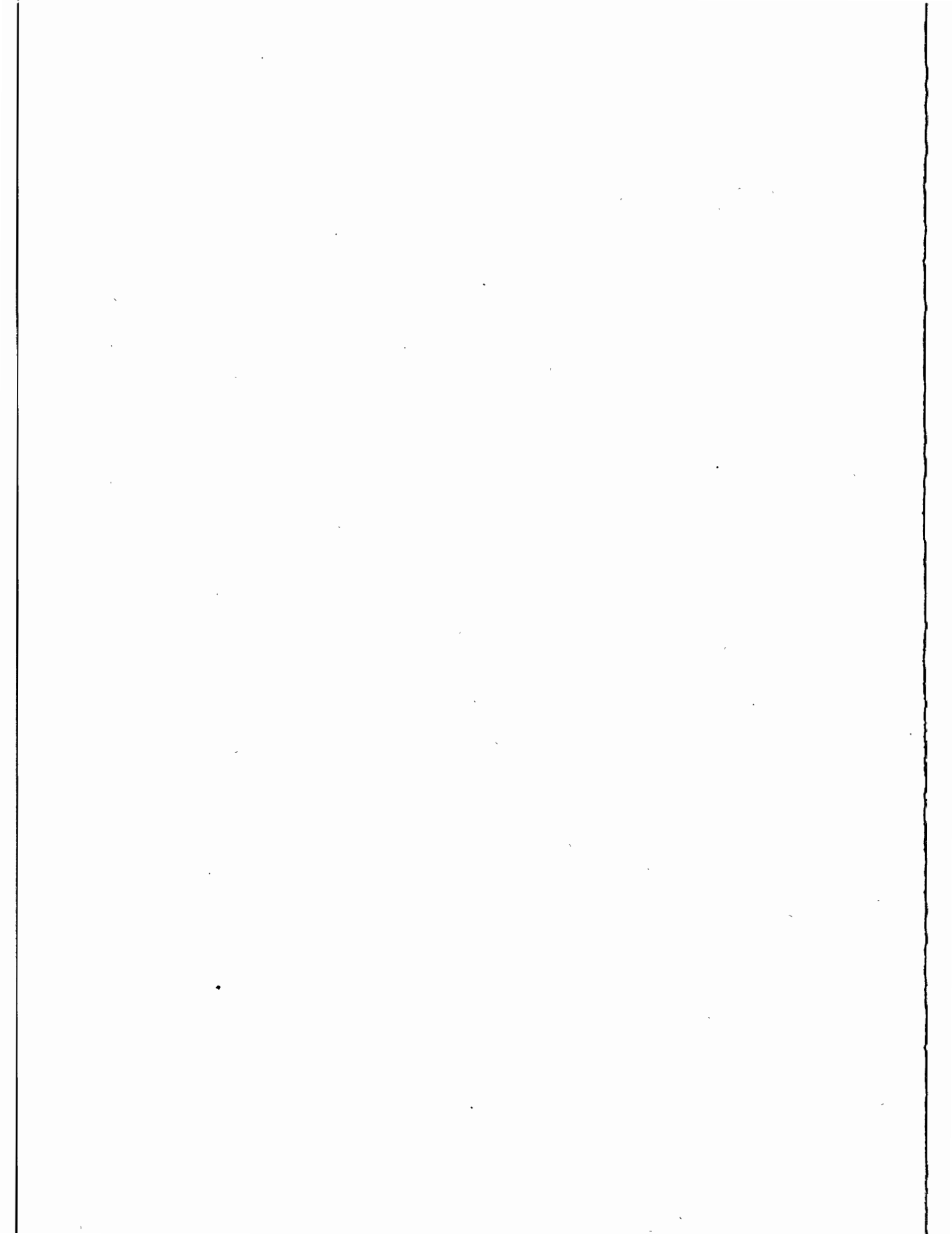
From what has been said above, we know that it is suitable for lasers to be able to generate the following pulses:

- stable wavelength laser pulses, so as to insure the optimal operation for SLR systems. If there should be any device which can effectively detect infrared lasers it would be very beneficial to use longer laser wavelength for SLR;
- higher repetition laser pulses, so as to acquire more ranging data in one satellite pass; but due to limitations of thermal transients which disturb the fine balance within the optical resonator and high peak power nonlinear effects which can lead to the irreversible breakdown of materials subnanosecond laser pulses are limited to about 20 pps repetition rate [Hyde and Whitehead, 1982];
- short sharp laser pulses, so as to improve the accuracy for measurements to the time interval between a transmitted and returned laser pulse;
- powerful peak laser pulses. so as to be able to measure the distances not only to the satellite-borne retroreflectors, but also to the moon-borne retroreflector array;
- purer fundamental laser pulses, so as to obtain an uniform and uniphase intensity profile for precise SLR.

Acknowledgement: The author would like to express his hearty gratitude to the Institut für Angewandte Geodäsie, Frankfurt, FR Germany, for its support.

11  
References

- [1] G. Mastrocinque, Feasibility of Satellite Tracking with a Dual-wavelength Laser Ranging System  
ESA Journal, 1985, Vol. 9, pp 273-286
  
- [2] Liu Jiyu, Satellite Laser Ranging Errors
  
- [3] W. Koechner, Solid-state Laser Engineering, 5.1.9 Mode Selecting techniques  
Springer-Verlag, Berlin, 1976
  
- [4] J.J. Degnan and T.W. Zagwodzki, A Comparative Study of Several Transmitter Types for precise Laser Ranging  
Proceedings of the Fourth International Workshop on Laser Ranging Instrumentation, published by the Geodetic Institute, University of Bonn, 1982, pp. 241 - 250
  
- [5] R.L. Hyde and D.G. Whitehead, Some Problems of Short Pulse, Low Energy, High Repetition Rate Lasers Applied to Satellite Ranging Systems  
Proceedings of the Fourth International Workshop on Laser Ranging Instrumentation, published by the Geodetic Institute, University of Bonn, 1982, pp. 251 - 259



ANALYSIS AND PERFORMANCE OF A PASSIVE  
POLARIZATION TELESCOPE COUPLING SWITCH  
FOR LUNAR LASER RANGING

S.R. Bowman, J.R. Rayner, C.O. Alley  
Department of Physics and Astronomy  
College Park, MD 20742

Telephone (301) 454 3405

ABSTRACT

A passive polarization switch is an attractive way to couple a laser transmitter and receiver to a telescope because it is so simple. However, few laser ranging stations have implemented such a switch because of concern about depolarization of the beam by the target. Here we show that the amount of depolarization is less than one might expect by considering the case of the Apollo lunar reflectors.

ANALYSIS AND PERFORMANCE OF A PASSIVE  
POLARIZATION TELESCOPE COUPLING SWITCH  
FOR LUNAR LASER RANGING

S. R. Bowman, J. R. Rayner, C. O. Alley  
Department of Physics and Astronomy  
College Park, MD 20742

Telephone (301) 454-3405

ABSTRACT

A passive polarization switch is an attractive way to couple a laser transmitter and receiver to a telescope because it is so simple. However, few laser ranging stations have implemented such a switch because of concern about depolarization of the beam by the target. Here we show that the amount of depolarization is less than one might expect by considering the case of the Apollo lunar reflectors.

INTRODUCTION

In order to separate the transmitted from the returned beams, some sort of switch is required. Most laser ranging systems incorporate a rotating mirrored chopper wheel for the switch. While this approach is conceptually simple it can lead to some practical problems. The wheel must spin stably while staying in phase with a high repetition rate laser. The limited extinction ratio between the two paths requires some additional blocking mechanism. Also, for realistic spin rates this type of switch is too slow for terrestrial ranging.

For the Goddard/Maryland Lunar Ranging System, a passive polarization switch was chosen.<sup>1</sup> It has the advantage of being very simple to implement, consisting of only a thin film Brewster angle polarizer and a zero order quarter wave plate. It has the disadvantage of losing some return light due to depolarization, but this is more than compensated for by its reduction of the noise by a factor of two. This section examines the efficiency of such a switch for lunar ranging.

DEPOLARIZATION FROM APOLLO REFLECTORS

After the second harmonic generator a half wave plate is used to rotate the linear polarization to the vertical, Figure 1. The "S" polarization is reflected off a thin film polarizer and passes through a zero order quarter wave plate into the telescope. (The zero order plate is needed to prevent temperature variation from affecting the polarization state.) Returning light of the correct polarization will become "P" polarized after a second trip through the quarter wave plate. Using Jones's calculus the polarization state can be computed each step of the way.<sup>2</sup>



Define a coordinate system on the optical table as shown in Figure 2. Transmission of the "S" polarization through the  $\lambda/4$  plate gives a polarization state

$$U_s = \frac{1}{2} \begin{pmatrix} 1-i \\ 1+i \end{pmatrix} \quad (1)$$

Multiple reflections off the telescope mirrors will change the polarization state. However measurements of this effect show it to be small. A helium neon laser with an arbitrarily oriented linear polarization was transmitted through the telescope. The attenuation of the transmitted beam by a crossed linear polarizer was measured at many telescope positions. The linearly polarized intensity was found to be preserved to within 5%. Since this change is small and is reversed upon returning through the telescope, it is ignored here. It cannot be ignored, though, that the polarization axis will rotate as the telescope tracks in azimuth. This effect combined with the changing orientation of the moon as it passes overhead will be accounted for by a rotation transformation of the corner cube array.

#### PASSIVE POLARIZATION SWITCH

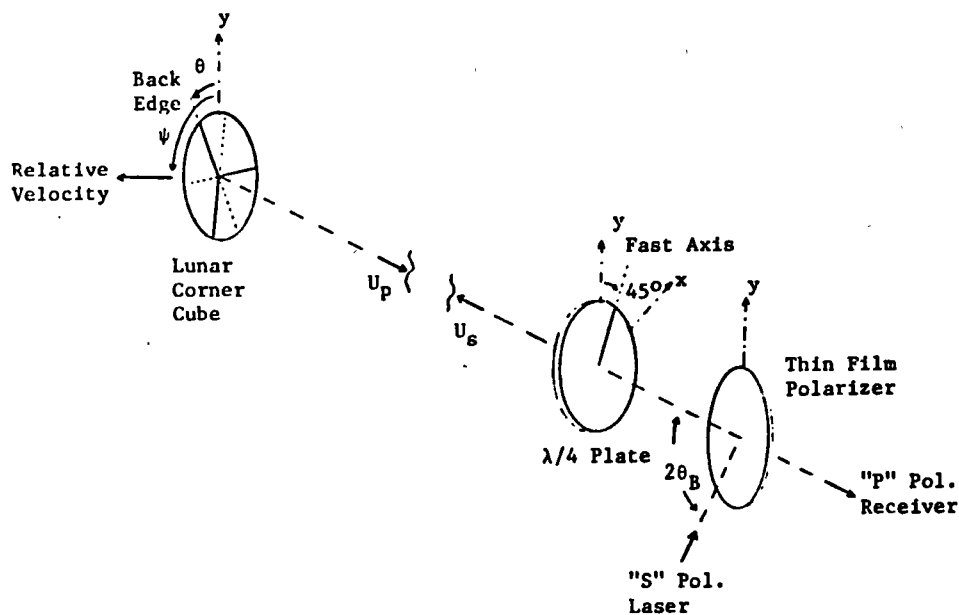


FIGURE 1

What happens to the polarization of a beam when reflected from a total internal reflection corner cube was first studied by E.R. Peck.<sup>3</sup> R.F. Chang et al.<sup>4</sup> extended the analysis to include far field diffraction of linear polarization from a corner cube. In a similar calculation, the Fraunhofer diffraction pattern for normally incident, circularly polarized light from a corner cube can be determined. Then the efficiency of the passive polarization switch can be evaluated once the velocity aberration effect is accounted for.

Upon reflection from a lunar corner, the incident beam is broken up into six wedge shaped beams. In general, each of these beams will have a different polarization. These six polarization states,  $\underline{V}^n$ , can be calculated from the equation

$$(\underline{V}_x^n, \underline{V}_y^n) = \underline{C}^n \cdot \underline{U}_s. \quad (2)$$

The authors mentioned above have calculated the polarization matrix  $\underline{C}^n$  consistent with the coordinates chosen here for the case of one back corner edge parallel to the "y" axis.

$$\begin{aligned} \underline{C}^1 &= \xi \underline{1} + \sqrt{1/2} \eta \underline{g}_z + \zeta \underline{g}_y + \sqrt{3/2} \eta \underline{g}_x \\ \underline{C}^2 &= \xi \underline{1} + \sqrt{2} \eta \underline{g}_z + \zeta \underline{g}_y \\ \underline{C}^3 &= \xi \underline{1} + \sqrt{1/2} \eta \underline{g}_z + \zeta \underline{g}_y - \sqrt{3/2} \eta \underline{g}_x \\ \underline{C}^4 &= \xi \underline{1} + \sqrt{1/2} \eta \underline{g}_z - \zeta \underline{g}_y - \sqrt{3/2} \eta \underline{g}_x \\ \underline{C}^5 &= \xi \underline{1} - \sqrt{2} \eta \underline{g}_z + \zeta \underline{g}_y \\ \underline{C}^6 &= \xi \underline{1} + \sqrt{1/2} \eta \underline{g}_z - \zeta \underline{g}_y + \sqrt{3/2} \eta \underline{g}_x \end{aligned} \quad (3)$$

In terms of the total internal reflection coefficients  $r_s$  and  $r_p$

$$\begin{aligned} \xi &= \frac{1}{16} (r_s + r_p) [3(r_s + r_p)^2 - 2(r_s - r_p)^2] \\ \eta &= \frac{\sqrt{2}}{16} (r_s + r_p)^3 \\ \zeta &= -i \frac{\sqrt{3}}{16} (r_s + r_p)^2 (r_s - r_p). \end{aligned} \quad (4)$$

For an arbitrary azimuthal orientation of the corner, the matrix  $\underline{C}^n$  must be rotated about the "z" axis. It is easy to see that only the "x" and "z" Pauli matrix components are affected by a rotation of angle  $\theta$ . To transform  $\underline{C}^n$  to  $\underline{C}^n(\theta)$ , one only need substitute

$$\underline{g}_x(\theta) = \begin{pmatrix} \cos 2\theta & \sin 2\theta \\ \sin 2\theta & \cos 2\theta \end{pmatrix} \quad \text{and} \quad \underline{g}_z(\theta) = \begin{pmatrix} \cos 2\theta & \sin 2\theta \\ \sin 2\theta & \cos 2\theta \end{pmatrix}. \quad (5)$$

Combining the last few equations gives the polarization state vectors,  $\underline{V}^n$ , for the six normally reflected beams from an azimuthally rotated total internal reflection corner cube. In order to evaluate the efficiency of the polarization switch, the components of each  $\underline{V}^n$  that are transmitted and rejected must be found. Transforming back through the  $\lambda/4$  plate shows that:

$$\underline{U}_p = \frac{1}{2} \begin{pmatrix} 1 & +i \\ 1 & -i \end{pmatrix} \quad (6)$$

is the transmitted polarization state. The components of the  $\underline{v}^n$ 's in the  $\underline{U}_p$  and  $\underline{U}_s$  directions are

$$\begin{aligned} \gamma_p^n &= \underline{v}^n \cdot \underline{U}_p = \begin{cases} \tau\xi + \zeta & (\text{for odd } n) \\ \tau\xi - \zeta & (\text{for even } n) \end{cases} \end{aligned}$$

and

$$\gamma_s^n = \underline{v}^n \cdot \underline{U}_s = \eta \delta_n e^{i2\theta}, \quad (7)$$

where the complex numbers  $\delta_n$  are given in Table (1).

The normalized reflected electric field from the  $n$ th subaperture of the  $j$ th corner cube in the array can now be written as

$$\underline{A}_j^n = [ \gamma_p^n(\theta_j) \underline{U}_p + \gamma_s^n(\theta_j) \underline{U}_s ] \exp(i\Delta_j). \quad (8)$$

The phase  $\Delta_j$  is the overall optical delay for the  $j$ th corner. For even slight variations in the physical dimensions or temperatures of the corners, the optical delay will vary over one wavelength. For this reason the following analysis assume  $\Delta_j$  to be random.

Records of the construction of the lunar corner reflector packages show that all the corners in the arrays were carefully oriented alike.<sup>5</sup> Therefore, the subscript on  $\theta_j$  can be dropped.

After propagating back from the moon, the beam from each of the corner cubes will be spread by diffraction. For the  $j$ th corner the field component in the  $\underline{U}_p$  direction at a point  $Q$  will be

TABLE 1

$n$	$\delta_n$
1	$\sqrt{3/2} - 1/2$
2	$+i$
3	$-\sqrt{3/2} - 1/2$
4	$-\sqrt{3/2} + 1/2$
5	$+i$
6	$\sqrt{3/2} - 1/2$

$$u_j^P(Q, \theta) = \frac{1}{\pi a^2} \exp(i\Delta_j) \int_0^a \rho d\rho \int_0^{2\pi} \gamma_p(\phi, \theta) e^{-ik\rho \sin\alpha \cos(\phi-\psi)} d\phi \quad (9)$$

Here  $(\rho, \phi)$  are polar coordinates on the corner aperture and  $(\alpha, \psi)$  are the angles locating the point Q relative to the center of the diffraction pattern. Dividing by the area of the corner,  $\pi a^2$ , normalizes the amplitude for  $\alpha = 0$ . Rewriting the  $\phi$  integral in terms of the six subapertures gives

$$u_j^P(Q, \theta) = \frac{1}{\pi a^2} \exp(i\Delta_j) \sum_{n=1}^6 \gamma_p(\theta) \int_0^a \rho d\rho \int_{\theta+(2n+1)\pi/6}^{\theta+(2n+3)\pi/6} \exp[-ik\rho \sin\alpha \cos(\phi-\psi)] d\phi \quad (10)$$

With the definition of  $x = k a \sin\alpha$  and the use of the Bessel series expansions

$$e^{i y \cos \beta} = J_0(y) + 2 \sum_{\ell=1}^{\infty} (-1)^\ell J_\ell(y) \cos(\ell\beta) \quad (11)$$

and

$$\int_0^x y J_\ell(y) dy = 2\ell x \sum_{m=0}^{\infty} \frac{(\ell + 2m + 1)}{(\ell + 2m + 2)(\ell + 2m)} J_{\ell+2m+1}(x)$$

the amplitude component becomes

$$u_j^P(Q, \theta) = \frac{1}{3x} \exp(i\Delta_j) J_1(x) \sum_{n=1}^6 \gamma_p^n + \frac{8}{\pi x} \exp(i\Delta_j) \sum_{\ell=1}^{\infty} (-1)^\ell \sin(\ell\pi/6) \sum_{n=1}^6 \gamma_p^n \cos\{\ell[\pi(n+1)/3 + \theta - \psi]\} * \sum_{m=0}^{\infty} \frac{(2m+\ell+1)}{(2m+\ell)(2m+\ell+2)} J_{2m+\ell+1}(x) \quad (12)$$

If the laser pulse duration is long enough, the fields from all of the N corners will superimpose. In the approximation that N is large, the transmitted intensity will be

$$I^P(Q, \theta) = \left| \sum_{j=1}^N u_j^P \right|^2 = N |u_j^P|^2 \quad (13)$$

Likewise, the rejected intensity will be

$$I^S(Q, \theta) = \left| \sum_{j=1}^N u_j^S \right|^2 = N |u_j^S|^2 \quad (14)$$

The polarization switch efficiency can now be written as

$$e(Q, \theta) = |u^P|^2 / [|u^P|^2 + |u^S|^2] \quad (15)$$

where the subscript j is now superfluous.

For small x, the  $J_1$  term dominates the expression for  $u^P$  and the efficiency approached unity. Realistically though, the diffraction pattern is never centered on the receiver. It was shown earlier that

$$4.0 \leq |\alpha| \leq 7.3 \text{ microradians.} \quad (16)$$

as a result of velocity aberration. Figure 2 shows the switch

POLARIZATION SWITCH EFFICIENCY  
FROM APOLLO REFLECTOR ARRAY

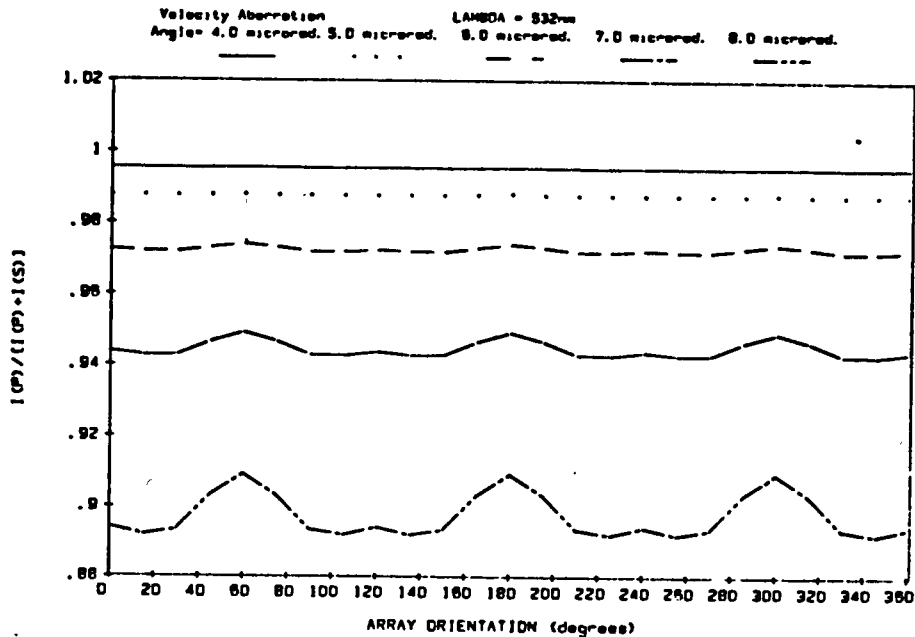


FIGURE 2

efficiency for several intermediate velocity aberration angles. It is clear from these curves that the depolarization is a weak function of the corner array orientation,  $\theta = \psi$ . More importantly though, the passive switch efficiency is better than 90% for all cases.

From the example calculation for lunar targets one would expect the depolarization losses to increase for other targets as the velocity aberration increases, although the exact calculation depends on the details of the targets structure. This means that the highest losses would be expected for the lowest satellites since they have the highest relative velocity. In practice, the passive polarization switch has been found to work very well for LAGEOS, BE-C, and GEOS-A.

CONCLUSIONS

Passive polarization switches are a simple, efficient way of coupling the laser and receiver to a laser ranging telescope. For lunar ranging operations, depolarization losses of less than 10% can be expected. Additional advantage is gained in noise reduction by the filtering of the unwanted polarization.

## REFERENCES

1. The idea of using a polarization switch for coupling the laser and detector was originally suggested by Professor Douglas G. Currie about 1976. Its first use was reported in: C.O. Alley et al., "Experimental Range Measurements at the Single Photo-Electron Level to the GEOS-A and BE-C Satellites," Third International Workshop on Laser Ranging, Lagonisi, Greece, May 1978.
2. R.C. Jones, "A New Calculus for the Treatment of Optical Systems," J. Opt. Soc. Am., 31 (1941), 488.
3. E.R. Peck, "Polarization Properties of Corner Reflectors and Cavities," J. Opt. Soc. Am., 52 (1962), 253.
4. R.F. Chang et al., "The Far Field Diffraction Pattern for Corner Reflectors with Complex Reflection Coefficients", J. Opt. Soc. Am., 61 (1971), 431.
5. Laser Ranging Retro-Reflector Array for the Early Apollo Scientific Experiment Package, Final Report to Aerospace Systems Division The Bendix Corporation, Arthur D. Little, Inc., Cambridge, Mass., June 30, 1969.
6. M. Born and E. Wolf, Principles of Optics, (New York: Pergamon Press, 1985), p. 394.

AN ACCURATE TEST OF THE AZIMUTH AXIS OF A 1.2M  
ALT-AZ TELESCOPE MOUNT FOR THE LUNAR LASER  
RANGING AND THE ANALYSIS OF THE RESULTS

H. Feng, Y. Xiong, Y. Zhang, J. Wang  
Yunnan Observatory  
Academia Sinica  
P.O Box 110  
Kunming - China -

Telephone 729 46  
Telex 64040 YUOBS.FN

ABSTRACT

The wobble of the azimuth axis of a 1.2m Alt-Az telescope mount for the Lunar Laser Ranging is measured by means of an accurate method. The systematic error is separated out and the random wobble is found to be about  $0''.08$ . The relation between the systematic error and the structure of the mount is also given in this article.

## I. Introduction

Because of the long distance between the Earth and the Moon, the lunar laser ranging works approximately to the threshold of detection for the current laser ranging technology. In addition, the aim actively pursued by all the lunar laser ranging stations today is to make the lunar laser ranging by means of the absolute pointing of a telescope so as to increase in the number of days for the ranging. But the necessary condition is that the telescope should have highly accurate pointing. However, the pointing is based on the stability of the axis system. It is known that because of the error in the level adjustment or mechanical faults of the mount even the effects of the environments, the azimuth axis of the mount can not coincide with the direction of the plumb line of the station. The deviation consists of the systematic error and random wobble. Our aim is to seek for an accurate testing method, analyse the measured data, extract the systematic error from them and make an exactly quantitative estimate of the random wobble. It is hopeful to make compensation for the systematic error extracted when a computer is used to correct the telescope pointing. Moreover, some very interesting details related to the structure of the telescope mount are also found as the systematic error is analysed.

## II. The Measuring Method

The most direct method for determining the deviation of the azimuth axis from the local plumb line is that the shift of a fine bubble, which is put at the top of the azimuth axis, is observed when the mount turns around the axis. Our measuring method still follows this principle, but the measurement accuracy is greatly improved.

The Talcott level used on the Zeiss transit instrument is adopted and one of the graduations is measured to be 1.17 arcsec (at about  $20^{\circ}\text{C}$ ). The level bubble is fixed on an adjustable support which is installed at the top of the azimuth axis. Two small measuring telescopes, each with a micrometer, are used to determine the position of either end of the bubble, respectively. As two measuring telescopes may be pointed to the targets within a short range and one graduation of the bubble may be equivalent to 130 divisions on the micrometer. And it is easy to estimate the readout of  $1/5$  division on the micrometer. In this way the readout resolution may be up to  $1/500$  arcsec. Of course, the actual measurement accuracy can not be so high, which is limited by the factors such as the sighting accuracy, the manufacture precision of the bubble, the effects of the environment and so on.

When the measurement is carried out the bubble is firstly put in the direction paralleled to the altitude axis. As the mount is turned at  $10^{\circ}$  around the azimuth axis, the positions of the two ends of the bubble are determined by the micrometers separately and the mean of the two readouts represents the position of the center of the bubble. Then place the bubble in the direction perpendicular to the altitude axis



and repeat the steps of the measuring method mentioned above. We have made the measurement of 46 circles in all (with 36 measuring points and 37 readouts per circle). The measured data of the last 20 circles are used for the quantitative calculation and analysis. When the measurements of half of the 20 circles are made, the bubble is parallel with the altitude axis, and for the other half is perpendicular to the altitude axis.

### III. The Results and their Analyses

When the measured results are shown graphically, it is not difficult to find that the systematic error is evidently included in the results and there appears good repeatability between the circles (Fig.1).

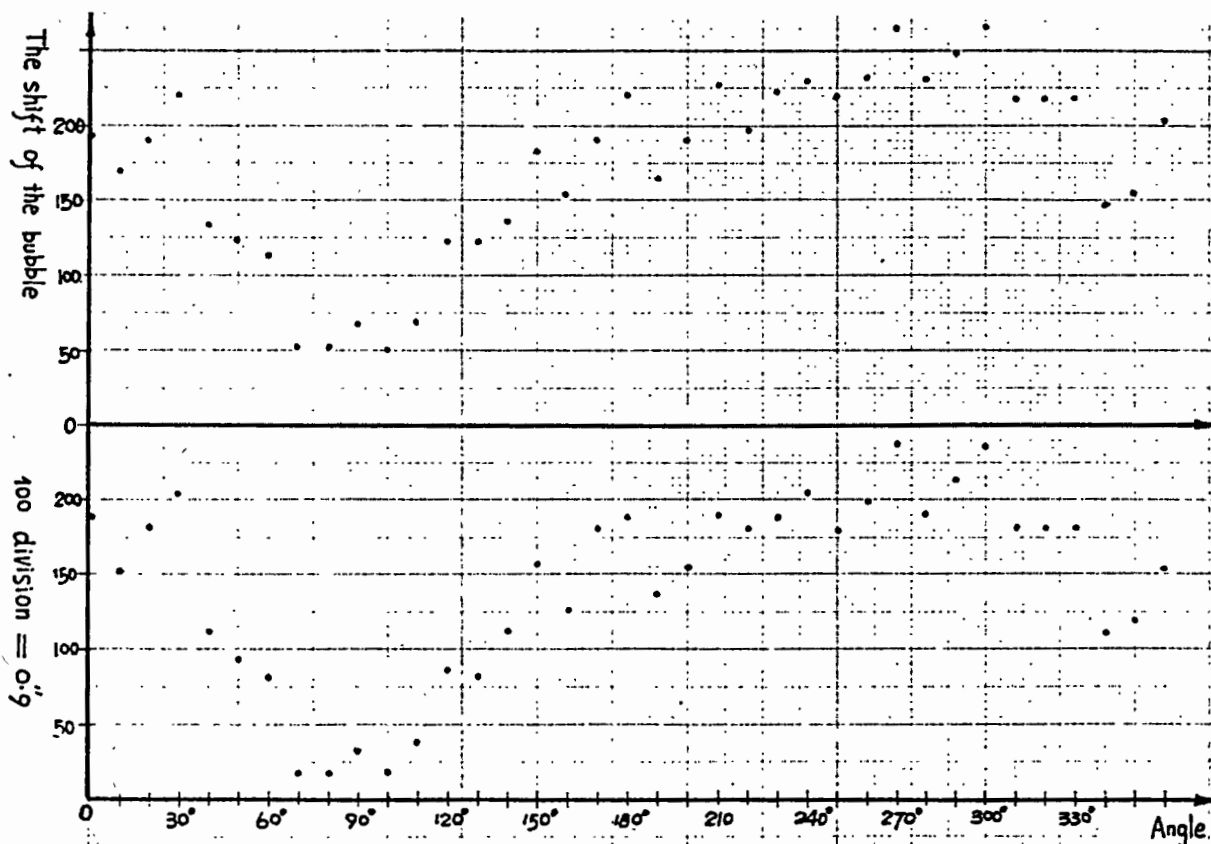


Fig.1. The positions of the bubble as the mount is turned at  $10^\circ$  around the azimuth axis

Using a trigonometric polynomial to fit the data, we can obtain the corresponding harmonic components. The first harmonic mainly originates from the level adjustment error of the mount, while the phases of the maxima of the third harmonic just correspond to the three bearing points of the mount, respectively. And it is of interest to note that the results also contain a twelfth harmonic, of which the amplitude is considerable and stable. The twelfth harmonic corresponds just right to the twelve oil pads of the revolving stage (Fig2).

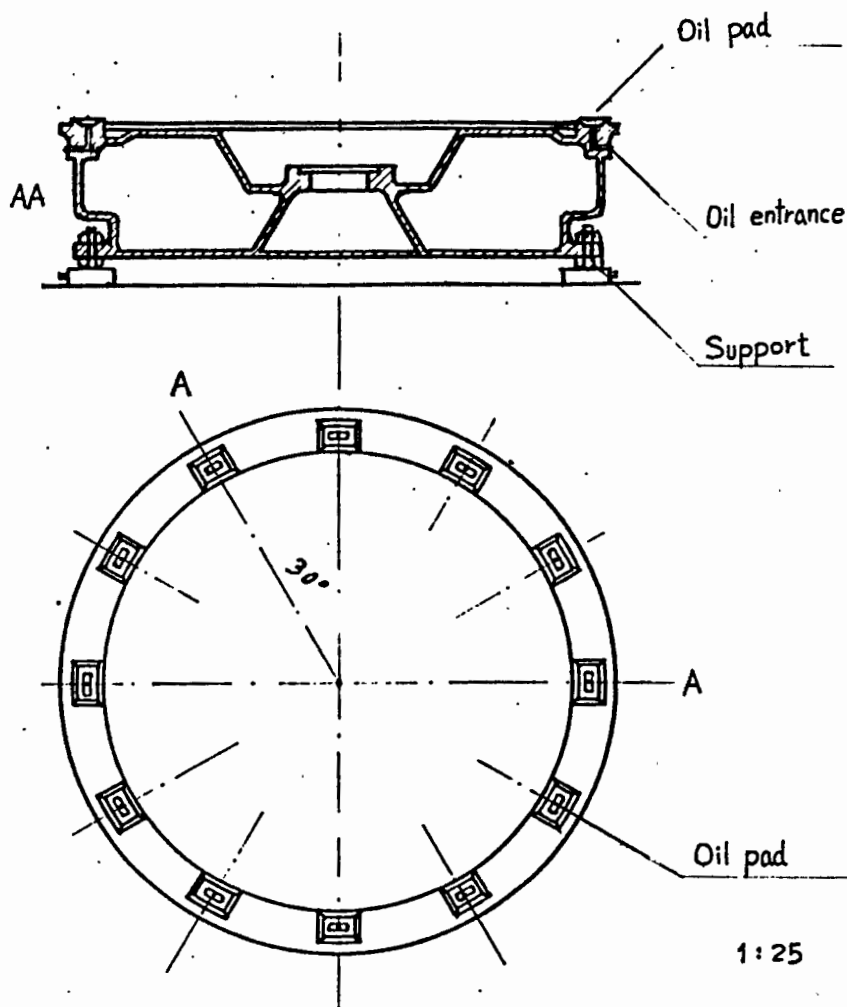


Fig.2. The twelve pads of the hydrostatic oil bearing

As for the second and fourth harmonics, they all originate from the deviation of the azimuth axis caused by the coupling of the drive roll with the rubbing disc (Fig.3). The drive roll is located at one side of the mount and its influence upon the azimuth axis may be regarded as the superimposition of both of the rigid and flexible compositions. The rigid composition influences the first harmonic and the flexible one produces the second and fourth harmonics. This analysis has been proved by the experiments. When the coupling of the driving roll with the rubbing disc is released, the second and fourth harmonics would nearly disappear and the first harmonic would have an obvious change. In addition, it is also found that both of the amplitude and phase of the first harmonic will have a slow and smooth change owing to the effects of the weather on the concrete pier, on which rests the mount. On the contrary, no notable variations would happen in the components, such as the third and twelfth harmonics, etc., which express the internal properties of the azimuth axis. It is necessary to note that a time-dependent linear term is included in the results, although its value

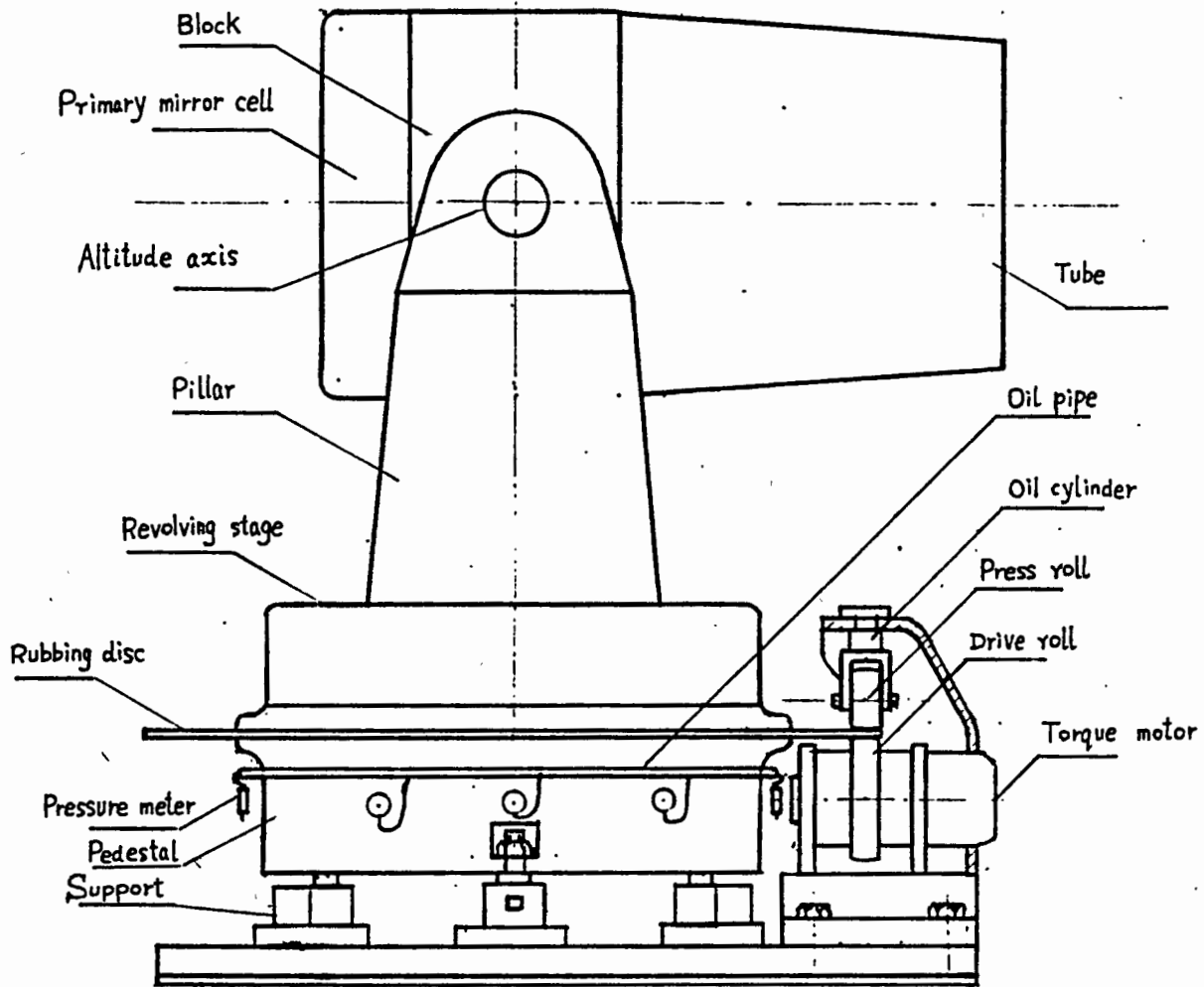


Fig.3. Azimuth axle drive assembly and its effects on the azimuth axis

is very small. The reason why there exists the linear term is that the measured value at  $0^\circ$  point at the beginning of the measurement may not be in accordance with that at the end of the measurement after running a circle. But if the measurement is repeatedly made at the  $0^\circ$  point in a short period, the measured values tally well with each other. Only in a rather long time interval when the measurement at the same point is made, the level bubble can shift in the same direction. It is considered that the reason why this phenomenon appears is that a substitute is used as the support of the bubble, of which the structure at either end is extremely unsymmetric. Even if there is no temperature gradient in the surrounding environment, the bubble will shift in the same direction owing to the time-dependent variation in the temperature within the dome. Therefore, it is reasonable to introduce the linear term to the measured results. It does not represent the internal characteristics of the axis, but shows that there is a linear variable term in the data, caused by the effects of the external environment on the measuring device.

Finally, the following formula is adopted to fit the measured data.

$$Y = a_1 \cos x + b_1 \sin x + a_2 \cos 2x + b_2 \sin 2x + a_3 \cos 3x + b_3 \sin 3x + a_4 \cos 4x + b_4 \sin 4x + a_{12} \cos 12x + b_{12} \sin 12x + kx + c \quad (1)$$

For the data of every circle (the 37 measured values are expressed by  $Y_i$ ), the twelve coefficients awaiting determination in the above equation can be calculated by the least square method. From the residua  $\Delta Y_i = Y_i - Y$  and equation (2) the root-mean-square of the fitting error  $M_f$  may be obtained, of which the mean is about 0.08.

$$M_f = \sqrt{\sum \Delta Y_i^2 / (37 - 12)} \quad (2)$$

The R.M.S. of the fitting contains the random wobble of the axis and the measuring error. The quantitative estimation should be made for our measuring method. It is found in the process of the analysis of the measured data that the random wobble of the axis does not happen in some small districts. So in this case the relation between the shift  $S$  of the bubble and the rotation angle  $\theta$  can be determined accurately (Fig.4). The data  $\theta_i, S_i$  can be fitted by a quadratic curve  $S = a \theta^2 + b \theta + c$ , which represents the motion model without wobble. The residua  $\Delta S_i$  of the measured values  $S_i$  with respect to the fitting curve can be used to estimate the measuring accuracy. The R.M.S. error in the measurement is

$$M_s = \sqrt{\sum \Delta S_i^2 / (N - 3)} \quad (3)$$

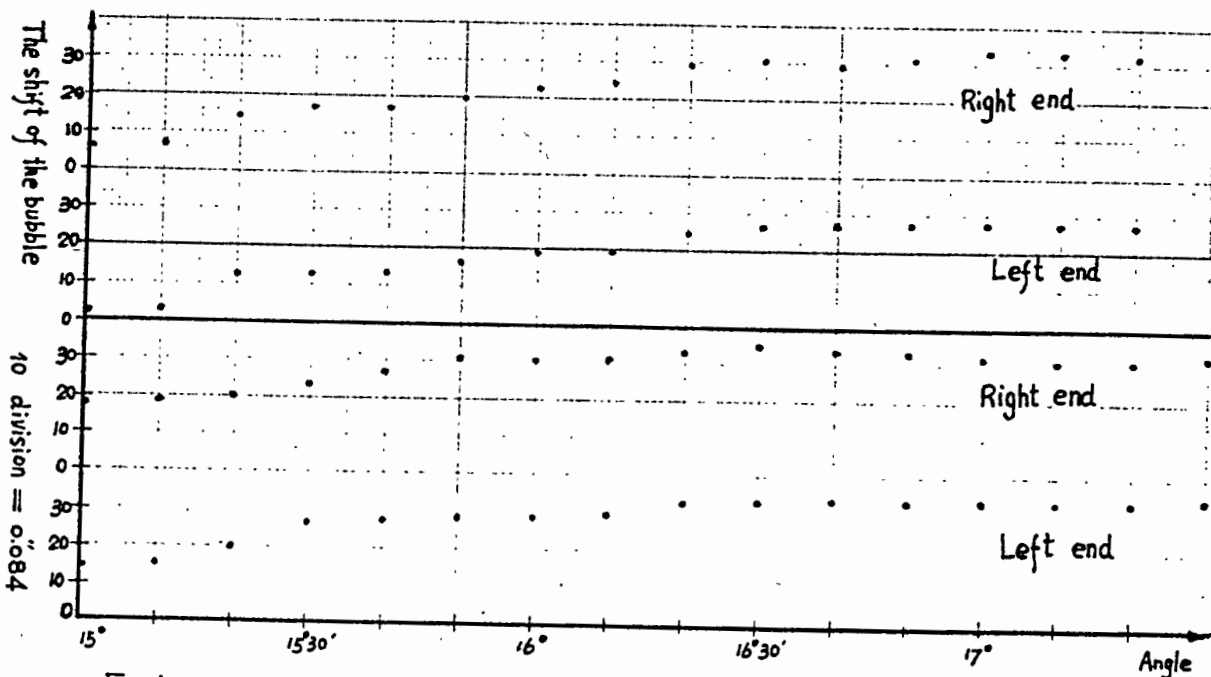


Fig.4. The relation between the shift of the bubble and rotation angle

where  $N$  is the number of the measuring points. A certain district of  $3^\circ$  is chosen where a measurement is made at every

10'. Fig. 4 shows two measured results. The repeatability of two measurements is very good and the root-mean-square error of the measurement is 0.015. Therefore, the values obtained from formula(2) primarily are the random wobble of the axis.

The data of 20 circles are listed in Table 1 and Table 2, where  $A_i$  represents the amplitude of the  $i$ th harmonic.

#### IV. Conclusions

(1) It can be seen from the data listed in Table 1 and Table 2 that the r.m.s. errors calculated from the measured data of every circle are quite approximate to one another. The standard deviation is used to express their dispersion, of which the value is about 0.01, being equivalent to the measuring error. It is shown that the tested result for the wobble of the azimuth axis is reliable.

(2) The systematic error model measured in a direction is different from that in the direction perpendicular to the former one. It is shown that a rigid model can not be used to describe the wobble of the axis. Hereafter, the correction for the telescope pointing must be made separately according to the results measured in the two directions.

(3) The first harmonic is affected by the influence of the environment on the concrete pier, but the other harmonics mainly have relation to the structure of the mount, and therefore they are all relatively stable. From now on, the first harmonic will be determined by the monitor of the relation between the first harmonic and the environments or by the observation of stars. Then the effect of the wobble of the azimuth axis on the telescope will be limited within the range approximate to that of the wobble of the azimuth axis stated in this paper. This is undoubtedly advantageous to the realization of the lunar laser ranging by means of the absolute pointing.

Unit: arc second

N	A <sub>1</sub>	A <sub>2</sub>	A <sub>3</sub>	A <sub>4</sub>	A <sub>12</sub>	M <sub>f</sub>
1	0.432	0.174	0.218	0.087	0.226	0.066
2	0.681	0.232	0.237	0.071	0.211	0.069
3	0.664	0.154	0.273	0.101	0.221	0.064
4	0.921	0.229	0.265	0.127	0.261	0.081
5	0.869	0.194	0.276	0.102	0.238	0.082
6	0.740	0.207	0.247	0.108	0.233	0.078
7	0.705	0.175	0.232	0.089	0.212	0.068
8	0.743	0.176	0.209	0.084	0.206	0.080
9	0.665	0.171	0.221	0.105	0.257	0.095
10	0.730	0.192	0.246	0.106	0.238	0.078
mean	0.715	0.190	0.242	0.098	0.230	0.076
$\sigma_x$	0.124	0.024	0.022	0.015	0.018	0.009

Table1 The bubble is parallel with the altitude axis.

Unit: arc second

N	A <sub>1</sub>	A <sub>2</sub>	A <sub>3</sub>	A <sub>4</sub>	A <sub>12</sub>	M <sub>f</sub>
1	2.014	0.478	0.203	0.086	0.159	0.094
2	2.046	0.470	0.209	0.080	0.161	0.091
3	2.056	0.465	0.228	0.095	0.140	0.096
4	2.235	0.462	0.259	0.137	0.146	0.077
5	2.338	0.481	0.222	0.124	0.150	0.074
6	2.323	0.463	0.212	0.119	0.131	0.059
7	2.265	0.482	0.245	0.123	0.143	0.074
8	2.159	0.466	0.233	0.111	0.143	0.063
9	2.190	0.499	0.243	0.122	0.176	0.075
10	2.141	0.475	0.245	0.124	0.155	0.064
mean	2.177	0.474	0.230	0.112	0.150	0.077
$\sigma_x$	0.109	0.011	0.017	0.018	0.012	0.012

Table2 The bubble is perpendicular to the altitude axis.

## DOUBLE PEAK POLARIZED INTERFERENCE FILTERS

M.L. White  
Lure Observatory  
Institute for Astronomy  
University of Hawaii  
Kula, HI 96790

Telephone (808) 878-1215  
Telex 7238459

### ABSTRACT

A new type of high transmission, narrow bandpass filter is tested at the University of Hawaii's Lunar Laser Ranging Observatory. In this article, the Daystar double peak, polarized interference filter is described. The filter performance is characterized through the evaluation of several tests.

## DOUBLE PEAK POLARIZED INTERFERENCE FILTERS

### I. Introduction

The Daystar double peak interference filter utilizes a solid spacer birefringent etalon. The etalon is cut to a half wave thickness and the refractive index of the etalon material is such that both orthogonal transmission modes are supported. This results in the transmission of both the vertical and horizontal light components at a desired wavelength. A single peak filter of the same type would pass only one polarization component resulting in a 50% loss of transmission at the desired wavelength. Finding birefringent material of acceptable quality and cutting the material at perfect half-wave plate thicknesses are the major limiting factors in the construction of double peak filters. Therefore, sources for these filters are limited.

Following are specifications for the filter described in this paper:

Transmission Wavelength: 532 Nanometers

Bandwidth: 1.0 Angstrom FWHM +/- 0.2 angstrom

Transmission: 28% per channel (This gives an actual throughput for our application of 28%)

Blocking: Full short side to x-ray optical density = 6.0  
Long side to 900 nanometers optical density = 5.0

Clear Aperture: 32 mm.

Filter components: Instrument quality, 60-40 scratch dig. Anti-reflection coated air/glass interfaces for minimum of 0.2 % reflectance. Installed in a temperature regulated oven providing +/- .05 angstrom on band control and minimum +/- 1.0 angstrom off-band search capability.

### II. Test Results

The filter was first tested on the University of Hawaii's, Mees Observatory solar spectrograph. The digitized signal from a silicon vidicon tube was used to measure the transmitted light through the filter and then without the filter. A graph was then plotted comparing the amount of light transmitted at 532 nanometers with no filter in place with the amount of light transmitted at 532 nanometers with the filter in place. The filter transmission was measured to be 28% with a FWHM bandpass of 1 angstrom (figure 1). At this time it was noted that the recommended on band temperature setting was not correct. In order to tune the filter on band, the recommended temperature had to be raised approximately 3 degrees centigrade to achieve maximum transmission at 532 nanometers. This was easily accomplished with the adjustable temperature controller, although the controller was near its maximum setting. The manufacturer doubted that the temperature calibration performed at the factory was nearly one angstrom off. However, the additional



tests performed also indicated that to achieve optimum transmission the filter temperature had to be raised.

The filter was then placed in the station's satellite calibration receive package. The average return signal off of the calibration target board was measured with a receive energy monitor through the filter and then without the filter in line with the detector. The comparisons of these two sets of data revealed that about 75% less energy was received with the filter in line with the detector than was received when the filter was not in line. This test was more subjective than the first and had an error factor of approximately plus or minus 10%.

Finally, the filter was tested during actual lunar ranging. The histograms in figures 2 and 3 show the number of photo-electron events obtained during several runs. It is difficult to apply a transmission efficiency number to the results, since one can only compare the data to other ranging data taken on nights when seeing conditions might be considerably different. A test of this nature is greatly affected by seeing conditions and equipment performance on a given night. However, when comparisons are made with lunar data taken with a four angstrom filter with a transmission of about 40%, the data rate is within expectation.

### III. Test Considerations

#### Angle of Incident Energy and Effects of Temperature Variance

Particular emphasis was placed on controlling the angle of incidence during these tests. When a narrow bandpass filter is tilted from the normal, the pass band will broaden while shifting its center to the shorter wavelengths. When testing the filter on the solar spectragraph a real-time display was monitored while the filter tilt was adjusted for maximum red shift.

Increasing the filter's correct operating temperature will shift the bandpass towards the longer wavelengths. Likewise, decreasing the filter's normal room temperature will shift the band pass toward the shorter wavelengths. The change in bandpass as a function of temperature depends on the spectral location of the filter and falls within a range of .15 to .4 angstrom per degree centigrade change. The Daystar 1 angstrom filter is installed in a temperature regulated oven providing +/- .05 angstrom on band control with a maximum +/- 1.0 angstrom off band search capability.

### IV. Conclusions

The filter performed at a level of efficiency consistent with the manufacturer's specifications with the exception of the discrepancy noted with the temperature controller. Daystar originally agreed to provide a filter with a throughput of 25%. The completed filter, however, was measured to have a throughput of 28%. This is an excellent overall transmission for a 1 angstrom bandpass filter and it should be useful to any lunar ranging station desiring to improve the receiver, signal-to-noise ratio. The problem with the temperature controller should lead future users of this filter type to verify on-band tuning since any deviation from the filter's correct operating temperature will lead to a significant change in the bandpass.

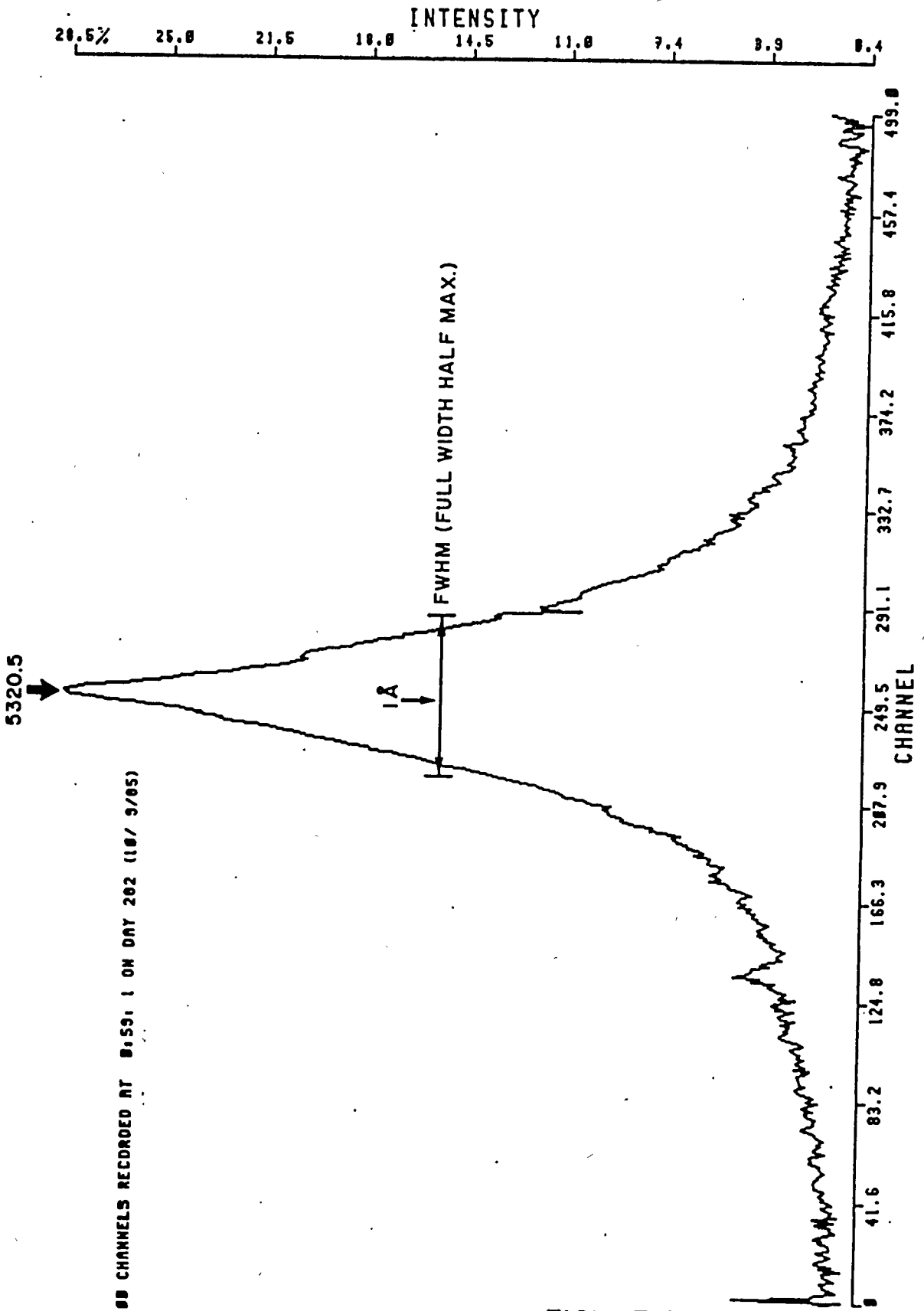
The filter was originally expected to increase the station's coverage through the maximum lunar illumination period. However, when the filter was tested during several full moon periods, a significant improvement in the signal to noise ratio was not observed. The background noise was considerably reduced as expected however, very few lunar events were observed. It is possible that more attempts at full moon ranging are needed to verify this result. More recently, other lunar stations have reported limited ranging success

during full moon that cannot be entirely related to increased lunar noise during full moon. This has led to some speculation that the Apollo reflectors lose some efficiency as they heat up during maximum lunar illumination.

Recently, the LURE Observatory achieved its first daylight lunar ranges. As a consequence normal lunar operations will be extended into daylight hours. More testing of the 1 angstrom double peak filter will be conducted during daylight hours where a significant improvement in the signal to noise ratio can be expected.

#### V. Acknowledgments

Special thanks to Dr. Donald Mickey for developing the solar spectrograph test and to the University of Hawaii, Institute for Astronomy for use of the Mees solar spectrograph. Thanks also to Richard Dawe and Lou Macknik for help with graphs and test ideas.



500 CHANNELS RECORDED AT 8:59:1 ON DAY 202 (10/ 9/05)

FIGURE 1

HISTP(8.30)

Data histogram for Input File : LUN31210.279

LUNAR Data Histogram

460 DATA RECORDS WITH 560 RANGES

Less than	50.0000	211	!*****
50.0000 TO	52.0000	3	!***
52.0000 TO	54.0000	2	!**
54.0000 TO	56.0000	3	!***
56.0000 TO	58.0000	2	!**
58.0000 TO	60.0000	1	!*
60.0000 TO	62.0000	1	!*
62.0000 TO	64.0000	3	!***
64.0000 TO	66.0000	7	!*****
66.0000 TO	68.0000	2	!**
68.0000 TO	70.0000	4	!****
70.0000 TO	72.0000	4	!****
72.0000 TO	74.0000	5	!*****
74.0000 TO	76.0000	5	!*****
76.0000 TO	78.0000	4	!****
78.0000 TO	80.0000	7	!*****
80.0000 TO	82.0000	2	!**
82.0000 TO	84.0000	3	!***
84.0000 TO	86.0000	30	!*****
86.0000 TO	88.0000	31	!*****
88.0000 TO	90.0000	2	!**
90.0000 TO	92.0000	3	!***
92.0000 TO	94.0000	0	!
94.0000 TO	96.0000	0	!
96.0000 TO	98.0000	3	!***
98.0000 TO	100.0000	3	!***
100.0000 TO	102.0000	4	!****
102.0000 TO	104.0000	0	!
104.0000 TO	106.0000	3	!***
106.0000 TO	108.0000	4	!****
108.0000 TO	110.0000	3	!***
110.0000 TO	112.0000	3	!***
112.0000 TO	114.0000	1	!*
114.0000 TO	116.0000	0	!
116.0000 TO	118.0000	1	!*
118.0000 TO	120.0000	1	!*
120.0000 TO	122.0000	2	!**
122.0000 TO	124.0000	2	!**
124.0000 TO	126.0000	2	!**
126.0000 TO	128.0000	2	!**
128.0000 TO	130.0000	1	!*
130.0000 TO	132.0000	4	!****
132.0000 TO	134.0000	4	!****
134.0000 TO	136.0000	0	!
136.0000 TO	138.0000	4	!****
138.0000 TO	140.0000	4	!****
140.0000 TO	142.0000	2	!**
142.0000 TO	144.0000	1	!*
144.0000 TO	146.0000	2	!**
146.0000 TO	148.0000	4	!****
148.0000 TO	150.0000	2	!**
More than	150.0000	163	!*****

A TOTAL OF 560 DATA POINTS PROCESSED

APOLLO 15  
OCTOBER 6, 1985 2:10 A.M.  
20 MINUTE RUN  
1 Å 30<sup>m</sup>

FIGURE 2

HISTP(8.30)

Data histogram for Input File : LUN01236.279

LUNAR Data Histogram

40 DATA RECORDS WITH		43 RANGES	
Less than	50.0000	6	*****
50.0000 TO	52.0000	0	!
52.0000 TO	54.0000	0	!
54.0000 TU	56.0000	0	!
56.0000 TO	58.0000	0	!
58.0000 TU	60.0000	0	!
60.0000 TU	62.0000	0	!
62.0000 TO	64.0000	0	!
64.0000 TU	66.0000	0	!
66.0000 TO	68.0000	0	!
68.0000 TO	70.0000	0	!
70.0000 TO	72.0000	0	!
72.0000 TO	74.0000	0	!
74.0000 TO	76.0000	1	!*
76.0000 TU	78.0000	0	!
78.0000 TO	80.0000	0	!
80.0000 TU	82.0000	0	!
82.0000 TO	84.0000	0	!
84.0000 TO	86.0000	1	!*
86.0000 TO	88.0000	5	*****
88.0000 TO	90.0000	5	*****
90.0000 TO	92.0000	0	!
92.0000 TO	94.0000	0	!
94.0000 TO	96.0000	0	!
96.0000 TO	98.0000	0	!
98.0000 TO	100.0000	0	!
100.0000 TO	102.0000	0	!
102.0000 TO	104.0000	0	!
104.0000 TO	106.0000	0	!
106.0000 TO	108.0000	1	!*
108.0000 TO	110.0000	0	!
110.0000 TU	112.0000	1	!*
112.0000 TO	114.0000	1	!*
114.0000 TO	116.0000	1	!*
116.0000 TO	118.0000	0	!
118.0000 TO	120.0000	0	!
120.0000 TO	122.0000	0	!
122.0000 TO	124.0000	0	!
124.0000 TO	126.0000	0	!
126.0000 TO	128.0000	1	!*
128.0000 TO	130.0000	2	!**
130.0000 TO	132.0000	0	!
132.0000 TO	134.0000	0	!
134.0000 TO	136.0000	0	!
136.0000 TO	138.0000	0	!
138.0000 TO	140.0000	0	!
140.0000 TO	142.0000	0	!
142.0000 TO	144.0000	0	!
144.0000 TO	146.0000	0	!
146.0000 TO	148.0000	0	!
148.0000 TO	150.0000	1	!*
More than	150.0000	17	*****

A TOTAL OF 43 DATA POINTS PROCESSED

APOLLO 11  
OCTOBER 6, 1985 2:36A.M.  
20 MINUTE RUN  
1 Å 30<sup>m</sup>

FIGURE 3

## FILTER ADVANTAGES

- GOOD TRANSMISSION, 28%, FULLY BLOCKED.
- DURABLE. (Survived Sounding Rocket Crash).
- COMPACT. (2" x 3")
- EASY TO CONTROL TEMPERATURE.
- SINGLE PASS BAND.
- WORKS IN SYSTEMS AS FAST AS  $f/20$ .
- REASONABLE COST  $\sim$  \$3,000.00 U.S.

## FILTER DISADVANTAGES

- LIMITED NUMBER OF VENDORS AVAILABLE.
- DIFFICULT TO MANUFACTURE.
- SENSITIVE TO  $>1^\circ$  DEVIATION FROM NORMAL.

## EFFECTS OF TELESCOPE DESIGN ON LASER BEAM POINTING ACCURACY

R. Korakitis  
Department of Topography  
National Technical University of Athens  
Heroon Polytechniou 9  
GR-157 73 Zografos - Greece -

Telephone (01) 777 3613  
Telex 215032 GEO GR

### ABSTRACT

This work presents some studies about the effects of the optical design of the telescope on the beam pointing accuracy of the SLR system at Dionysos Satellite Geodesy Observatory.

A brief description of telescope and mount is given, with emphasis on components critical to beam alignment. Possible torsional flexure of the horizontal axis is examined and is found to be unimportant.

The path of the laser beam through the mount is softwaremodelled and beam deviations upon exit are computed for different positions of adjustable optical components. At the same time, it is shown that precession of the beam, due to improper alignment, has practically no effect on the optical path length, so no system delay changes are expected for different orientations of the mount. This prediction is experimentally confirmed down to the performance limit of the system (about 2 cm).

## 1. Introduction

This work reports some results of studies, conducted at Dionysos Satellite Geodesy Observatory, concerning the mechanical and optical performance of the mount and telescope used in the Satellite Laser Ranging system. The purpose of the studies is to establish the accuracy limit of the system with regard to laser beam pointing and system delay stability, since the mount was originally designed to be used with a 1st generation Ruby laser, having much lower precision capabilities.

In the first part, a brief description of mount and telescope is given, indicating components critical to mechanical and optical adjustments. A possible torsional flexure of the horizontal axis is examined both theoretically and experimentally and is found to be unimportant.

The second part describes the laser beam path and its software model. In this model, all optical components are suitably represented and ray-tracing results show how each individual adjustment affects the alignment of the beam and the optical path length. For all reasonable values of beam deviation, the path length does not depend on the orientation of the mount. The last section of the work describes the experimental verification of this prediction, through system delay measurements at various orientations.

## 2. Characteristics of the mount

The SLR system at Dionysos uses a conventional altitude over azimuth design, with separate transmit and receive optics and a coude optical path. The overall lay-out of the mount and telescope is shown in Fig.1.

Both rotation axes are realized by pairs of conical roller bearings and their exact orientation can be adjusted by suitably located screws. A precision level permits alignment of the primary (azimuth) axis within 3 arcsec of the local vertical. Similarly, the tilt of the secondary (altitude) axis is adjustable to within 3 arcsec of the horizontal plane. In addition to the roller bearings, the altitude axis is supported by preloaded bronze bushings, in order to minimize flexure. Rotation angles of the axes are read by optical encoders, which have a resolution of 1 millidegree and are situated by the respective drive gears. The rotation of the axes is accomplished by step-motors having a resolution of 0.001 per step and repeatability 1 millidegree (RMS). Therefore, the positioning accuracy of the mount is limited to about 5 arcsec.

With regard to the distribution of masses, one should note that the center of mass (CM) of the receiving telescope lies behind the altitude axis (when the telescope is in the horizontal plane), whereas the CM of the transmitter lies in front of the axis. Since the corresponding moments have opposite direction, the altitude axis is rotationally balanced. However, these moments can cause a torsional flexure of the steel tube that realizes the axis. The rotation angle of this axis (i.e. the altitude) is determined at the transmitting end of the tube, where the altitude drive and the encoders are situated, so any torsional flexure will show itself as a vertical deflection of the receiving telescope. A rough estimate of the magnitude of this deflection can be made using elementary elasticity theory [1]:

To a first approximation, the deflection angle  $\phi$  due to torsional flexure of a thin cylindrical tube is given by:

$$\phi = \frac{M l}{G r^2 S}$$



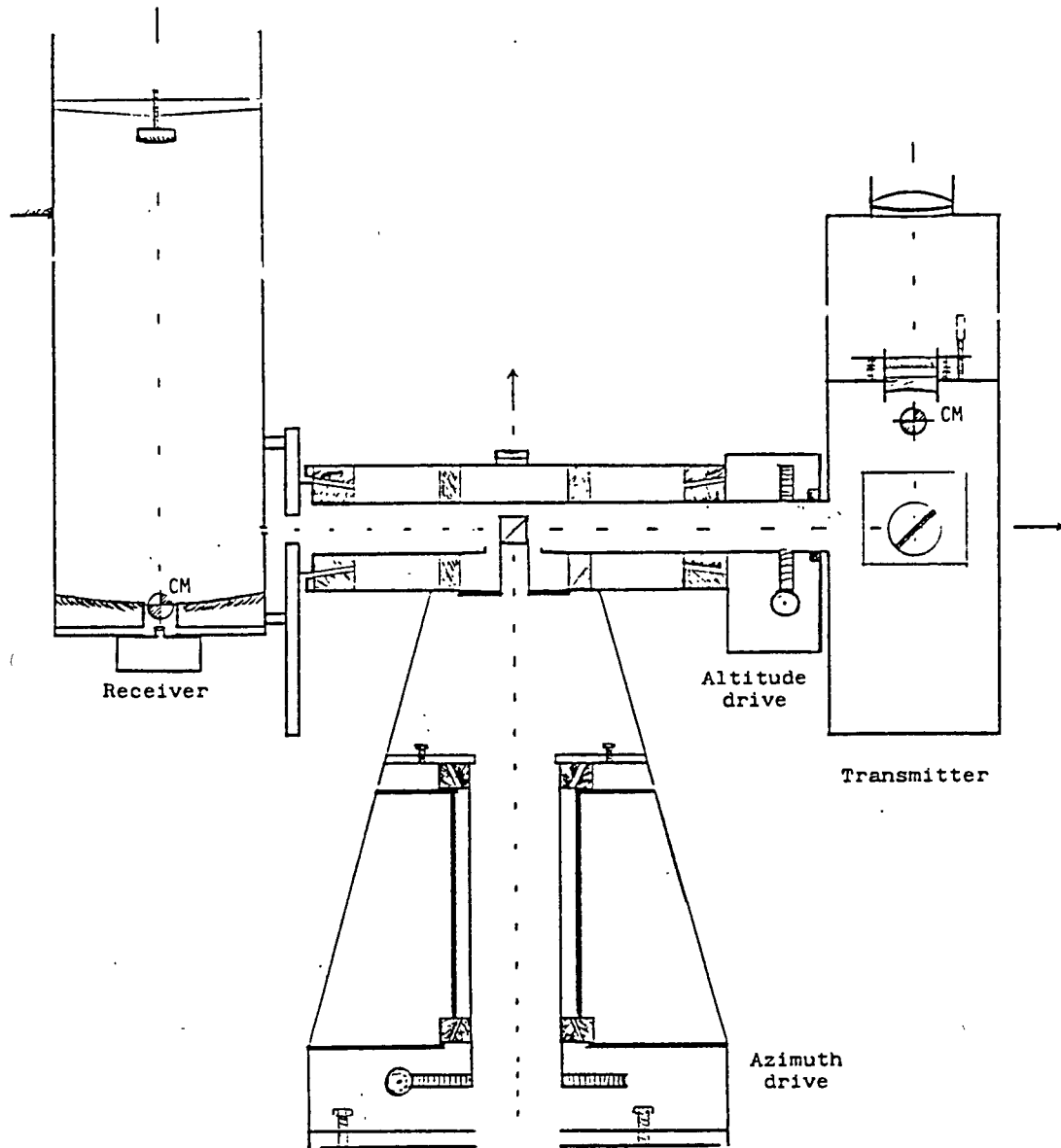


Fig. 1 : Mechanical lay-out of mount and telescopes

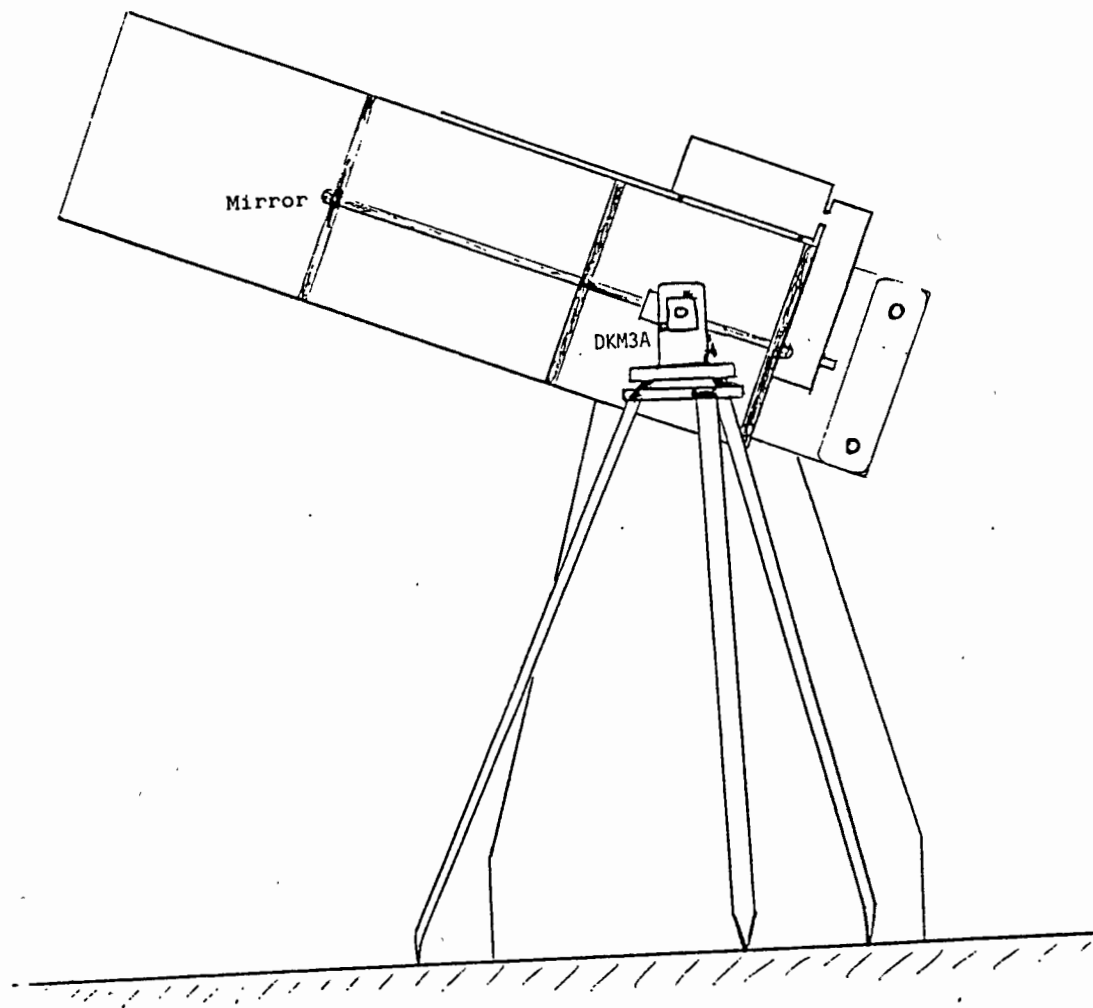


Fig. 2 : Set-up for the torsional flexure experiment

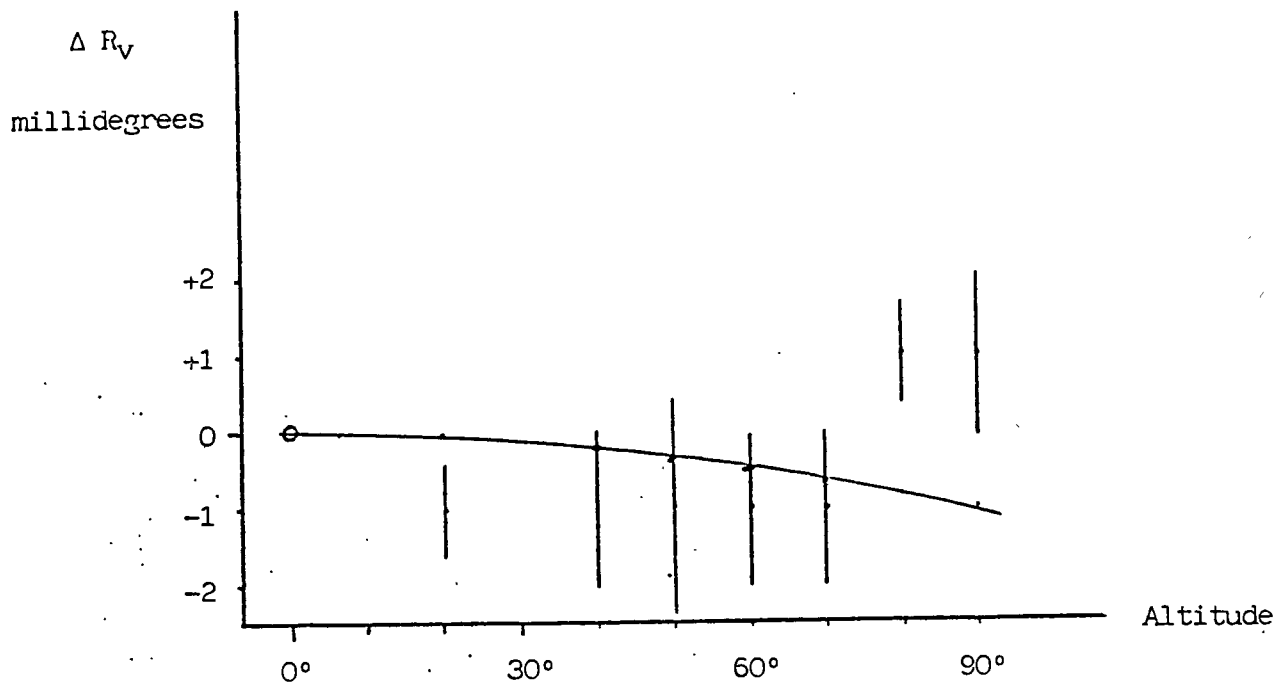


Fig. 3. Vertical reading differences (theodolite-telescope) vs. altitude.  $\Delta R_v$  defined to be zero at  $v = 0^\circ$ . The solid curve shows the effect of the expected torsional flexure.

where the symbols and their values for this particular case are:

M = the applied torque	= 100 kgr* × 20 cm × cosv
l = the length of the tube	= 100 cm
G = the shear modulus of the material	= 8 × 10 <sup>5</sup> kgr* cm <sup>-2</sup>
r = the radius of the tube	= 10 cm
S = the cross-section of the tube	= 157 cm <sup>2</sup>

Therefore, the maximum deflection (at altitude  $v=0^\circ$ ) is about 16 microradians or  $0^\circ.001$ . Since the predicted value of the deflection is similar to the positioning accuracy of the axis, torsional flexure is considered to be unimportant. In any case, an experimental check was performed as follows:

A small mirror was fixed on the outside wall of the receiving telescope, perpendicular to the optical axis. A precision theodolite, type Kern DKM3A, was placed by the receiver so that its horizontal axis roughly coincided with the altitude axis of the mount (Fig.2). The theodolite was used as an autocollimator, projecting the image of an illuminated crosshair to the mirror. In this way a direction, approximating the optical axis, was realized that remained fixed with regard to the receiver. The altitude of the telescope was varied and the encoder readings were compared with the corresponding readings of the vertical angle of the theodolite. Two independent series of such measurements were taken and the mean values of the differences are shown in Fig.3, along with the expected value of the deflection. No systematic deviation that can be attributed to torsional flexure is evident. The deviation of the measurements near the zenith, currently under further investigation, is probably connected with the behaviour of the anti-backlash torque motors of the altitude drive.

### 3. The laser beam path model

A general schematic of the laser beam path is shown in Fig 4. Upon exit from the laser unit, the beam is twice deflected through  $90^\circ$  by dichroic mirrors that separate the 532nm radiation from the IR. The laser beam, after expansion, is directed to the 1st mirror of the coude path that sends it upwards, along the vertical (azimuth) axis of the mount.

In order to facilitate the alignment of the beam, an auxilliary optical setup is under construction by the vertical axis. It mainly consists of an autocollimator and a fixed mirror, that will realize a permanent reference direction for the laser beam. A sample of the laser beam will be brought into this path by inserting a pellicle beam-splitter. At the same time, this setup will permit direct viewing through the transmitting telescope, enabling thus a direct check of the pointing of the telescope using observations of stars.

The alignment procedure consists of three main parts:

- Adjustment of the last dichroic mirror, together with expander, for pitch, yaw and linear position. Then, adjustment of the 1st coude mirror for pitch, yaw and transverse linear position so that the beam exactly follows the azimuth axis of the mount.
- Adjustment of the 2nd coude mirror, which actually is a right-angle prism situated at the intersection of the axes, for pitch, yaw and linear position so that the beam follows the altitude axis.

When these adjustments are completed, the laser beam should not precess when the mount is rotated to different orientations. At present, that can be achieved within 15 arcsec but this figure is expected to decrease using the alignment setup described earlier.

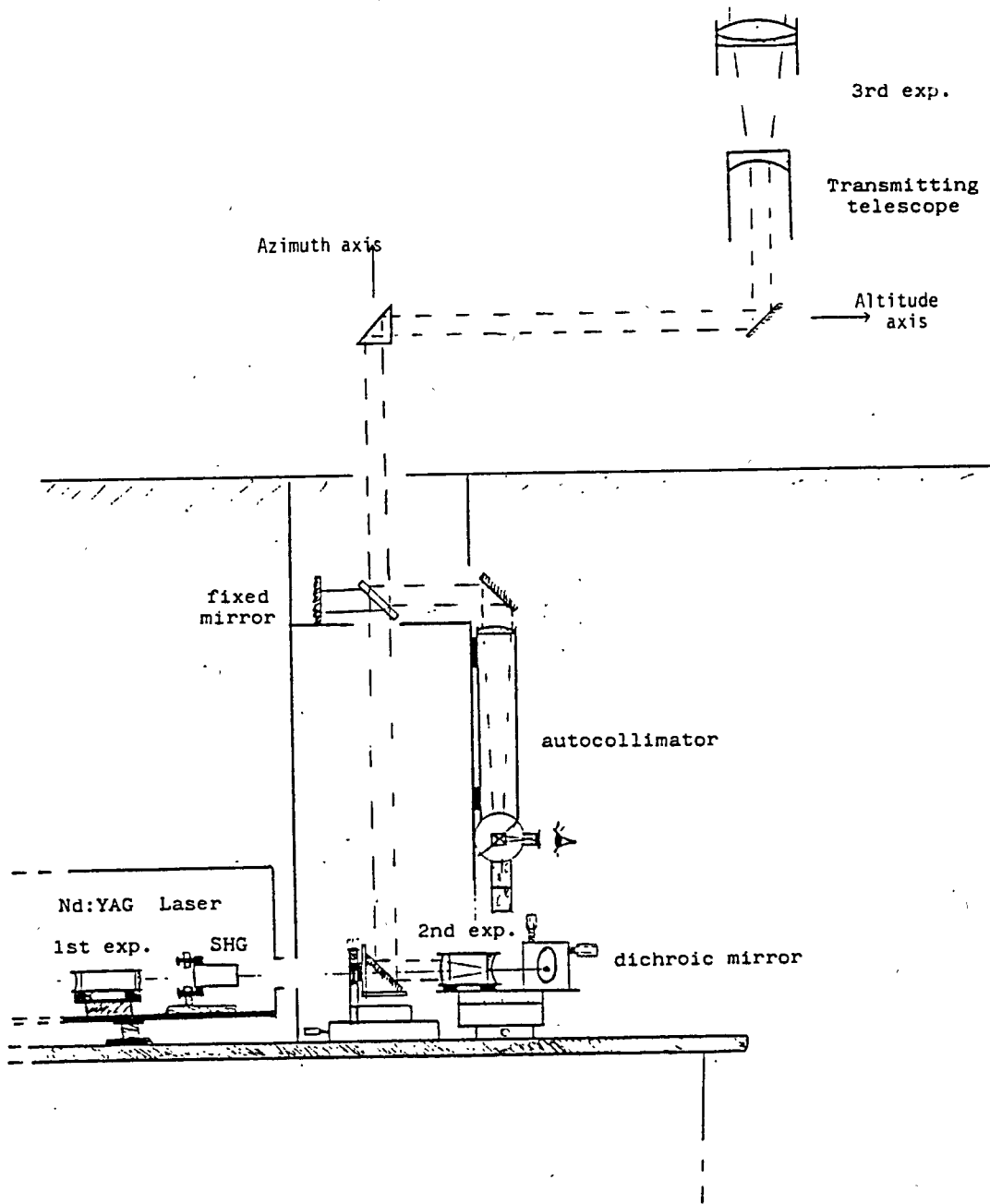


Fig. 4 : Schematic of the laser beam path

- c. The last step involves the adjustment of the 3rd coude mirror, located inside the transmitter, in order to bring the exit laser beam into alignment with the pointing direction of the mount (common direction of transmitter and receiver optical axes). In addition, the final beam expander adjusts the full angle divergence of the beam in the range 10 to 100 arcsec.

Referring to Fig.1, one should note the internal calibration path that is established inside the receiver end of the altitude axis. A very small drop of clear glue, at the hypotenuse face of the central coude prism, scatters some radiation towards the receiver. There, a small prism deflects it towards the main mirror so that it can be acquired by the detection package.

In order to study quantitatively the effects of the several adjustments needed for the alignment of the beam, the optical path was modelled in the computer. This software model analytically treats the deflections of the beam at all mirrors and prisms in the path, the position and orientation of which can be varied in accordance with the degrees of freedom of the actual components. The starting point and initial direction of the laser beam, as it leaves the 2nd expander, is taken into account, as well as the distances between the components, which were measured using a Chesterman stainless-steel tape.

The computations are performed using matrix representations of vectors in three rectangular coordinate systems: the  $\{X_0, Y_0, Z_0\}$  system remains fixed in space, with  $Z_0$  along the azimuth axis of the mount (local vertical) and  $Y_0$  towards the local astronomical North. The  $\{X_1, Y_1, Z_1=Z_0\}$  system is produced by rotating the previous one around  $Z_0$  through the azimuth angle  $A$ ; the  $X_1$  axis is along the altitude axis of the mount. Finally, the  $\{X_2=X_1, Y_2, Z_2\}$  system is derived by rotating the previous one around  $X_1$  through the altitude angle  $v$ ; the  $Y_2$  axis is along the optical axis of the transmitting telescope. The program outputs the direction of the laser beam upon exit, expressing it as an angular deviation from the  $Y_2$  axis towards a certain direction in the  $\{X_2, Z_2\}$  plane. Figures 6 and 7 are typical examples of the output, showing different locii of beam deviations for constant azimuth or altitude and for different adjustments of the components. In addition, the program computes the total path length, from the starting point of the beam up to a fixed plane outside the last lens of the system, where a retroreflector can be actually placed.

At present, the effects of the final beam expander are computed using the paraxial approximation. Since the overall alignment precision will increase with the installation of the auxiliary optics, a revised program is under development that will perform accurate ray-tracing using the exact refraction matrices.

It is worth mentioning that the program also handles the possibility that the two rotation axes of the mount are skew lines. In such case, the beam will rotate around the  $Y_2$  axis without changing its direction, in the paraxial approximation. In reality, though, the direction of the beam may be affected and this problem is another motivation for developing the exact treatment.

It is apparent that a similar program can be used to study any other telescope design as well, provided that all relevant positions and orientation of components are properly introduced.

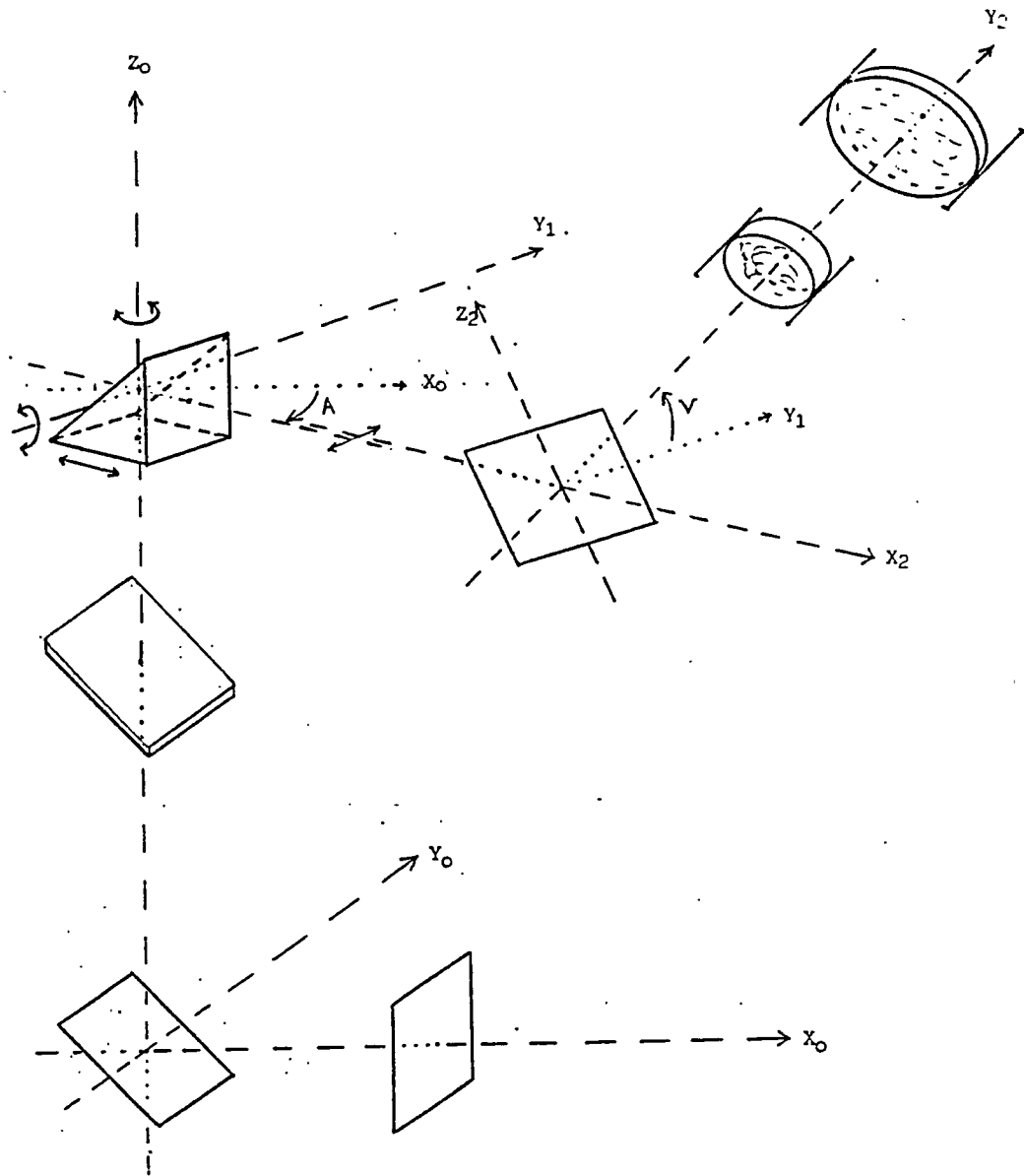
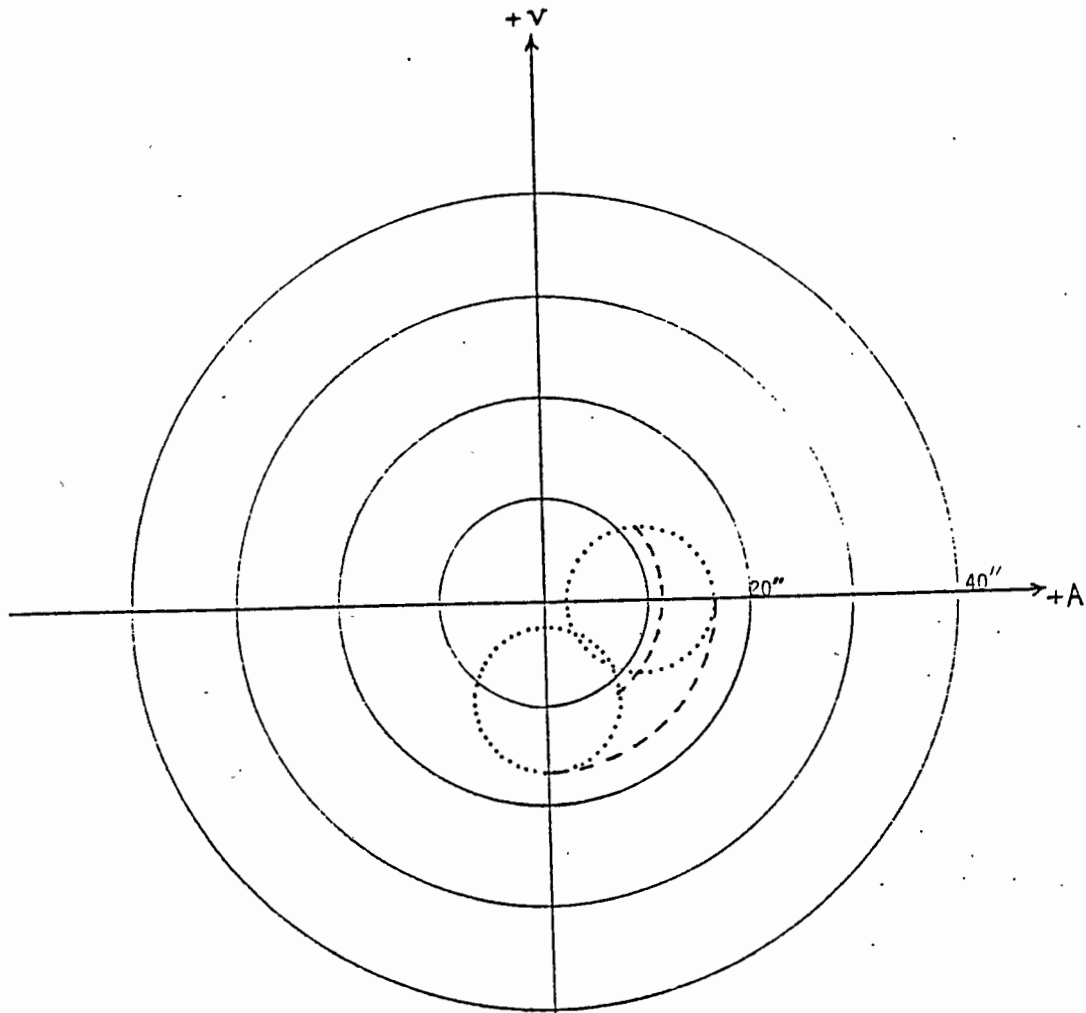


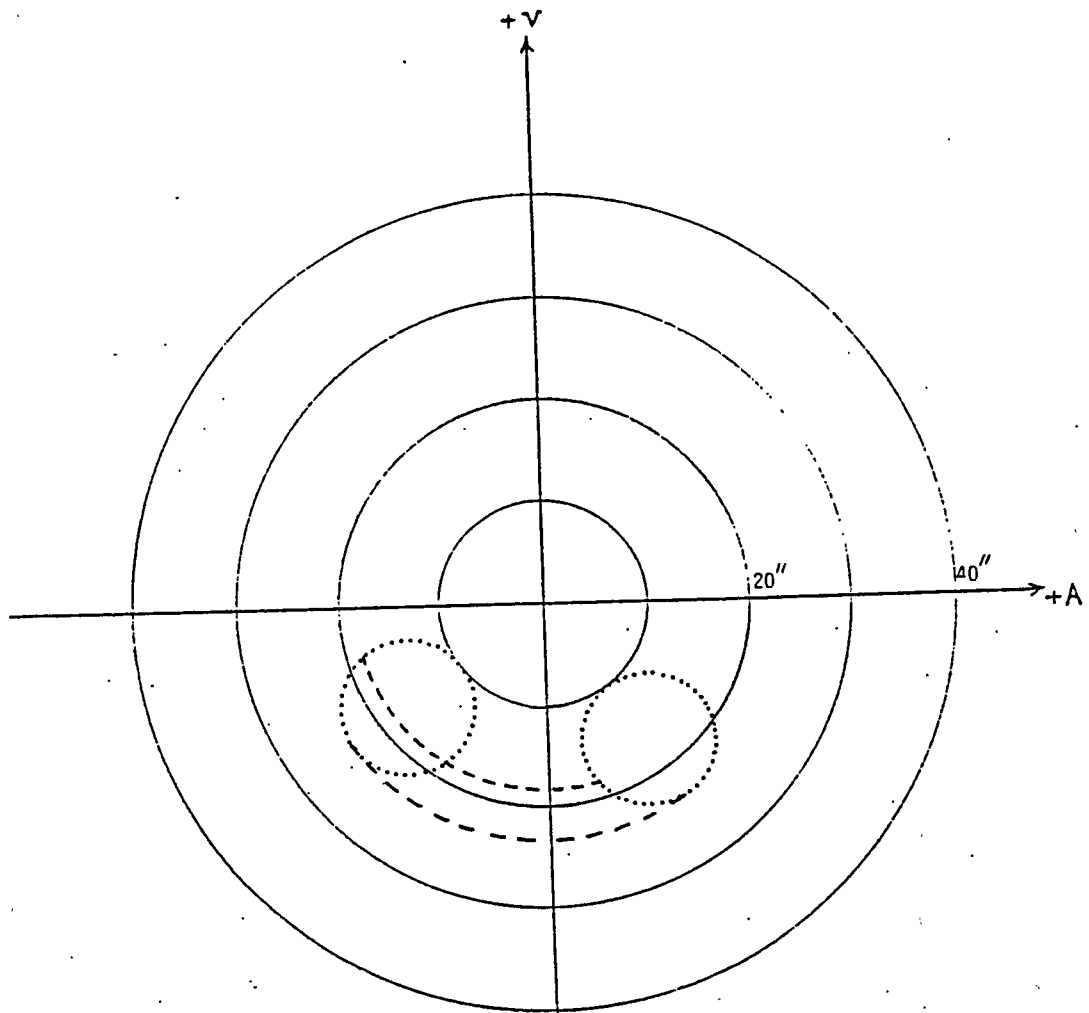
Fig. 5 : Geometry of the laser beam path model



Initial beam tilt :  $20''$  to  $-Z_0$   
 Prism displacement:  $0$  mm  
 angular dev. :  $-20''$  az  
                    $0''$  alt

Fig. 6 : Laser beam deviation curves  
 at constant azimuth (dashed lines)  
 and constant altitude (dotted lines)





Initial beam tilt :  $10''$  to  $-Y_0$  and  $18''$  to  $-Z_0$   
 Prism displacement: 0 mm  
 angular dev. :  $-20''$  az  
                    $-20''$  alt  
 Hor. axis displaced by 1 mm

Fig. 7 : Laser beam deviation curves  
 at constant azimuth (dashed lines)  
 and constant altitude (dotted lines)

#### 4. System delay measurements

As was mentioned earlier, the software model of the mount includes the total path length of the laser beam, which is directly related to the overall system delay. The computations indicate that the path length is only affected either by a linear displacement of the central coude prism or by the skewness of the two rotation axes. However, for any fixed adjustment of components, the path length is invariant for every orientation of the mount, at least for reasonably small beam deviations (up to several arcminutes!). The implication is that, once the alignment of the beam is even approximately correct, the system delay should not change with orientation of the mount.

This prediction was experimentally tested by measuring the travel time of the laser pulse from a point behind the last dichroic mirror, where a fiber optic link to the START photodiode of the system was placed, to a retroreflector at the transmitter exit and back. The travel time was measured at several different values of azimuth and altitude of the mount and a total of 40 individual measurements were taken in each position. The results are shown in figures 8 and 9 and no variation larger than the resolution of the measurements (about 2 cm [2]) is evident. In addition, one should note that the measurements were taken when the spatial profile of the laser beam was greatly distorted by a damaged SHG crystal. Therefore, a second test is scheduled, to be done after the installation of a new SHG crystal and which will also include a stability check of the internal calibration path.

#### 5. Conclusion

It has been shown that the particular telescope design of the SLR system at Dionysos Observatory presents some problems regarding the alignment of the beam in the coude path, which are studied using a software model of the mount. The results of the study dictate several improvements that can be made to increase the pointing accuracy of the system, with beneficial effects on received energy and return rate. On the other hand, it has been shown, both theoretically and experimentally, that the mount is free from appreciable flexure and is quite immune to system delay (i.e. calibration) changes for different orientations.

I would like to thank Mr. D. Paradissis for his kind help during the flexure test of the telescope.

#### REFERENCES

1. R.Feynman : "Lectures on Physics" , Addison Wesley Publ. Co. , 1964
2. R.Korakitis : "Performance considerations of the SLR system at Dionysos Observatory", 2nd WEGENER-MEDLAS Conference, Athens, 1986

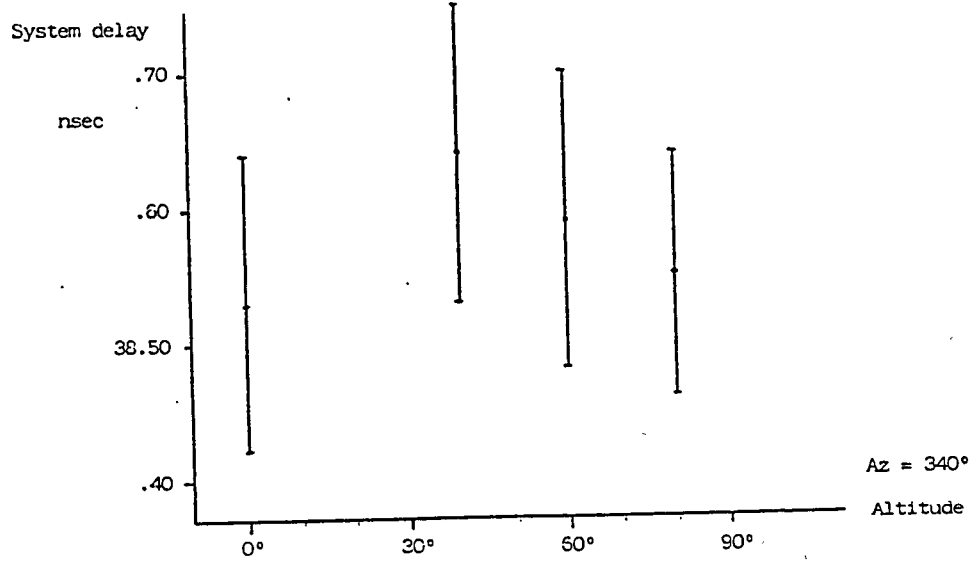
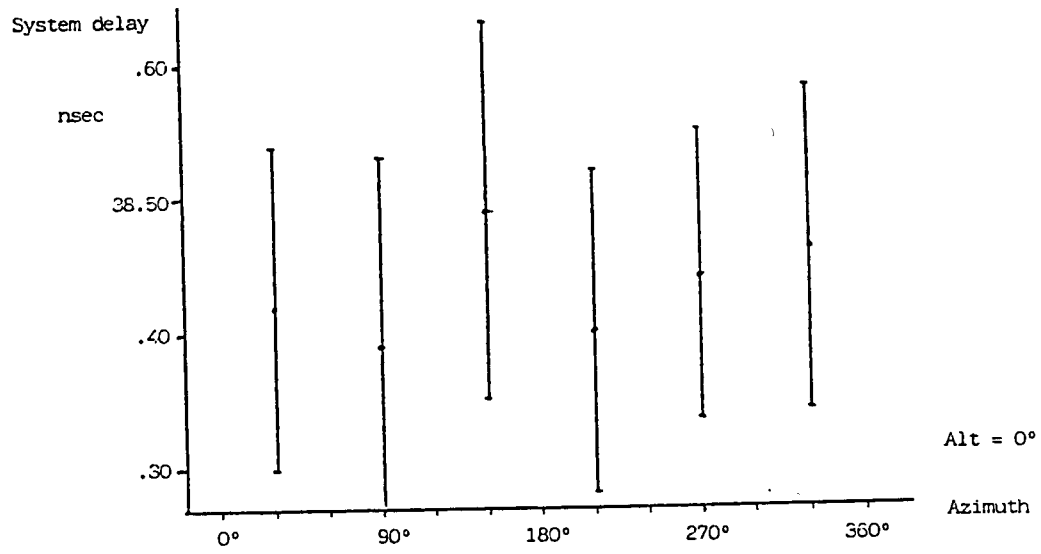


Fig. 8,9 : System delay measurements

